

**Mitochondrial Dysfunction in Uraemic
Cardiomyopathy. Technetium 99m
Sestamibi Washout As A Novel Marker Of
Mitochondrial Function.**

Dr Paul Callan MBChB, MSc Clinical Trials (Dist)

Thesis being submitted for Medical Doctorate

The University of Hull and University of York

Hull York Medical School

September 2018

Abstract

Introduction

Cardiovascular disease is the most common cause of morbidity and mortality in patients with chronic kidney disease. Uraemic cardiomyopathy describes a classical phenotype of left ventricular hypertrophy, diastolic impairment, myocardial fibrosis and altered response to ischaemic injury. Mitochondrial dysfunction plays a key role in the development and progression of this condition. Technetium 99m sestamibi washout is a novel tool that can be used for the non-invasive assessment of cardiac mitochondrial function.

Methods

Clinical studies

We undertook a retrospective analysis of the utility of myocardial SPECT imaging in patients with end stage renal failure referred for kidney transplantation. We assessed its ability to predict mortality and cardiovascular events.

A study of early vs delayed SPECT imaging using Technetium 99m sestamibi was performed in healthy subjects to develop a protocol for measuring Technetium washout in clinical studies.

Animal studies

Uraemia was induced in rats using a 5/6ths nephrectomy model. *Ex-vivo* measurement of cardiac function was performed using a Langendorff perfusion mode after 12 weeks, followed by *in-vitro* measurement of mitochondrial respiration and enzymatic activity of respiratory chain complexes.

Myocardial single positron emitted computed tomography (SPECT) was performed on isolated rat hearts using a modified perfusion rig, and perfused with buffer containing Technetium 99m sestamibi tracer. Technetium washout from the myocardium was recorded. Mitochondrial uncoupling agents were added to assess its effect on Technetium washout.

In vivo myocardial SPECT imaging was performed on rats to develop a protocol for measuring Technetium washout in pre-clinical studies.

Results

Clinical studies

The presence of resting perfusion defects or moderate to severe stress perfusion defects on myocardial SPECT scans performed in patients with end stage renal failure were independent predictors of adverse cardiovascular outcomes. The scan findings did not add to the risk prediction models based on clinical risk factors alone, highlighting the need for more robust tools to assess cardiovascular prognosis.

Evaluation of early Technetium kinetics in clinical practice found marked variability in early Technetium washout within the first hour. Inducible cardiac ischaemia was associated with higher washout rates.

Animal studies

A rat model of uraemic cardiomyopathy by subtotal nephrectomy was characterised, which identified a reduction in respiratory complex II/III enzyme activity, and an increase in state 4 mitochondrial respiration in the presence of glutamate and malate, when compared with controls.

An isolated perfused heart system for assessing ex vivo Technetium sestamibi washout was developed. Washout rates increased significantly with the addition of mitochondrial uncoupling agent CCCP, indicating that Technetium retention is dependent upon an intact mitochondrial membrane potential. We developed a method of measuring Technetium washout *in vivo*, and demonstrated stable Technetium retention in control rats.

Conclusion

We have developed a robust model for assessing Technetium 99m sestamibi washout both in an isolated heart model and *in vivo*. It has the potential to be utilised as a tool to increase our understanding of the role of mitochondrial dysfunction in the progression of uraemic cardiomyopathy, and to evaluate novel treatments for targeted at myocardial metabolism.

Table of Contents

Abstract.....	2
List of figures	9
List of tables	13
List of abbreviations.....	15
Acknowledgements	18
Declaration	19
Chapter 1: Introduction	21
1.1 Renal physiology.....	22
1.2 Cardiac physiology	26
1.3 Blood pressure.....	33
1.4 Hypotension.....	35
1.5 Uraemic Cardiomyopathy	35
1.6 Left Ventricular Hypertrophy	36
1.6.1 Diagnosis of LVH.....	37
1.6.2 Cellular level changes in LVH	40
1.6.3 LVH and Renal Failure	41
1.6.4 Pathophysiology of LVH	41
1.7 Mitochondrial function.....	45
1.8 Role of mitochondria in uraemic cardiomyopathy.....	49
1.8.1 Mitochondrial biogenesis in heart failure.....	50
1.8.2 Mitochondrial bioenergetics in heart failure.....	50
1.8.3 Mitochondrial dysfunction in uraemic cardiomyopathy.....	51
1.9 Myocardial Perfusion Imaging	52
1.10 Methods of stress testing.....	53
1.10.1 Exercise Stress	53
1.10.2 Dipyridamole.....	53
1.10.3 Adenosine	54
1.10.4 Dobutamine	54
1.10.5 Regadenoson	55
1.11 Prognostic Markers of Myocardial Perfusion Imaging.....	55
1.11.1 Stress testing.....	55
1.11.2 Reversible perfusion defects.....	56

1.11.3 Transient Ischaemic Dilation.....	56
1.11.4 ²⁰¹ Thallium Lung uptake.....	56
1.11.5 Left ventricular dysfunction	57
1.12 Technetium 99m Sestamibi	57
1.12.1 The ideal tracer	58
1.12.2 Tracer kinetics.....	59
1.12.3 Clinical aspects of ²⁰¹ Thallium Imaging	60
1.12.4 Technetium-99m terofosmin	61
1.13 Technetium 99m Sestamibi Washout.....	63
1.14 Objectives.....	64
1.15 Overall hypothesis	64
Chapter 2: Materials and Methods.....	65
2.1 Ethical Approval.....	66
2.2 5/6ths Nephrectomy Surgical Procedure.....	66
2.3 Preparation of Krebs Henseleit buffer.....	71
2.4 Isolated heart perfusion.....	71
2.5 Assessment of cardiac contractility	74
2.6 Biochemical analysis.....	75
2.7 Mitochondrial Isolation.....	76
2.8 Mitochondrial Respiration	76
2.9 Enzyme assays	78
2.9.1 Citrate Synthase	78
2.9.2 Aconitase	79
2.9.3 Complex I.....	79
2.9.4 Complex II.....	81
2.9.5 Complex II and III.....	82
2.9.6 Complex IV	83
2.10 Electrocardiogram.....	83
2.11 Ex vivo SPECT imaging.....	84
2.12 In vivo SPECT imaging	86
2.13 Clinical SPECT imaging protocol	87
2.14 Statistical analysis.....	89
Chapter 3: Myocardial Perfusion Imaging Prior To Renal Transplantation	91
3.1 Cardiovascular screening in end stage renal disease	92
3.1.1 Pharmacological interventions	92

3.1.2	Pre-operative cardiovascular screening guidelines	93
3.1.3	Clinical risk prediction tools.....	94
3.2	Diabetes and cardiovascular disease risk	95
3.2.1	Differences in cardiovascular disease in type 1 and type 2 DM.....	96
3.3	Myocardial perfusion imaging prior to non-cardiac surgery	97
3.4	Hypothesis.....	97
3.5	Methods.....	98
3.6	Ethical Approval	102
3.7	Statistical Analysis.....	102
3.8	Results.....	102
3.8.1	Cardiac Stress Testing.....	103
3.8.2	Scan results.....	103
3.8.3	Subsequent investigation	103
3.8.4	Renal transplantation.....	103
3.8.5	Mortality	107
3.8.6	Cardiovascular events.....	107
3.8.7	Factors associated with increased mortality	107
3.8.8	Factors associated with mortality and cardiovascular events	107
3.8.9	Mortality and CV event rates by MPI findings	107
3.8.10	Mortality and CV event rates by transplant suitability	108
3.8.11	Mortality and CV events by Sum Stress Score.....	108
3.9	Risk scores.....	110
3.9.1	Results.....	112
3.10	Discussion.....	117
3.11	Conclusion.....	119
	Chapter 4: Mitochondrial function in an experimental model of uraemia	121
4.1	Mitochondrial function in heart failure	122
4.2	Objectives	124
4.3	Hypothesis	125
4.4	Methods.....	125
4.5	Results	126
4.5.1	Model characterisation	126
4.5.2	Biochemical analysis	127
4.5.3	Assessment of cardiac function.....	129
4.5.4	Mitochondrial respiration.....	130

4.5.5 Mitochondrial enzyme activity.....	132
4.5.6 Respiratory complex assays.....	134
4.6 Discussion.....	137
4.7 Conclusion.....	140
Chapter 5: Technetium 99m Sestamibi Washout	141
5.1 Myocardial Perfusion Imaging.....	142
5.1.1 Technetium 99m sestamibi.....	142
5.1.2 Technetium washout.....	142
5.2 Objectives.....	144
5.3 Hypothesis.....	145
5.4 Methods.....	145
5.4.1 Developing an isolated perfusion system.....	145
5.4.2 Mitochondrial uncoupling.....	147
5.4.3 Phantom Studies.....	147
5.4.4 SPECT imaging of control hearts.....	148
5.4.5 In vivo SPECT imaging.....	151
5.4.6 Alternative methods of analysis.....	152
5.5 Results.....	152
5.5.1 Phantom studies.....	152
5.5.2 Washout data – ex vivo control hearts.....	152
5.5.3 Alternative method of measuring washout rate.....	154
5.5.4 Prolonged washout.....	155
5.5.5 Comparing washout rates with and without CCCP.....	157
5.5.6 In vivo Technetium SPECT washout studies.....	158
5.6 Discussion.....	161
5.6.1 Methods of analysis.....	163
5.7 Conclusion.....	164
Chapter 6: Early Technetium 99m sestamibi kinetics in clinical practice	165
6.1 Early Technetium kinetics.....	166
6.2 Objectives.....	166
6.3 Hypothesis.....	167
6.4 Methods.....	167
6.4 Results.....	168
6.5 Discussion.....	170
6.6 Conclusion.....	172

Chapter 7: Discussion and future work	173
7.1 Project findings.....	174
7.2 Limitations	175
7.2.1 Clinical Studies	175
7.2.2 Animal studies	176
7.3 Implications for clinical practice	177
7.4 Future pre-clinical studies	178
7.5 Future clinical work	179
7.5.1 Perhexilene	179
7.5.2 Sacubitril- Valsartan	179
References	181

List of figures

Figure 1.1 Glomerular Structure

Figure 1.2 Structure of the Nephron

Figure 1.3 Cellular anatomy of a cardiomyocyte

Figure 1.4 Mechanism of sarcomeric contraction

Figure 1.5 Mechanism of muscle contraction

Figure 1.6 Cellular effects of Norepinephrine

Figure 1.7 Frank Starling curve

Figure 1.8 Composition of Extracellular matrix

Figure 1.9 Definition of Normal Blood Pressure and Hypertension

Figure 1.10 Different types of Left Ventricular Hypertrophy

Figure 1.11 a) Normal ECG b) ECG with Left Ventricular Hypertrophy

Figure 1.12 2-Dimensional Transthoracic Echocardiogram view demonstrating measurement of LV dimensions.

Figure 1.13 Fatty acid oxidation pathway

Figure 1.14 Glycolysis pathway

Figure 1.15 Citric acid cycle

Figure 1.16 Electron transport chain

Figure 1.17 Chemical structure of Technetium 99m-sestamibi

Figure 1.18 Schematic of Technetium 99m decay

Figure 1.19 Relationship between myocardial blood flow and commonly used radiotracers

Figure 1.20 Example of a normal stress/rest myocardial perfusion study

Figure 1.21 Example of an abnormal myocardial perfusion scan

Figure 2.1 Figure 2.1 Schematic diagram of 5/6ths nephrectomy

Figure 2.2 Modified Langendorff perfusion rig

Figure 2.3 Isolated heart within perfusion rig

Figure 2.4 Example blood pressure trace for the assessment of cardiac contractility

Figure 2.5 Derived pressure trace to determine dp/dt_{max} and dp/dt_{min}

Figure 2.6 Example mitochondrial respiration traces

Figure 2.7 Standard lead position for a 12 lead Electrocardiogram

Figure 2.8 ECG complex showing waveforms and key wave durations

Figure 2.9 Annotated photograph of modified imaging cell

Figure 2.10 Annotated photograph of isolated perfused heart imaging system

Figure 3.1 Seventeen segment model

Figure 3.2 Study flowchart and patient outcomes

Figure 3.3 Survival curves for all-cause mortality by scan findings

Figure 3.4 Survival curves for all-cause mortality and CV events by scan findings

Figure 3.5 Mortality and CV events by transplant suitability

Figure 3.6 Survival curves of all-cause mortality and CV events by sum stress score

Figure 3.7 ROC analysis comparing ACDE score and a risk score incorporating ACDE score plus any reported abnormality on perfusion imaging for predicting cardiac events

Figure 3.8 ROC analysis comparing ACDE score and a risk score incorporating ACDE score plus any reported abnormality on perfusion imaging for predicting cardiac events

Figure 3.9 ROC analysis comparing ACDE score with a score incorporating ACDE plus a resting or stress perfusion defect >8 on sum score for predicting all-cause mortality

Figure 3.10 Kaplan Meier curves of all cause mortality stratified by ACDE score

Figure 3.11 Kaplan Meier curves of all cardiovascular events stratified by ACDE score

Figure 4.1 Principles of aortic banding

Figure 4.2 Timeline of events

Figure 4.3 Wet heart weights in both the uraemic and control arms

Figure 4.4 Serum urea levels at 12 weeks post nephrectomy or sham procedure in uraemic and control groups

Figure 4.5 Serum creatinine levels at 12 weeks post nephrectomy and their controls

Figure 4.6 *In vitro* left ventricular pressure recordings of 12 week uraemic and control rat hearts

Figure 4.7 *In vitro* derived rate of LV pressure change of 12 week uraemic and control rat hearts

Figure 4.8 –State 3 and 4 cardiac mitochondrial respiration states with the addition of complex 1 and complex 2 substrates

Figure 4.9 Respiratory control ratios with the addition complex I and II substrates

Figure 4.10 Citrate synthase and aconitase enzyme activity of isolated cardiac mitochondria comparing uraemic (n=4) and control (n=5) rats

Figure 4.11 Complex enzyme activity of isolated cardiac mitochondria comparing uraemic (n=4) and control (n=5) rats

Figure 5.1 Photograph of modified imaging cell

Figure 5.2 Photograph of isolated perfused heart system

Figure 5.3 Technetium washout protocol, isolated rat hearts

Figure 5.4 Technetium washout protocol, prolonged washout phase

Figure 5.5 Example planar SPECT image from isolated heart perfusion

Figure 5.6 Decay corrected counts in control hearts, addition of CCCP at 55 mins

Figure 5.7 Decay corrected counts/mm² in isolated control hearts, addition of CCCP at 55 minutes

Figure 5.8 Example washout curve demonstrating lines of best fit for calculation of washout rate

Figure 5.9 Washout curves of decay corrected counts with a prolonged washout phase

Figure 5.10 Washout curves of decay corrected counts/mm² with prolonged washout

Figure 5.11 Initial and late washout rates with and without the addition of CCCP

Figure 5.12 Technetium washout traces for *in vivo* SPECT imaging, control hearts

Figure 5.13 *In vivo* Technetium washout – standard uptake values

Figure 5.14 Peak intensity - *in vivo* controls

Figure 5.15 Ratio of peak cardiac to peak background counts - *in vivo* controls

Figure 5.16 Modal intensity - *in vivo* controls

Figure 5.17 Peak intensity to modal intensity - *in vivo* controls

Figure 6.1 Graph showing differences in washout rate according to sum stress score, age, and ejection fraction

Figure 6.2 Tracer washout curves from Liu et al, 2008

List of tables

Table 1.1 Differences in properties of Technetium and Thallium radiotracers

Table 2.2 Summary of major differences between animal and human SPECT imaging protocols

Table 3.1 Current guidelines for pre-operative assessment in kidney transplant candidates

Table 3.2 Components of Lee Index and NSQIPM MICA risk prediction tools

Table 3.3 Baseline characteristics according to transplant suitability

Table 3.4 Perfusion Imaging findings

Table 3.5 Risk scores assessed

Table 3.6 ROC areas for a range of risk scores for predicting all-cause mortality

Table 3.7 ROC areas for a range of risk scores for predicting all-cause mortality and CV events

Table 4.1 Comparing measures of left ventricular hypertrophy at 12 weeks post nephrectomy vs control

Table 4.2 Comparison of *in vitro* left ventricular pressure recordings, comparing 12 week old uraemic and control rat hearts

Table 4.3 Comparison of *in vitro* derived rate of LV pressure change, comparing 12 week old uraemic and control rat hearts

Table 4.4 State 3 and 4 respiration rates in the presence of glutamate/malate

Table 4.5 State 3 and 4 respiration rates in the presence of succinate/rotenone

Table 4.6 Citrate synthase activity in isolated mitochondria from uraemic and non-uraemic rat hearts

Table 4.7 Aconitase activity in isolated mitochondria from uraemic and non-uraemic rat hearts

Table 4.8 Respiratory complex I activity

Table 4.9 Respiratory complex II activity

Table 4.10 Complex II and III activity

Table 4.11 Complex IV activity

Table 5.1 Count Rates measured by SPECT using a range of Technetium activities within a phantom study

Table 5.2 Washout rates before and after the addition of CCCP

Table 5.3 Washout rates using line of best fit method

Table 5.4 Washout rate for prolonged washout studies

Table 5.5 Washout rate using line of best fit method for prolonged washout studies

Table 5.6 Calculated washout rate for in vivo control studies

Table 6.1 Technetium activity and washout rates, with decay correction

Table 6.2 Technetium activity and washout rates, without decay correction

Table 6.3 Comparing non-decay corrected washout rates, stratified by age, ejection fraction and sum stress score as binary outcomes

List of abbreviations

123 I BMIPP 123 Iodine Beta methyl-p-Iodophenyl-Pentadecanoic acid

AC Attenuation Correction

ACE Angiotensin converting enzyme

ACE- I Angiotensin converting enzyme inhibitor

ADP Adenine Diphosphate

ARB Angiotensin receptor blocker

ATP Adenosine tri-phosphate

BNIP Bcl2/adenovirus protein interacting protein

BNP Brain Natrietic peptide

BP Blood pressure

BSA Bovine serum albumin

CAD Coronary artery disease

CCCP Carbonyl cyanide m-chlorophenyl hydrazine

CKD Chronic kidney disease

COX Cytochrome oxidase

CPT-1 Carnitine Palmitoyltransferase 1

CT Computed tomography

CV Cardiovascular

DMSO Dimethyl sulfoxide

DNA Deoxyribonucleic acid

ECG Electrocardiogram

EF Ejection fraction

EGTA Ethylene glycol-bis tetra-acetic acid

ER Estrogen receptor

ESRD End stage renal disease

ETC Electron transport chain

FA Fatty acid

FAD Flavin Adenine Dinucleotide

FFA Free fatty acids

FMN Flavin mononucleotide

GFR Glomerular filtration rate

keV Kiloelectronvolt

LAO Left Anterior Oblique

LBBB Left bundle branch block

LV Left ventricle

LVEF Left ventricular ejection fraction

LVH Left ventricular hypertrophy

MCAD Medium chain co A dehydrogenase

METS Metabolic equivalents

MI Myocardial infarction

MPI Myocardial perfusion imaging

MRI Magnetic resonance imaging

mRNA Messenger Ribonucleic acid

NAC Non attenuation corrected

NAD Nicotinamide adenine dinucleotide

NMR Nuclear magnetic resonance

NO_x Nitric Oxide

NYHA New York Heart Association

PC Phosphocreatinine

PGC1 alpha Peroxisome gamma co-activator alpha

PPAR gamma Peroxisome proliferator- activated receptor gamma

RAS Renin angiotensin system

ROC Receiver Operator Curve

ROS Reactive oxygen species

SDS Sum difference score

SMS Sum motion score

SPECT Single positron emission computed tomography

SRS Sum stress score

SSS Sum stress score

Tc Technetium

TCA Tricarboxylic acid

TTE Transthoracic echocardiogram

UQ Ubiquinone

Acknowledgements

I am indebted to Dr Ann Tweddel, who contributed to the concept and design of the project, and provided me with support and guidance throughout. I am especially grateful for the funding provided, through the nuclear medicine department research fund, for the purchase of materials and consumables.

I am equally indebted to my co-supervisor, Dr Anne- Marie Seymour, who provided me with excellent support and guidance in the pre-clinical aspects of the project.

I am very grateful to Dr Chris Cawthorne for his knowledge, efforts and considerable time in helping to perform the SPECT/CT imaging studies, and assistance in image processing.

I am also grateful to Professor Sunil Bhandari for his support throughout the project, particularly in developing the clinical audit.

I wish to thank Mrs Kathleen Bulmer for her expert support with mitochondrial function assessment, particularly in enzymatic assays and Langendorff heart perfusions. I am also grateful to Ms Laura Goodlass and the animal welfare team for their expert animal care, and support during surgical procedures.

Thank you to Mr Manos Papadopoulos and Dr Graham Parker for their considerable support with clinical SPECT work. Mr Papadopoulos provided data from a trial that he performed, which I used to measure early and delayed Technetium washout in humans (Chapter 7).

I am extremely grateful to Dr Robert Atkinson who allowed me to use a modified rat imaging cell that he designed, which was used in the preclinical SPECT studies, as well as providing assistance with biochemical analysis of serum samples obtained from rats.

I am also extremely thankful to Faisal Nuhu, who also assisted in the biochemical analysis of serum samples from rats. Both he and Dr Atkinson were supported me as I developed skills in mitochondrial isolation, mitochondrial respiration and enzymatic analysis.

I am forever grateful to my parents, who have supported me throughout my education, and are central to all that I have achieved.

Finally I am indebted to my unimaginably patient and long-suffering wife, who has supported me immeasurably throughout the research project.

Declaration

I confirm that this work is original and that if any passage(s) or diagram(s) have been copied from academic papers, books, the internet or any other sources these are clearly identified by the use of quotation marks and the reference(s) is fully cited. I certify that, other than where indicated, this is my own work and does not breach the regulations of HYMS, the University of Hull or the University of York regarding plagiarism or academic conduct in examinations. I have read the HYMS Code of Practice on Academic Misconduct, and state that this piece of work is my own and does not contain any unacknowledged work from any other sources. I confirm that any patient information obtained to produce this piece of work has been appropriately anonymised

Chapter 1: Introduction

1.1 Renal physiology

The kidneys play an essential role in regulating both the volume and composition of fluids within the body. They act as a filtration system that removes surplus water, electrolytes including sodium and potassium, and waste products such as urea, to produce urine (Peterson, 2007). The kidneys also produce erythropoietin, essential for red blood cell formation; calcitriol, the active form of vitamin D that plays a key role in calcium and phosphate metabolism; and renin, a hormone that helps to regulate blood pressure and electrolyte balance (Vander, 1980).

1.1.1 Renal filtration

The kidneys receive approximately 20% of the total cardiac output, filtering 180 litres per day, and producing, on average, 1.5 litres of urine (Jacobson, 1981). A healthy kidney is composed of approximately 1 million functional units, known as nephrons. They receive blood via an afferent arteriole, which flows into a bed of intertwined capillaries termed the glomerulus. The capillary bed is surrounded a cup like structure, known as Bowman's capsule. They are lined with podocytes – specialised cells that allow the passage of fluid into the nephron, but prevent the movement of larger molecules, such as red blood cells and albumin (Figure 1.1). The rate of filtration through the glomeruli is dependent upon the hydrostatic pressure within the capillaries, as well as the pressure exerted by proteins within blood, known as the osmotic pressure (Cogan, 1991). The control of renal blood flow, and hence filtration is predominantly auto-regulated by the kidney through adjustments in resistance within arterioles. Extrinsic control of renal blood flow is mediated by the sympathetic nervous system through vasoconstriction.

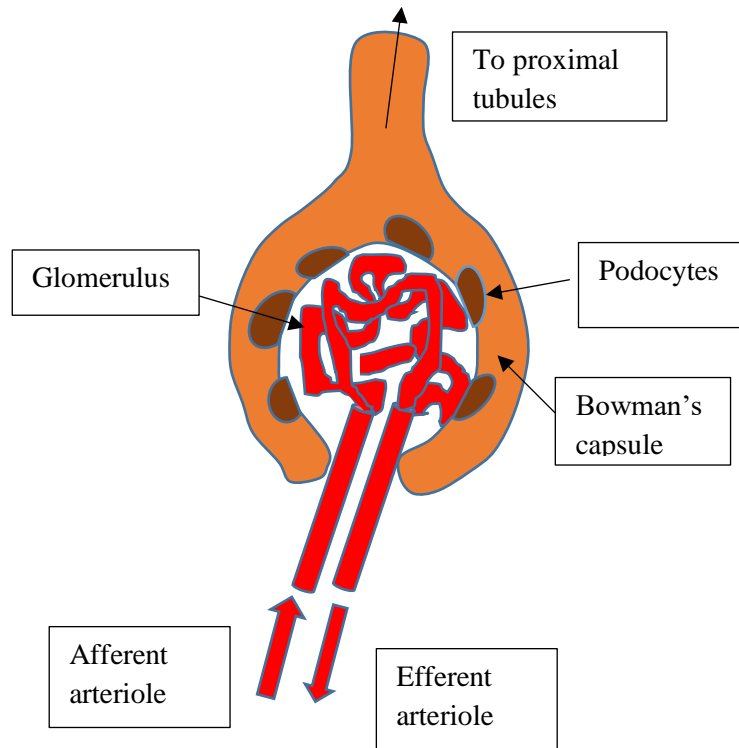


Figure 1.1 Glomerular structure

1.1.2 Tubular reabsorption

The filtrate that collects in Bowman's capsule passes into a series of tubules and collecting ducts. Blood that remains within the glomerular capillaries drain into efferent arterioles, into the peritubular capillaries which closely traverse the tubules and collecting ducts (Figure 1.2). This enables reabsorption of electrolytes and other molecules from the tubules back into the circulatory system (Peterson, 2007). This highly regulated process ensures the homeostasis of blood volume, acid/base balance, and osmolarity (concentration of ions within the blood). Reabsorption occurs via active and passive mechanisms. Passive diffusion describes the movement of substances from areas of high to low concentration. Active transport requires membrane bound pumps to transport substances across the epithelial cells (Knepper, 1987). These pumps, such as Na^+/K^+ ATPase pumps require energy, in the form of ATP to drive this transfer of molecules back into the capillaries.

The proximal tubules are lined with less tightly packed epithelial cells, which facilitates the reabsorption of glucose, amino acids, organic acids, phosphates and other solutes. Na^+/K^+ ATPase pumps transports sodium into the blood. This leads to co-transport of water and

chloride ions, as well as glucose and amino acids (Maddox et al, 2002). The proximal tubules lead to the loop of Henle, located deeper within the kidney, in the renal medulla. The descending limb allows passive transport of H₂O out of the tubules, but are relatively impermeable to salts, resulting in high ion concentrations (osmolarity) within the ducts. The ascending loops are highly permeable to NaCl, allowing active salt transport and thus a reduction in osmolarity. The peri-tubular capillaries are closely arranged in loops, which are adjacent to the loops of Henle. The Na⁺ concentration increases progressively from the superficial renal cortex to the renal medulla. This means that that the relative osmolarity in the ascending loops is higher than that in the descending loops, thus enabling passive diffusion from the ascending to descending loops. In contrast water diffuses in the opposite direction. This mechanism, known as counter-current exchange, helps to maintain a constant osmotic gradient whilst maintain high blood flow through the capillaries (Imai & Kokko, 1974).

Further adjustments to the solute content occur in the distal tubules, where reabsorption of Na, Cl and HCO₃ occurs. These drain into the collecting ducts, which are water permeable, and determine the final concentration of urine. The permeability of the ducts is controlled by anti-diuretic hormone (ADH), which acts via cyclic AMP and adenylate cyclase to activate channels known as aquaporins that enable water to diffuse from the ducts into the interstitial space (Nielsen, 1995).

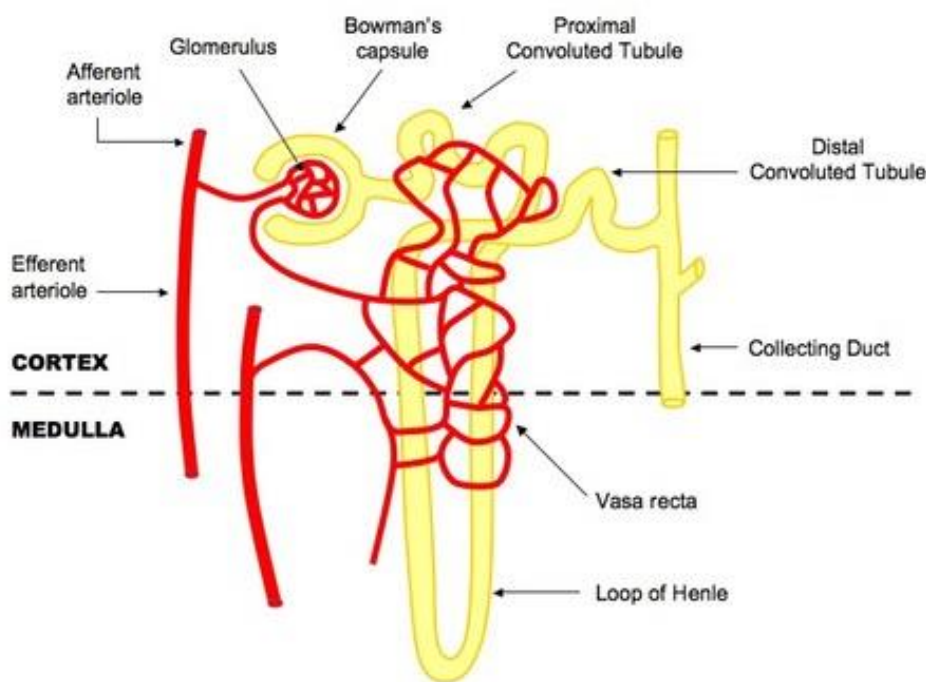


Figure 1.2 Structure of the Nephron Adapted from <https://pmgbiology.com/tag/nephron/>

Secretion

Secretion is the opposite process to reabsorption, whereby substances within the blood are transferred back into the tubular fluid in order to be excreted in the urine. This includes potassium, hydrogen, ammonium, and waste products such as urea and creatinine. Many pharmaceutical drugs are excreted, either wholly or partially, in the urine, through the process of secretion (Ullrich, 1993).

Transport of molecules occurs via both passive and active diffusion. Secretion of organic acids and bases, as well as hydrogen ions occurs in the proximal tubules. Ammonium, potassium and hydrogen ions are secreted in the distal tubules and collecting ducts (Pritchard, 1992).

Glomerular filtration rate

Glomerular filtration rate (GFR) is a method of measuring renal function in clinical practice, developed by Lubowitz *et al.* This is calculated using the formula;

$$\text{GFR} = \frac{UV}{P}$$

U = Concentration of solute in urine (ml/min) P = Concentration of solute in plasma

V = Volume of urine produced per minute

To select a substance to use for the measurement of GFR, it must be small enough to be freely filtered within the glomerulus; not be reabsorbed, secreted or metabolised within the kidney; non-toxic; and easily measurable in blood and urine. Inulin is a polysaccharide that fits these criteria. However, measurement requires a constant infusion to maintain a steady state plasma concentration (Hood *et al.*, 1971). In clinical practice, creatinine is used to measure eGFR, which is a breakdown product of creatine phosphate in muscle. There is a small amount of tubular secretion of creatinine, but measurement methods tend to overestimate the concentration in plasma, which offsets the amount secreted (Sjostrom *et al.*, 1988).

1.2 Cardiac physiology

1.2.1 Structure of the cardiomyocyte

Peterson et al describe the heart as ‘an electrically controlled and chemically driven mechanical pressure-suction pump’. It contains muscle cells, known as cardiomyocytes, which are responsible for co-ordinated contraction and relaxation. Cardiomyocytes are cylindrically shaped, and contain bundles of contractile proteins, known as myofibrils, which comprise 50-60% of total cell volume (Opie, 2005). Each myocyte is bound by a sarcolemma, which forms a complex tubular network in the extracellular space and transmits a wave of electrical excitation between cells. Cardiomyocytes have abundant mitochondria (23% of cell volume in adults), which provide energy in the form of ATP to supply the high demand required to maintain contractile function (Libby, 2008). The sarcoplasmic reticulum (SR) forms a fine network spreading throughout the myocytes. It plays a key role in controlling calcium release to initiate myocardial contraction, and reuptake to allow myocardial relaxation (Figure 1.3). Myocytes are held together by an extracellular matrix that predominantly contains collagen. They are arranged in an end-to-end formation and electrically coupled by protein channels, known as connexions (Tada & Katz, 1982).

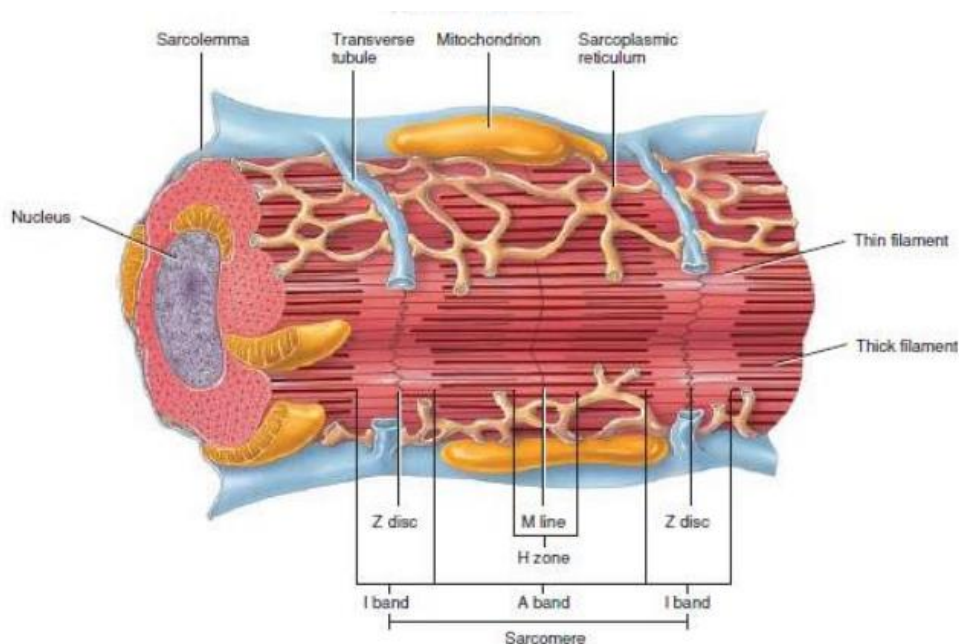


Figure 1.3 Cellular anatomy of a cardiomyocyte (Taken from Libby *et al*, 2008)

1.2.2 Myocardial contraction

Each contractile unit within a myofibril is known as a sarcomere. The principle contractile proteins within myofibrils are thin actin and thick myosin filaments. In its relaxed state, actin and myosin interaction is inhibited by tropomyosin on the actin chain. Calcium binding with troponin C produces a conformational change of troponin I, which shifts the position of the inhibitory tropomyosin molecule, and allows coupling of actin and myosin (Rayment et al, 1993). Myosin filaments contain a series of myosin heads, each formed by the terminal ends of a myosin heavy chain and myosin light chain, with two ATP binding sites. ATP produces a conformational change in the myosin head to detach actin from a myosin head. ATPase splits ATP into ADP and Pi, flexing the myosin head and levering the actin molecule to bind with the next myosin head (Figure 1.4). Actin is attached to the ends of the sarcomere, known as Z-lines. As the actin filaments slide over the myosin heads, the sarcomere shortens and thickens, leading to myocardial contraction (Figure 1.5). Titin is a very large elastic protein that tethers myosin to the Z-line to provide stability. Increase in cardiac volume and pressure lead to greater stretch of the titin molecules, resulting in more forceful contraction (Knoll et al, 2002).

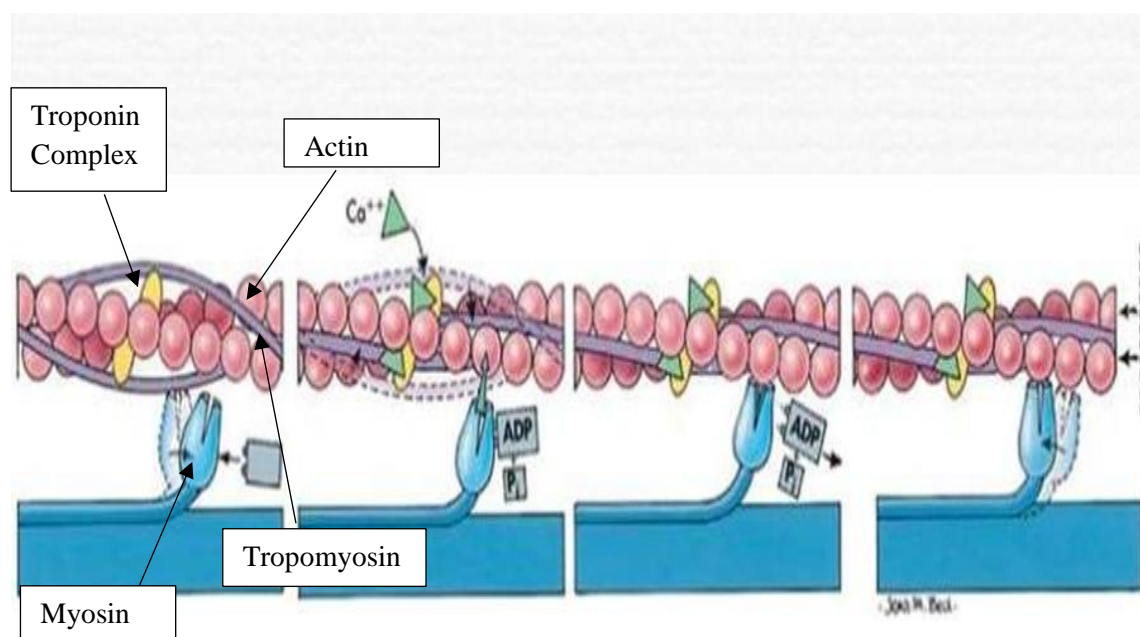


Figure 1.4 Mechanism of sarcomeric contraction From Thibodeau GA, Patton KT 1999. Calcium binds with Troponin complex to release Tropomyosin and allow actin-myosin binding. ATP binding enables detachment of the myosin head, leverage of the actin filament to bind with the next actin filament.

1.2.3 Cardiac excitation contraction coupling

As described above, calcium binding is essential to initiate myocardial contraction. A relatively small amount of calcium enters the cardiomyocyte with each contraction, but this triggers a much larger release of calcium from the SR (calcium-induced calcium release). A wave of electrical depolarisation travels down the T-tubules, which triggers the opening of L-type calcium channels, to allow calcium influx into the cytosol. These channels are located in close proximity to the SR. Ryanodine receptors located on the SR are activated by the trigger calcium, opening calcium release channels, and enabling a large flux of calcium from the SR to cytosol (Wehrens et al, 2004). As the electrical excitation wave passes, cytosolic calcium entry ceases, and switches off calcium release from the SR. Calcium that entered the cytosol from the extracellular space is extruded from the cell via sodium/calcium exchange pumps. Re-uptake of calcium back into the SR is controlled by the Sarco Endoplasmic Reticulum Calcium ATPase (SERCA) pump. This large protein constitutes 90% of the protein content of the SR. For each mole of ATP consumed, 2 calcium ions are taken up by the SR (Peterson, 2007).

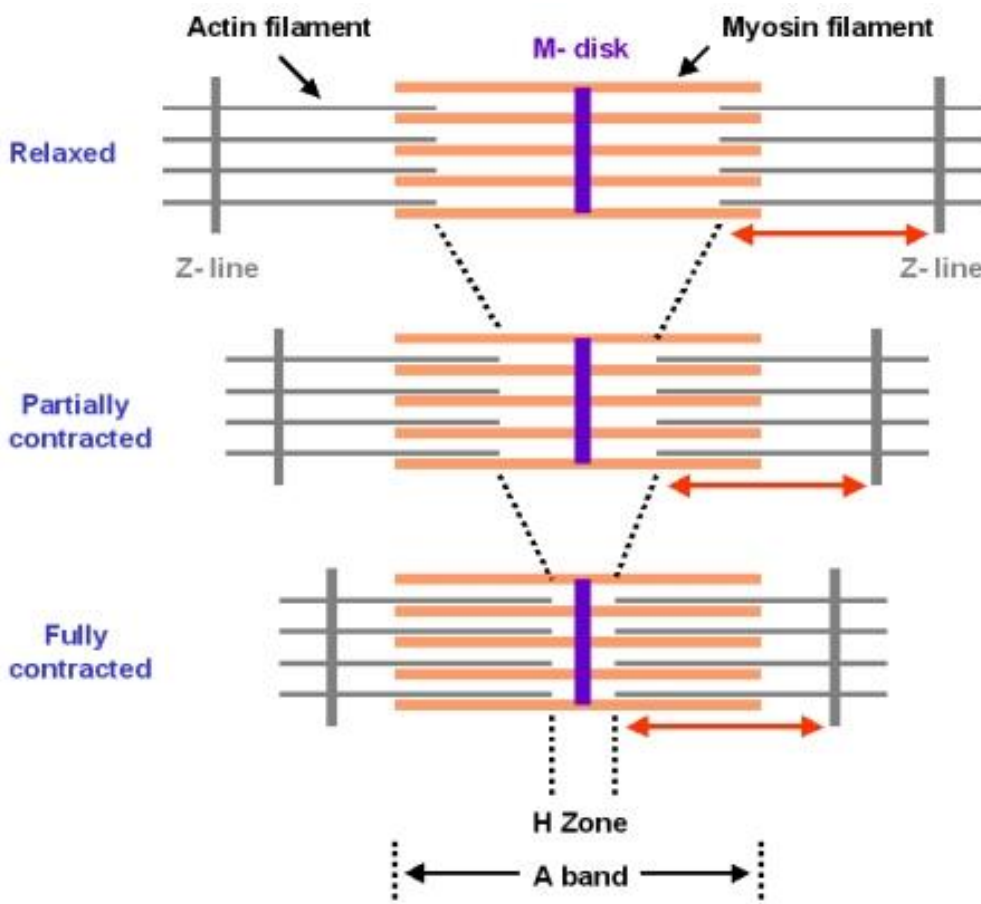


Figure 1.5 Mechanism of muscle contraction Adapted from M. Blaber, 2001.

1.2.4 Adrenergic signalling

In a steady state, the amount of calcium released into the cytosol during contraction equals that removed during the relaxation phase. This can be altered by a number of neurohormonal signalling systems, most importantly the beta adrenergic system. Stress and exercise increases the number of adrenergic impulses. This leads to increased norepinephrine (NE) granule release from the synaptic clefts. Beta-adrenergic receptors located on the cell membranes of cardiomyocytes are stimulated in response to elevated NE levels. Beta 1 subtypes are the predominant receptor within cardiomyocytes, with a smaller proportion of beta 2 receptors (Opie, 2004). Beta stimulation leads to activation of a cascade of secondary messenger G – proteins. Ultimately this leads to the formation of cyclic adenosine monophosphate (cyclic AMP), activation of protein kinase A, and phosphorylation of a key sarcolemmal protein p27. This leads to increased influx of extracellular calcium through L-type calcium channels, greater calcium release from the SR, and increased rate and force of the resulting myocyte contraction (Figure 1.6). Protein Kinase A phosphorylation of phospholamdan enables greater calcium reuptake via SERCA, thereby enhancing myocyte relaxation in parallel (Peterson, 2007).

Parasympathetic nervous system stimulation produces the opposite effect on myocardial contractility. Acetylcholine release from the vagal nerves activates M2 muscarinic receptors on the cardiomyocyte cell membrane. This activates inhibitory G proteins (Gi), which subsequently stimulates the second messenger cyclic GMP, and consequently protein kinase G. This inhibits calcium entry within the cell, leading to a reduction in rate and force of myocardial contraction. Protein kinase G also directly inhibits stimulatory G- protein activation, further limiting the stimulatory beta adrenergic effects (Floras, 2003).

1.2.5 Effect of loading conditions on contractility

The force of cardiac contractility can also be modulated by the degree of stretch within the cardiac muscle, independent of changes in cytosolic calcium levels. This was initially described by Otto Frank through experiments on isolated frog hearts. Starling and colleagues demonstrated that increasing venous

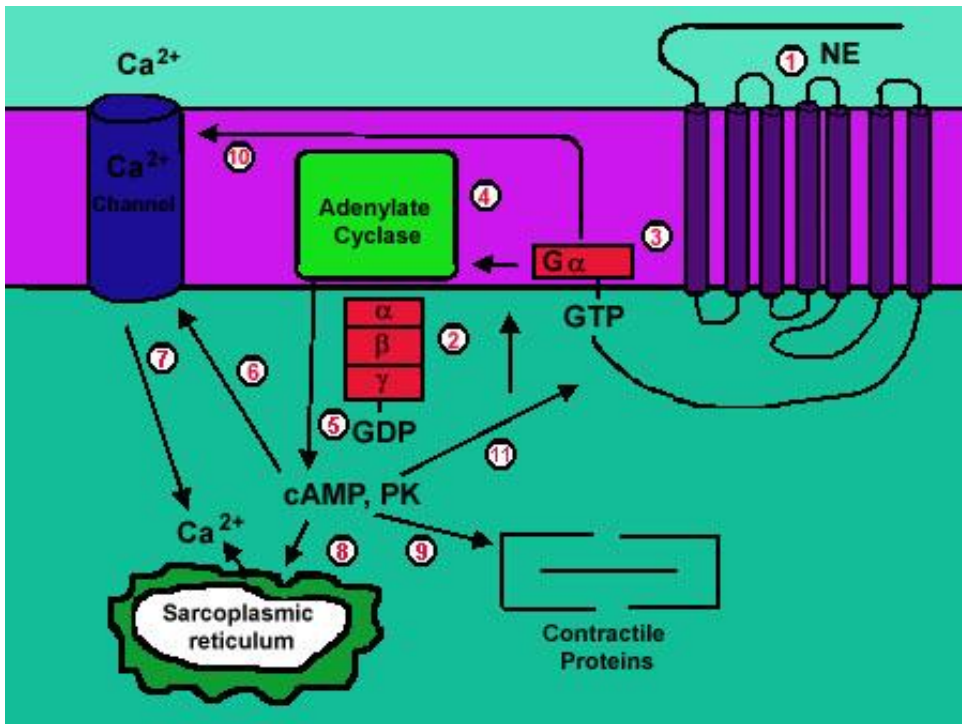


Figure 1.6 Cellular effects of norepinephrine. NE-Norepinephrine, GTP-Guanosine triphosphate, cAMP- cyclic Adenosine Monophosphate, PK-Protein Kinase, GDP-Guanosine diphosphate. Taken from Piascik, 2008.

return leads to a rise in end-diastolic pressure within the left ventricle (Sequeira *et al*, 2005). This results in increased cardiac contractility, as evidenced by an increase in stroke volume - the amount of blood ejected from the ventricle with each beat. The ability of the heart to alter its force of contraction in response to changes in venous return, or preload, is known as the Frank-Starling mechanism.

Frank-Starling curves demonstrate the effect of rising LV end diastolic pressure on stroke volume. These curves are altered by the adrenergic effects on cardiac contractility (inotropy), and afterload. The latter is defined as the pressure that the heart must overcome to eject blood in systole. Afterload is affected by blood pressure within the systemic circulation, as well as conditions such as aortic stenosis, in which there is a reduction in the degree of aortic valve opening. As afterload rises, there is a shift in the Frank-Starling curve, such that for a given increase in LVEDP, there is a lesser increase in the stroke volume. Conversely, increased inotropy leads to a greater rise in stroke volume for a given rise in LVEDP (Figure 1.7).

A postulated mechanism for the Frank-Starling phenomenon is that increased stretching of the sarcomeres leads to a greater calcium affinity to Troponin C. Enhanced calcium binding leads to removal of the inhibitory effect of tropomyosin on actin/myosin binding. This means that at a given calcium concentration, there is earlier activation and greater force of contraction

(Libby *et al*, 2008). Myocardial stretch may increase cross bridging between neighbouring troponin C/tropomyosin complexes. These linkages may allow calcium induced activation of one actin chain to produce conformational changes in other tropomyosin complexes, thus directly affecting actin/myosin binding at other sites. This augmented response may explain why a 5% increase in sarcomere length can lead to a 2-3 fold increase in cardiac force contractility (Peterson, 2007).

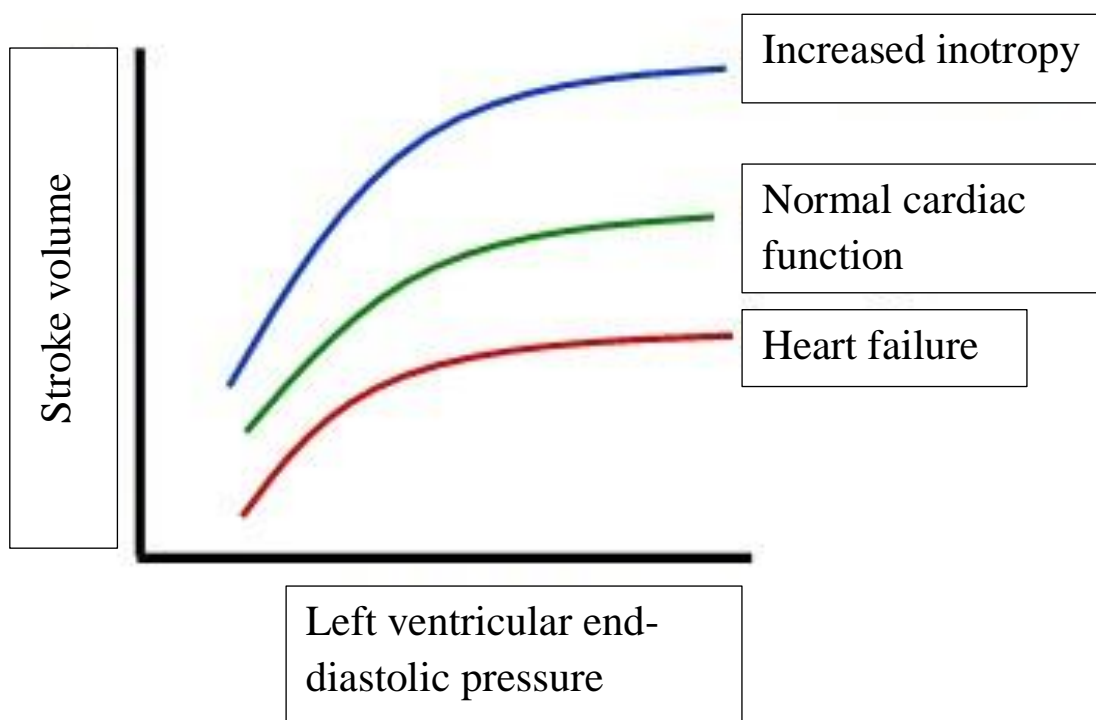


Figure 1.7 Frank Starling Curve Heart failure leads to a less pronounced increase in stroke volume for a given rise in left ventricular end-diastolic pressure. Conversely, increased inotropy leads to a greater increase in stroke volume.

1.2.6 Extracellular matrix

Cardiomyocytes and cellular components of the myocardium cellular components of the myocardium are surrounded by an extracellular matrix. It enables coordinated contraction of myocardial tissue. The fluid component of the extracellular space provided stores a wide variety of soluble proteins and other molecules related to many cardiac processes. It also plays a crucial role in accumulating water, which provides excellent resistance to compression (Libby, 2008). The organization, composition and density of the matrix and the extracellular

space are dynamic not only in pathological conditions, but also under normal conditions. These three properties are in a constant change in response to different demands, and they all have an impact on the function of the myocardium (Baudino, 2006).

The extracellular space can be divided into three components. The basement membrane is a specialized structure that underlies all cellular layers of tissue. Its close relationship with cells is critical as it provides tissues with mechanical stability as well as signals that determine cellular polarity and migration. In the heart, its main constituents at the protein level are laminins, collagens IV, XV and XVIII, perlecan, agrin and nidogens 1 and 2 (van Agtmael, 2010; LeBleu, 2007; Iozzo, 2009).

The interstitial matrix contributes to the mechanical properties of the tissue. It appears physically anchored to the basement membrane but forms a different functional unit that, in addition to providing mechanical resistance and structural support to the myocardium, provides the extracellular compartment through which signals and nutrients are distributed and the fibroblasts migrate. In the heart, its main components are collagens I, III, VI and XII, proteoglycans and the matricellular proteins that appear associated with the previous components (Harvey, 1999) (Figure 1.8). Extracellular fluid surrounds all the cellular and extracellular structures of a tissue. It contains the elements necessary for cellular functioning and viability such as ions (Na^+ , K^+ , Ca^{2+} , Cl^- and HCO_3^-), glucose and other sugars, amino acids, fatty acids, neurotransmitters, hormones and growth factors, cytokines and other proteins. These elements are secreted from blood plasma, in a process of continuous exchange with the extracellular fluid by capillary endothelial filtration. The secretory and waste products of the cells exert important roles in the autocrine and paracrine regulation and are drained into the circulation through the lymphatic system (Mow, 1999)

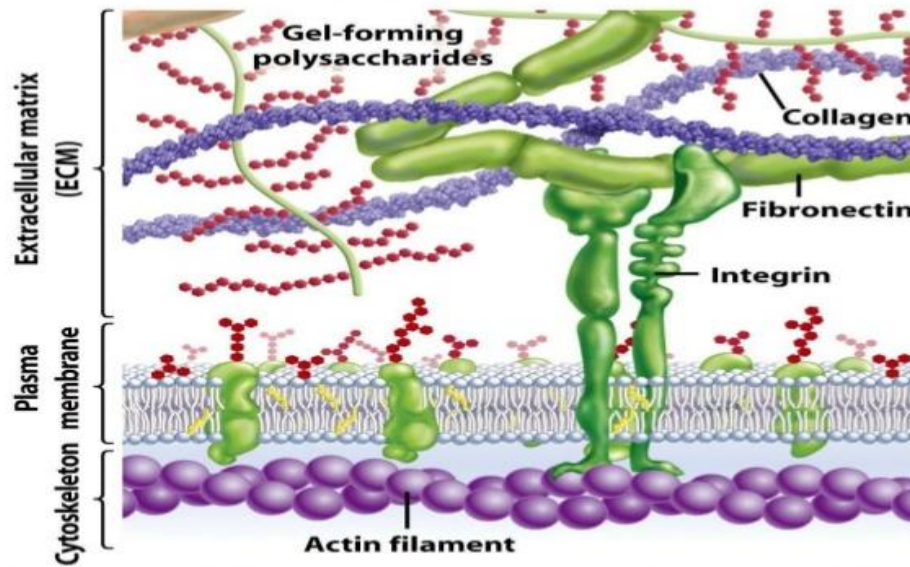


Figure 1.8 Composition of the extracellular matrix From Prof M A Shaheen Open Access image <https://www.slideshare.net/ahmedaamer986/barrier-function-biomechanical-properties-of-the-skin>

1.3 Blood pressure

Blood pressure is the force exerted by circulating blood on the walls of arteries. The first blood pressure measurements were performed by Hales in 1733, who inserted fine tubes in the carotid arteries of horses, and measured the height of blood in the column (Lewis, 1994). Scipione Riva-Rocci invented the sphygmomanometer, a non-invasive method of blood pressure measurement (Booth, 1977). This consists of an inflatable cuff attached to a pressure gauge. The cuff is typically positioned on the upper arm, at the level of the heart, and a stethoscope is placed on the brachial artery. The cuff is inflated to above arterial pressures, and slowly deflated. The pressure at which the pulsatile sounds can be heard with the stethoscope is the systolic pressure. The pressure at which the sounds disappear completely is the diastolic pressure. Systolic blood pressure represents the force exerted on blood vessels at the heart ejects blood (systole), whereas diastolic pressure measures the force exerted whilst the heart relaxes and the aortic valve is closed (diastole). Blood pressure is conventionally measured in millimetres of mercury (mmHg), as this has been formally validated to invasively measure arterial pressures. One millimetre of mercury pressure is defined as the force exerted on a 1 millimetre high column of mercury with a density of 13595.1kg/m^3 when gravitational

acceleration is 9.80655m/s^2 . One millimetre mercury is $1/760$ of standard atmospheric pressure (British Standards, 1974).

High blood pressure, or hypertension, is associated with an increased risk of cardiovascular events (stroke, coronary artery disease, peripheral vascular disease), and kidney disease (Lewington, 2002). Defining a ‘normal’ blood pressure is challenging, as there is a continuous relationship between high blood pressure and cardiovascular disease from systolic pressures as low as 115mmHg in adults. From a pragmatic viewpoint, high blood pressure is defined as the level at which the benefits of treatment outweigh the risks. The ESC 2018 guidelines for the management of hypertension define hypertension as a systolic blood pressure greater than 140, and/or a diastolic blood pressure of greater than 90 (Williams, 2018). Figure 1.9 shows the definition of normal blood pressure, and grades of hypertension.

Category	Systolic		Diastolic
Optimal	<120	and	<80
Normal	120–129	and/or	80–84
High normal	130–139	and/or	85–89
Grade 1 hypertension	140–159	and/or	90–99
Grade 2 hypertension	160–179	and/or	100–109
Grade 3 hypertension	≥ 180	and/or	≥ 110
Isolated systolic hypertension	≥ 140	and	<90

Figure 1.9 Definition of normal blood pressure and hypertension ESC 2018 Guidelines on the management of systemic arterial hypertension.

Blood pressure should be measured 3 times whilst seated, 1-2 minutes apart, with the average of the last two readings used as the final measurement. There is significant within-person variability in blood pressure throughout the day, and depending on stress levels, physical activity etc. Ambulatory home blood pressure monitors, which can perform repeated measurements over a 24 hour period, typically provide lower readings than those measured in clinic, and are more reproducible (Bliziotis, 2012). The overall prevalence of hypertension in adults is 30-45%, which rises to >60% in those aged >60 (Chow *et al*, 2012). The prevalence is expected to rise by 15-20% over the next 10 years, due to an aging population, and increasingly sedentary lifestyles (Kearney *et al*, 2005). Hypertension is the leading

contributor to premature mortality, responsible for 4.9 million deaths due to ischaemic heart disease, and 3.5 million deaths due to stroke worldwide (Forouzanfar *et al* 2017). Diastolic hypertension is risk factor particularly in middle aged patients. Diastolic BP tends to fall in later life due to increasing arterial stiffness (Franklin *et al*, 1999).

1.4 Hypotension

Hypotension is low blood pressure, typically defined as a systolic BP <90mmHg, and diastolic BP <60mmHg. Whereas hypertension is a recognised disease, hypotension is typically considered a physiological state (Braunwald, 2005). There are multiple causes, including vasodilating medications, dehydration, infection, blood loss, cardiac failure. Healthy young people, and those with chronic conditions such as heart failure may have hypotension without any symptoms, due to physiological adaptations to low BP (Parwani, 2012). A sudden reduction in BP can result in reduced organ perfusion, leading to light headedness, confusion, impaired kidney and liver function, and circulatory collapse in severe cases. Treatment focuses on identification and correction of the underlying cause, replacement of blood and fluid, and medications that cause arterial vasoconstriction (vasopressors) and increased cardiac contractility (inotropes) in severe cases (Worthley, 2000).

1.5 Uraemic Cardiomyopathy

Uraemic cardiomyopathy, or type 4 cardiorenal syndrome, is broadly defined as any structural cardiac abnormality affecting patients with chronic kidney disease (Ronco *et al* 2008). Magnetic resonance imaging studies have shown that the most common abnormality is left ventricular hypertrophy (LVH) followed by left ventricular dilation, and systolic dysfunction (Parfrey *et al* 1996). These three morphological abnormalities may be viewed as a continuum of progressive cardiac impairment, although dilation and systolic dysfunction may also be a consequence of other conditions such as ischaemic and valvular heart disease. We typically view uraemic cardiomyopathy as the presence of left ventricular hypertrophy, in association with impaired diastolic function, changes within the extracellular matrix, and an altered response to myocardial insult (Alhaj 2013).

1.6 Left Ventricular Hypertrophy

Left ventricular hypertrophy is defined as a demonstrable increase in LV muscle mass. In adults, growth of the heart is usually closely matched to its functional load and, under normal circumstances, is mainly constitutive in nature. In response to changes in functional load, the heart triggers a hypertrophic response to counterbalance the increase in wall stress (Opie *et al*, 2006). This hypertrophic response can broadly be classified as either physiological or pathological.

Pathological hypertrophy can be induced by pressure overload, from conditions including systemic arterial hypertension and aortic stenosis. It can also be triggered by conditions leading to volume overload, such as valvular heart disease or primary cardiomyopathies (Zac, 1984). Physiological hypertrophy is induced by physical training. Endurance activities, such as long distance running or swimming leads to a volume loading. Explosive, power based activities such as weight-lifting leads to pressure loading of the left ventricle (Scharag *et al*, 2006). Both pathological and physiological forms lead to cardiac hypertrophy - an increase in myocyte volume, as well as hyperplasia with formation of new sarcomeres and an increase in cell DNA content. The pathological form also leads to interstitial fibrosis, myocyte necrosis, and ultimately a reduction in cardiac function (McMullen & Jennings, 2007). The changes seen in pathological forms of LVH are largely irreversible, whereas in the setting of physiological hypertrophy, detraining leads to a reversal of the phenotypical changes (Pelliccia *et al*, 2002).

A pathological stimulus causing pressure overload produces an increase in systolic wall stress that results in concentric hypertrophy – LV wall thickening with a reduction in cavity size (Figure 1.10). In contrast, a pathological stimulus causing volume overload produces an increase in diastolic wall stress and results in eccentric hypertrophy – a dilated LV cavity with relatively thin walls (Grossman *et al*, 1975).

Pathological hypertrophy is accompanied expansion of the extracellular matrix. Matrix metalloproteinases 1, 3 and 9 stimulate fibroblasts to produce type I and type III collagen (Karthikeyan & Lip, 2006). This leads to the clinical finding of myocardial fibrosis, which initially affects the sub-endocardial layer. This results in reduced compliance of the myocardium, resulting in a ‘stiff’ heart which affects diastolic ventricular filling. Whilst systolic function is initially preserved, there is a reduction in longitudinal function and a

reduction in torsion – the rotational movement of the apex of the heart that contributes to left ventricular emptying (Aurigemma *et al*, 2006).

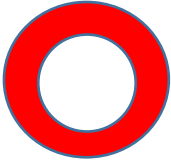
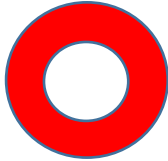
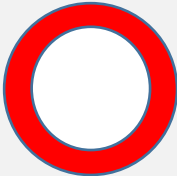
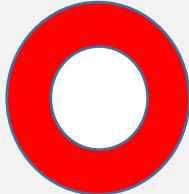
		Relative wall thickness	
		Normal	Increased
Left Ventricular Mass	Normal	Normal 	Concentric remodelling 
	Increased	Eccentric hypertrophy 	Concentric hypertrophy 

Figure 1.10 Different types of left ventricular hypertrophy

Changes in the titin protein isoforms also contribute to the increased LV stiffness. As described earlier, titin is a key protein regulating passive sarcomeric tension and elasticity. Shortened isoforms lead to an increase in passive tension for a given load, and thus a reduction in elasticity (van Heerebeek *et al*, 2006). The additional collagen deposition also affects electrical signalling within the left ventricle, leading to a loss of synchrony of myocardial contraction (Brower *et al*, 2006). In advanced disease processes, the compensated form of hypertrophy progresses to a decompensated form, where there is impairment of systolic function, and frequently signs of overt heart failure (Hein *et al*, 2003).

1.6.1 Diagnosis of LVH

Establishing a ‘normal range’ of LV mass has been challenging for pathologists, as it is strongly influenced by a person’s size, gender, age, and level of physical activity. A total heart weight above 500 grams has often been used for diagnosis (as LV weight correlates

closely with total heart weight), however this may be normal for larger subjects (Lorell and Carabello 2000). A number of methods can be used to diagnose LVH *in vivo*.

Electrocardiographic criteria are a specific but insensitive marker. The commonly used Sokolow-Lyon criteria have been shown to have a sensitivity of 22%, and specificity of 79% (Cabezas *et al* 1997). This is calculated using the formula;

Amplitude of S wave in lead V1 + amplitude of R wave in V5 or V6 (whichever is greater).

Left ventricular hypertrophy is defined as a value greater than 35mm (see Figure 1.11).

Transthoracic echocardiography (TTE) is the most widely used imaging technique for the detection of LVH. The normal thickness of the inter-ventricular septum and posterior wall is 6- 10mm (see figure 1.12). The normal range is affected by a number of factors – greater LV wall thickness is seen in men, people of Afro- Caribbean ethnicity, higher body surface area, and trained athletes. Calculating left ventricular mass is a more reliable measure of LVH. It can be estimated by measuring wall thicknesses using either M-mode or 2 D echocardiography. The Devereux formula for estimating LV mass, shown below, correlates closely with LV weight at autopsy (Devereux, 1986)

$$\text{LV mass (grams)} = 0.8 \times (1.04((\text{IVSd} + \text{LVIDd} + \text{PWTd})^3 - \text{LVID}^3) - 13.6\text{g}$$

IVSd – Interventricular septal diameter in diastole, LVIDd – Left ventricle internal diameter in diastole, PWTd – Posterior wall thickness diameter in diastole.

LVH by this method is defined as an LV mass (indexed for body surface area) of 125g/m² in men, and 110g/m² in women (Alhaj *et al* 2013). Studies have shown that indexing for body surface area significantly underestimates LVH prevalence in obese patients, and indexing for height is more useful clinically and scientifically. Relative wall thickness is another important echocardiographic measure, providing complementary information on the mode of cardiac remodelling (Foppa *et al*, 2005). This is calculated using the following formula;

$$\text{Relative wall thickness} = (2 \times \text{PWT}) / \text{LVID}$$

PWT - Posterior wall thickness

LVID – Left ventricle internal diameter

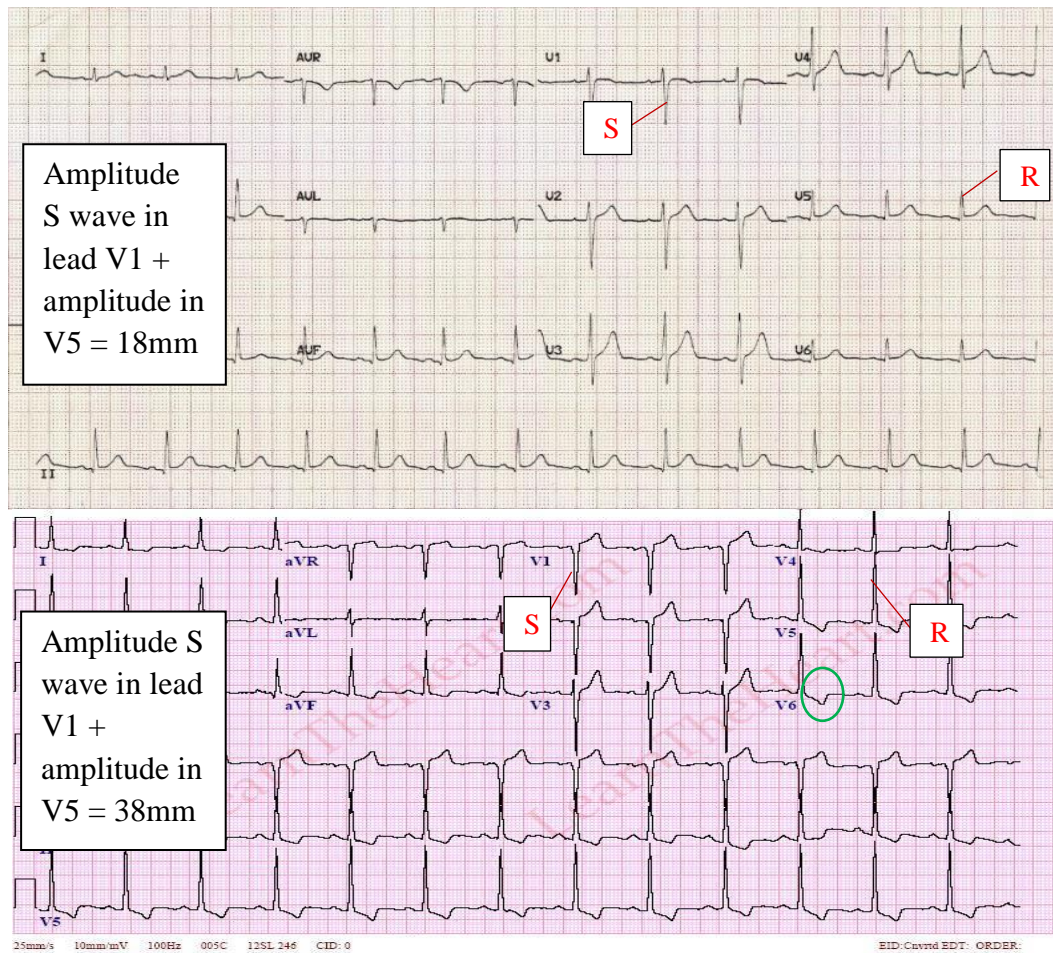


Figure 1.11 a) A normal ECG and b) ECG with changes associated with LVH The lower ECG demonstrates increased height of S wave in V1 and R wave in V5 (red lines). There is also depression of the ST segment and inversion of T waves in the chest leads (green circle) due to prolonged depolarisation, also known as ‘LVH strain’ pattern.

Values greater than 0.45 indicate concentric hypertrophy, defined as an increase in LV wall thickness with a normal or reduced LV volume, in contrast to eccentric hypertrophy, where there is a proportional increase in wall thickness and chamber size. Concentric hypertrophy occurs in pressure overloaded hearts, whereas eccentric hypertrophy develops in response to volume overload (see Figure 1.10).

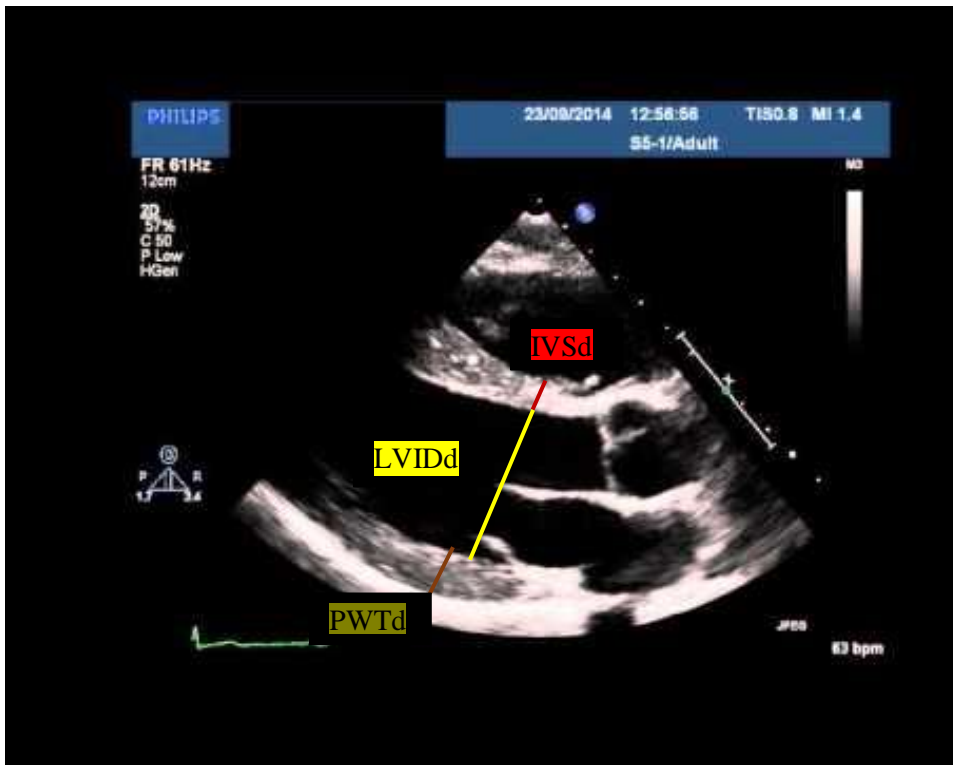


Figure 1.12 Two- Dimensional transthoracic echocardiogram view demonstrating measurement of LV dimensions IVSd – Interventricular septum in diastole, LVIDd – Left ventricular internal diameter in diastole, PWTd – Posterior Wall Thickness in diastole

Echocardiographic studies of patients with CKD reveal that both forms of hypertrophy are common, reflecting the fact that both volume and pressure overload contribute to the remodelling process (Nardi *et al* 2009). Echocardiography is limited by poor image quality due to suboptimal acoustic windows in up to 25% of patients (Fernando 2007). The calculations are also based on the assumption of normal LV geometry, and may be inaccurate in patients with prior myocardial infarction. MRI largely overcomes these issues due to its improved spatial resolution and 3- dimensional volumetric analysis methods, and is now considered the gold standard for LV mass quantification. Studies have shown close correlation between MRI derived LV mass measurements and post-mortem weights (Armstrong *et al* 2012).

1.6.2 Cellular level changes in LVH

A number of changes in myocyte morphology been demonstrated in LVH. In animal models of cardiac hypertrophy, there is an increase in myocardial mass proportional to the increase in myocyte size. An increase in cell width is seen in pressure overloaded rat heart models, due to

the addition of myofibrils, leading to the concentric LVH phenotype (Sheridan *et al* 1998). In contrast, chronic volume overload results in a predominant increase in myocyte length, which results in an increased ventricular circumference (Frey, 2003). It was previously believed that cardiac hypertrophy consists of hypertrophy of cardiomyocytes and hyperplasia of other cell types in the heart, such as fibroblasts. In recent years the discovery of cardiac stem cells and the finding that cardiomyocytes have capacity to proliferate challenged that concept and raised significant interest in investigating the molecular mechanisms of myocyte hyperplasia. Increased expression of the transcription factors G1 cyclin and cyclin D in response to hypertrophic stimuli, suggesting that cardiomyocytes can re-enter the cell cycle, leading to myocyte proliferation (Li *et al*, 1998). The transcription factor Myc is a regulator of cell growth and differentiation. Transgenic mice overexpressing Myc displayed hypertrophic growth through proliferation of adult cardiac myocytes (Xiaou *et al*, 2001). Conversely, Myc deficient mice have an attenuated hypertrophic response to pressure overload stimuli (Zhong *et al*, 2005).

1.6.3 LVH and Renal Failure

LVH is frequently detected by echocardiography in renal failure patients. It is found in 10-40% of all CKD patients, and in 70-90% of those with end stage renal failure (Griffiths 2003). Independent predictors of LVH in CKD include declining glomerular filtration rate (GFR), ambulatory systolic and diastolic blood pressure, and anaemia (Peterson 2007). Concentric LVH is the more common form of remodelling, and becomes increasingly common in ESRD patients. Approximately 20% of patients exhibit a mixed form of remodelling. LVH is an important, independent determinant of survival in ESRD, conferring a 2.9 times increased relative risk of all-cause mortality and 2.7 times increased risk of cardiac mortality (Silberberg *et al*, 1989) Furthermore, regression of LVH through treatment with ACE inhibitors has been shown to improve prognosis over and above what would be expected from the BP reduction effect alone (Mathew *et al*, 2001).

1.6.4 Pathophysiology of LVH

Pressure overload

Hypertension and CKD have a bidirectional relationship. Essential hypertension is the principle cause of ESRD in 26% of Caucasians and 46% of black patients (Hsu *et al* 2005).

Systemic hypertension leads to glomerular hypertension, hyperfiltration, and glomerular sclerosis. Once renal dysfunction is established, hypervolaemia as a result of sodium and water retention, and reduced arterial compliance cause further blood pressure elevation, and progressive renal damage. Renin-angiotensin system (RAS) hyperactivity is seen commonly in patients with hypertension and renal failure, and is a trigger for the development of LVH (Santos *et al* 2012). Angiotensin II and aldosterone induce cardiac myocyte hypertrophy and hyperplasia through the activation of Src family tyrosine kinases. Furthermore, administration of ACE inhibitors and angiotensin receptor blockers lead to regression of LVH in a blood pressure independent manner. Increased cardiac afterload also leads to an increase in sympathetic activity, which stimulates cardiac hypertrophy through activation of alpha 1 adrenoceptors (Zimmer *et al.* 1995). Although this has been shown to produce a marked LVH response in experimental studies, conditions that produce catecholamine excess in humans e.g. pheochromocytoma do not appear to lead to significant hypertrophy (Shub *et al* 1986).

Volume overload

Fluid retention associated with end stage renal disease leads to a significant increase in intramyocardial blood volume. MRI studies demonstrate an average reduction in end-diastolic volume of 20% following dialysis (Hunold *et al.*, 2003). Arterio-venous fistulae and anaemia also contribute to the increased circulating blood volume. Upon mechanical strain, stretch-activated channels are activated rapidly and lead to increased ion transients, which result in rapid alterations of cardiac electrical activity (McCain & Parker, 2011). There is an influx of Na^+ and Ca^{2+} ions, through Na^+/H^+ exchanger and Ca^{2+} -channels, respectively, into the intracellular space. Elevated intracellular Na^+ levels can lead to a further increase of intracellular Ca^{2+} through $\text{Na}^+-\text{Ca}^{2+}$ exchange. Subsequently the additional Ca^{2+} -triggered Ca^{2+} release from the sarcoplasmic reticulum then leads to an increase in cardiomyocyte contractility (Frank & Frey, 2011). In cardiomyocytes, activation has been shown to result in membrane depolarization, and to increase action potential duration. It also activates secondary signalling pathways by activating kinases such as calmodulin-dependent protein kinases or protein kinase C. The Ca^{2+} -binding protein calmodulin has emerged as an important regulator of cardiomyocyte hypertrophy, as overexpression of CaM resulted in the development of cardiomyocyte hypertrophy (Paluch 2015, Ross 2004).

Fibrosis

Myocardial fibrosis is defined as an increase in the collagen volume fraction of myocardial tissue. It is associated with worsening ventricular systolic function, increased ventricular stiffness, and is a risk factor for sudden death (Gross and Ritz, 2008).

Uraemia induces a reactive fibrosis, in which interstitial fibroblasts are activated, initially in the perivascular space, progressing to diffuse involvement of the interstitium.

Hyperaldosteronism has been postulated as a trigger for enhanced collagen synthesis, which is supported by the identification of aldosterone receptors on cardiac fibroblasts (Brown 2013). Furthermore, the use of ACE inhibitors has been shown to limit fibrosis in experimental uraemia models (Gross *et al*, 2004). Parathyroid hormone also appears to be a key regulator of fibrosis, however clinical studies are required to further examine its effects (Cha *et al*, 2010).

Until recently, endomyocardial biopsy was the only method of assessing fibrosis clinically, however this was problematic due to the need for an invasive procedure, and is also unable to determine the degree of fibrosis within the entire ventricle. Cardiac MRI with delayed gadolinium contrast imaging has now emerged as a useful non-invasive imaging method for the detection and quantification of myocardial fibrosis (Mark *et al*, 2006). Unfortunately, the use of gadolinium contrast in patients with advanced renal disease has been linked to nephrogenic systemic fibrosis, a potentially debilitating multi-organ disorder, which severely limits its use. Retrospective studies reveal an association between lower GFR and increased myocardial fibrosis on MRI in patients with mild to moderate renal impairment. In patients with ESRD, a patchy, diffuse pattern of late gadolinium enhancement has been demonstrated, which is in contrast to the discrete, localised enhancement typically seen following myocardial infarction (Amann *et al*, 1994). This pattern appears to be specific to uraemia, and correlates with post-mortem studies that demonstrate a diffuse non-coronary inter-cardiomyocyte fibrosis (Mall, 1990).

Functional Cardiac Impairment

Left ventricular systolic function measured by ejection fraction is often preserved even in the presence advanced cardiac remodelling, however diastolic dysfunction is ubiquitous. LVH and interstitial fibrosis are key contributors to the reduced elasticity and distensibility of the left ventricle, leading to impaired cardiac filling and reduced performance. Contractile functional analysis of isolated cardiomyocytes from a rat model of renal failure reveal a

prolongation of early cell shortening, with impairment of intracellular calcium transients (Kennedy *et al*, 2003).

Numerous echocardiographic markers of diastolic impairment have been identified that can aid clinical diagnosis and risk stratification. Many of the measures are preload dependent, and therefore consistency is required around the timing of imaging in relation to dialysis, particularly when performing serial measurements on the same patient. Increased left atrial volume is a marker of diastolic impairment, and has been shown to be an independent prognostic marker in patients with ESRD (Tripepi *et al*, 2007). Early myocardial diastolic velocity measured using tissue Doppler imaging is a relatively preload independent marker of diastolic function (Shan *et al*, 2000). Reduced diastolic velocity is independently associated with worsening renal function, and is inversely correlated with the degree of myocardial fibrosis.

Left ventricular dilation and systolic dysfunction are both poor prognostic markers. One study revealed a mean life expectancy of 38 months in patients with LV systolic impairment and 48 months in those with LV dilation and ESRD (London, 2003).

Increased susceptibility to ischaemic injury

Patients with renal failure have a significantly higher mortality, following acute myocardial infarction. Two year mortality following an MI is 50% - twice as high as seen in the general population (Sarnak 2003). The risk of heart failure following acute myocardial infarction is approximately 3 times higher than the general population (Anavekar *et al*, 2003). This is likely, in part, due to the reduced use of reperfusion therapies and secondary prevention medications in this group, however they also appear to be more susceptible to ischaemia-reperfusion injury. Experimental animal model studies show that ligation of the left coronary artery leads to significantly larger areas of necrosis in uraemic rats compared with controls (Dikow *et al*, 2004). Persistent functional cardiac impairment following ischaemic insult has also been demonstrated in a separate study of uraemic rats. These functional changes were accompanied by decreased endothelial nitric oxide synthase and NOx levels, with an increase in free radicals, suggesting that oxidative stress may be a key contributor to the more pronounced ischaemic injury (Combet *et al*, 2001). A reduction in capillary density in uraemic hearts leads to impaired oxygen diffusion, which may explain why they are more likely to develop hypoxia and subsequent necrosis in the peri-infarct myocardium. Insulin resistance is also likely to play a role, as glucose becomes the main substrate utilised for ATP generation under ischaemic conditions. Reduced insulin sensitivity leads to lower GLUT 4 translocation,

which impairs the heart's ability to increase energy production at this critical time (Aksentijević, 2009).

1.7 Mitochondrial function

Myocardial contraction requires a large and continuous supply of energy. Most of the energy is generated in the form of adenosine triphosphate, produced through oxidative phosphorylation within the cardiac mitochondria. The mitochondria comprise approximately 30% of myocardial cell volume, compared with just 2% in skeletal muscle, which reflects its high energy demands. Cardiac mitochondria are located in the sub-sarcolemmal and inter-fibrillar regions, both populations have distinct biochemical properties in terms of rates of respiration and protein synthesis, as well as response to metabolic stress (Holmuhamedov *et al*, 2012). In the fasted state, free fatty acids are the principal substrate utilized in oxidative phosphorylation. Following a carbohydrate meal, glucose oxidation becomes the predominant source of ATP. Lactate is also an important fuel source, particularly following intense exercise. Free fatty acids are transported into the mitochondria in the form of Acyl CoA via a carnitine carrier. The long chain Acyl CoA undergoes β -oxidation, a series of transformational steps until a two carbon Acetyl Co A fragment is produced, which can then enter the citrate cycle (Figure 1.13). Glucose is oxidized to form pyruvate via the glycolytic pathway (Figure 1.14). Pyruvate is subsequently converted to Acetyl Co A by pyruvate dehydrogenase, or to oxaloacetate by pyruvate carboxylase. Both of these substrates can then enter the citric acid cycle.

Within the citrate cycle (figure 1.15), acetyl CoA and oxaloacetate combine to form citrate. A number of enzymatic reactions convert citrate back into oxaloacetate, where it can then combine with another unit of acetyl CoA to reinitiate the cycle. During the stepwise conversion from citrate to oxaloacetate, $8H^+$ atoms are generated for use in the electron transport chain, and one molecule of GTP. This will generate 10 molecules of ATP per cycle. The hydrogen atoms removed within the citric acid cycle undergo a series of oxidation and reduction steps in the electron transport chain (ETC). The ETC proteins are located within the inner mitochondrial membrane. Transfer of protons across the mitochondrial membrane generates a proton motive force that leads to the generation of ATP from ADP and phosphate (figure 1.16). The linking of proton movement and creation of an electrochemical gradient to the generation of ATP is termed coupled oxidative phosphorylation. Nicotinamide adenine dinucleotide (NAD^+) and flavin adenine dinucleotide (FAD) are key co-enzymes within the process of oxidative phosphorylation, and are involved in a number of oxidation/reduction

reactions, catalysed by dehydrogenases. Metabolism of 1 unit of glucose yields 31 molecules of ATP, whereas metabolism of 1 unit of the free fatty acid palmitate provides a net yield of 104 ATP molecules. In anaerobic conditions, pyruvate is reduced to lactate, catalysed by the enzyme lactate dehydrogenase. This enables oxidization of NADH, which is required for glycolysis (Marin-Garcia, 2005). This metabolic process is a far less efficient than aerobic metabolism, yielding 5 molecules of ATP for each unit of glucose, but is vital in periods of oxygen deficiency, such as cardiogenic shock, when there is generalized tissue hypoxia due to an inadequate cardiac output

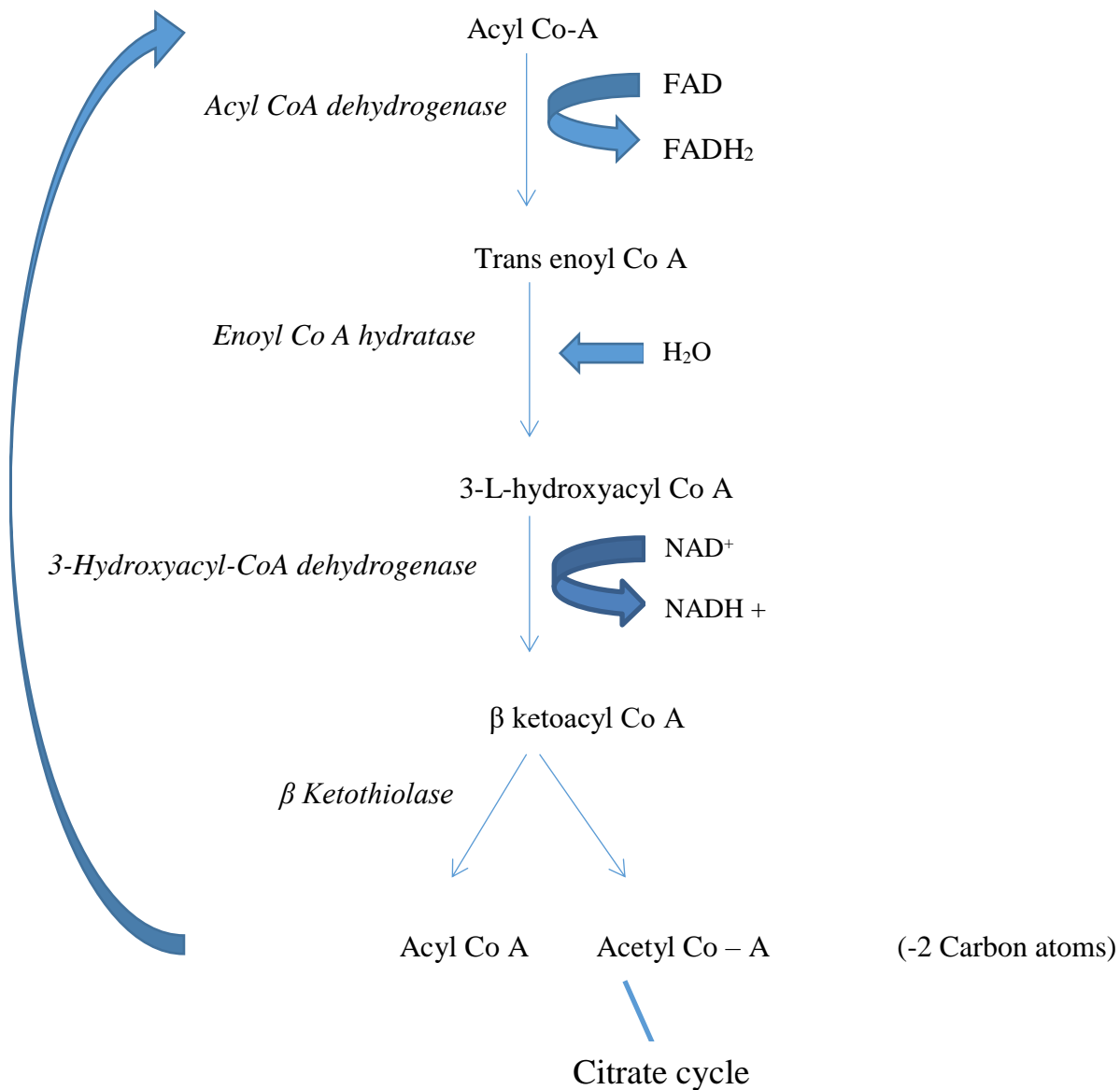


Figure 1.13 Fatty acid oxidation

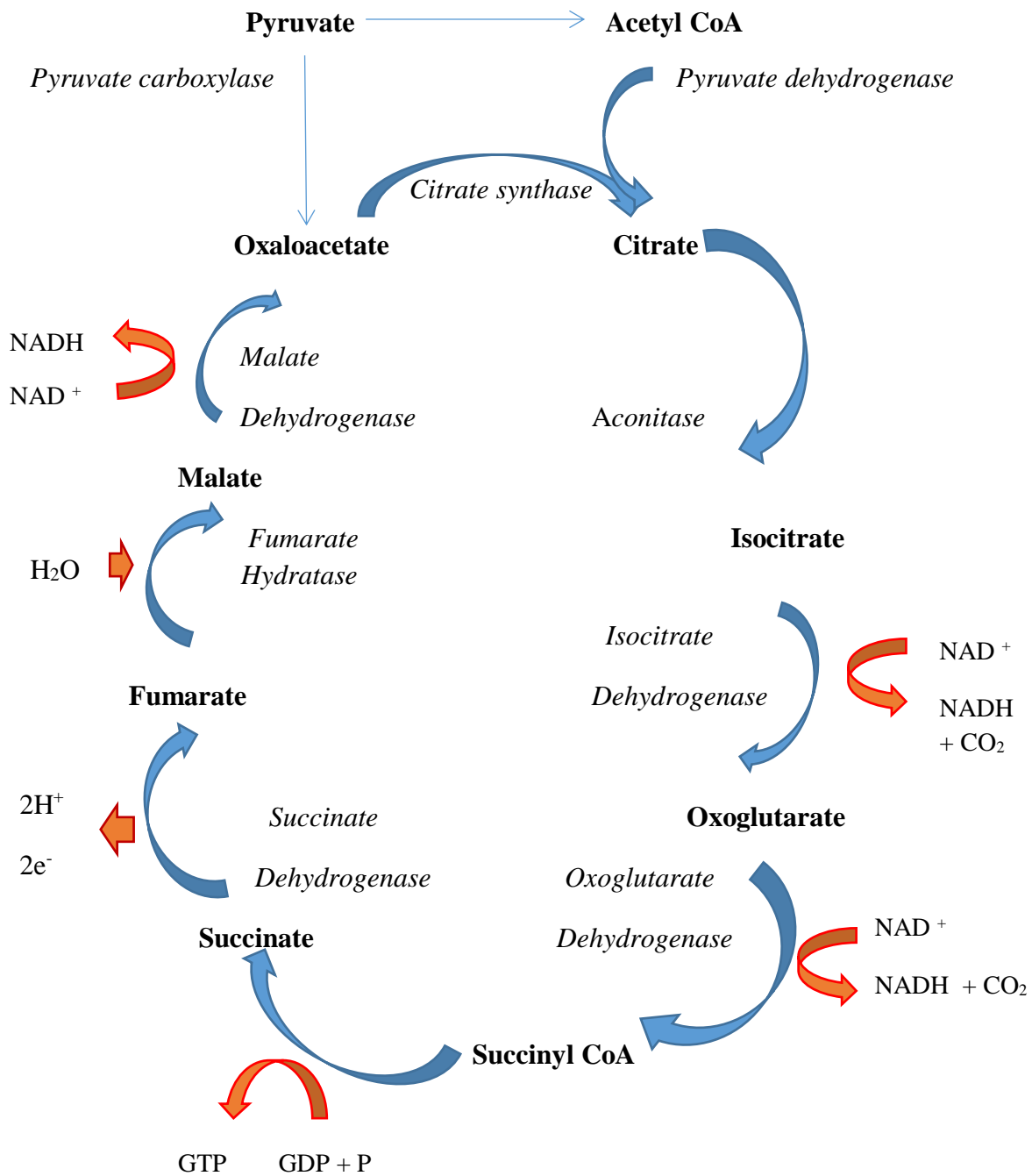


Figure 1.15 Citric acid cycle

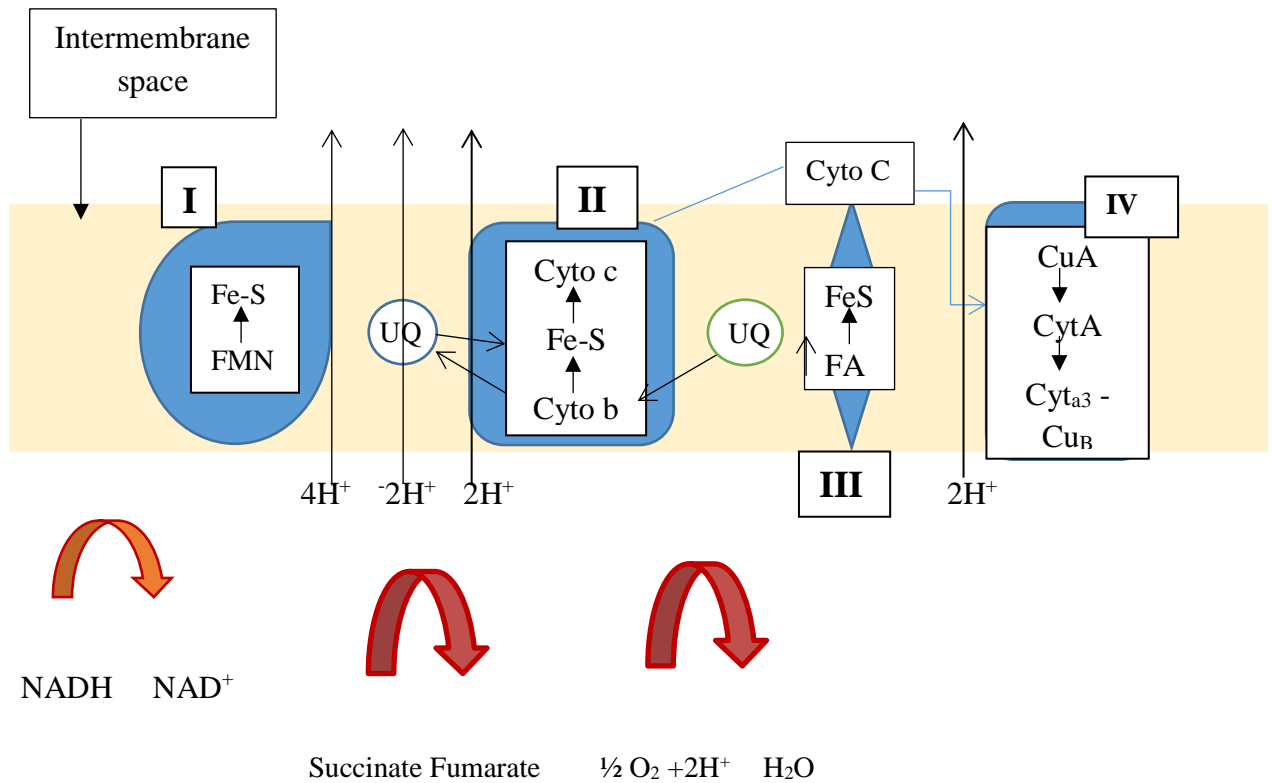


Figure 1.16 Electron transport chain FMN Flavin Mononucleotide, NADH Nicotinamide Adenine Dinucleotide, UQ Ubiquinone, Cyto c Cytochrome C, FAD Flavin Adenine Dinucleotide

1.8 Role of mitochondria in uraemic cardiomyopathy

Mitochondria are essential eukaryotic cell organelles, with a primary role of providing energy in the form of ATP. They also play a central role in iron metabolism, calcium storage, generation of reactive oxygen species (ROS), steroid synthesis, and programmed cell death. Cardiac muscle is highly dependent on aerobic respiration. Cardiac mitochondria occupy approximately 30% of cardiomyocyte space, and during maximal exercise the heart utilises up to 90% of its oxidative capacity (Marin-Garcia, 2005). Intuitively, any condition that impairs the bioenergetic function of cardiac mitochondria is likely to have a significant impact on cardiac function, which could ultimately lead to heart failure.

1.8.1 Mitochondrial biogenesis in heart failure

Mitochondrial replication is dependent upon both nuclear encoded and mitochondrial DNA transcription. The peroxisome proliferator-activated receptor gamma (PPAR- γ) family of transcriptional coactivators are key regulators of this process. PGC-1 α in particular is a master synchroniser of both genomes, activating nuclear respiratory factors that lead to mitochondrial protein transcription. During compensated hypertrophy, expression is upregulated, with mitochondrial density closely matching energy demand. The progression to decompensated heart failure is associated with a downregulation of transcription factors, and a blunting of the hypertrophic response to angiotensin II (Liang *et al*, 2003).

Reactive oxygen species are free radicals that are highly reactive to lipids and proteins, including DNA. Superoxide (OH⁻) anion is a commonly encountered free radical created by partial reduction of water. It is released by the complexes I and III of the electron transport chain. It is typically scavenged by antioxidants, such as manganese superoxide dismutase, and converted to water (Seddon *et al*, 2007). In the setting of impaired mitochondrial function, the antioxidant scavenger mechanisms may be overwhelmed by the reactive oxygen species. This can lead to damage of key cellular components, opening of mitochondrial permeability transition pores, which ultimately triggers the apoptotic cascade. Cell death leads to further free radical release, and can create a cycle of ROS induced ROS release (Zorov *et al*, 2000). Patients with advanced CKD have been shown to have increased circulating levels of the ROS 8-hydroxydeoxyguanosine compared with controls, with a reduction in total antioxidant status (Granata *et al*, 2009; Dounousi *et al*, 2006). Expression of PGC-1 α , 1 β , and angiotensin II are increased by low level concentrations of ROS; they also deactivate class II histone deacetylases which inhibit cardiac hypertrophy.

1.8.2 Mitochondrial bioenergetics in heart failure

Alterations in substrate utilisation are a key adaptation within the failing heart. Free fatty acid (FFA) oxidation is the preferential substrate for ATP generation in a healthy human heart, as this provides the highest energy yield per molecule. Carbohydrates are more efficient than FFAs in terms of oxygen required to produce an equivalent amount of ATP, and therefore become the principal substrate in conditions of increased energy demand and/or reduced oxygen delivery, such as ischaemia and heart failure. FFA utilisation is preserved or even increased in the early stage of cardiac remodelling (Doenst *et al*, 2013). During transition to

the decompensated phase, there is a downregulation of mitochondrial fatty acid oxidation enzymes, and glucose oxidation is favoured. This also appears to be mediated via PGC-1 α and PPAR- γ , as well as oestrogen receptor regulators (ERRs), which regulate FA metabolism. The accumulating lipid intermediates have a direct toxic effect on cellular function, and leads to progressive cardiac dysfunction. In the more advanced stages of decompensation, glucose oxidation is unable to meet demand, leading to an energy deficit and ventricular failure.

ATP levels are preserved in moderate LV hypertrophy, but have been shown to fall in experimental models of severe LV hypertrophy. A more sensitive indicator of impaired bioenergetics is a reduction in phosphocreatinine (PC):ATP ratio. Phosphocreatinine acts as a rapidly mobilisable high energy phosphate store within the cardiomyocyte. There is a negative correlation between LV mass and PC:ATP ratio. Furthermore low PC:ATP ratio is associated with reduced ejection fraction and poorer prognosis in dilated cardiomyopathy (Conway *et al*, 1991). The reduced levels may be due to the shift in substrate utilisation, as FA oxidation increases the redox potential of NADH/NAD, which is linked to PC formation. It may also be related to an over-expression of foetal isoenzymes that accompanies pathological cardiac remodelling, as lower PC:ATP ratios are seen during development.

1.8.3 Mitochondrial dysfunction in uraemic cardiomyopathy

A number of metabolic abnormalities commonly seen in renal failure patients, such as insulin resistance, hyperlipidaemia, and obesity, promote ROS production through oxidative stress. Studies suggest a causal link between oxidative stress and many of the hallmark features of uraemic cardiomyopathy, namely impaired cardiac function, fibrosis and increased susceptibility to ischaemia-perfusion injury (Taylor *et al*, 2015).

Genomic analysis of peripheral mononuclear cells have revealed a specific genetic ‘fingerprint’ common to CKD patients, compared with healthy subjects. Approximately one quarter of the genes demonstrating altered expression encode subunits of the mitochondrial oxidative phosphorylation pathway (Granata *et al*, 2009). Impaired mitochondrial respiration was subsequently demonstrated in skeletal muscle, in particular a reduction in complex IV activity.

Decreased myocardial phosphocreatinine levels and PC:ATP ratios have been confirmed in a rat model of renal failure induced by subtotal nephrectomy, associated with functional cardiac

impairment (Raine *et al*, 1993). This is in keeping with changes in PC levels seen in other mechanisms of cardiac hypertrophy, as described in section 1.3.2.

Cardiac mitochondrial respiration was also assessed in a subtotal nephrectomy rat model of renal failure, which demonstrated increased state IV respiration, suggesting reduced mitochondrial efficiency. They also demonstrated an increased vulnerability of mitochondria to calcium induced stress (Taylor *et al*, 2015). Animal models of uraemic cardiomyopathy reveal reduced activity of sarcoplasmic reticulum Ca^{2+} ATPase 2a and $\text{Na}^{+}/\text{K}^{+}$ -ATPase which affects calcium reuptake during diastole. Exposure to an ischemic insult with subsequent reperfusion leads to impaired calcium extrusion, resulting in high cellular calcium and cellular hypercontracture (Kennedy *et al*, 2003).

ROS production (described in section 1.8.1) has been shown to stimulate matrix metalloproteinase (MMP) expression, specifically interstitial collagenase (MMP-1) and stromolysin (MMP-3) (Spinale *et al*, 1993). MMPs play a key role in collagen synthesis and fibroblast formation, and provide an explanation for the diffuse pattern of fibrosis specific to uraemic cardiomyopathy (Tsutsui *et al*, 2011) The OH^{-} scavenger dimethylthiourea has been shown to reduce MMP expression in an experimental model of myocardial infarction (Kinugawa 2000).

1.9 Myocardial Perfusion Imaging

Myocardial perfusion imaging (MPI) was first performed in 1973 by William Strauss, and has subsequently developed into a key diagnostic tool for clinical cardiologists. Approximately 9 million myocardial perfusion scans were performed in the USA alone (2008 Nuclear Medicine Market Summary, 2008). MPI provides a functional assessment of the regional distribution of blood flow within the myocardium, using an intravenously administered radiopharmaceutical. Studies are usually performed both at rest and following cardiovascular stress, which allows the clinician to distinguish between ischaemic and infarcted myocardium. Ischaemic areas will typically demonstrate reduced relative tracer uptake following stress, with normal uptake at rest, whereas infarcted myocardium or scar will display reduced uptake on both stress and rest images. The introduction of Single Photon Emission Computed Tomography (SPECT), in which images are taken from multiple angles in order to develop a 3-D representation of the heart, was a key development in perfusion imaging. It enables better depth localisation and spatial resolution than traditional 2-D planar imaging, and allows integration of anatomical information using other modalities, such as CT (Hacot *et al*, 1993).

Electrocardiograph (ECG) gating techniques allow an assessment of ventricular function, which provides additional prognostic information and improved diagnostic accuracy (Bateman *et al*, 1999).

A wealth of data has been accrued over the last 40 years that validates the diagnostic and prognostic power of MPI in a broad range of patient populations, in many clinical settings. A meta-analysis of 33 studies demonstrated a mean sensitivity of 87% with a specificity of 73% for the detection of coronary stenoses greater than 50%, which is superior to exercise stress testing, and comparable to other functional tests such as dobutamine stress echocardiography (Klocke *et al*, 2003). It has the best discriminatory diagnostic utility, and hence its greatest clinical value, in patients with an intermediate pre-test probability of coronary artery disease.

1.10 Methods of stress testing

1.10.1 Exercise Stress

Exercise increases metabolic demand on the heart. A graded exercise protocol, commonly the Bruce protocol, provides stepwise increases in effort levels at timed intervals to provide a progressive rise in heart rate. Age predicted target heart rate in beats per minute is calculated by subtracting a patient's age from 220. Target heart rate is achieved at 85% of age predicted target heart rate, at which point the tracer is injected. It is a safe form of stressing, with a very low incidence of adverse events. Exercise stress testing provides complementary prognostic information to the perfusion imaging (El-Hajj, 2014). Approximately 50% of patients referred for studies are unable to exercise, predominantly due to mobility issues e.g. arthritis, prior stroke, peripheral vascular disease (Rozanski *et al*, 2013).

1.10.2 Dipyridamole

Dipyridamole is a pyradopyrimidine compound that acts by inhibiting cellular uptake of adenosine into platelets and red blood cells. This increases circulating levels of adenosine, leading to coronary vasodilation 2 – 4.5 times above baseline (McLaughlin *et al*, 1994). Maximal vasodilation occurs in unobstructed coronary vessels, whereas segments of coronary arteries with significant obstructions are already maximally dilated. This produces a relative perfusion deficit in the area of myocardium supplied by the diseased coronary vessel.

Approximately 50% of patients develop side effects during dipyridamole infusion, commonly chest discomfort, flushing, and headache. More severe side effects include bronchospasm and severe hypotension (Ranhosky *et al* 1990). Caffeine inhibits the vasodilatory effects of dipyridamole, and therefore should be avoided for 24-48 hours prior to a test.

1.10.3 Adenosine

Adenosine is a purine analogue that modulates a range of cardiovascular processes. A2A receptors are found in abundance in vascular smooth muscle. Activation by adenosine leads to G-protein mediated adenylyl cyclase activation, resulting in vasodilation. Adenosine triphosphate (ATP) is converted to cyclic Adenosine Monophosphate (cAMP), which inhibits calcium uptake by sarcolemma, leading to smooth muscle relaxation and vasodilation. It produces a more pronounced and consistent coronary vasodilation than dipyridamole (Wilson *et al*, 1990). It also has a much shorter half-life, therefore any adverse effects can be reversed quickly by discontinuing the infusion. Side effects are common, similar to those experienced with dipyridamole (Cerqueira *et al*, 1994). Low level exercise performed during the infusion attenuates the severity of side effects.

1.10.4 Dobutamine

Dobutamine is a synthetic catecholamine that directly stimulates beta 1 receptors of the sympathetic nervous system. It activates post-synaptic receptors leading to Gs protein coupled adenylyl cyclase activation. Adenosine triphosphate (ATP) is converted to cyclic Adenosine Monophosphate (cAMP). Its primary effects within the heart are to increase heart rate through increased automaticity of the sino-atrial node (positive chronotropy), more rapid electrical cardiac conduction (dromotropy), and increases contractility of atrial and ventricular myocardium, thus increasing cardiac output (positive inotropy).

Dobutamine stress protocols produce an increase in myocardial oxygen demand and heart rate similar to that seen with exercise. It produces less coronary vasodilation than dipyridamole and adenosine, therefore has a lower sensitivity for detecting milder perfusion defects (Ankur Gupta, 2016). Side effects include chest pain, palpitations, flushing and breathlessness. More severe side effects include arrhythmias and hypotension, which can be reversed using beta-blockers. It is generally regarded a second line agent, reserved for patients with contraindications to vasodilator stress, such as asthma, or cardiac conduction system disease. Patients with end stage renal failure have impaired endothelial function, leading to impaired

vasodilation. This may limit the effectiveness of vasodilator stress agents, therefore dobutamine stress in this group of patients may improve the diagnostic yield.

1.10.5 Regadenoson

Regadenoson is a synthetic selective A_{2A} agonist that produces a rapid coronary vasodilator effect. Because of its low affinity for A₁, A_{2B} and A₃ receptors, it leads to far fewer side effects, including headaches/flushing, bronchospasm, and conduction defects (Al-Jaroudi *et al*, 2009). Its rapid onset of action means that it can be given as a bolus, resulting in a significantly shorter time to tracer injection. Twenty six myocardial infarctions and 29 deaths were reported in the first 5 years of clinical use, therefore it should not be used in patients with unstable angina symptoms or haemodynamic instability (Hage, 2014).

1.11 Prognostic Markers of Myocardial Perfusion Imaging

A number of findings from an MPI study have been shown to provide independent prognostic information, and are described below.

1.11.1 Stress testing

See section 1.10 for a more detailed review of stress agents. Exercise stress testing provides complementary information that can aid diagnosis and guide subsequent patient management (Vítola *et al*, 2016). Pharmacological stressing agents are commonly used for patients that are unable to exercise, or have left bundle branch block (LBBB). Vasodilators are the most commonly used agents, which include adenosine, dipyridamole and the newer selective adenosine receptor agonist, regadenoson. Dobutamine is generally reserved for patients that are both unable to exercise and have a contraindication to vasodilator stress. Pharmacological stress has widened the clinical use of MPI, and can achieve more pronounced vasodilation than physiological stress, although at a cost of the loss of an objective measure of exercise capacity (Wilson *et al*, 1990). A retrospective analysis revealed that ST depression during adenosine infusion was an independent predictor of cardiac events (0.5% vs 7.6% in the normal ECG and ST depression groups respectively), although this was only seen in 7% of patients administered adenosine (Yap *et al*, 2005). The requirement of pharmacological stress, is in itself an adverse prognostic sign, irrespective of the reason. A meta-analysis of 24 studies that included nearly 15,000 patients showed a 3 fold increase in the cardiac event rate in

patients with a normal MPI study that underwent pharmacological stress compared with those receiving exercise stress, and a 2 fold increase in those with an abnormal study (Navare *et al* 2004). This meta-analysis found that exercise capacity was the most powerful predictor of cardiac events, although this was prior to the widespread use of ECG gating for LV function assessment.

1.11.2 Reversible perfusion defects

Reversible defects are those in which a relative reduction in tracer uptake is seen following stress, which improves significantly at rest, and typically indicates ischaemia. Larger defects are associated with higher cardiac event rates. Furthermore, patients with a total volume of ischaemic myocardium of less than 10% fare worse with revascularisation compared with pharmacological therapy, whereas the converse is true in defects greater than 20% (Papaioannou and Heller, 2003). The sum stress score (SSS) is a semi-quantitative index that incorporates the size and severity of a defect. This has been shown to be a powerful predictor of future CV events; a score of 0-3 indicates a rate of cardiac death or myocardial infarction of 0.3%/year, whereas a score of greater than or equal to 9 gives a rate of 10%/year (Leslie *et al*, 2003).

1.11.3 Transient ischaemic dilation

This refers to an increase in LV cavity size on stress images when compared with rest, with a ratio of stress to rest volume of 1.22 considered abnormal with Technetium tracers. It is a marker of extensive coronary disease, although the exact cause has not been determined; it may represent true dilation due to myocardial stunning, or an apparent increase in LV size due to global sub-endocardial ischaemia. In a large prospective study, transient ischaemic dilation was associated with a rate of cardiac death/ non-fatal MI of 11.8%, compared with 1.9% without a significant change in cavity size (McLaughlin and Danias, 2002).

1.11.4 ²⁰¹Thallium Lung uptake

Significant tracer uptake of Thallium radiotracer in the lung parenchyma is a poor prognostic marker. It is closely correlated to elevated end left ventricular end diastolic pressure, and is a marker of severe underlying coronary artery disease (CAD). A ratio of lung to heart uptake of

>0.5 is commonly used to define abnormality. Its presence confers a 3.5 times increase in relative risk for cardiac death/non-fatal MI (Gill *et al*, 1987).

1.11.5 Left ventricular dysfunction

Left ventricular (LV) impairment is one of the most powerful predictors of cardiac death (Cowie *et al*, 2000). Gated SPECT enables measurement of LV volumes and ejection fraction (EF), as well as providing information on diastolic function and LV synchrony. The incremental prognostic value of gated SPECT was assessed in a large prospective study, which showed that an ejection fraction of <45%, an end systolic volume of >70ml were strong independent predictors of cardiac death and coronary events (Sharir *et al*, 2006). Patients with an EF <30% have a poor prognosis that is unaffected by the presence of underlying ischaemia.

1.12 Technetium 99m Sestamibi

Technetium 99m-hexakis 2-methoxy-2-methylpropylisonitrile (sestamibi) received FDA approval for cardiac imaging in 1990, and is currently the most commonly used radiopharmaceutical agent for this purpose (American College of Radiology Imaging Network, 2017). Technetium-99m is produced via spontaneous beta decay of its parent nuclide, Molybdenum-99. It is then bound to six methoxyisobutylisonitrile ligands, as shown in Figure 1.17.

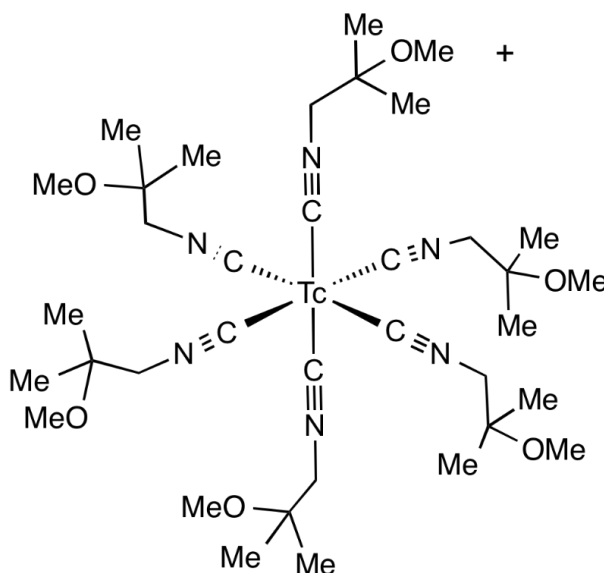


Figure 1.17 Chemical structure of Technetium 99m-sestamibi Me – Methyl O – Oxygen
N – Nitrogen C – Carbon

Technetium 99m- sestamibi has a physical half-life of 6 hours, and a biological half-life of 24 hours, leading to an effective half-life of 5 hours. It produces gamma ray photons predominantly at energy of 140.5 kiloelectronvolts (keV), which is convenient for medical imaging as it has a similar wavelength to conventional x-rays used in diagnostic imaging (Pinwica-Worms et al, 1992). A schematic of Technetium-99m decay is shown in Figure 1.18. A typical dose used in clinical practice will give a total-body radiation dose of 0.5 rad, the organ receiving the highest dose is the gallbladder.

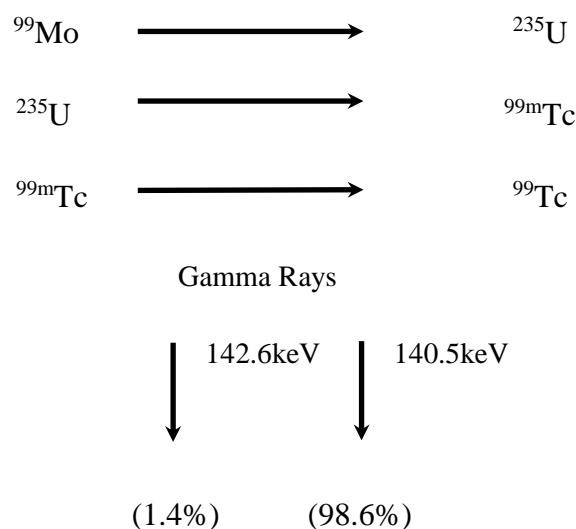


Figure 1.18 Schematic of Technetium 99m decay

Sestamibi is a lipophilic cationic tracer that passively diffuses into the myocardium. Over 90% is selectively incorporated into mitochondria because of their more negatively charged membrane potential (Pinwica-Worms et al, 1990). In the presence of normally functioning mitochondria, technetium sestamibi is fully retained within the myocardium, with minimal redistribution. It clears rapidly from the blood pool ($1/2$ life 4.3 minutes at rest, 1.6 minutes following exercise). Only 1.2% of the injected tracer is taken up by the myocardium at rest; approximately 20% is taken up by the liver, as it is excreted via the hepatobiliary system (Wackers *et al*, 1989). This means that immediate imaging following tracer injection will result in significant image attenuation, and it is therefore recommended to wait for approximately 45 minutes in order to allow hepatobiliary clearance.

1.12.1 The ideal tracer

The ideal tracer for myocardial perfusion imaging would have myocardial uptake directly proportional to blood flow that would provide a measure of absolute coronary flow. It should have a high extraction fraction, meaning that a high proportion of tracer is taken up by the myocardium, rather than other organs. This would mean that the injected dose could be

minimised without compromising image quality. It should have a high target-to-background ratio – clear distinction between uptake from the heart and surrounding organs to reduce the risk of imaging artefact. It should also have good myocardial retention to allow for repeated scans in order to optimise image quality.

1.12.2 Tracer kinetics

The relationship between coronary blood flow and the myocardial uptake of radiotracers is non-linear. All of the above tracers show a plateau at higher blood flow levels (Figure 1.19). The radiotracers show a significant plateauing at coronary blood flow levels exceeding 2.5 mL/min/g. This is smallest for Thallium 201 and is larger for Technetium 99m sestamibi and tetrofosmin (Zaret, 2005).

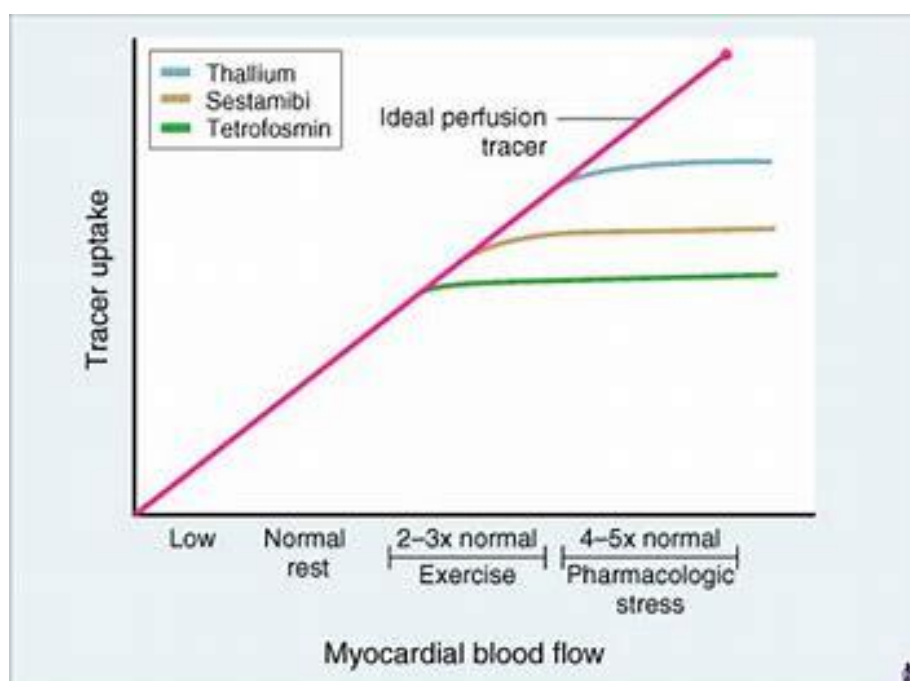


Figure 1.19 Relationship between myocardial blood flow and commonly used radiotracers Taken from Braunwalds Heart Disease: A textbook of Cardiovascular Medicine, 7th Ed.

The myocellular uptake of Thallium 201 is dependent on Na-K adenosine triphosphatase. The myocardial uptake of Thallium declines with Na-K pump inhibition from adenosine triphosphate depletion (Pinwica-Worms et al, 1992). The myocellular uptake of Tc-99m sestamibi reflects the mean plasma membrane potential. It is retained within the mitochondria as a result of an electrostatic interaction. It declines to low levels with severe cell injury (Leppo et al, 1989).

Myocardial microvascular transport of Thallium and Technetium is variable at different blood flow levels. The capillary permeability for Thallium 201 is greater than that for Tc-99m sestamibi. The parenchymal cell permeability surface area for Tc-99m sestamibi is much higher than that for Thallium (Ayalew et al, 2002). Table 1.1 outlines the key differences in tracer kinetics between Technetium and Thallium tracers.

1.12.3 Clinical aspects of ²⁰¹Thallium Imaging

Prior to the introduction of technetium agents, Thallium 201 was the principle radiotracer used for perfusion imaging. A major disadvantage is its long half-life of 2.4 days. This means that significantly lower doses are given in order to limit radiation exposure to an acceptable level. Additionally, it produces lower energy x-rays of 75-80keV, which are more susceptible to attenuation. The reduced number of detectable rays (counts) results in poorer image resolution, and an insufficient count number for gated LV function assessment (Crawford, 2003).

Factor	^{99m} Tc-Sestamibi or ^{99m} Tc-tetrofosmin	²⁰¹ Tl
Extraction fraction	Lower	Higher
Myocardial retention	Prolonged	Comparatively shorter
Myocardial washout	Slower	Rapid
Redistribution	Minimal	Significant
Myocardial perfusion at high blood flow	Same	Same
Injected dose	Higher	Lower
Counting statistics	Better	Fair
Physical half-life	6 h	73.1 h
Photon energy	140 keV	68–80 keV (abundance), 170 keV (~10%), and 135 keV (~3%)
Radiation dosimetry	More favourable	Less favourable

Table 1.1 Differences in properties of Technetium and Thallium radiotracers

Adapted from Hussain SS, 2007

Thallium 201 is in continual flux between the intracellular and extracellular space, and is taken up by ischaemic, but not infarcted tissue within 20 to 30 minutes (Hussain, 2007). This

means that imaging needs to be undertaken within 10 -15 minutes of tracer injection, and severely limits the scope for image re-acquisition should the initial images prove sub-optimal. It does mean, however, that only a single dose of radiotracer is required to obtain both stress and redistribution images. Technetium agents allow re-acquisition of images, because of permanent tracer retention, however separate injections are required for stress and rest images, commonly on separate days in order to allow tracer decay. Thallium-201 has a much higher extraction fraction (84% vs 65%), meaning that tracer uptake is proportional blood flow at higher flow rates (Leppo and Meerdink, 1989). A higher extraction fraction allows detection of more subtle degrees of ischaemia, however this beneficial imaging property is negated by the lower energy/ lower count images obtained with thallium. A number of direct comparative studies demonstrate that technetium agents provide better defect contrast when compared with thallium (Gray and Gewirtz, 1991; Lee *et al*, 1991; Narahara *et al*, 1990). The diagnostic sensitivity and specificity for both tracers are similar when assessed in a broad range of patient populations.

1.12.4 Technetium-99m tetrofosmin

Technetium-99m tetrofosmin is currently the only other radiotracer in clinical use for MPI. It has a lower myocardial extraction fraction than sestamibi, resulting in reduced sensitivity for the detection of subtle areas of ischaemia. A head to head study of 88 patients with known mild-moderate coronary disease that underwent imaging with both technetium agents demonstrated defects were, on average, smaller with reduced severity when using tetrofosmin compared with sestamibi labelling (Reyes *et al*, 2006). There was no difference in the diagnostic performance of the two tracers, although this may be because the study was underpowered. Other small studies have failed to show a difference in diagnostic performance between the two agents. It is cleared more rapidly through the hepatobiliary system, meaning that image acquisition can be performed 10 - 15 minutes after tracer injection. A large prospective study confirmed that imaging with tetrofosmin resulted in higher patient throughput, and a significant reduction in the number of repeated scans (21.4% vs 10%) compared with sestamibi (Ravizzini *et al*, 2002).

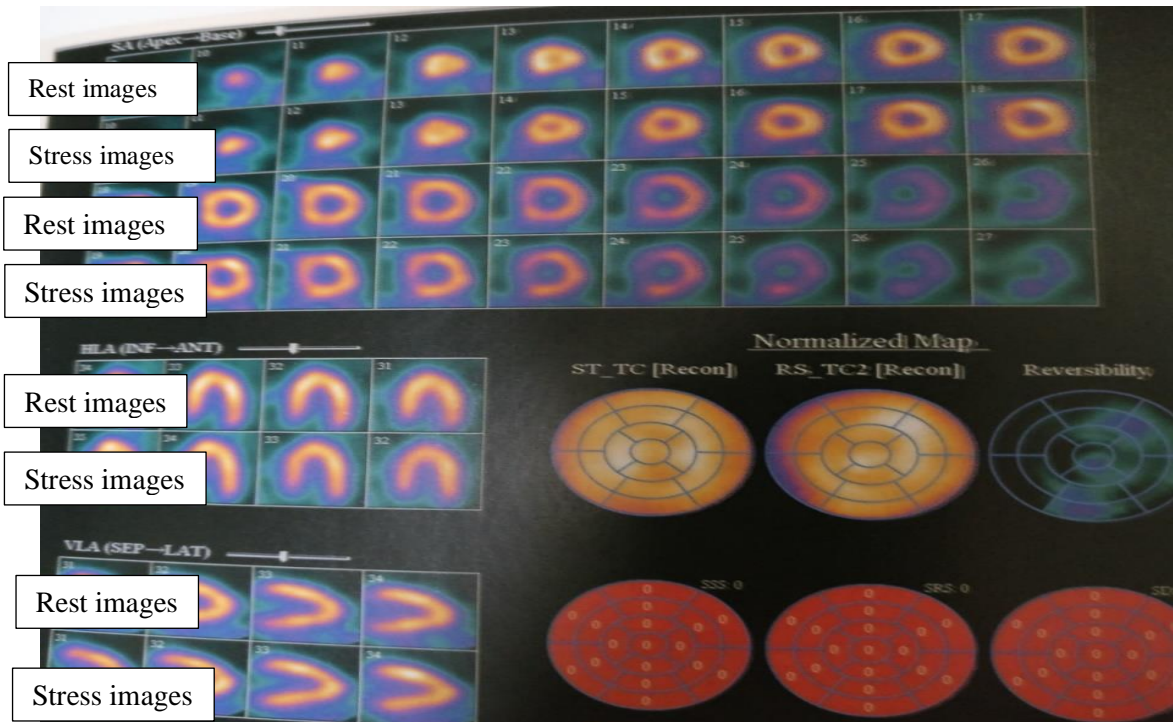


Figure 1.20 Example of a normal stress/rest myocardial perfusion study in a patient referred with chest pain Rest and stress scans, as labelled, from short-axis, horizontal and long axis views. Perfusion is identical both at stress and rest.

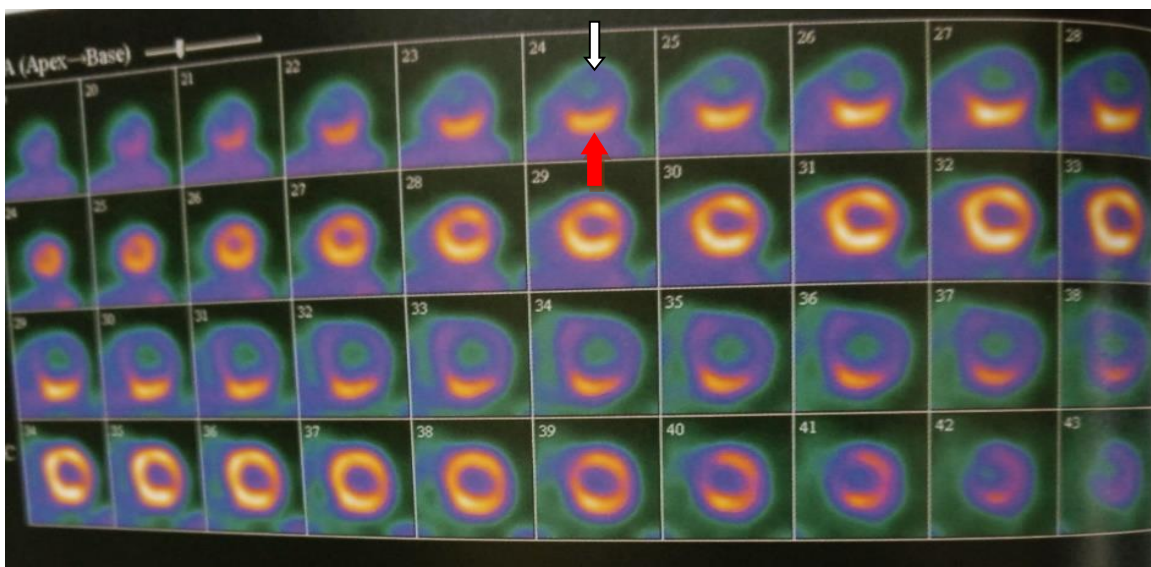


Figure 1.21 Example of an abnormal myocardial perfusion scan in a patient referred with chest pain Stress images (1st and 3rd rows) show darker areas in the anterior, lateral and septal regions of the left ventricle, indicating reduced perfusion (white arrows), The brighter area in the inferior region of the left ventricle suggests improved perfusion to that region (red arrow). Rest images (2nd and 4th rows) show normal perfusion throughout. Findings indicate a reversible perfusion defect in the proximal left sided coronary system.

1.13 Technetium 99m Sestamibi Washout

A distinct characteristic of Tc99m sestamibi is its uptake and prolonged retention within mitochondria. This has led to further investigation to establish whether these unique pharmacokinetic properties could be used to detect mitochondrial dysfunction. Impaired sestamibi retention (also referred to as increased washout) was first demonstrated *in vitro* by examining the effect of both calcium overload and acidaemia in isolated rat hearts (Beanlands *et al*, 1990). Experimental *in vivo* animal studies of ischaemia - reperfusion injury subsequently demonstrated a significant reduction in Tc99m retention after 3 hours, compared with controls (Okada *et al*, 1995). A more recent study by Liu *et al* (2008) showed that ischaemic preconditioning in isolated rat hearts resulted in reduced Tc99m retention compared with those subjected to ischaemia/ reperfusion injury. These studies established the assessment of technetium washout as a reliable indicator of myocardial viability in the pre-clinical setting.

In vivo assessment of technetium washout has principally focused on the assessment of heart failure. Sugiura *et al* (2006) found that washout rates were significantly increased at 4 hours post tracer injection in 17 heart failure patients compared with 10 healthy controls. Washout rate correlated with higher beta natriuretic peptide (BNP) levels, and lower ejection fraction, both of which are powerful predictors of mortality. A larger study of 61 patients with non-ischaemic cardiomyopathy confirmed that increased washout correlated with higher BNP level, poorer LV function as well as increasing New York Heart Association (NYHA) class, a marker of worsening functional capacity (Matsuo *et al* 2007).

The first study that assessed the utility of myocardial washout rate specifically in mitochondrial cardiomyopathy was conducted by Ikawa *et al* (2007). Again they were able to demonstrate an association between higher washout rates and poorer functional status, as well as an increase in interventricular septal thickness measured by echocardiography. Participants with the highest washout rates were also shown to have increased 123I-BMIPP uptake, a free fatty acid analogue, on SPECT imaging, reflecting a switch to anaerobic respiration. Enhanced Tc99m washout has also been demonstrated in patients with coronary vasospastic angina, and hypertrophic cardiomyopathy (Ono *et al*, 2003; Isobe *et al*, 2010).

A recent translational study was the first to demonstrate that myocardial washout rate was specifically linked to mitochondrial dysfunction (Fukushima *et al*, 2010). Rats were

administered carbonyl cyanide m-chlorophenylhydrazone (CCCP), an agent known to cause mitochondrial uncoupling and reduce membrane potential. Tc99m washout was markedly increased and associated with reduced ATP and phosphocreatinine levels on NMR spectroscopy. They subsequently demonstrated increased washout rates in an animal model of hypertensive heart failure and a group of 19 patients with chronic heart failure following a recent exacerbation.

To date, there have been no studies that have specifically assessed technetium washout in uraemic cardiomyopathy.

1.14 Objectives

The aims of this study were;

To evaluate current practice with respect to the use of MPI in patients with end-stage renal failure referred for renal transplantation.

To assess the structural and cellular changes associated with uraemic cardiomyopathy using a subtotal nephrectomy model of renal failure.

To develop an isolated perfused heart system for the assessment of technetium washout.

To develop a method for measuring *in vivo* technetium washout studies in rats.

To develop a protocol for assessing technetium washout in clinical practice.

1.15 Overall hypothesis

1. Current methods of myocardial perfusion imaging provide additional prognostic information beyond clinical risk factors alone in asymptomatic patients with end stage renal disease.

2. A rat model of uraemia via 5/6ths nephrectomy will lead to reduction in cardiac contractility and impaired mitochondrial respiration.

3. Technetium washout can be measured in isolated rat hearts using a perfused heart system.

4. Technetium 99m sestamibi washout rates are higher in the presence of uraemic cardiomyopathy, reflecting underlying cardiac mitochondrial dysfunction.

Chapter 2: Materials and Methods

2.1 Ethical Approval

All animal procedures conformed to the UK Home Office guidelines on the operation of laboratory animals (Scientific Procedures Act 1986, Amendment Regulation 2012). The procedures were performed in accordance with the conditions set out in the respective personal, project and establishment licenses.

Clinical studies were conducted in accordance with the Declaration of Helsinki on Ethical Principles for Medical Research Involving Human Subjects, adopted by the General Assembly of the World Medical Association (1996). Studies received favourable approval from Hull and East Yorkshire NHS Trust research and ethics department.

2.2 5/6ths Nephrectomy Surgical Procedure

Induction of experimental uraemia was achieved using a one stage 5/6ths surgical nephrectomy (adapted from Raine et al, 1993). The 5/6ths nephrectomy model is a well established technique for studying renal failure, its haemodynamic and cardiovascular consequences. It was developed as an experimental model by Chanutin and Ferris in 1932, although the initial technique led to high mortality. Subsequent refinements led to significant reductions in blood loss, and consequently became a reliable and reproducible experimental model. The model requires the animal to undergo surgical removal of the entire right kidney and two thirds of the left kidney. This acute loss of renal tissue leads to progressive glomerular and tubular-interstitial dysfunction, loss of remnant nephrons, and systemic hypertension (Van Koppen *et al*, 2003). There is compensatory growth of the remnant kidney over the first 7-10 days following nephrectomy. This is predominantly due to hypertrophy of the proximal convoluted tubules, and there is also an increase in glomerular volume of up to 75%. Early hyperplasia has also been demonstrated in nephrectomy models of very young rats, with a proliferation in glomerular endothelial cells. A hyperfiltration state is induced, with an increase in glomerular filtration of up to 40% in the remnant tissue. This initial adaptive response ultimately results in glomerular hypertension and injury. It leads to accumulation of inorganic phosphates and reactive oxygen species, and mitochondrial uncoupling leading to impaired energy production (Fine, 1986). There is downregulation of key mitochondrial enzymes of fatty acid oxidation and oxidative phosphorylation, MCAD and

COXIV, and upregulation of BNIP3 and Beclin 1, which are associated with mitochondrial autophagy, 19 (Fedorova *et al*, 2013).

The 5/6ths nephrectomy model produces physiological changes that mimic those of patients with chronic kidney disease. In a study by Gava *et al*, model characterisation demonstrated a 67% reduction of creatinine clearance, systemic arterial hypertension (BP 170/105mmHg in nephrectomy model, compared with 136/90 mmHg in controls), and a 30% rise in proteinuria levels after 2 weeks. Prior studies from this department (Taylor *et al*, 2015; Smith *et al*, 2010) have confirmed structural and function cardiac adaptations following subtotal nephrectomy, including the development of left ventricular hypertrophy (12% increase in wet heart weight), There is evidence of mitochondrial uncoupling, with a 44% increase in state 4 respiration using complex I substrates, and 22% increase in state 3 respiration using complex II substrates, as well as impaired resilience to ischaemia-reperfusion injury. The model produces an immediate loss of nephrons, unlike chronic kidney disease in humans, where there is a progressive loss of nephron numbers. Compensatory renal hypertrophy that occurs with the model is not seen in renal failure in humans. However, the progressive nephron loss that follows the early phase of hypertrophy and hyperfiltration more closely resemble kidney injury seen in chronic kidney disease (Komers *et al* 2012).

The model has been most extensively studied in rats, but it is also validated in mice and rabbits. It has been used in pre-clinical studies of a range of therapeutic interventions, including dialysate solutions, antihypertensives, and treatments intended to attenuate the progression of renal dysfunction (Aubertin *et al* 2012, Eliahou *et al* 2000, Sanchez-Lozada *et al* 2008). Subtotal nephrectomy has been combined with nitric oxide depletion and a high salt diet in order to produce renal failure in Lewis rats, which are more resistant to developing chronic kidney disease, but are useful for assessing cell based therapies (Van Koppen *et al*, 2013).

An alternative to surgical nephrectomy is vascular ligation, whereby renal arteries are selectively occluded, with the degree of discolouration of the renal tissue used to determine the extent of infarction (Al-Banchaabouchi *et al*, 1998 , Shapiro 1993). The remnant kidney model involves surgical right sided nephrectomy , followed by ligation of 3 of the 4 renal arteries. This technique is technically challenging in smaller animals and leads to prolonged operative times. Furthermore, collateral vessel development can lead to reperfusion beyond ligated arteries. Direct comparison of surgical nephrectomy and ligation methods reveal a much wider variability in the degree of renal dysfunction of the former, thus making it less reliable as an experimental model (Liu *et al* 2003).

Renal mass reduction can also be achieved by ablation, using either electrocautery or cryoablation. This has the advantage of improved haemostasis, however it adds additional expense, and still leads to significant variation in the degree of induced renal dysfunction (Gagnon and Gallimore, 1988; Kumano *et al* 1986).

Chemically induced renal failure has also been used in experimental models, with agents such as adenine, cisplatin, and adriamycin (Okuda *et al*, 1986, Yokozama *et al*, 1986). These models have the theoretical advantage of causing progressive renal dysfunction, more akin to chronic kidney disease in humans, as opposed to the sudden loss of nephrons resulting from surgical nephrectomy. It also avoids the need for a surgical procedure that can lead to death of animals. However, a major disadvantage is that the medications used will have extra-renal effects that may lead to physiological alterations. Therefore it may be difficult to distinguish whether changes are solely due to chronic kidney disease, or due to medication toxicity. Furthermore, animals show significant variability in their susceptibility to drug induced renal injury, which can lead to an inconsistent experimental model.

5/6ths Nephrectomy Procedure

Male Sprague Dawley rats (Charles River Laboratories, Kent) aged 4-5 weeks were selected for the procedure. This is within the peri-adolescent period of a rat's life cycle, as they progress to sexual maturity (Sengupta, 2013). At this age, the rats had completed the weaning phase, and were considered sufficiently robust to withstand the physiological demands of surgery. Rats are the most commonly used animals in experimental models of cardiovascular function in renal disease (Zaragoza *et al*, 2011). There are several validated rat models of hypertensive and non-hypertensive renal disease which display the characteristic cardiovascular changes seen in humans, including ventricular hypertrophy, interstitial fibrosis, and progression to systolic dysfunction and heart failure (Doggrell & Brown, 1998). The 5/6ths nephrectomy model is one that is well characterised in the study of uraemic cardiomyopathy. There are physiological differences between rats and humans; the former have faster heart rates, shorter cardiac action potentials, and an inverse cardiac force-frequency relationship (Coleman, 2004). Caution is required, therefore, when interpreting data from animal models and applying this to humans. Mouse models of renal failure have been characterised, however their smaller size make surgical procedures more technically challenging. Larger animals, such as rabbits and pigs, share many anatomical and physiological characteristics with humans in respect of cardiovascular function (Zaragoza, 2011). However, the higher costs, and additional resources required to house and care for such animals made it unfeasible to use these in our experiments. The Sprague Dawley strain

of rats are known have a docile nature, making them generally easy to handle. They are the most widely used outbred rat in biomedical research, and commonly used to study metabolism and cardiac function (Taconic life sciences website).

Anaesthesia

Anaesthetic induction was achieved using isoflurane 3.5% in a closed Perspex induction chamber, with an oxygen supply of 3 litres/minute. Maintenance anaesthesia was provided using 2.5% isoflurane and 1 litre/minute oxygen.

Isoflurane is an inhalational anaesthetic that has the advantages of being easy to control, and allows animals to recover quickly (Steffey *et al* 2006). It is predominantly excreted through exhalation, therefore it undergoes minimal biotransformation and has minimal effects on metabolism (Brunsun *et al.* 1997). Isoflurane was shown to be superior to injected ketamine/medetomidine as an anaesthetic agent for abdominal surgery in Sprague Dawley rats (Hedenqvist 2008). It resulted in a reduction in pain-related behaviour, and faster recovery of body weight. Acute neurotoxicity, as well as delayed neurological effects have been seen with prolonged isoflurane use, however this was only seen with anaesthetic times in excess of 4 hours, and not with shorter exposures (Stratmann *et al.*, 2009). The maximum anaesthetic time in our study was 90 minutes. Isoflurane has been shown to have an adverse effect on cardiac contractility (Yang *et al.*, 2014). This was only significant at isoflurane concentrations of 3%, higher than those used in our study. Furthermore, the changes in cardiac function were seen in older rats (8-12 months). Aging is associated with reductions in cardiac contractility and myocardial performance (Pacher *et al.*, 2004); studies of the effect of isoflurane on adolescent mice demonstrated no significant changes in cardiac function at a 2.5% concentration of isoflurane (Reddy *et al.*, 2009).

An experienced animal welfare officer monitored anaesthetic requirements throughout the procedure through assessment of respiratory rate, depth of respiration, and heart rate. Sufficient depth of anaesthesia was confirmed by absence of pedal withdrawal reflex. Aseptic conditions were maintained throughout. The abdominal area was shaved and iodine applied to the surgical field. A midline incision was performed to expose the abdominal organs. The left kidney was identified and decapsulated. Two thirds of the kidney was removed, estimated by weight of tissue. Haemostasis was achieved using surgical haemostatic polymer (Johnson and Johnson, Georgia USA). The right kidney was subsequently exposed and decapsulated. The renal vessels were ligated using silk sutures and the entire kidney was removed (Figure 2.1). Isotonic saline was injected into the abdominal cavity to compensate for intraoperative fluid

loss. The wound was closed in layers; with deep tissue closure achieved using 3.0 Vicryl absorbable suture (Ethicon, Johnson and Johnson, Georgia USA). Superficial dermal closure was achieved using 4.0 Monocryl absorbable suture (Ethicon, Georgia USA).

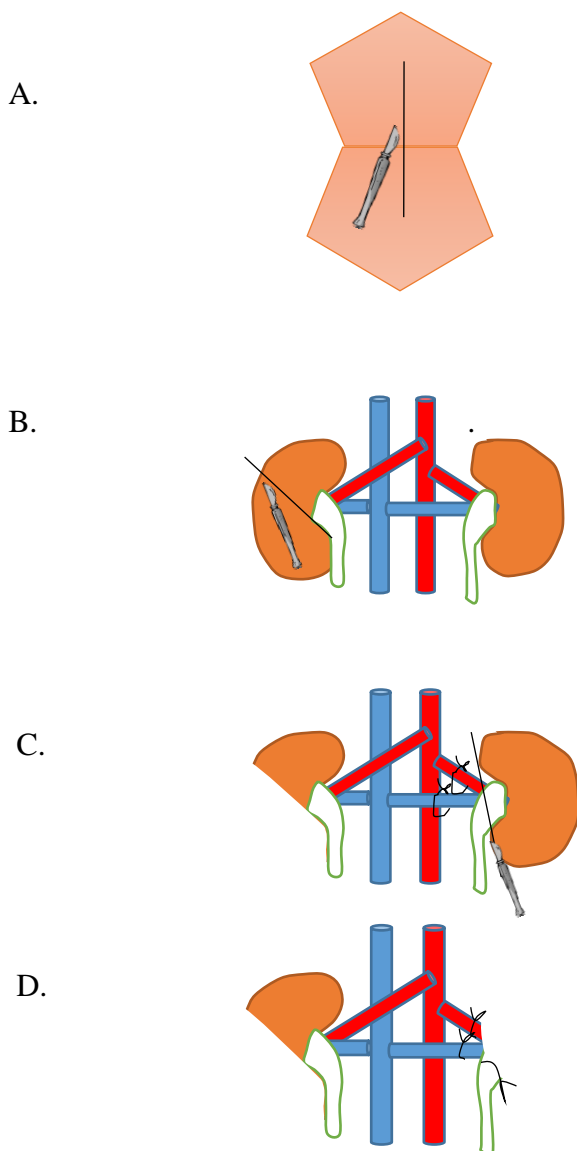


Figure 2.1 Schematic diagram of 5/6th nephrectomy A. Midline abdominal incision B. Decapsulation and excision of 2/3rds of left kidney C. Ligature of renal vessels and removal of left kidney D. Final appearance following 5/6ths nephrectomy

Animals in the control group were selected at random, and underwent a sham procedure. A midline laparotomy was performed and both kidneys were decapsulated, but no renal tissue was removed. Anaesthetic protocol, aseptic technique and wound closure were identical to animals undergoing 5/6ths nephrectomy procedure.

The animals were maintained for 12 weeks, individually housed with a 12 hour light: dark cycle. The animals were pair fed with standard rat chow, whereby an animal in the control

group was provided with the same amount of food by weight as a paired animal in the control arm. Water was available *ad libitum*.

2.3 Preparation of Krebs Henseleit buffer

Krebs Henseleit buffer was used as the perfusate for ex vivo isolated heart perfusion, including the isolated heart SPECT studies. The following constituents were combined (mM); NaCl (118.5), NaHCO₃ (25), KCl (4.8), KH₂ PO₄ (1.2), MgSO₄ (1.2), CaCl₂ (1.25), glucose (5). These were added to ultrapure water that had been gassed with a mixture 95% O₂ and 5% CO₂ for a minimum of 15 minutes. The buffer was subsequently filtered using 0.45µm Millipore filter paper.

2.4 Isolated heart perfusion

Ex vivo assessment of cardiac function was undertaken using a Langendorff perfusion mode (Langendorff, 1895). This technique was developed in 1895, and despite subsequent modifications, the fundamental principles remain very similar to those described over 100 years ago. Retrograde perfusion of isolated hearts is achieved by cannulating the proximal aorta, and delivering perfusate by means of peristaltic pumps at a constant hydrostatic pressure. The aortic valve is closed, therefore the perfusate flows through the coronary arteries, which arise from the sinuses of Valsalva in the aortic root. Gottleib and Manus (1904) adapted the technique by inserting a non-compliant balloon in the left ventricular cavity, which maintains a constant diastolic pressure, and enables assessment of ventricular performance. Coronary effluent can be collected via the coronary sinus, and cardiac efficiency is determined through analysis of the differential oxygen content between the perfusate and effluent.

It provides reproducible measures of cardiac function, and has a wide range of applications. It has improved our understanding of normal cardiac physiology, and the pathophysiology of a host of cardiac conditions, including coronary ischaemia, heart failure and arrhythmias (Bell *et al*, 2011).

An alternative to retrograde perfusion is the ejecting heart model (Neely *et al*, 1967). This technique requires a left atrial cannula, through which antegrade perfusion is delivered. The

heart is initially perfused in a retrograde manner, until atrial cannulation is secured. The aortic cannula subsequently becomes an outflow cannula, when antegrade flow is established. This method has the advantage of producing physiological coronary perfusion, and gives the operator greater control over ventricular preload and afterload. It is technically more demanding than the Langendorff perfusion mode, and requires additional apparatus.

Isolated heart perfusion was performed using a modified Langendorff perfusion mode (Smith *et al*, 2010). The animals were anaesthetized using intraperitoneal thiopentone. Appropriate depth of anaesthesia was confirmed by loss of pedal withdrawal reflex. The hearts were excised via an extended thoracotomy, ensuring that sufficient length of proximal aorta was removed intact for cannulation. The heart was immediately placed in ice – cold KH buffer. Excess fat and vessels were trimmed, then transferred to the perfusion rig, as shown in Figure 2.2. The proximal aorta was positioned over the inflow cannula, ensuring that the cannula tip was within the aortic root, whilst avoiding damage to the aortic valve. The position was initially secured using a metal clip, before tying silk suture to maintain position during perfusion (Figure 2.3). The KH buffer was delivered at a rate of 14ml/minute, oxygenated with a 95% O₂/5% CO₂ mixture, and maintained at a temperature of 37 degrees Celsius.

A 21G needle was inserted into the left ventricle to vent the left heart and prevent LV distension. A cling-film balloon attached to the tip of a cannula was placed into the LV cavity via the left atrium. The cannula was attached to a pressure transducer (SensNor, Horten Germany) and the volume of the balloon was adjusted using a micrometer syringe (Gilmont Instruments, Barrington USA) to achieve an end diastolic pressure of 5-7mmHg.

Two hooked copper wires were placed in the right and left ventricles using a 25G needle. The wires were attached to a Powerlab stimulus generator (AD instruments, Hastings UK) to deliver ventricular pacing with a pulse width of 1msec, and voltage adjusted to achieve consistent capture at 300 beats per minute.

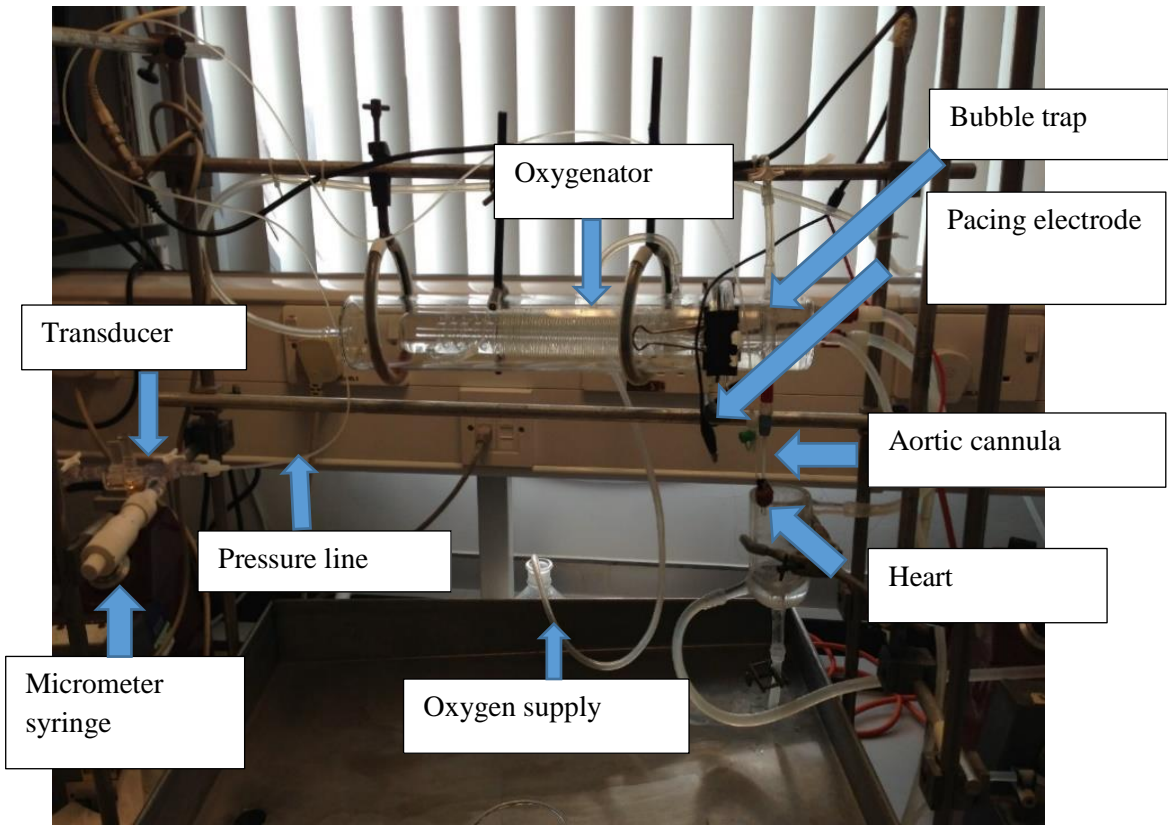


Figure 2.2 Modified Langendorff perfusion rig

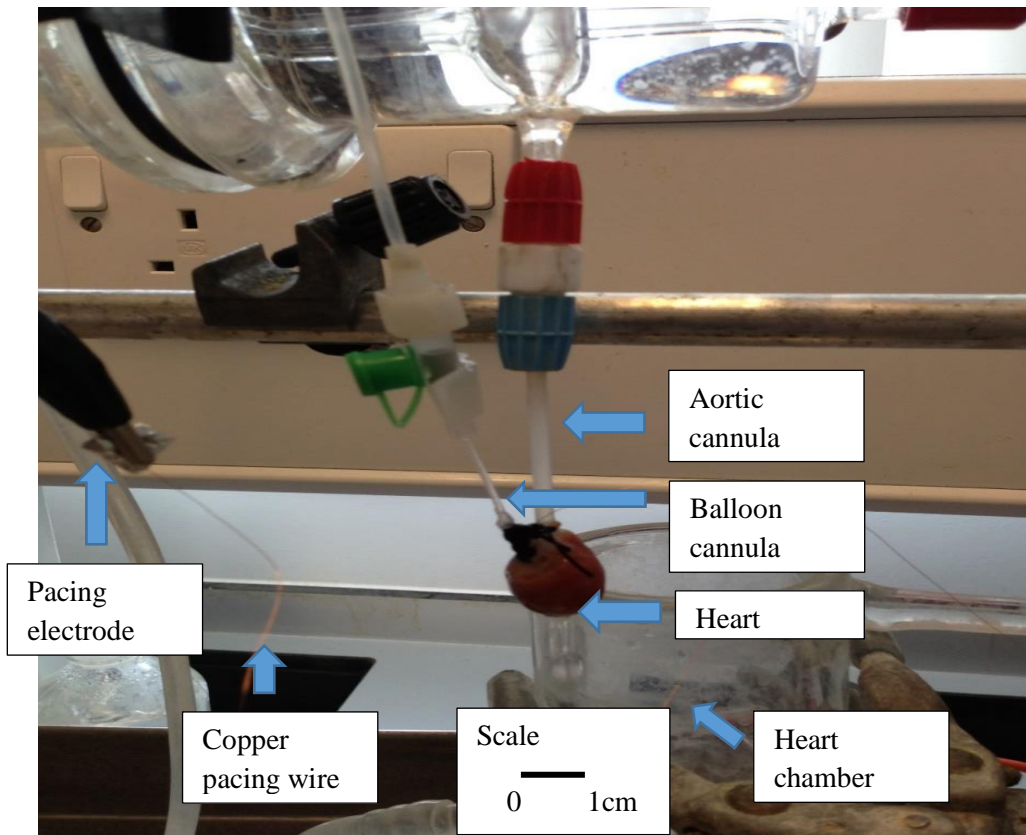


Figure 2.3 Isolated heart within perfusion rig

2.5 Assessment of cardiac contractility

Indices of cardiac function were recorded using a Powerlab data acquisition module, and analysed using Chart 5 software (AD instruments, Hastings UK). Following a 20 minute period of equilibration, heart rate and left ventricular pressure traces were recorded continuously. A period of equilibration was incorporated as our preliminary studies revealed a delay in achieving maximal cardiac contractility from initial incorporation into the perfusion rig. This is likely to be related to a degree of myocardial stunning following hypothermic cardioplegia, as well as the brief period of ischaemia between heart explantation and aortic cannulation. It is recognized that the isolated heart is a constantly deteriorating preparation, with a reduction in cardiac contractility of 5 -10% per hour (Gamble *et al*, 1970). However myocardial architecture and ultrastructure is relatively preserved up to 120 minutes in an adequately perfused heart (Bergman *et al*, 1979). In our preliminary studies, all hearts had reached maximal contraction at 20 minutes, with preservation of myocardial contractility throughout the 90 minute perfusion period.

Left ventricular developed product is defined as the difference between systolic and end diastolic pressure (Figure 2.4).

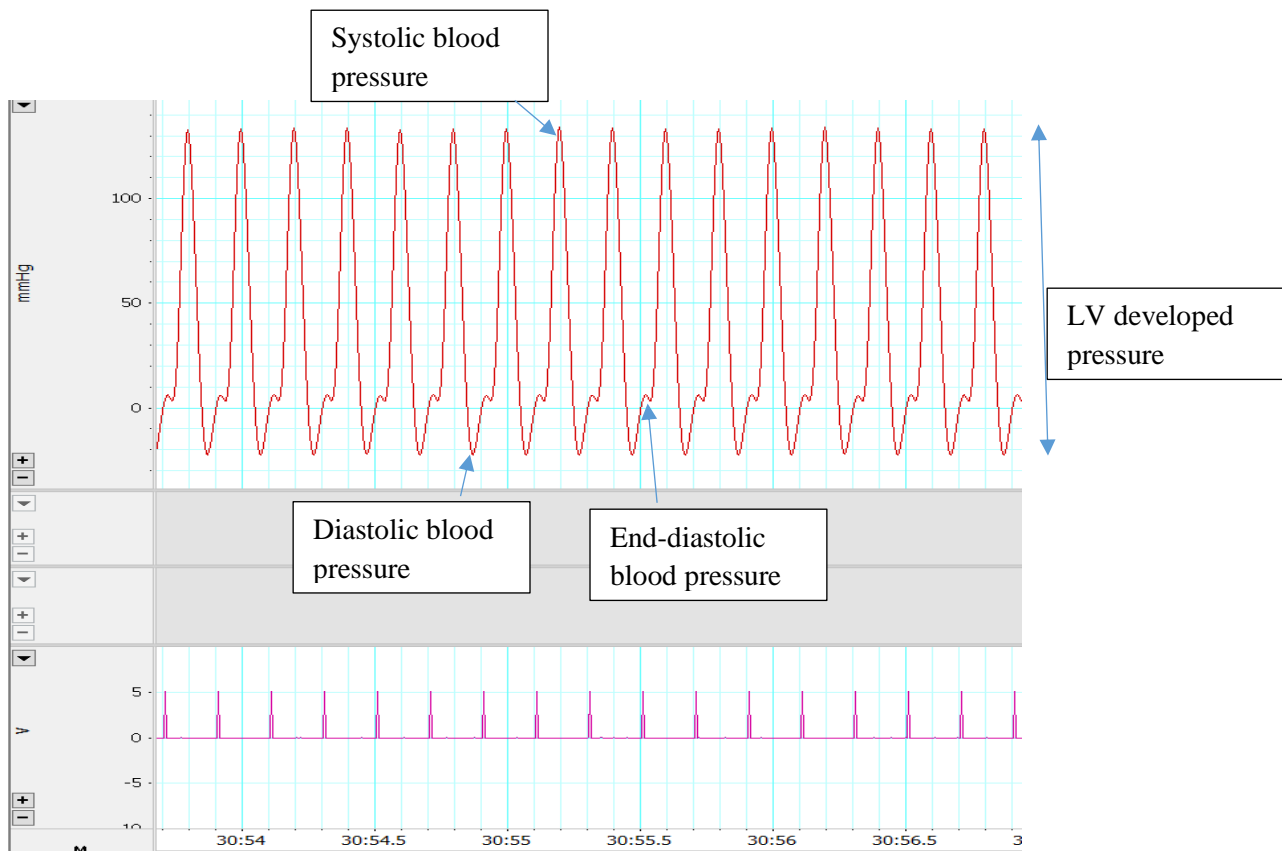


Figure 2.4 Example blood pressure trace to assess cardiac contractility

Rate pressure product is calculated by multiplying the heart rate (bpm) by LV developed pressure (mmHg). Derived pressure traces were produced, which delineate the change in left ventricular pressure with time. dP/dt max and dP/dt min were recorded, as shown in Figure 2.5.

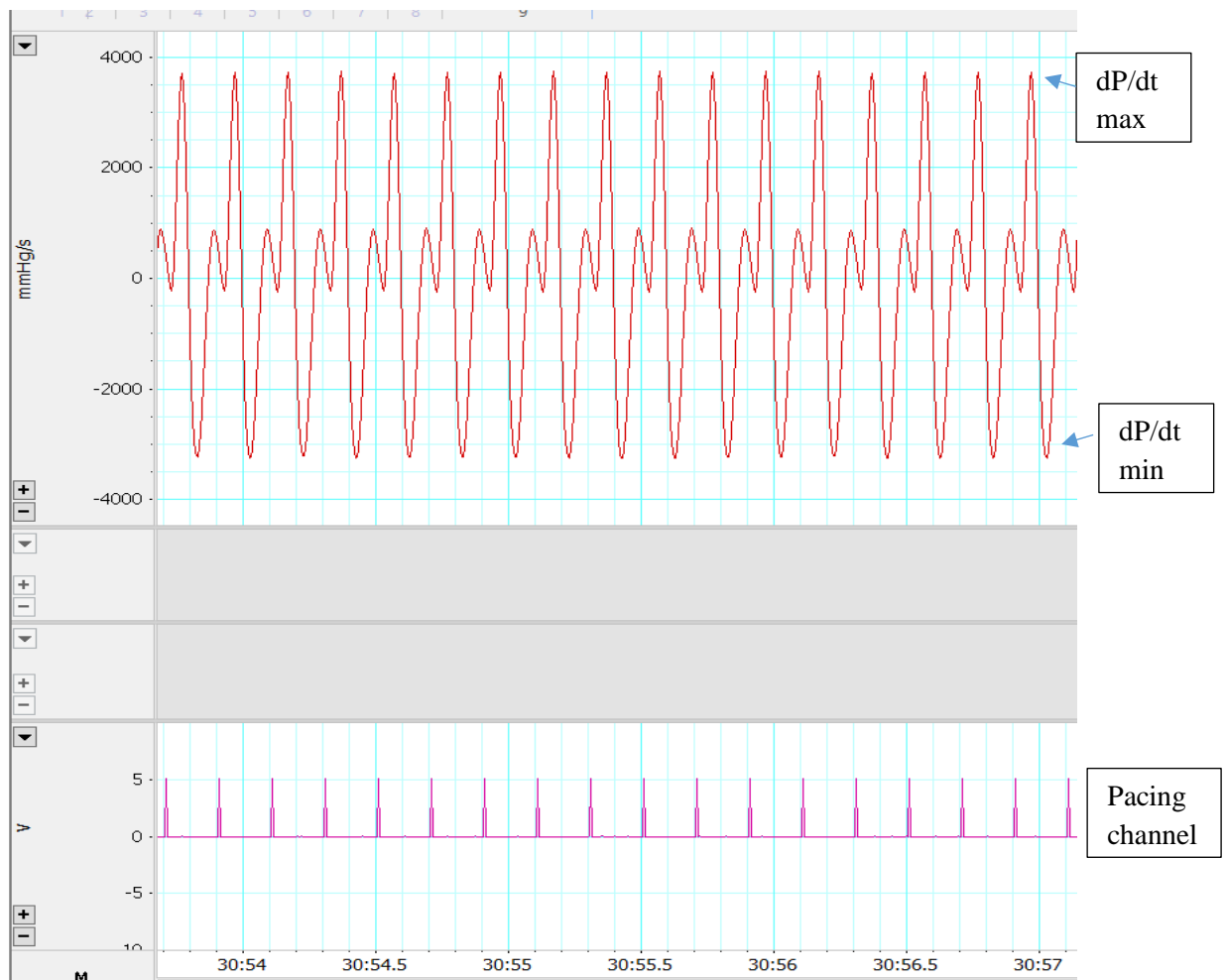


Figure 2.5 Derived pressure trace to determine dP/dt_{max} and dP/dt_{min}

2.6 Biochemical analysis

Blood was taken from the thoraco-abdominal cavity at the time of sacrifice. It was spun in a centrifuge at 4000g for 10 minutes at 4 degrees Celsius, and the serum was removed.

Biochemical analysis was performed using an RX chemical analyser (Randox, Co. Antrim) to determine the serum urea and creatinine concentrations.

2.7 Mitochondrial Isolation

Cardiac mitochondria were isolated using a modification of Boehm et al. (2001). Excised hearts were placed in ice cold isolation buffer containing 0.3mM sucrose, 10mM HEPES and 2mM EGTA, with pH adjusted to 7.2.

Hearts were minced to form a suspension, and transferred to a 30cm³, 19mm OD glass Teflon homogeniser (Scientific Laboratory Supplies, UK). In order to break down the cellular structure of cardiomyocytes, 1 millilitre trypsin solution containing 1.25mg/mL trypsin, 0.3M sucrose, 10mM HEPES and 2mM EGTA was added to the suspension and left for 15 minutes. During this time, the suspension was homogenised using a loose fitting Teflon pestle (Scientific Laboratory Supplies, UK).

Ten millilitres of trypsin inhibitor solution containing 1mg/ml BSA, 0.3M sucrose, 10mM HEPES, 1mg/mL trypsin inhibitor and 2mM EGTA (pH 7.2) was added and the suspension homogenised using a combination of loose and tight fitting Teflon pestles (Scientific Laboratory Supplies, UK) for a further 5 minutes until homogenous.

The mitochondrial fraction was then isolated from the suspension by a sequence of low speed centrifugation (600g at 4 degrees Celsius for 10 minutes), followed by high speed centrifugation (8000g at 4 degrees Celsius for 15 minutes).

The resulting supernatant was discarded, and the pellet was re-suspended in isolation buffer containing 0.3M sucrose, 1mg/mL BSA, 10mM HEPES and 2mM EGTA (pH 7.4). This was subjected to a further high speed centrifuge (8000g at 4 degrees Celsius for 15 minutes), to produce a purified mitochondrial fraction. The mitochondrial pellet was re-suspended in 600µl of isolation buffer. Mitochondrial protein content was determined using the Bio-Rad protein assay.

2.8 Mitochondrial Respiration

The principle role of mitochondria is to convert oxygen and energy substrates into ATP. Mitochondrial function can be assessed *in vitro* by measuring oxygen consumption by polarography using a Clark electrode (Rank brothers, Cambridge UK).

The Clark electrode consists of a silver anode and a platinum cathode, separated by insulating material. The isolated mitochondria and substrates are placed in a sealed chamber that is continuously stirred to produce a homogenous solution, and separated from the electrode

using a Teflon membrane. Dissociation and re-association of water at the charged platinum electrode leads to the release of electrons that is directly proportional to the concentration of dissolved oxygen. This electron flow can be measured as a voltage, which can be converted to an oxygen concentration. Oxygen consumption rates can be measured in the presence of various substrates to investigate individual components of the electron transport chain.

Mitochondrial isolate at a concentration of 0.4mg/ml was added to respiratory buffer containing 125mM KCL, 20mM MOPS, 10mM Tris (base), 0.5mM EGTA, 2.5mM KH_2PO_4 , and 2.5mM MgCl_2 . The respiratory chamber was maintained at 37 degrees by a water jacket and the contents were continuously mixed using an electromagnetic stirrer. The electrode was separated from the chamber by a Teflon membrane, filter paper, and 1 ml of 3mM KCl.

Data was collected using a Powerlab 4/30 (AD instruments, Hastings UK) digital acquisition console which records oxygen consumption within the chamber, and is represented graphically using Chart 5 software (AD instruments Hastings UK). After a 2 minute period of equilibration, state 2 respiratory activities were measured in the presence of the NADH linked (complex I) substrates glutamate (5 mM) + malate (1 mM) and FADH₂ linked (complex II) substrates succinate (5 mM) + rotenone (1 μM) (to inhibit electron transport to and from complex I).

After a further period of equilibration 0.3mM ADP was added to the mixture and the chamber sealed with a plunger. ADP is then converted to ATP, and the oxygen consumption during this period was analysed to determine state 3, or ADP-stimulated respiration. Oligomycin was then added to the mixture, which blocks ATP synthase and therefore ADP stimulated respiration. State 4 respiration rates are measured, where ATP production is uncoupled from oxidative phosphorylation (Figure 2.6). Respiratory control ratio was determined by the ratio of state 3 to state 4 respiration.

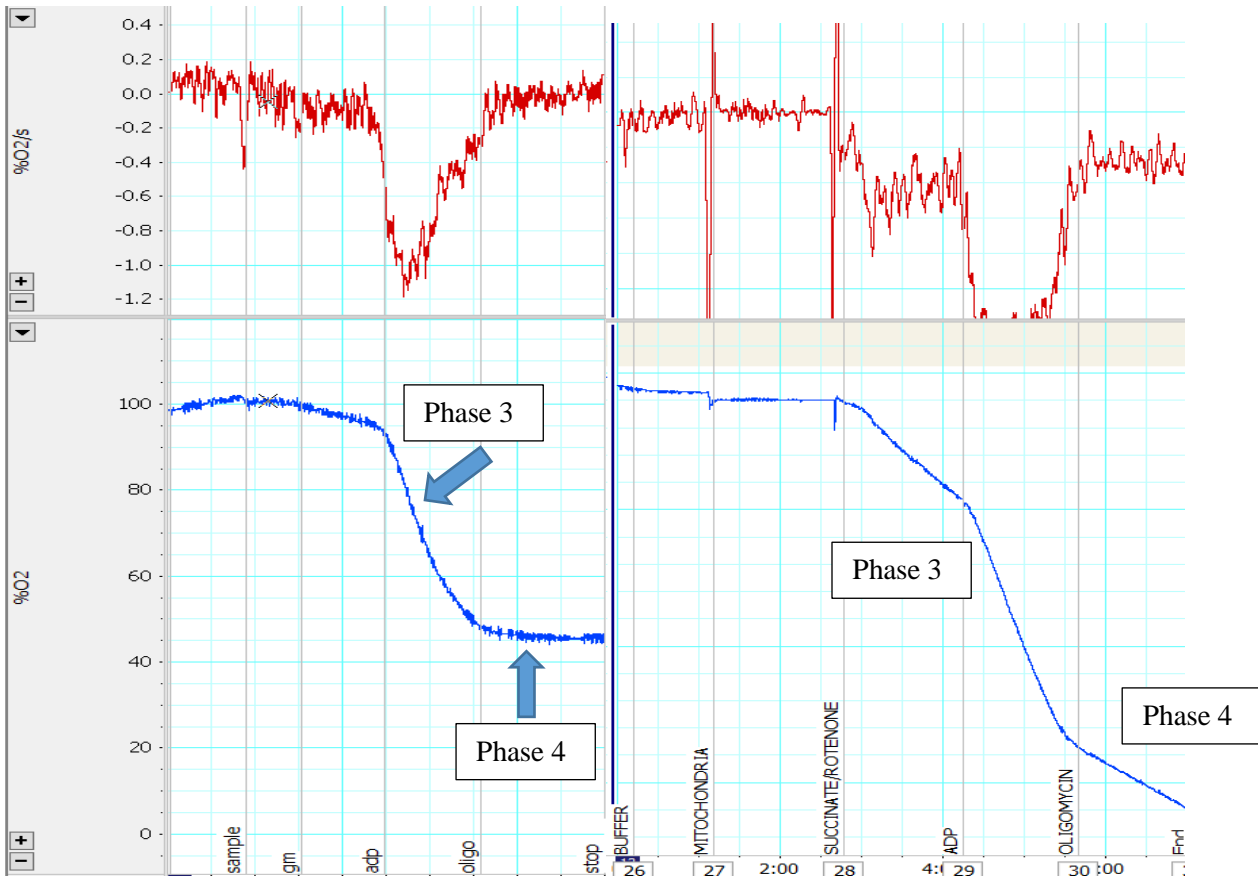


Figure 2.6 Example mitochondrial respiration traces Addition of complex I substrates glutamate/malate (left) and complex II substrates succinate/rotenone (right)

2.9 Enzyme assays

2.9.1 Citrate Synthase

Citrate synthase is a central enzyme within the Krebs cycle. It catalyses the condensation reaction between acetyl coenzyme A and oxaloacetate to form citric acid, coenzyme A, and water. Citrate synthase levels are used as a quantitative measure of tissue mitochondrial content. Citrate synthase catalyses the reaction between acetyl coenzyme A and oxaloacetate to form citrate. The activity of citrate synthase can be measured via colorimetric reaction as DTNB is reduced to TNB by a thiol group produced in the above reaction. TNB has a yellow colour that can be measured spectrophotometrically.

The test was performed according to a modified protocol of Pon and Schon (2007). To perform the assay, 1.85ml of buffer containing 50mM tris, 50mM DTNB, 0.1mM acetyl CoA and 0.1% (v/v) Triton X-100 was added to a cuvette and equilibrated at 25 degrees celsius. One hundred microliters of mitochondrial suspension (40µg of mitochondrial protein) was added to the cuvette and incubated for a further minute. The reaction was initiated by adding

50µl of 10mM oxaloacetate Absorbance was measured over 3 minutes, at a wavelength of 412nm. The enzyme activity was calculated using the extinction coefficient of $13.6\text{mM}^{-1}\text{cm}^{-1}$, with the following formula;

Enzyme activity (nmol/ml/mg protein) =

Absolute Change x Cuvette Volume (ml) x Homogenate buffer vol (ml)

Extinction Coefficient x Volume supernatant (ml) x Weight tissue (g)

2.9.2 Aconitase

Aconitase is an iron sulphur cluster which is an integral protein within the Krebs cycle. It catalyses the conversion of citrate to isocitrate through the dehydration of citrate to cis-aconitate, followed by the stereospecific hydration to isocitrate. It is therefore an essential component to ensure normal metabolic function.

Aconitase catalyses the isomerisation of citrate to isocitrate via the intermediate isoaconitate. The reaction turns a colourless solution to a coloured mixture that can be detected spectrophotometrically. Aconitase activity was measured according to the protocol developed by Fransler and Lowenstein (1969). A reaction buffer containing 20mM Tris HCl, 100mM NaCl and 0.3mM cis-aconitic acid was added to a 3ml cuvette, and incubated at 30 degrees Celsius. The reaction was activated by adding 200µl mitochondrial suspension (80µg mitochondrial protein) and measuring the change in absorbance over 2 minutes at a wavelength of 240nm. The enzyme activity was calculated using the extinction coefficient of $3.6\text{mM}^{-1}\text{cm}^{-1}$.

2.9.3 Complex I

Principle

Respiratory complex I is, as the name suggests, the first step in the transport chain. NADH CoQ-oxioreductase is responsible for the oxidation of NADH to NAD^+ via the reduction of flavin mononucleotide (FMN). The reduced FMNH_2 molecule transfers electrons to an iron sulphur cluster, which in turn transfers to form ubiquinone (Q). This process generates 4

protons for each 2 electrons that enter the complex, and actively transport across the inner mitochondrial membrane to generate an electrochemical gradient which will ultimately lead to ATP generation.

Complex I activity can be measured colorimetrically according to the method devised by Long et al (2009), as DCPIP is reduced by ubiquinol to produce a colour change from a blue to a colourless solution.

Assay Condition

Reaction buffer (pH 7.4)	Concentration
Bovine Serum Albumin	3mg/ml
DCPIP (in ethanol)	0.24mM
NADH	0.13mM
Antimycin A (in ethanol)	2µg/ml
Decylubiquinone (in ethanol)	0.06mM
KH ₂ PO ₄	25mM
MgCl ₂	5mM
KCN	2mM

Protocol

909µl of buffer was added to a cuvette, and incubated for 5 – 10minutes at 30 degrees Celsius. The reaction was initiated by adding 91µl of mitochondrial suspension, and measuring absorbance (negative slope) at 600nm wavelength over 3 minutes. After 2 minutes, 10µl of rotenone was added to measure the rotenone insensitive rate. This is subtracted from the reaction rate to produce the final rate. The DCPIP extinction coefficient $19.1\text{mM}^{-1}\text{cm}^{-1}$ was used to calculate enzyme activity.

2.9.4 Complex II

Principle

Complex II, or succinate dehydrogenase, accepts two electrons from succinate produced via the Krebs cycle. The electrons are transferred to FAD to form FADH₂. They are then transferred, via iron-sulphur clusters, to convert ubiquinone (Q) to the fully reduced form ubiquinol (QH₂). No protons are transferred to the inner mitochondrial membrane during this process.

As in the complex I assay, DCPIP is reduced by ubiquinol to produce a colorimetric reaction. The assay protocol was described by Pon and Schon (2007).

Assay conditions

Reaction Buffer (pH 7.4)	Concentration
Succinic Acid	20mM
DCPIP (in ethanol)	0.16mM
Antimycin A (in ethanol)	2µg/ml
Decylubiquinone (in ethanol)	0.06mM
KH ₂ PO ₄	25mM
MgCl ₂	5mM
KCN	2mM

Protocol

909µl of reaction buffer is added to a cuvette and incubated at 30 degrees Celsius. 15µg mitochondrial protein is added and incubated for 5 minutes. To initiate the reaction, 15µl decylubiquinone is added to the mixture and a decrease in absorbance is monitored over 2 minutes at 600nm wavelength. The DCPIP extinction coefficient 19.1mM⁻¹cm⁻¹ was used to calculate enzyme activity.

2.9.5 Complex II and III

Principle

Complex III, also known as cytochrome reductase, transfers electrons from ubiquinol produced in complex II, to cytochrome c. One electron is transferred via a 2 iron, 2 sulphur group, to the heme group of cytochrome c. The other electron is transferred to cytochrome c, then partially reduces ubiquinone. This generates 2 protons, in addition to the 2 protons released by ubiquinol, leading to the transfer of 4 protons to the inner mitochondrial membrane. Complex 2 and 3 activity measures the process of electron transfer from succinate to cytochrome c

Reduction of cytochrome c results in a colour change that can be used to measure enzyme activity. The method used was described by Pon and Schon (2007).

Assay Conditions

Reaction buffer (pH 7.4)	Concentration
Succinic Acid	20mM
Rotenone (in ethanol)	2µg/ml
KH ₂ PO ₄	25mM
MgCl ₂	5mM
KCN	2mM

Protocol

909µl of reaction buffer is added to a cuvette and incubated at 30 degrees Celsius. Mitochondrial protein 5µg is incubated with the buffer for 10 minutes. The reaction is initiated by the addition of 10µl cytochrome c. Absorbance is measured over 3 minutes at a wavelength of 550nm. The extinction coefficient of cytochrome c is 21mM⁻¹cm⁻¹.

2.9.6 Complex IV

Principle

Complex IV, also known as cytochrome oxidase transfers electrons from cytochrome c to molecular oxygen. This leads to the release of 8 protons, 4 of which are transferred across the mitochondrial membrane to contribute to the creation of the electrochemical gradient.

Oxidisation of cytochrome c leads to a reversal of the colour change seen in the complex II and III assay. Complex IV assay protocol was undertaken as described by Pon and Schon (2007).

Assay conditions

Reaction buffer (pH 7.0)	Concentration
KH ₂ PO ₄	20mM
n-dodecyl-beta-D-maltoside	0.45mM

Protocol

909µl of reaction buffer is added to a cuvette and incubated for 5 minutes at 30 degrees Celsius. 2.5µg mitochondrial protein was added to the buffer and incubated for a further 5 minutes. The reaction was initiated by adding 10µl of 2mM cytochrome c, and absorbance measured at a wavelength of 550nm for 2 minutes.

2.10 Electrocardiogram

Resting 12 lead electrocardiogram (ECG) recordings were performed using a MAC 3500 ECG diagnostic system (GE healthcare, Chicago, Illinois, USA). Recordings were performed with the patient lay in a supine position. Ten ECG electrodes were placed on the limbs and anterior chest wall, as shown in Figure 2.7, and leads were attached. A 10 second recording was taken whilst the patient lay still. A standard paper speed of 25mm/s was used, with an amplitude of 10mm per millivolt signal, and a frequency filter of 150 Hertz to remove high frequency signal artefact. Marquette 12SL ECG computerized analysis algorithm (GE healthcare, Chicago, Illinois, USA) provided data on heart rate and QRS duration and PR

interval (see figure 2.8). ECG recordings were performed by a cardiac physiologist, and data interpreted by an experienced cardiologist.

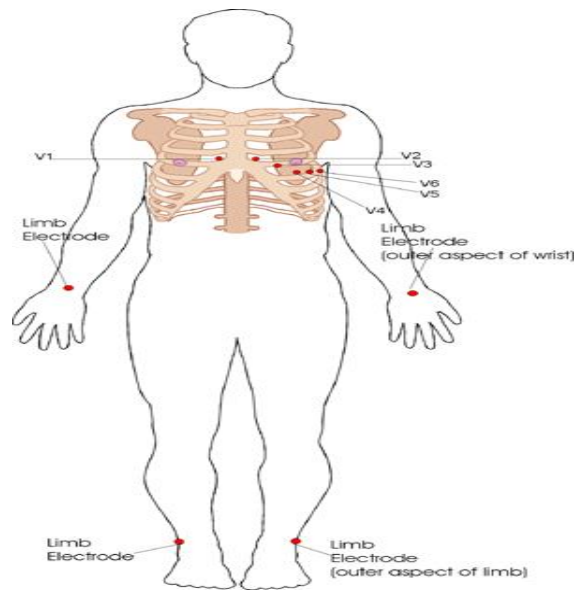


Figure 2.7 Standard lead position for a 12 lead ECG Taken from University of Glasgow online ECG training module

<https://www.gla.ac.uk/researchinstitutes/healthwellbeing/electrocardiology/trainingandsupport/howtorecordecgs/#d.en.42250>

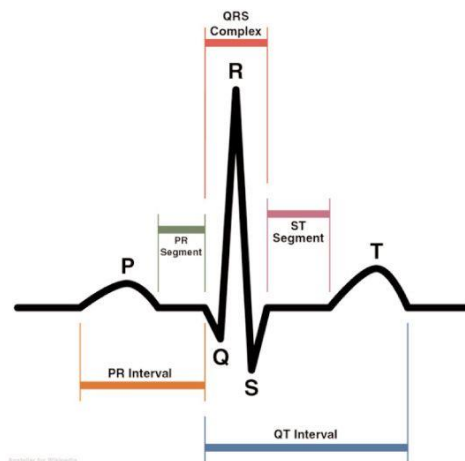


Figure 2.8 ECG complex showing waveforms and key wave durations

2.11 Ex vivo SPECT imaging

Krebs –Henseleit buffer was produced as described above. A beaker was filled with 300ml KH buffer, oxygenated using 95% O₂/5% CO₂ mix, and placed in a water bath maintained at 37°C. An insulated inflow tube was placed in the beaker, and attached to the modified imaging cell via a peristaltic pump. An outflow tube was attached to a collecting dish in the

imaging cell, which was connected to a waste beaker positioned behind lead blocks, to create a non-recirculating model.

A modified imaging cell incorporated an aortic cannula, and collection dish for buffer (see Figure 2.9).

The protocol for anaesthesia, heart excision and aortic cannulation was described in section 2.4. The buffer flow rate was set at 10ml/minute. After a 10 minute equilibration period, 150 MBq Technetium 99m sestamibi was added to the beaker.

After a 30 second delay, planar SPECT images were taken using a Nanospect SPECT/CT scanner (Mediso Budapest Hungary), with a single pinhole collimator in an LAO projection (gantry rotation 270°). 5 x 5 minute acquisitions were taken during the ‘wash-in’ phase (Figure 2.10).

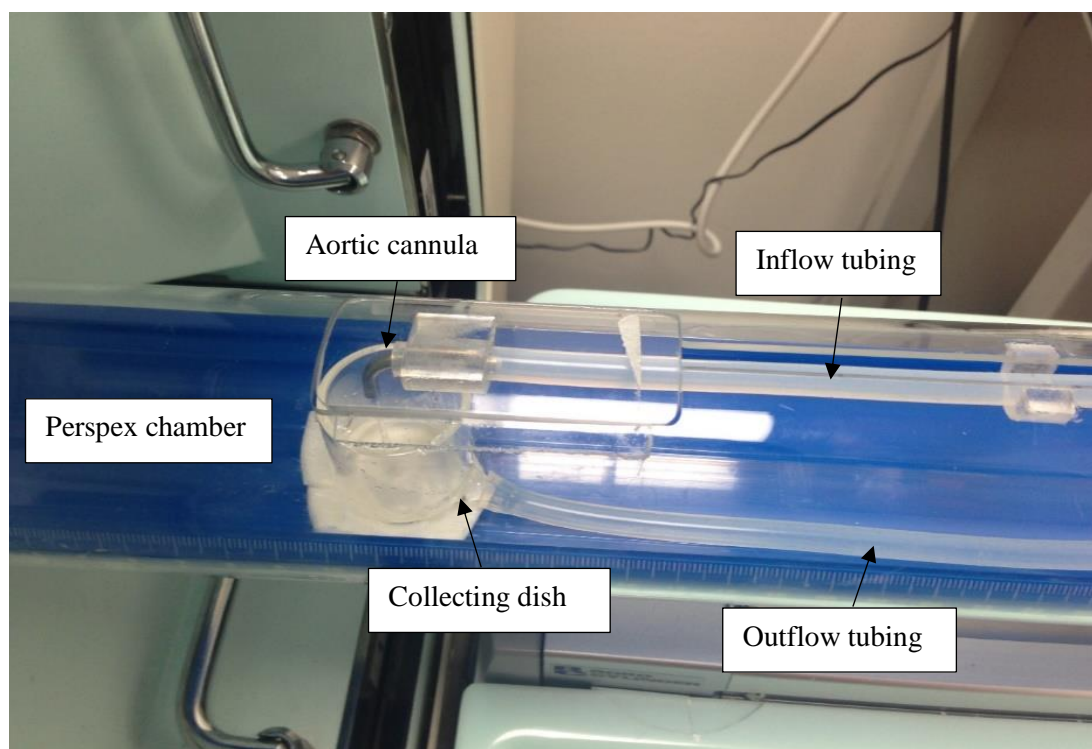


Figure 2.9 Modified imaging cell

The inflow tube was then transferred to a beaker containing fresh KH buffer, and a further 5 x 5 minute acquisitions were obtained during this ‘washout’ phase.

The uncoupling agent CCCP was then added at a concentration of 1mM in DMSO. A further 8 acquisitions were taken, with an acquisition time of 5 minutes.

In a subset of studies, CCCP was not added to the buffer and a prolonged washout phase of 12 x 5 minute acquisitions was performed.

The images were processed using Vivoquant software (Invicro, Boston USA), with absolute and decay corrected counts collected for each acquisition. Wash-in and washout curves were created, and wash-out rates were calculated using the following formula.

Washout rate (%/hour) =

$$\frac{\text{Early decay corrected counts} - \text{Delayed decay corrected counts}}{\text{Early decay corrected counts}} \times 100$$

Early decay corrected counts x (60/time in minutes)

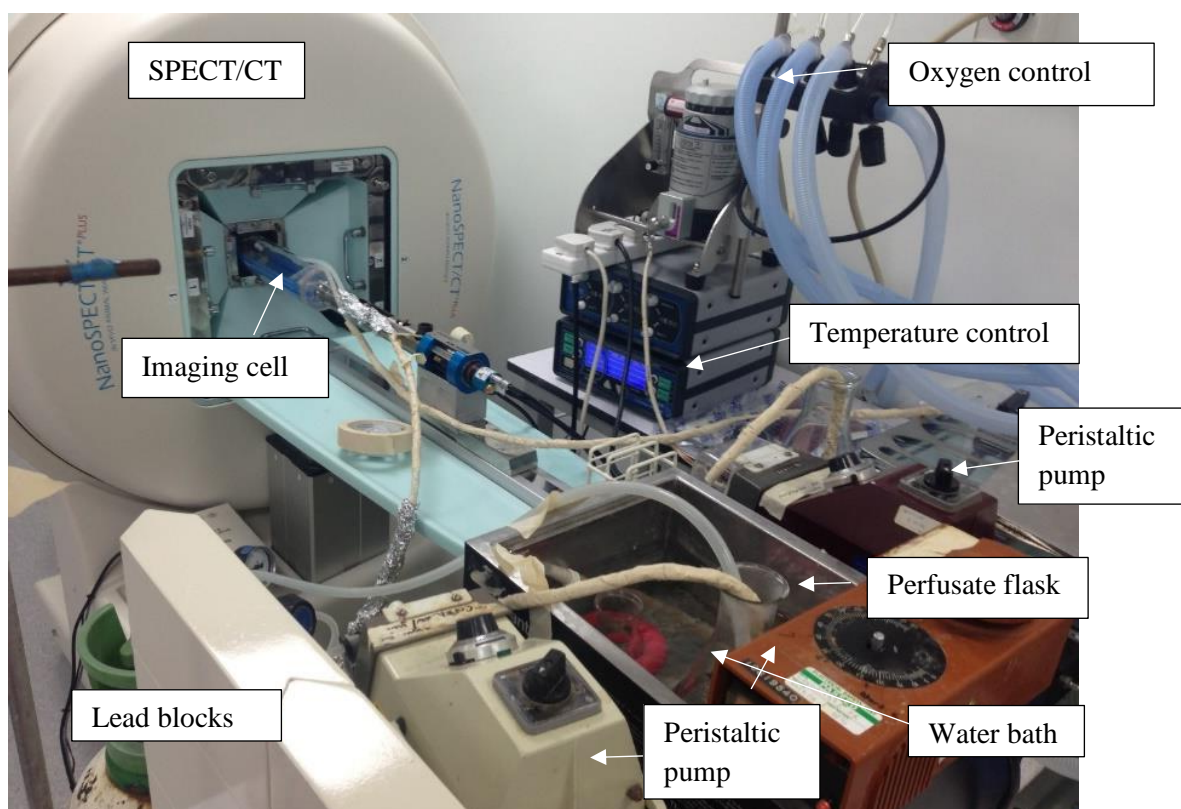


Figure 2.10 Isolated perfused heart imaging system

2.12 In vivo SPECT imaging

Rats were brought down to the holding room within the imaging facility the night before the scan. Food was withheld from midnight on the eve of the procedure.

The rats were placed in a closed Perspex anaesthetic chamber and induced with 3.5% isoflurane and 3 litres/minute O₂. The rats were transferred to a dedicated imaging module

where anaesthesia was maintained using 1.5-2.5% isoflurane and 1litre/minute O₂. The depth of anaesthesia was confirmed by loss of pedal withdrawal reflex. Respiratory rate was monitored continuously during induction of anaesthesia, then at 2 minute intervals during imaging.

The temperature within the imaging module was maintained at a temperature of 37°C. ECG electrodes were attached to the rat using cuffs positioned on each limb, and heart rate was monitored throughout the procedure.

The distal tail vein was cannulated using a 22 G cannula. The rat bed and imaging module were positioned under the SPECT/CT system, a scout topogram and a helical CT (pitch 0.5, 180 projections) was acquired for accurate localisation and attenuation correction.

150MBq Technetium sestamibi was injected through the cannula, followed by a 200µl flush to account for the cannula dead space.

SPECT images were obtained using a Nanospect SPECT/CT system (Mediso, Budapest, Hungary), with a pyramid collimator and multi-pinhole detector. Each reconstruction consisted of 20 projections over 180° (9° rotation per projection), with an acquisition time of 45 seconds per projection. Data was acquired using a 256 x 256 matrix. Imaging commenced at 5 minutes following injection, and subsequent reconstructions were taken at 25, 40, 55, 70 and 85 minutes.

The animals were recovered, and condition monitored until they were fully conscious. They were housed individually in the holding bay for the duration of at least 5 half-lives of 99m Technetium sestamibi before transferring back to the main animal housing area.

Image reconstruction was processed using HISPECT multi-pinhole reconstruction software (Scvis GmbH, Gottingen Germany). Image analysis was undertaken using Vivoquant software (Invicro, Boston USA). Standard uptake values (SUV) were calculated according to the equation: $SUV = \text{activity per g target tissue} / \text{activity applied per gram}$. Cardiac distribution of 99m Technetium sestamibi was determined by drawing a region of interest around the left ventricle. The quantification of cardiac uptake using the Vivoquant processing tool was performed by determination of the sum of count activity within the left ventricle.

2.13 Clinical SPECT imaging protocol

A standard 2 day pharmacological stress/ rest protocol was used for imaging patients. . During the stressing component, patients received continuous ECG monitoring and non-invasive blood pressure measurement at 2 minute intervals. Dobutamine was infused at an initial dose of 10mcg/kg/min, with a stepwise increase every 3 minutes to a peak dose of 40mcg/kg/min. Atropine was administered in 600mcg boluses, up to a maximum of 1.2mg in patients that had not achieved 85% target heart rate on maximum dose dobutamine. Images were acquired 45 minutes following tracer injection in an attempt to minimize hepatic and gastrointestinal uptake artefact, with an Infinia Hawkeye gamma camera (GE Healthcare, Milwaukee, Wisconsin, USA). Two heads were placed in an L-Shaped configuration. Attenuation correction acquisitions were performed for each phase. Images were acquired with a low-energy high-resolution collimator, using a 180 degree non-circular orbit from 45-degree right anterior oblique to 45-degree left posterior oblique in the step and shoot mode (32 projections, 25 seconds per projection), 20% symmetric energy window centred at 140 keV and gating at 8 frames/ cardiac cycle. Images were stored in 64×64 matrices in the computer. Non attenuation corrected images were processed with filtered back projection algorithm, using Butterworth filter with a cut off frequency of 0.45 and order of 10. Attenuation correction images were processed using Iterative Reconstruction (Flash 3D, Siemens) algorithm. For the quantification of data, Quantitative Perfusion SPECT-Quantitative Gated SPECT (QPS:QGS) (Cedars Sinai, Los Angeles, California) was used for both AC and NAC methods. Resting images were acquired using the same imaging protocol on a separate day.

Animal SPECT studies	SPECT studies in clinical subjects	Implications
Performed under general anaesthesia	Performed whilst awake	Prolonged general anaesthetic may affect cardiac contractility. Greater risk of movement artefact in humans.
Scanned within a Perspex chamber	Scanned in very close proximity to camera heads	Chamber may lead to artefact due to scatter.

Single head gamma camera	Dual headed gamma camera	Dual headed camera enables the acquisition of a greater number of projections within the same scanning period, increasing image resolution.
Pyramid collimator	Low energy, high resolution (LEHR) collimator	LEHR collimator provides images of greater resolution, at the expense of reduced counts. Will not affect measurement of calculated washout rates.
Vivoquant image analysis software (GE Healthcare, Milwaukee, Wisconsin, USA)	QGS:QPS image analysis software (Cedars- Sinai, California, Los Angeles)	Differences in image processing and analysis software may lead to output data.

Table 2.2 Summary of major differences between animal and human SPECT imaging protocols

2.14 Statistical analysis

Results are expressed as mean and standard error. Statistical significance was assessed for continuous variables using unpaired student t-test when comparing data between subjects. Paired t-test was used when comparing data on the same subject at two distinct time points. Non- continuous variables were compared using the Chi Squared test. In the clinical studies, long term survival data was evaluated through the construction of Kaplan-Meier curves, and groups were compared using the log rank test. Associations between clinical variables and outcomes were analysed using Cox-proportional hazards model. For the development of clinical risk scores, non-parametric receiver operating curves were created, and analysed using logistic regression models. A significance level of $p < 0.05$ was using for all statistical tests.

Chapter 3: Myocardial Perfusion Imaging Prior To Renal Transplantation

3.1 Cardiovascular screening in end stage renal disease

Cardiovascular disease remains the leading cause of death in patients with end-stage renal disease (Foley *et al*, 1998). Although many patients with ESRD progress to needing dialysis, the optimal therapy for both quality and quantity of life in suitable patients remains renal transplantation (RT) (Schnuelle *et al*, 1998; Port *et al*, 1993). Renal transplantation is defined as the surgical implantation of a human kidney from a compatible donor into a recipient (Collins Dictionary).

The estimated incidence rates of myocardial infarction following transplantation are 3.5 – 5% at 1 year, with a particularly high frequency in the first three months (Ojo, 2006; Lentine *et al*, 2005). In an era where the number of available donor kidneys is limited, pre-transplant assessment is particularly important when trying to maximise the benefit from each transplantation. Pre-transplant identification of high risk patients would allow plans to be put in place for enhanced monitoring in the perioperative period. Specific pharmacological therapies could also be initiated to reduce the risk of perioperative cardiovascular events. Cardiovascular events are typically defined as;

Unstable angina – Prolonged episodes of anginal chest pain whilst at rest, without evidence of myocardial damage (no elevation in cardiac enzymes).

Myocardial infarction - Evidence of myocardial damage, as evidenced by elevation in cardiac enzymes, or typical ECG changes ST segment elevation or depression, T-wave inversion. It is notable that a significant proportion of post-operative myocardial infarctions are clinically silent i.e. occur in the absence of classical symptoms of chest pain and breathlessness.

Cardiac death – death attributable to a cardiac cause, typically cardiac pump failure, or arrhythmias.

Need for coronary revascularisation – Identification of significant coronary artery disease that requires treatment with percutaneous coronary intervention or coronary artery bypass grafts.

3.1.1 Pharmacological interventions

Statins

Statins (3-hydroxy-methylglutaryl coenzyme A reductase inhibitors) are an established class of lipid lowering drugs. Although their principal effect is through reduction of low density

lipoprotein levels, they have pleiotropic effects, including increased endothelial nitric oxide synthesis, reduction in oxidative stress, anti-inflammatory properties (Libby et al, 2002, Liao et al 2005). Large retrospective cohort studies have demonstrated an association between statin use and reduction in perioperative mortality (Poldermans et al 2003; Lindenauer et al, 2004) A meta-analysis that included twelve randomised controlled trials involving 4707 patients demonstrated a reduction in post-operative myocardial infarction, and a composite outcome of death, myocardial infarction and stroke (Ma et al, 2018).

Beta blockers

There is significant heterogeneity and controversy surrounding the results of randomised controlled trials of perioperative beta blocker use in non-cardiac surgery. The DECREASE studies were a prominent series examining perioperative beta blocker use which demonstrated benefit. However, major concerns subsequently arose surrounding trial conduct and fabrication of data, and the trial was subsequently discredited. A number of smaller trials produced neutral results, or showed modest benefit. The POISE trial enrolled 8351 patients with CV risk factors scheduled for high risk vascular surgery. There was a significant increase in post-operative mortality in the beta blocker arm, compared with placebo (Devereux *et al* 2008). Current ESC guidelines recommend that pre-operative beta blockade may be considered in patients with established ischaemic heart disease or myocardial ischaemia, or those at high clinical risk.

A number of medication classes have shown no evidence of benefit for reducing perioperative cardiac events, including nitrates, angiotensin converting enzyme inhibitors, calcium channel blockers and aspirin. (Auerbach *et al*, 2002; Hindler *et al*, 2006).

3.1.2 Pre-operative cardiovascular screening guidelines

Current guidelines differ significantly in their recommendations for cardiac screening (Table 3.1), including whether to screen asymptomatic patients, the number of clinical risk factors that should prompt further investigation, and the form of assessment. As a result, there is a huge variation in clinical practice between centres (Friedman *et al*, 2011).

3.1.3 Clinical risk prediction tools

Risk prediction tools provide a broad estimation of perioperative risk. They can be useful in determining the need for further cardiac evaluation and counselling patients regarding procedural risks. The Lee index is a widely used, validated tool for predicting risk prior to non-cardiac surgery (Lee *et al*, 1999).

Association	Guideline	Recommendations
The Renal Association	Assessment of the potential kidney transplant recipient 2011	No compelling evidence for use of pre-transplant screening. May be used to identify high risk patients for exclusion from transplant waiting list.
Academic College of Cardiology Foundation	Appropriate use of cardiac radionuclide imaging 2009	Appropriate prior to intermediate risk surgery in asymptomatic patients with >1 risk factor and poor functional capacity (<4 METS).
National Kidney Foundation	Clinical Practice guidelines for cardiovascular disease in dialysis patients 2001	Annual non-invasive testing for potential transplant recipients with diabetes mellitus or known ischaemic heart disease. Twice yearly assessments for those with >2 risk factors, left ventricular ejection fraction <40%, peripheral vascular disease
National Kidney Foundation/ Transplantation Society	Lisbon Conference 2007	Non-invasive testing in high risk patients with diabetes mellitus, known cardiovascular disease, multiple risk factors (> 1 year on dialysis, age >60 years, hypertension, dyslipidaemia, smoking, left ventricular hypertrophy)

Table 3.1 Current guidelines for pre-operative assessment in kidney transplant candidates

It was designed to predict post-operative myocardial infarction, acute heart failure and cardiac arrest. The six variables are shown in table 3.2. It has been found to have moderate discriminatory power in determining low vs high risk surgical candidates. It is less effective in patients undergoing vascular surgery. A newer risk prediction model was recently developed by the American College of Surgeons National Surgical Quality Improvement Program (Gupta *et al*, 2011). The risk factors were derived and validated using much larger datasets by those used in developing the Lee Index (>200,000 cases in both derivation and validation cohorts, vs <5000 in Lee Index). It is not a traditional scoring system, but provides an estimate of the probability of myocardial infarction or cardiac arrest in an individual patient. It was shown to be superior to the Lee index in predicting cardiovascular events up to 30 days post-operatively.

Lee Index	National Surgical Quality Improvement Program Myocardial Infarction or Cardiac Arrest (MICA) model
History of ischaemic heart disease	Type of surgery
History of heart failure	Functional status (Independent/partially dependent/fully dependent)
History of symptomatic cerebrovascular disease	Age
Treatment with insulin for diabetes	American Society of Anaesthesiologists (ASA) class.
Pre-operative creatinine >170µmol/L	Pre-operative creatinine >130 µmol/L
High risk surgery (Major cardiothoracic or vascular surgery, procedures > 4hours, emergency surgery)	

Table 3.2 Components of Lee Index and NSQIPM MICA risk prediction tools.

3.2 Diabetes and cardiovascular disease risk

Diabetes mellitus is a group of metabolic disorders in which persistent hyperglycaemia (random plasma glucose more than 11 mmol/L) is caused by deficient insulin secretion, resistance to the action of insulin, or both. Type 1 diabetes is defined as an absolute insulin deficiency due to T cell mediated

autoimmune destruction of pancreatic beta islet cells (American Diabetes Association, 2010). It is commonly identified in childhood or early adulthood. Cardiovascular events are more common and occur earlier in patients with type 1 DM than non-diabetics. There is an approximate 10 fold increase in age adjusted risk of cardiovascular disease in type 1 diabetics. For example, the incidence of major CV events in young adults is 0.98% per year, compared with an incident risk of first CV event of 0.1% in the general population (Secrest *et al*, 2010). Events occur on average 10-15 years earlier than in matched non-diabetic controls (Soedamah-Muthu *et al*, 2006). Sub-clinical CVD is also much more common in patients with type 1 DM, demonstrated by increased coronary artery calcification, sub-clinical carotid artery disease, and vascular endothelial dysfunction (Dabalea *et al*, 2006; Larsen *et al*, 2005; Costacou *et al*, 2005). Duration of diabetes is an important factor in terms of risk of CV events. A disease duration of >20 years is associated with an event rate of >3% per year (Secrest *et al*, 2010).

Type 2 diabetes is due to insulin resistance and a relative insulin deficiency, resulting in persistent hyperglycaemia. It accounts for >90% of all cases of diabetes worldwide (Morrish *et al*, 2008). It is most commonly diagnosed in middle aged and older patients, although can occur at younger ages, often associated with obesity. Cardiovascular disease is the leading cause of mortality in type 2 diabetes, with a two to fourfold increase in fatal and non-fatal myocardial infarction (Williams & Pickup, 2008). Patients who suffer a cardiovascular event have a poorer long term prognosis than non-diabetics. Type 2 DM rarely occurs as an isolated CV risk factor; it is more commonly associated with dyslipidaemia, hypertension, obesity and microalbuminuria. Insulin resistance is likely to play a central role in the development of this group of linked disorders, commonly referred to as the metabolic syndrome (World Health Organisation, 1999).

3.2.1 Differences in cardiovascular disease in type 1 and type 2 DM

Cardiovascular disease presents at a younger age in type 1 DM, and women are affected at rates equal to those in men. In terms of underlying pathophysiology, autopsy studies have shown that coronary lesions in type 1 DM are more soft and fibrous (Mountner *et al*, 1992). Type 2 diabetics have been found to have more obstructive lesions and more non-calcified lesions than patients with type 1 DM (Djaberi, 2009). Inflammation is considered a more prominent driver of atherosclerosis in type 1 diabetics. Studies have demonstrated higher inflammatory markers, including C-reactive protein, interleukin-6 and fibrinogen. (Scholin *et al*, 2004). Elevated inflammatory markers are associated with faster progression of coronary artery calcification, and a higher prevalence of coronary artery disease.

It is well established that surgery in patients with diabetes is associated with longer hospital stay, greater use of healthcare resources, and higher perioperative mortality. Elevated levels of glycosylated haemoglobin (HbA1c)—a marker of poor glycaemic control—are associated with worse outcomes in surgical and critical care patients (Marik *et al*, 2010).

3.3 Myocardial perfusion imaging prior to non-cardiac surgery

Myocardial perfusion imaging (MPI) is an established tool for the assessment of patients prior to non-cardiac surgery. A meta-analysis of dipyridamole stress MPI prior to vascular surgery in high risk patients found that the extent of reversible ischaemia was associated with perioperative cardiac events (Etchells *et al*, 2002). Whether MPI is helpful as a stratification tool prior to renal transplantation listing remains debatable. A recent prospective study found that MPI has a sensitivity of just 53% for detecting obstructive coronary disease, significantly lower than computed tomography angiography (Winther *et al*, 2015). The gold standard used was coronary angiography, which leads to inherent limitations when attempting to directly compare anatomical and functional tests. Furthermore the study used vasodilator stress, and did not examine clinical outcomes. Studies that have assessed the prognostic value of thallium perfusion imaging prior to RT found that an abnormal perfusion scan is associated with increased risk of perioperative myocardial infarction (MI) and cardiac death (Rabbat *et al*, 2003). No prior studies have examined how MPI results affect decisions regarding suitability for transplantation.

Hypothesis

1. Dobutamine stress myocardial perfusion imaging using Technetium 99m sestamibi provides additional prognostic information to clinical risk factors alone for predicting both all-cause mortality and cardiovascular events in patients with end-stage renal disease being considered for renal transplantation.
2. The identification of myocardial ischaemia or infarction on myocardial perfusion scans using Technetium 99m sestamibi predict an increased risk of cardiovascular events and all-cause mortality in patients with end-stage renal disease being considered for renal transplantation.
3. Perfusion abnormalities detected with myocardial perfusion imaging correlate with coronary artery disease on subsequent invasive coronary angiography.
4. Dobutamine stress studies are safe in patients with end stage renal disease
5. A risk prediction score incorporating clinical risk factors and perfusion scan findings will accurately stratify patients with end stage renal disease for determination medium to long term risk of cardiovascular events and all-cause mortality.

Methods

We conducted a retrospective review of the use of myocardial perfusion imaging (MPI) for transplant assessment in a tertiary referral centre serving a population of approximately 1.2 million.

Patients were seen in a dedicated renal transplant assessment clinic by a nephrologist, who referred patients directly for MPI scans.

Technetium 99m- sestamibi was the radiotracer used in all studies. The choice of stress agent was at the discretion of the physician conducting the test. As the majority of studies were performed by a single operator, dobutamine was the used in the majority of cases. A standard 2 day stress-rest imaging protocol was employed. During the stressing component, patients received continuous ECG monitoring and non-invasive blood pressure measurement at 2 minute intervals. Dobutamine was infused at an initial dose of 10mcg/kg/min, with a stepwise increase every 3 minutes to a peak dose of 40mcg/kg/min. Atropine was administered in 600mcg boluses, up to a maximum of 1.2mg in patients that had not achieved 85% target heart rate on maximum dose dobutamine. Images were acquired 45 minutes following tracer injection in an attempt to minimize hepatic and gastrointestinal uptake artefact, with an Infinia Hawkeye gamma camera (GE Healthcare, Milwaukee, Wisconsin, USA). Resting images were acquired using the same imaging protocol on a separate day. Referral to a cardiologist for consideration of further investigation was at the clinical discretion of the treating nephrologist.

All patients undergoing MPI as part of a kidney or kidney-pancreas transplant assessment between January 2005 and June 2012 are included in the study. A hand search of paper copies of all scan reports between these dates was performed, and those with the appropriate indication selected. A standard data collection proforma was used: demographic and clinical information was obtained from the request card and clinic letters stored on the hospital Patient Centre electronic database. Clinical information obtained included aetiology of renal disease, dialysis modality, history of previous renal transplants, co-morbidities (hypertension, diabetes, previous cardiac events, prior stroke, peripheral vascular disease, respiratory disease, prior percutaneous coronary intervention (PCI) or coronary artery bypass grafting (CABG), and medications).

Electrocardiogram (ECG) data collected included heart rate, QRS duration and, presence of left ventricular hypertrophy (LVH). An abnormal ECG was identified if any of the following

were present on the trace: any non-sinus rhythm, pathological Q waves, left or right bundle branch block, ST depression or T wave inversion, or LVH as defined by Sokolow-Lyon criteria (de Vries *et al*, 1996). Baseline and peak heart rate and blood pressure were recorded, in addition to percentage of target age predicted heart rate achieved, and ECG evidence of ischaemia or arrhythmias.

Available scans were reanalysed to obtain the following variables: LV volumes and ejection fraction during both stress and rest studies; sum stress score, sum difference score, sum rest score, sum motion score; presence and location of fixed and reversible perfusion defects and their size as a percentage of total left ventricular area. The summed scores are a validated semi-quantitative method of assessing the extent and severity of perfusion defects, calculated automatically by the Cedars Sinai QGS/QPS analysis software using a 17 segment model (Leslie *et al*, 2005). Each myocardial segment is scored on a scale of 0 to 4, with 0 being normal tracer uptake, and 4 indicating a complete absence of tracer. The score for each segment is added together. Sum stress score is the calculated value from stress images, and conversely sum rest score from the resting images. A sum stress score of less than 4 is normal, whereas a score of greater than 13 is severely abnormal according the Cedars-Sinai classification system. Sum difference score is calculated by subtracting the SRS from SSS. Sum motion score is a measure of left ventricular function that incorporates wall motion and thickening in each myocardial segment (figure 3.1).

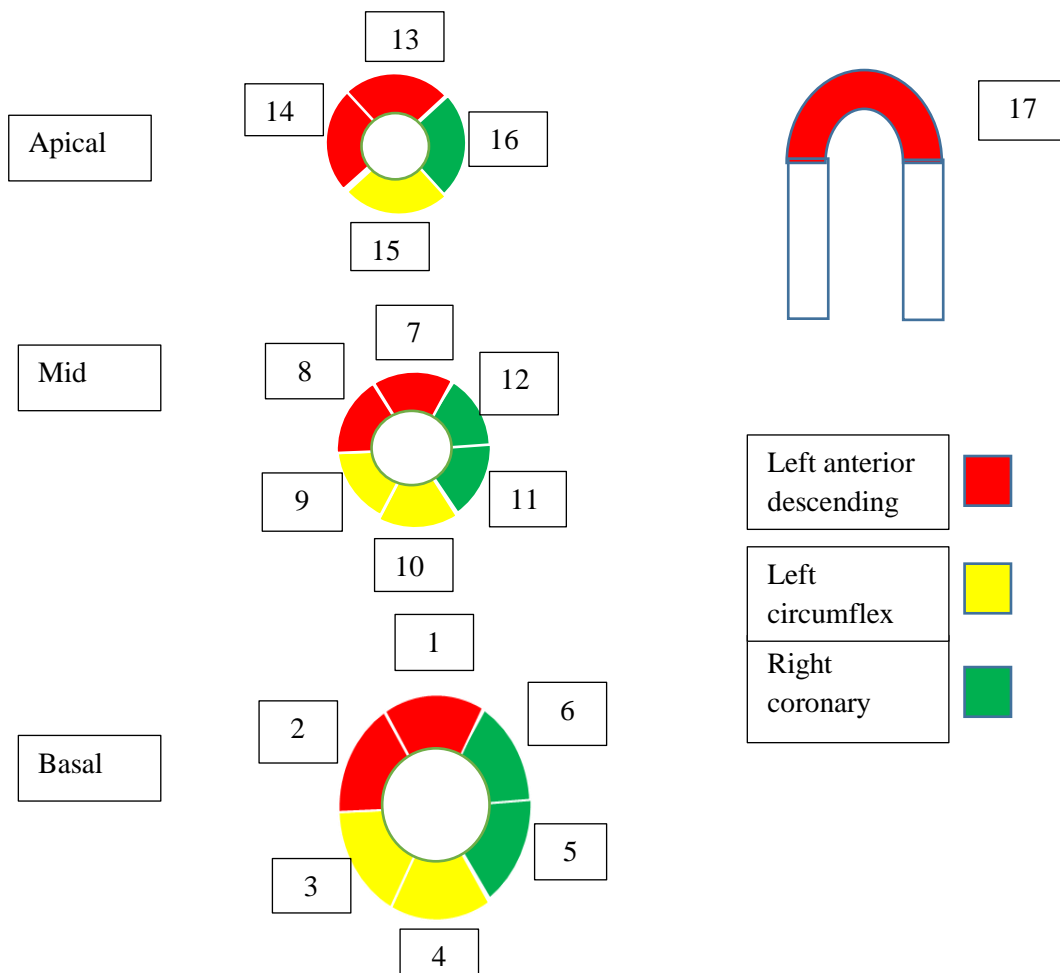
Follow up data was obtained from Patient Centre (iSOFT, Banbury UK) electronic database and included further cardiac investigations undertaken, specifically invasive coronary angiogram, cardiac magnetic resonance imaging, computed tomography coronary angiogram.

The decision of the transplant team as to whether the patient was deemed suitable for renal transplantation was recorded. In those patients deemed not suitable, the reason for this decision was documented, further categorised into cardiac or non-cardiovascular reasons. Date of transplant and type of transplant (deceased donor, live donor, and combined kidney-pancreas) were recorded.

Clinical events were defined as;

Myocardial infarction (MI) – According to the third universal definition of MI (Tehrani *et al*, 2013)

Elevated serum Troponin levels plus at least one of the following; -Symptoms of myocardial ischaemia (chest pain, breathlessness, diaphoresis, epigastric discomfort)



1.Basal anterior	7.Mid anterior	13.Apical anterior
2.Basal anteroseptal	8.Mid anteroseptal	14.Apical septal
3.Basal inferoseptal	9.Mid inferoseptal	15.Apical inferior
4.Basal inferior	10.Mid inferior	16.Apical lateral
5.Basal inferolateral	11.Mid inferolateral	17.True apex
6.Basal anterolateral	12.Mid anterolateral	

Figure 3.1 Seventeen segment model Regions of the left ventricle and supplying coronary arteries

- New ST-segment or T-wave changes or new left bundle branch block on ECG
- Development of pathologic Q waves on ECG
- Imaging evidence of new loss of viable myocardium or new wall-motion abnormality
- Finding of an intracoronary thrombus by angiography or autopsy

Coronary revascularisation – Coronary artery bypass grafting, insertion of an intracoronary stent, balloon dilation of stenosed vessel, intracoronary thrombus aspiration

Stroke - defined as an acute episode of focal or global neurological dysfunction caused by brain, spinal cord, or retinal vascular injury as a result of haemorrhage or infarction.

Peripheral vascular disease - Significant (>50%) narrowing of one or more arteries supplying the upper or lower limbs, leading to symptomatic claudication, acute ischaemia, or requiring vascular intervention (balloon dilation, insertion of an arterial stent, embolectomy, or amputation).

Heart failure hospitalisation defined as an event that meets ALL of the following

Criteria (Modified from the CDISC standard definition, 2014):

- The patient is admitted to the hospital with a primary diagnosis of heart failure
- The patient's length-of-stay in hospital extends for at least 24 hours
- The patient exhibits documented new or worsening symptoms due to HF on presentation including at least ONE of the following:
 - a. Breathlessness
 - b. Decreased exercise tolerance
 - c. Fatigue
 - d. Other symptoms of worsened end-organ perfusion or volume overload
- The patient has objective evidence of new or worsening HF from physical examination, radiological findings and/ or elevation of natriuretic peptides.

Biopsy proven acute rejection- Grade II or III acute rejection according to the Banff working classification of kidney transplant pathology (Solez *et al*, 2003)

Cardiovascular death- Death resulting from an acute myocardial infarction (MI), sudden cardiac death, death due to heart failure (HF), death due to stroke, death due to cardiovascular (CV) procedures, death due to CV haemorrhage, and death due to other CV causes.

Non-cardiovascular death- Defined as any death with a specific cause that is not thought to be cardiovascular in nature, as listed above.

Ethical Approval

The study was part of the service evaluation and quality improvement programme and received favourable opinion from the Hull and East Yorkshire Hospitals NHS Trust Clinical Governance and Audit department with approval number 3239.

Statistical Analysis

The two primary endpoints used in our analyses were;

1. Death due to any cause (cardiovascular or non-cardiovascular)
2. The combined endpoint of all-cause mortality and cardiovascular events

Cardiovascular events were defined as myocardial infarction, ischaemic stroke, and heart failure requiring hospitalisation (as defined in previous section). Mean values and interquartile ranges were calculated for continuous variables. Kaplan Meier survival curves were constructed to show all-cause mortality and cardiac events stratified by MPI findings, transplant suitability and sum stress score. Differences between groups were assessed by the log-rank test. Chi squared tests were used to compare clinical characteristics between transplanted and non-transplanted groups. Univariable analysis with Cox proportional hazards were used to test for an association between clinical/scan variables and all-cause mortality and the combined endpoint of all-cause mortality and cardiovascular events. All variables with a $p < 0.2$ were included in a subsequent multivariable analysis using Cox proportional hazards.

Results

One hundred and forty nine scans and reports were identified, performed between 03/10/2003 and 13/05/2012. Complete follow up data was available for 138 patients (6 patients moved area, 2 patients had 2 scans, 3 died during transplant assessment). These patients were

included in the final analysis. Damage to the optical discs containing the data of 18 scans meant that 120 sets of images were available for calculation of summed scores and LV volumes. The mean age of the 138 patients was 53.2, standard deviation (SD) 10.36, 95 (69%) were male, 43 (31%) female. One hundred and seventeen scans (85%) were for a first transplant assessment, 21 (15%) for previously failed graft recipients. Diabetes was the most common cause of renal failure, accounting for a third of cases. Baseline characteristics are shown in table 3.3, patient flowchart in figure 3.2.

3.8.1 Cardiac Stress Testing

One hundred and thirty patients (94%) received dobutamine stress, 4 (2.9%) received adenosine, 1 underwent exercise stressing, 1 received dipyridamole. As this was a pragmatically designed study with the principal aim of evaluating the role of myocardial perfusion imaging, I included the patients receiving all types of stress in the final analysis. Two patients had a rest only scan as further invasive investigations were already planned. Median peak dobutamine dose was 40micrograms/kilogram/minute, median peak adenosine dose was 600micrograms.

3.8.2 Scan results

Mean left ventricular ejection fraction (LVEF) at rest was 58.5% (SD 8.7%), and 56.6% (10.3%) post stress. There was a mean decrease in LVEF from rest to stress of 1.9% (5.7%). The tests were interpreted as normal in 77/138 patients (55.8%), as showing a significant fixed defect in 10/138 (7.2%), reversible defects in 51/138 (37%). Defect sizes and summed scores are shown in table 3.4.

3.8.3 Subsequent investigation

Ninety eight patients (71%) had no further investigations, 39 (28%) underwent diagnostic angiography, 1 patient refused further investigation. Fourteen angiograms (36%) demonstrated epicardial coronary disease that correlated with the MPI findings, but in 25 (64%) the angiogram findings did not correlate with the MPI findings. Five patients underwent PCI, two underwent CABG. One patient died whilst awaiting CABG.

3.8.4 Renal transplantation

Forty six patients (33.3%) underwent kidney transplantation, of whom 6 subsequently suffered graft loss. 49 (35.5%) are still active or currently suspended on the transplant list.

Reasons for suspension were: Stable/improving renal function, infected leg ulcers, required to lose weight prior to surgery, undergoing anaemia investigation, and awaiting other surgical

procedures. Forty three patients (31.1%) were deemed not suitable for transplantation. Reasons for not transplant listing are shown in figure 3.3.

Baseline Characteristic	Not suitable n=43	Transplanted +active n=95	P value
Age years	57.3	50.69	0.004
Male sex %	65.1	70.5	0.53
BMI	27.5	26.4	0.24
1 st transplant%	88.4	79	0.43
Type 1 DM %	25.6	29.5	0.64
Type II DM %	11.6	7.4	0.56
Hypertension %	76.7	60	0.46
Vascular %	11.6	9.5	0.70
MI %	4.6	6.3	0.70
Angina %	4.6	3.2	0.66
PCI %	0	3.2	0.24
CABG %	4.6	2.1	0.41
Haemodialysis %	60.5	51.6	0.44
Peritoneal dialysis	18.6	18.9	0.74
Pre-dialysis %	20.9	29.5	0.25
Aspirin use %	39.5	29.5	0.20
Statin use %	46.5	33.7	0.20
>1 BP agent %	46.5	60	0.11
Abnormal ECG %	34.9	35.8	0.78

Table 3.3 Baseline characteristics according to transplant suitability

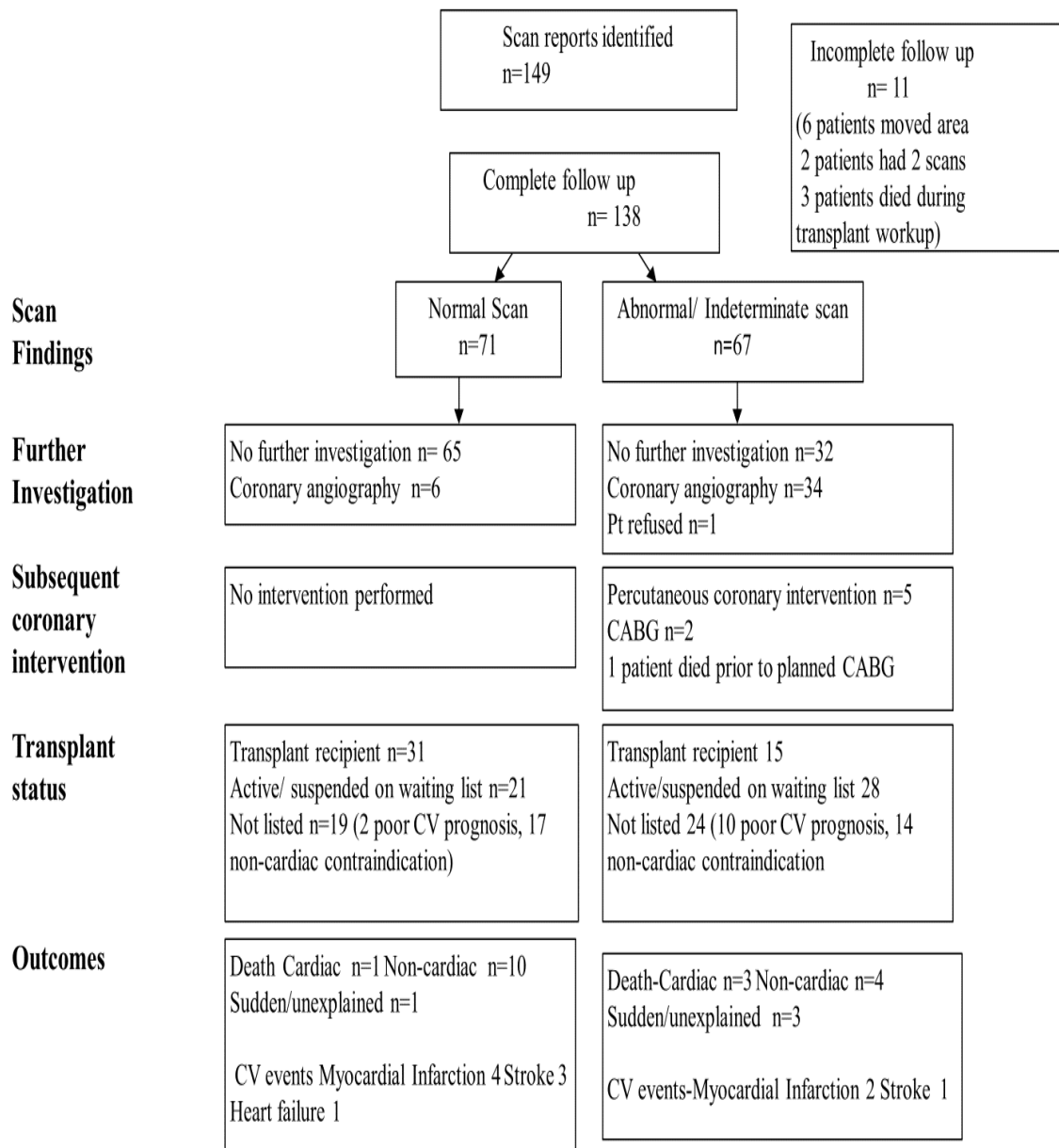


Figure 3.2 Study flowchart and patient outcomes

		No. (percentage)
Sum rest score N=120	0 – 4 (Normal)	107 (89.2)
	5 – 8 (Mildly abnormal)	9 (7.5)
	9 – 13 (Moderately abnormal)	4 (3.3)
	>13 (Severely abnormal)	0
Sum stress score N=118 (2 rest only scans)	0 – 4	80 (67.7)
	5 – 8	27 (22.9)
	9 – 13	7 (5.9)
	>13	4 (3.4)
Sum difference score N=118	0 – 4	85 (72)
	5 – 8	25 (21.2)
	9 – 13	5 (4.2)
	>13	3 (2.5)
Sum motion score N=120	0 – 4	61 (50.8)
	5 – 8	20 (16.7)
	9 – 13	12 (10)
	>13	27 (22.5)

Table 3.4 Perfusion Imaging findings

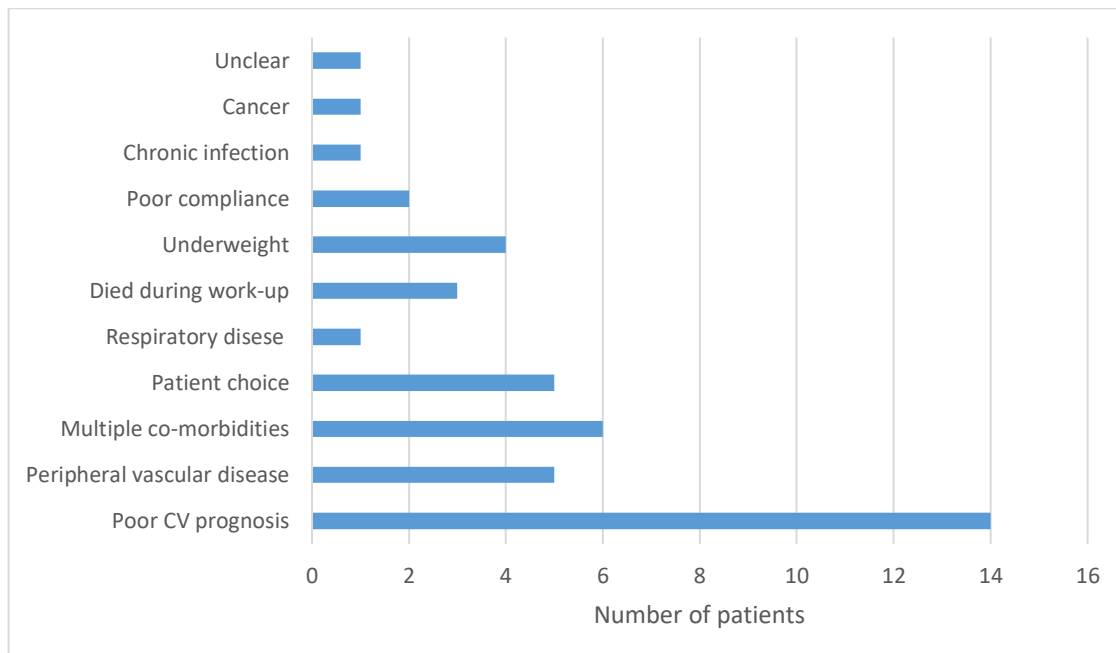


Figure 3.3 Reasons for not transplanting

3.8.5 Mortality

During a median follow up of 40.4 months, 21 (15.2%) patients died, 4 from cardiac causes, 13 from non-cardiac causes. Four deaths were sudden and unexplained.

3.8.6 Cardiovascular events

Eleven confirmed cardiovascular events occurred during the follow up period, 6 myocardial infarctions, 4 strokes, and 1 heart failure hospitalisation.

3.8.7 Factors associated with increased mortality

On univariable analysis, abnormal baseline ECG ($p=0.041$), higher sum rest score ($p=0.008$), and decision not to transplant ($p=0.005$) were associated with increased mortality.

Multivariable analysis included transplant indication, prior myocardial infarction, QRS duration, resting systolic blood pressure, decision to transplant, change in left ventricle end systolic volume, post stress ejection fraction, percentage fixed defects, sum rest score, sum motion score and abnormal ECG. Patients who were accepted for transplant had a significantly lower all-cause mortality ($p<0.001$). Greater left ventricular dilation (measured in systole) between rest and stress scans was associated with reduced survival ($p=0.03$). Higher sum rest scores ($p=0.002$) and an abnormal baseline ECG ($p<0.001$) were also associated with increased all-cause mortality on multivariable analysis.

3.8.8 Factors associated with mortality and cardiovascular events

On analysis, abnormal baseline ECG ($p=0.011$), QRS duration ($p=0.038$), transplant indication ($p=0.028$), sum rest score (0.019), and decision not to transplant ($p=0.025$) were associated with increased mortality and cardiovascular events. Multivariable analysis included age, indication, extra-cardiac vascular disease, QRS duration, abnormal ECG, change in left ventricular end systolic volume, change in left ventricular end diastolic volume, percentage fixed defect, sum stress score and sum rest score. An abnormal ECG was the only factor significantly associated with increased mortality and cardiovascular events combined ($p<0.001$)

3.8.9 Mortality and CV event rates by MPI findings

Patients with fixed perfusion defects were at an increased risk of cardiovascular events and all-cause mortality, although this did not reach statistical significance. Log rank for mortality $p=0.17$, mortality and CV events $p=0.06$. Kaplan Meier survivor curves are shown in figures 3.4 and 3.5.

3.8.10 Mortality and CV event rates by transplant suitability

There was a significantly lower mortality and cardiac event rate in those that underwent kidney transplantation, or are currently active/ suspended on the list, when compared with those deemed not suitable for transplant. Log rank $p < 0.001$ for both mortality, and CV events + mortality combined. Kaplan Meier survival curve for all-cause mortality and CV events shown in figure 3.6.

3.8.11 Mortality and CV events by Sum Stress Score

When sum stress score was analysed as a categorical variable, there was a significantly higher combined mortality and cardiac event rate in patients with moderate to severe stress perfusion defects (SSS>8). Log rank for all-cause mortality + CV events

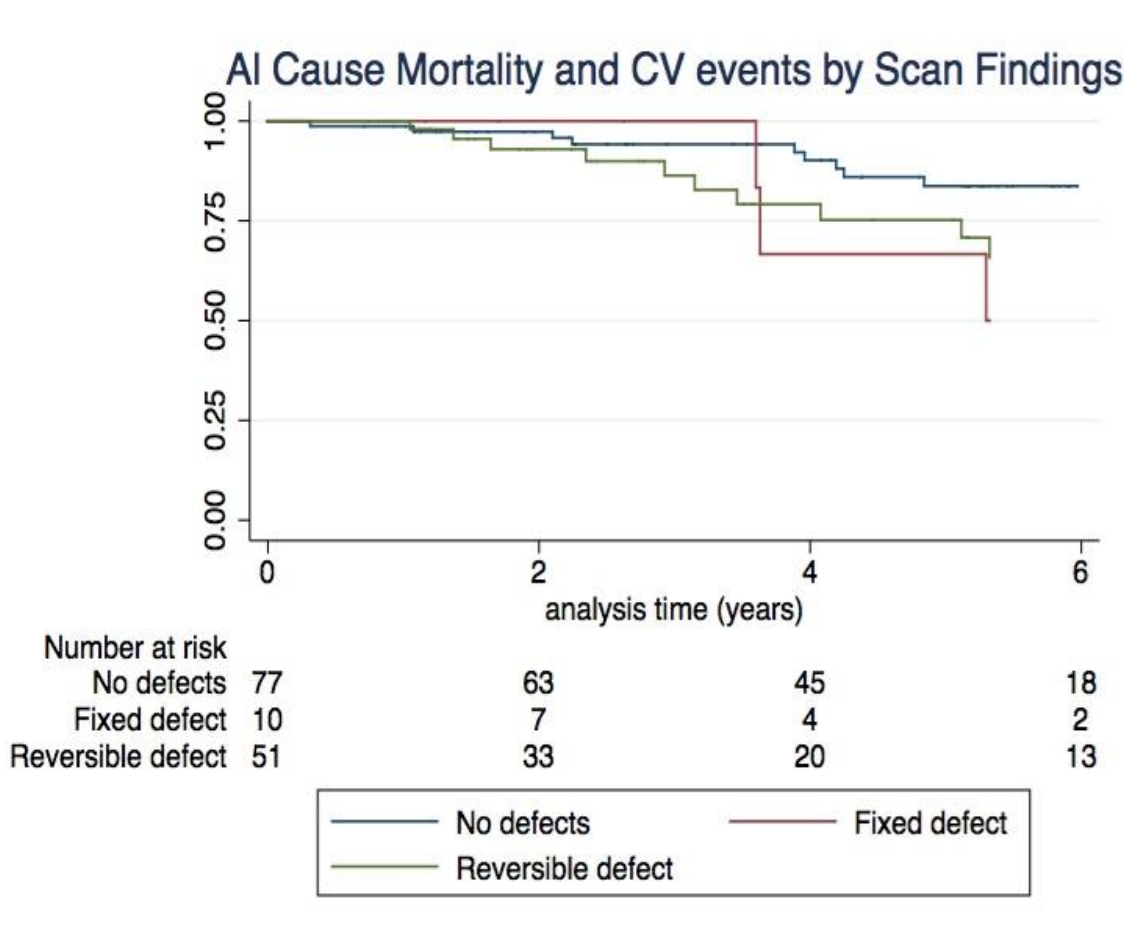


Figure 3. 4 Survival curves for all-cause mortality by scan findings



Figure 3.5 Survival curves for all-cause mortality and CV events by scan findings

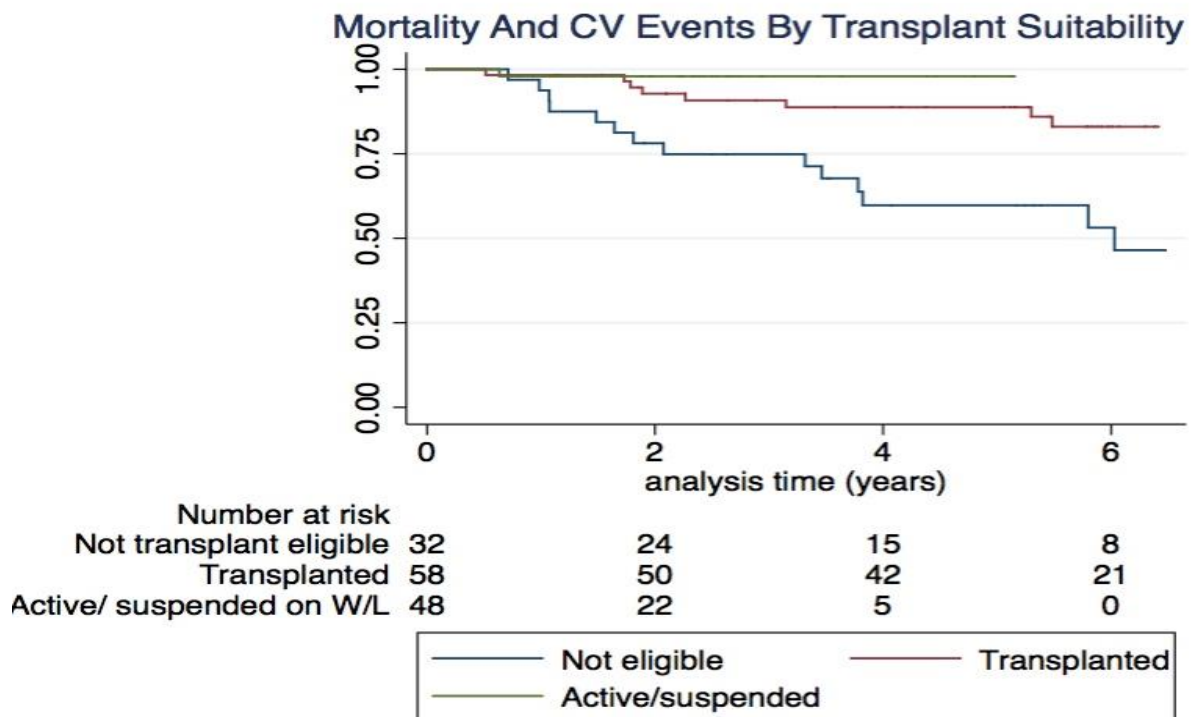


Figure 3.6 Mortality and CV events by transplant suitability

combined $p=0.028$. Kaplan Meier curve shown in figure 3.7. Eleven patients had moderate to severe defects; two of these patients underwent CABG, 3 were deemed unsuitable for RT due to their cardiovascular status, 1 died of cardiovascular causes, and 1 suffered a stroke.

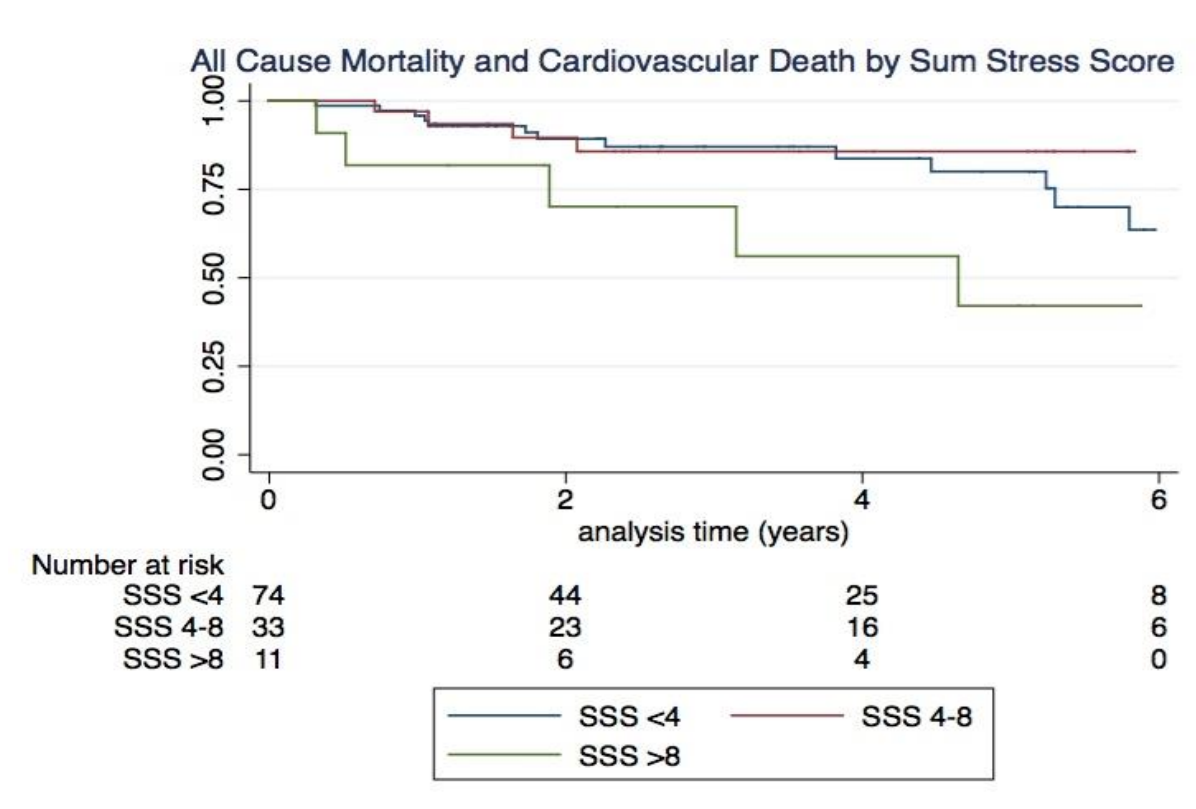


Figure 3.7 Survival curves of all-cause mortality and CV events by sum stress score

3.9 Risk scores

As a *post hoc* analysis, I examined the ability of risk scores that incorporate established cardiovascular risk factors and test findings to predict future cardiac events in this population. For the purposes of this analysis I assessed the following outcomes;

- All-cause mortality
- The combined endpoint of death due to cardiac causes, non-fatal myocardial infarction, new onset angina, and post-transplant coronary revascularisation (percutaneous coronary intervention/coronary artery bypass grafting).

The initial risk score incorporated 3 factors: age over 50, past history of cardiac disease (prior myocardial infarction, angina, revascularisation), and presence of diabetes. Although none of

these factors were significantly associated with adverse outcomes in this study, they are well established risk factors for both mortality and cardiovascular events in ESRD In larger registries (O'Hare *et al* 2007; Churchill *et al* 1992; Kahn *et al*, 2011).

An abnormal ECG was an independent predictor of both outcomes in our study, therefore its impact on risk discrimination was assessed. The definition of an abnormal ECG is described above.

Hypertension is associated with increased cardiovascular risk in the general population, and is an important contributor to the development of renal failure. In patients with established end stage renal failure, there is a u-shaped relationship between blood pressure and outcomes, as low blood pressure is associated with increased mortality. We assessed the impact of incorporating treated hypertension into the risk prediction model. In our cohort, diabetes was more prevalent in younger patients. As age is consistently the strongest predictor of outcomes in epidemiological studies, there may be confounding between age and diabetes, therefore I included a model with diabetes removed.

I assessed the additive impact of the presence of an abnormal perfusion scan in determination of risk. I separately assessed the impact of including only moderate to severe perfusion defects (sum rest score or sum difference score >8), given that these were associated with adverse outcomes. For each risk score, all factors were given equal weighting, with the presence of a risk factor or abnormality allocated 1 point, and the absence scoring 0 points. A logistic regression model was used to assess binary outcomes. Non-parametric receiver operating curves were created for each risk score analysed, and compared using Chi² test, with a significance level of 0.05.

Risk scores	Factors
ACD	Age, Cardiac disease history, Diabetes
ACDE	Age, Cardiac disease history, Diabetes, ECG abnormality
ACE	Age, Cardiac disease history, ECG abnormality
ABCDE	Age, elevated Blood pressure Cardiac disease history, Diabetes, ECG abnormality
ABCDE + P	Age, elevated Blood pressure Cardiac disease history, Diabetes, ECG abnormality, Perfusion abnormality
ABCDE + MP	Age, elevated Blood pressure Cardiac disease history, Diabetes, ECG abnormality, Moderate-Severe Perfusion abnormality

Table 3.5 Risk scores assessed

3.9.1 Results

There were 21 deaths due to any cause and 10 cardiac events (4 confirmed cardiac death, 6 non-fatal MI) during the follow up period.

The risk score with best discrimination for predicting both all-cause mortality and cardiovascular events in our cohort was the ACDE score (ROC area 0.701 for all-cause mortality, 0.813 for cardiovascular events). There was a statistically significant difference in ROC areas for cardiovascular events, whereas this did not reach statistical significance for all-cause mortality, tables 3.6, 3.7, figure 3.8. Addition of the perfusion scan findings to the score reduced its discriminatory ability (ROC area 0.666 for all-cause mortality, 0.760 for cardiovascular events).

Score	ROC area	Standard Error
ACD	0.646	0.094
ACDE	0.701	0.092
ACE	0.694	0.086
ABCDE	0.666	0.092

Table 3.6 ROC areas for a range of risk scores for predicting all-cause mortality

Score	ROC area	Standard Error
ACD	0.731	0.093
ACDE	0.813	0.092
ACE	0.777	0.086
ABCDE	0.760	0.093

Table 3.7 ROC areas for a range of risk scores for predicting all-cause mortality and CV events

A score that incorporated only moderate to severe perfusion defects, as defined by sum stress and rest scores >8, did not provide additional discriminatory power to the ACDE score for both endpoints (ROC area 0.71 vs 0.687 for mortality, 0.772 vs 0.778 for CV events), see figures 3.9 and 3.10. The ROC area for ACDE is lower in this comparison. This is because it only included patients that had calculated sum scores (122 patients vs 138 patients in the initial ROC analysis)

The discriminatory ability for each risk score was higher for predicting cardiovascular events than all-cause mortality, as would be expected.

Figures 3.11 and 3.12 illustrate the Kaplan Meier survival curves for each risk score in the ACDE score, for both all-cause mortality and cardiac events.

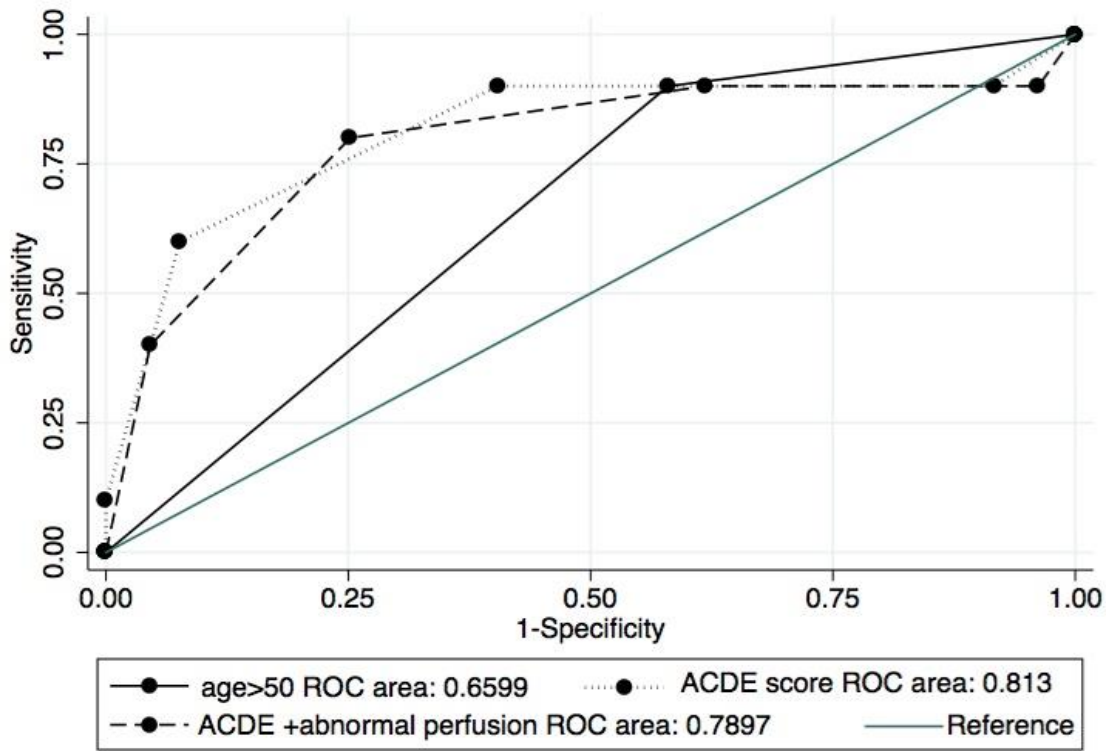


Figure 3.8 ROC analysis comparing ACDE score (age>50, known cardiac disease, diabetes, abnormal ECG), and a risk score incorporating ACDE score plus any reported abnormality on perfusion imaging for predicting cardiac events.

There is clear separation in the risk scores; patients with scores of 0 or 1 have improved survival and freedom from cardiac events than those with scores of 2 or more. Ninety percent of cardiac events occurred in patients with a score of 2- 4, occurring in 9/61 patients (14.8%). Conversely, in patients with a score of 0 or 1, there was only one event in 77 patients (1.2%).

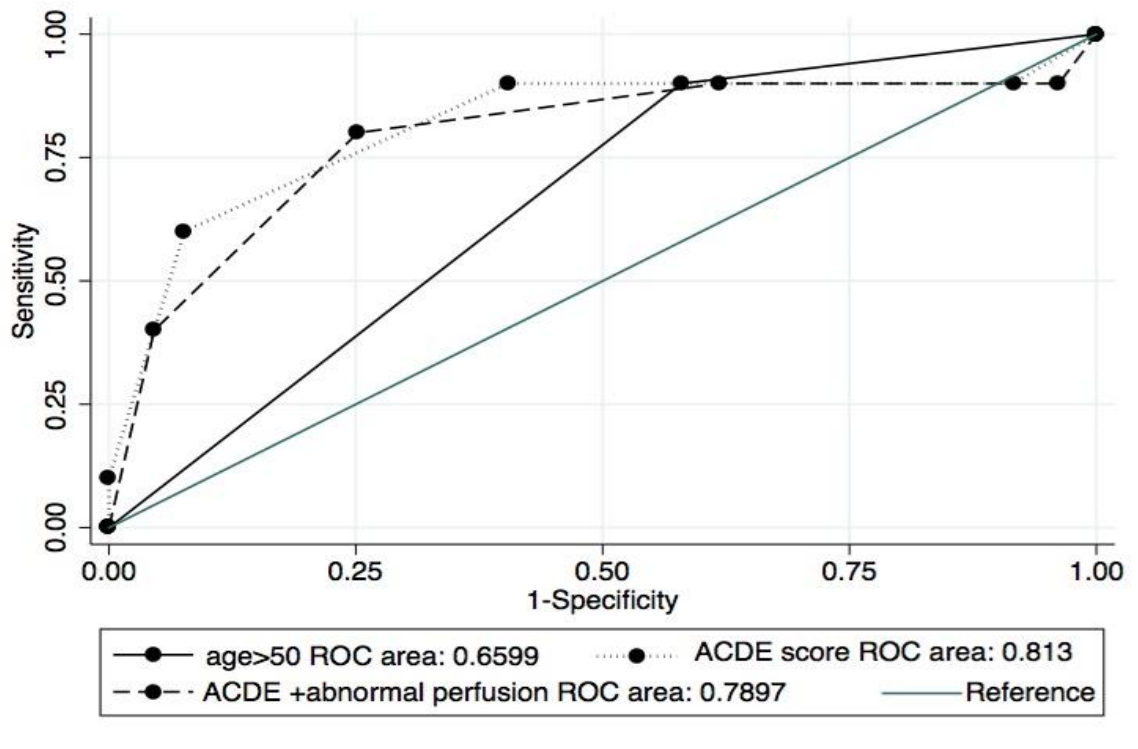


Figure 3.9 ROC analysis comparing ACDE score (age>50, known cardiac disease, diabetes, abnormal ECG), and a risk score incorporating ACDE score plus any reported abnormality on perfusion imaging for predicting cardiac events.

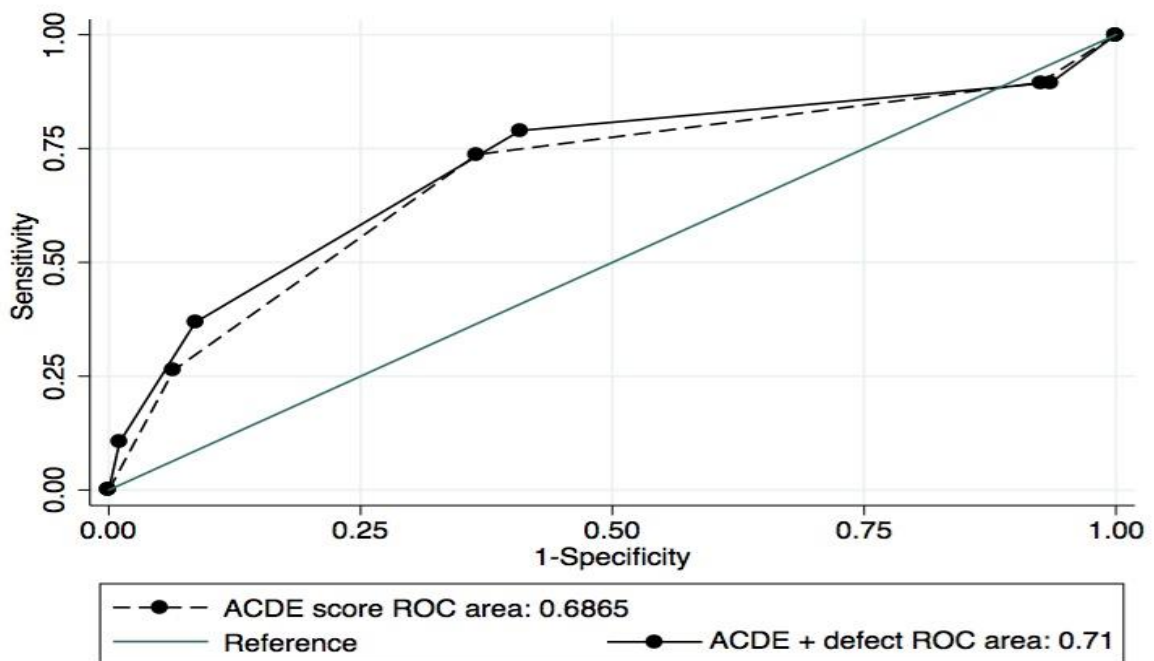


Figure 3.10 ROC analysis comparing ACDE score (age >50, known cardiac disease, diabetes, abnormal ECG) with a score incorporating ACDE plus a resting or stress perfusion defect >8 on sum score for predicting all-cause mortality

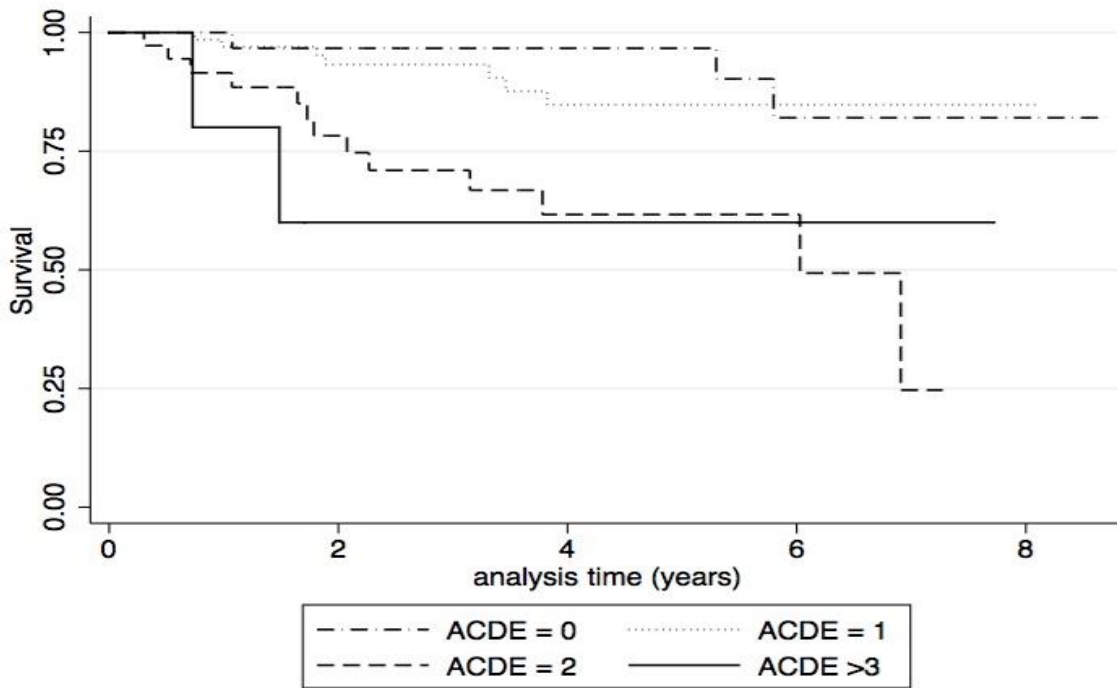


Figure 3.11 Kaplan Meier curves of all cause mortality stratified by ACDE score

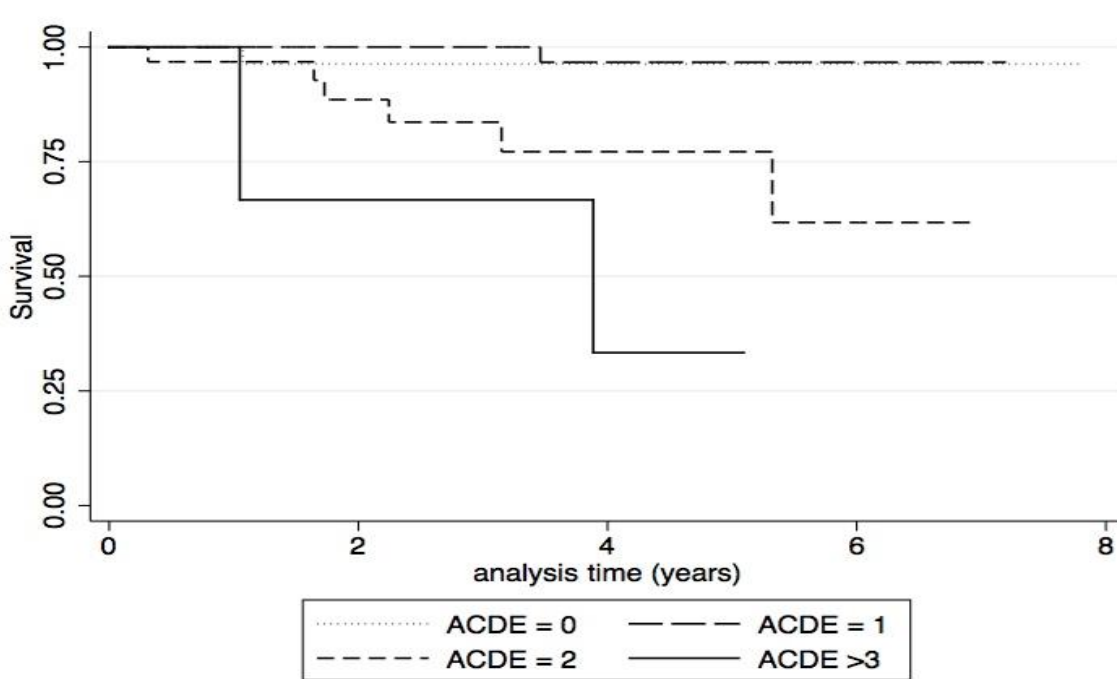


Figure 3.12 Kaplan Meier curves of all cardiovascular events stratified by ACDE score

3.10 Discussion

The presence of an abnormal MPI scan was not predictive of mortality or cardiac events, when an abnormal scan was defined as any reported, non-artefactual, perfusion defect. Patients with larger stress and resting perfusion defects were shown to have reduced survival, and an increased risk of cardiovascular events. Patients with mild perfusion defects appear to have a similar risk of adverse events as those with normal scans.

Two recent retrospective studies of pre-transplant patients in USA and Australia also found that the presence of an abnormal scan in itself was not associated with an increased risk of major adverse outcomes, although the latter group did find an increased rate of ‘softer endpoints’ (unstable angina, coronary revascularisation) (Chew *et al*, 2013; De Lima *et al*, 2012).

Higher sum rest scores in MPI analysis, which are typically suggestive of prior myocardial infarction, were associated with increased mortality on multivariable analysis. Interestingly, a clinical history of myocardial infarction was not associated with increased mortality. This may have been due to the low rates of prior infarction in this cohort, meaning that the analysis lacked power to detect a difference. A significant proportion of myocardial infarctions are clinically silent, particularly amongst diabetic and hypertensive patients, and are associated with higher mortality (De Luca *et al*, 2006). MPI has the ability to detect these prognostically important defects, although it is possible that a significant proportion of these could be detected on 12 lead ECG or transthoracic echocardiography. ECG abnormalities were indeed a strong independent predictor of mortality in our cohort.

Moderate to severe perfusion defects as measured by sum stress score were associated with an increase in rates of the combined endpoint of all-cause mortality and cardiac events. Hakeem *et al* (2008) previously showed that defects of at least moderate severity are poor prognostic markers in chronic renal failure. A prior meta-analysis by Rabbat (2003) of thallium scintigraphy prior to renal transplantation demonstrated a six-fold increased risk of myocardial infarction and fourfold increase in cardiac death in patients with reversible defects. In our study there were only eleven patients with moderate to severe defects; the majority of CV events and deaths occurred in patients with SSS less than 8, making it an insensitive prognostic marker.

Abnormalities on MPI correlated with coronary angiogram findings in 40% of cases. MPI has been shown to have lower performance in identifying epicardial coronary artery disease for

patients with ESRD compared with the general population, with sensitivities and specificities varying from 37-90% and 40-90% respectively (Lentine *et al*, 2010). MPI is a functional measure of myocardial perfusion, whereas angiography is an anatomical assessment and they are therefore not wholly equivalent tests. Microvascular coronary disease affects 20-25% of patients with renal failure, which may result in reversible perfusion abnormalities in the absence of large vessel coronary disease (Rostand *et al*, 1991). Furthermore, technetium 99m uptake into myocardial tissue is dependent on mitochondrial function, which is impaired in ESRD, and may also result in perfusion abnormalities (Victor *et al*, 2011). A strategy of routine coronary angiography in all patients may lead to high rates of contrast nephropathy, which would be particularly detrimental at the pre-dialysis stage. This should be reserved for patients at high risk or with symptoms. A non-invasive assessment would be a more appropriate screening test for those at intermediate risk, whereas there is currently no compelling evidence for testing in asymptomatic low risk patients.

A significantly longer life expectancy was seen in those considered suitable for transplantation, compared with those deemed unsuitable. This suggests that the assessment process appropriately selects patients that survive longer, and thus have the greatest potential to benefit from transplantation. RT itself confers a prognostic benefit, however improved survival was also seen in those still awaiting transplantation, suggesting that this did not significantly influence the findings. The patients considered suitable were younger, but otherwise similarly matched in terms of co-morbidities. This suggests that there may be features other than classical risk factors which are important when determining the appropriateness of transplantation, such as frailty and treatment compliance. Therefore, a detailed clinical evaluation undertaken by experienced physicians remains the most important part of the assessment process. In almost one third of cases, cardiovascular disease was the primary reason for transplant non-suitability; the MPI findings played a key role here in determining suitability.

In our study, 5.6% of patients were referred for revascularisation procedures, which is in line with rates from previous studies by Chew (2013) and DeLima (2012). Revascularisation of asymptomatic patients prior to non-cardiac surgery remains a contentious issue. Large randomised trials have failed to show a benefit from revascularisation in patients prior to major vascular surgery (McFalls *et al*, 2004; Poldermans *et al*, 2007). Renal transplantation is considered an intermediate risk surgical procedure, and current ESC guidelines state that prophylactic myocardial revascularisation is not recommended in those with proven ischaemic heart disease prior to low to intermediate risk surgery (class III, level of evidence

B) (Poldermans *et al*, 2009). One randomised trial of prophylactic revascularisation has been undertaken in patients with ESRD, which demonstrated that adverse cardiac event rates were lower in those that underwent revascularisation compared with the medically managed group (Manske *et al*, 1992). This was a small trial of twenty six patients, with short follow up, and suboptimal use of evidence based medical therapies. Further large scale randomised controlled trials are required to establish the effectiveness of prophylactic revascularisation in this high risk group.

Evaluation of a range of risk prediction models identified a score incorporating age, history of cardiac disease, presence of diabetes, and presence of ECG abnormalities as providing good accuracy for predicting cardiac events, with a ROC area of >0.8 , and fair accuracy for all-cause mortality at >0.7 . A score that incorporated the perfusion scan findings did not add to the accuracy of the score, even when only significant defects were included. The number of fatal and non-fatal cardiac events in this group was low, and these risk prediction tools would need to be validated in larger prospective cohorts. Chew *et al* also performed a risk stratification using age >50 , presence of diabetes and history of CV disease. They found, similarly, that there was clear separation between groups in terms of risk of adverse CV outcomes. Those with 1 risk factor did gain incremental benefit from the MPI study, whereas patients with no risk factors had very low event rates irrespective of scan findings. Equally, the high risk patients did not gain additional prognostic information for the scan.

The findings of our retrospective study add further support for a targeted, risk factor based approach to selecting patients for additional CV imaging prior to renal transplantation, in line with both the American College of Cardiology and National Kidney Foundation/Transplantation guidelines. This would reduce radiation exposure for low risk patients, and reduce costs and service pressures for the imaging department, compared with current practice. The utility and safety of such an approach would need to be assessed prospectively, ideally as a multicentre study.

3.11 Conclusion

Dobutamine stress MPI is a safe, non-invasive method of cardiovascular assessment in patients with ESRD, and its findings influence decisions regarding transplant suitability in a significant proportion of patients. High sum stress and sum rest scores were associated with poorer outcomes, and should be quoted in scan reports in order to guide the clinician in decision making. An abnormal pre-operative ECG was associated with increased

cardiovascular events and mortality. Further studies are required to establish whether specific patient subgroups benefit from further cardiovascular investigation e.g. diabetics, and the role of prophylactic revascularisation prior to kidney transplantation.

Chapter 4: Mitochondrial function in an experimental model of uraemia

4.1 Mitochondrial function in heart failure

In the setting of physiological or compensated pathological cardiac hypertrophy, there is an increase in mitochondrial density that matches the increase in cardiac energy requirements (Nishio *et al*, 1995). Mitochondrial biogenesis requires the synchronous transcription of mitochondrial and nuclear encoded DNA, which is controlled by peroxisome proliferator activated gamma co-activator 1 α (PGC1 α). In the transition from compensated hypertrophy to decompensation and overt heart failure, there is a downregulation of PGC1 α (Barger *et al*, 2000).

Aortic banding is a technique used to create a pressure overload model of cardiac hypertrophy. A metal clip or suture applied to the aorta reduces the luminal area of the aorta, leading to constriction. This leads to an increased cardiac afterload, a rising left ventricular diastolic pressure, leading to cardiac hypertrophy, and ultimately cardiac failure (see Figure 4.1). Using a rat model of pressure overload induced by aortic banding, Garnier *et al* (2003) found a linear relationship between PGC1 α RNA expression and levels of citrate synthase and cytochrome c oxidase (markers of mitochondrial activity).

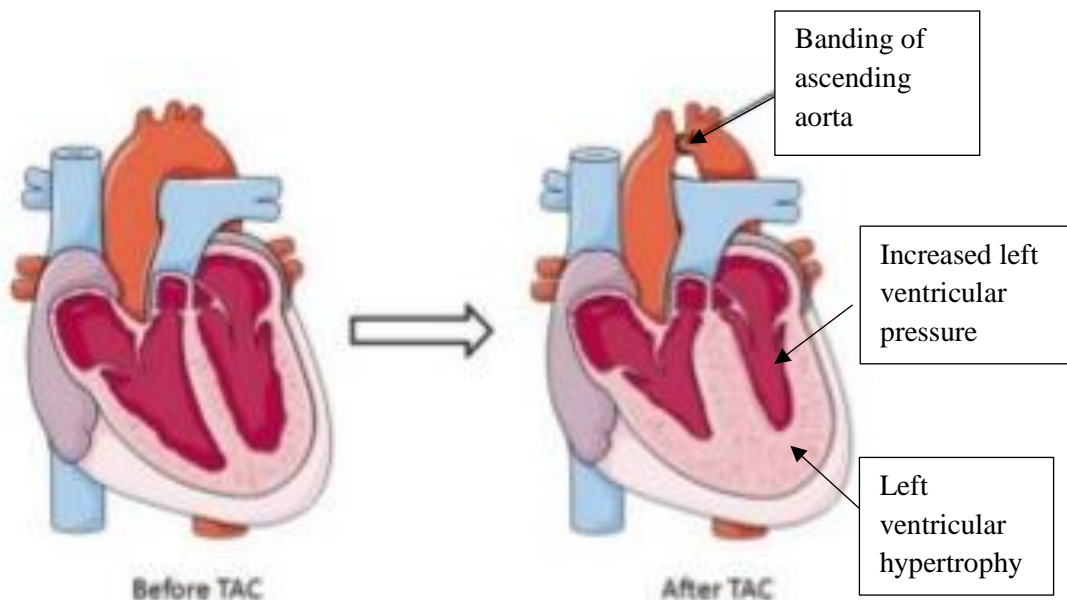


Figure 4.1 Principles of aortic banding Adapted from open access slideshare presentation by Dr BA Mohamed <https://www.slideshare.net/InsideScientific/dont-miss-a-beat-arrhythmia-detection-for-preclinical-ecg-research>

Interestingly, increased adrenergic signalling and renin-angiotensin system activation and cytokine stimulation that are ubiquitous in advanced heart failure have been shown to stimulate PGC1 α expression (Tian *et al*, 2001). It is therefore unclear what drives the downregulation of PGC1 α in the transition to decompensated heart failure.

There is an increase in basal metabolic oxygen consumption in the failing heart. Endothelial nitric oxide attenuates mitochondrial respiration through its inhibitory effects on the iron-sulphur groups of the electron transport chain, and the heme group of cytochrome c oxidase (Xie *et al*, 1996). Nitric oxide also plays a key role in intracellular calcium influx, which is necessary for excitation-contraction coupling within myocytes. Canine models of pacing induced heart failure have demonstrated a reduction in nitric oxide production, associated with an increased in basal myocardial oxygen consumption (Recchia *et al*, 1998).

In the healthy heart, free fatty acid (FFA) metabolism accounts for 70-90% of ATP production. In experimental models of heart failure there is a change in substrate metabolism, with a marked reduction in free fatty acid metabolism and thus a greater reliance on glucose oxidation, akin to fetal metabolism (Olson, 1959). The shift in substrate metabolism is thought to be an adaptive response to the increased energy demand, as glucose oxidation provides more ATP for a given amount of oxygen (Stanley *et al* 1997). Furthermore, ATP derived from glycolysis is preferentially used for Ca reuptake within sarcoplasmic reticulum, and therefore plays an important role in ventricular relaxation and contraction. The regulatory processes that lead to this shift in substrate utilisation remain unclear. PGC1 α , a key controller of mitochondrial biogenesis, also plays a role in the co-activation of peroxisome proliferator-activated receptors (PPAR) and oestrogen related receptors. PPAR alpha is responsible for activation of carnitine palmitoyl transferase (CPT-1) and medium chain acyl CoA dehydrogenase (MCAD), both important regulators of fatty acid oxidation.(Desvergne and Wahli, 1999). Reduced PPAR alpha and PGC1 alpha activity have been confirmed in rat models of pressure overload hypertrophy, and canine models of pacing induced heart failure (Huss *et al* 2001; Osorio *et al*, 2002). There is also a post-transcriptional down-regulation of PPAR alpha in the hypertrophic heart, leading to further reductions in the ability of the failing heart to utilise FA oxidation (Barger *et al*, 2000). Cardiac myocytes are ill suited for substrate storage, and the accumulation of intracellular lipids leads to the activation of apoptotic pathways.

Oxidative stress plays an important role in the progressive mitochondrial dysfunction found in heart failure. The electron transport chain is the predominant source of reactive oxygen species within cardiomyocytes. These are generated as high energy electrons produced in the

Krebs cycle for ATP production bind directly to oxygen to form superoxide and hydrogen peroxide. In healthy tissues approximately 1-2% of electrons entering the ETC form reactive species, which are rapidly scavenged by manganese superoxide dismutase (MnSOD).

ROS play an important role in cell signalling, acting as a second messenger to pro-hypertrophic factors, including transcriptional growth factor B1, angiotensin II, and endothelin. They are also an important regulator of the inflammatory response, and are essential for phagocyte function. Conditions such as cardiac ischaemia/hypoxia lead to disruption of the electron transport chain, and blockage of electron transfer at complexes I and III lead to the formation of large amounts of ROS that overwhelm scavenging mechanisms. This leads to lipid peroxidation, protein denaturation, DNA mutation, and ultimately apoptosis (Tsutsui *et al*, 2011). Specific forms of heart failure such as alcoholic and anthracycline induced cardiomyopathies have shown to be directly linked to ROS accumulation, however *in vivo* evidence of increased ROS activity in ischaemic and other forms of dilated cardiomyopathy is limited (Jing *et al*, 2012; Vander Heide and L'Ecuyer, 2007). Furthermore, large scale clinical trials of antioxidant therapies in both primary and secondary prevention of cardiovascular disease have shown no benefit (Myung *et al*, 2013).

Heart failure due to primary mitochondrial disorders is likely to represent a very small proportion of cases of clinical heart failure, however there is mounting evidence of the role of secondary mitochondrial dysfunction in the progression of cardiac failure.

4.2 Objectives

The aims of the following experimental chapter are;

To characterise an experimental model of uraemic cardiomyopathy.

To examine the effect of uraemia on indices of cardiac function *in vitro*, by means of a Langendorff isolated heart perfusion preparation.

Assess the effect of uraemia on the activity of key mitochondrial enzymes, including the respiratory complex enzymes of the electron transport chain.

Assess the effect of uraemia on mitochondrial respiration *in vitro* using polarography.

4.3 Hypothesis

1. Induction of uraemia using a 5/6ths nephrectomy model will lead to an increase in heart weight at 12 weeks post nephrectomy.
2. Induction of uraemia will lead to reduction in indices of cardiac contractility at 12 weeks.
3. Induction of uraemia results in an increase in state 4 respiration due to mitochondrial uncoupling at 12 weeks post-nephrectomy.
4. Induction of uraemia will lead to a reduction in respiratory complex enzymatic activity measured in isolated cardiomyocytes when compared with controls at 12 weeks.

4.4 Methods

Five male Sprague-Dawley rats aged 6 weeks underwent surgical 5/6ths nephrectomy using the technique described in the methods section. A further 5 rats underwent a sham procedure. The rats were given a pair matched diet, whereby a rat that underwent nephrectomy was paired with a control animal, and provided with the same amount of food by weight. They were provided with water *ad libitum*, and housed with a 12 hour day-night cycle. One animal from the nephrectomy group died around 2 weeks following surgery. Examination revealed a large haematoma surrounding the remnant kidney.

At 12 weeks post surgery the animals were sacrificed. Heart weight, body weight, and tibia length were recorded. Blood taken from the thoracic and abdominal cavity was analysed to calculate urea and creatinine levels.

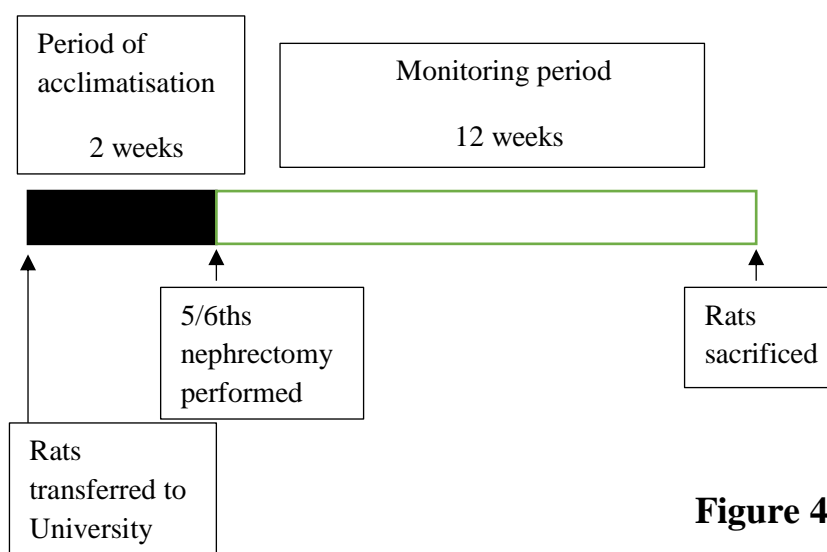


Figure 4.2 Timeline of events

Ex vivo cardiac function was assessed using a Langendorff perfusion preparation, as described in the methods section. Ventricular pressures and heart rate were recorded using PowerLab data acquisition device, and analysed with Chart5 software (AD instruments, Hastings).

Fresh mitochondrial isolates were prepared as described in the methods section.

Mitochondrial function was assessed *in vitro* by assessing mitochondrial respiration. Oxygen consumption was determined by polarography using a Clark-type electrode, as described in the methods section. Complex I function was assessed by adding the substrates glutamate and malate. Complex II and III function was assessed by adding rotenone, which inhibits complex I respiration, and succinate, the substrate required to initiate complex II transport. Coupled oxidative phosphorylation is assessed by comparing state 3 and 4 respiration. State 3 respiration occurs when ADP is added to the incubated mitochondrial isolate and substrate. This leads to an increase in oxygen consumption as ADP is converted to ATP. When all of the ADP is phosphorylated, the preparation enters state 4 respiration. Measuring the ratio between state 3 and 4 respiration provides an assessment of the degree of coupling between respiration and phosphorylation.

Enzymatic assays were performed to assess citrate synthase and aconitase activity.

Respiratory complexes I, II, II and III, IV were assayed according to the procedure described in the methods section.

4.5 Results

4.5.1 Model characterisation

There was no significant difference in mean body weight between the uraemic and control arms at 12 weeks post nephrectomy (486.5g vs 483.8g, $p=0.79$). Wet heart weight was significantly higher in the uraemic rats compared with control (2.08g vs 1.79g, $p=0.00102$), see figure 4.3.

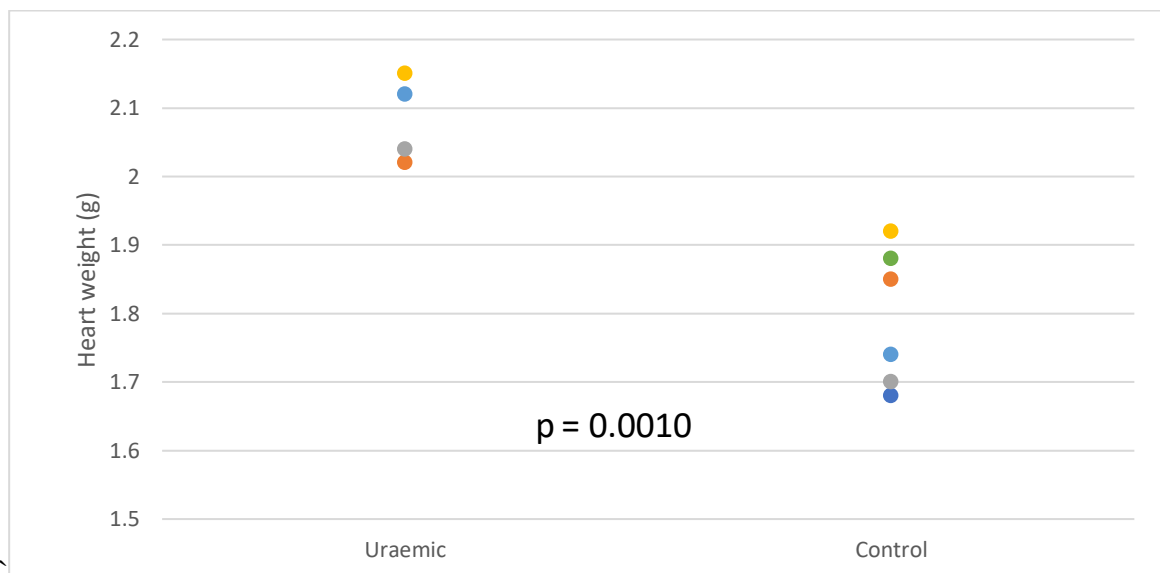


Figure 4.3 Wet heart weights in both the uraemic and control arms

The mean ratio of heart weight to tibia length was higher in uraemic hearts, although this difference was not statistically significant (0.42 vs 0.38, $p=0.12$). The ratio of heart weight to body weight was significantly higher in the uraemic arm compared with control (0.0043 vs 0.0037, $p=0.0043$), Table 4.1.

	Body Weight (g) Mean (S.E)	Heart weight (g) Mean (S.E.)	Heart weight:tibia length Mean (S.E.)	Heart weight:body weight Mean
Uraemic (n=4)	486.5 (7.54)	2.08 (0.062)*	0.4225 (0.056)	0.0043*
Control (n=5)	483.83 (8.46)	1.795 (0.1)	0.375 (0.031)	0.0037

* $p<0.01$. g-grams S.E. – standard error

Table 4.1 Comparing measures of left ventricular hypertrophy

4.5.2 Biochemical analysis

Serum urea levels were 3.7 times greater in the uraemic rats at 12 weeks compared with those undergoing sham procedure (17.93mmol/L vs 4.8mmol/L, $p<0.0001$). Similarly, serum

creatinine levels were 2.3 times greater in the uraemic arm compared with control (87.5µmM/l vs 38.67µmM/l, $p < 0.0001$), figures 4.4 and 4.5.

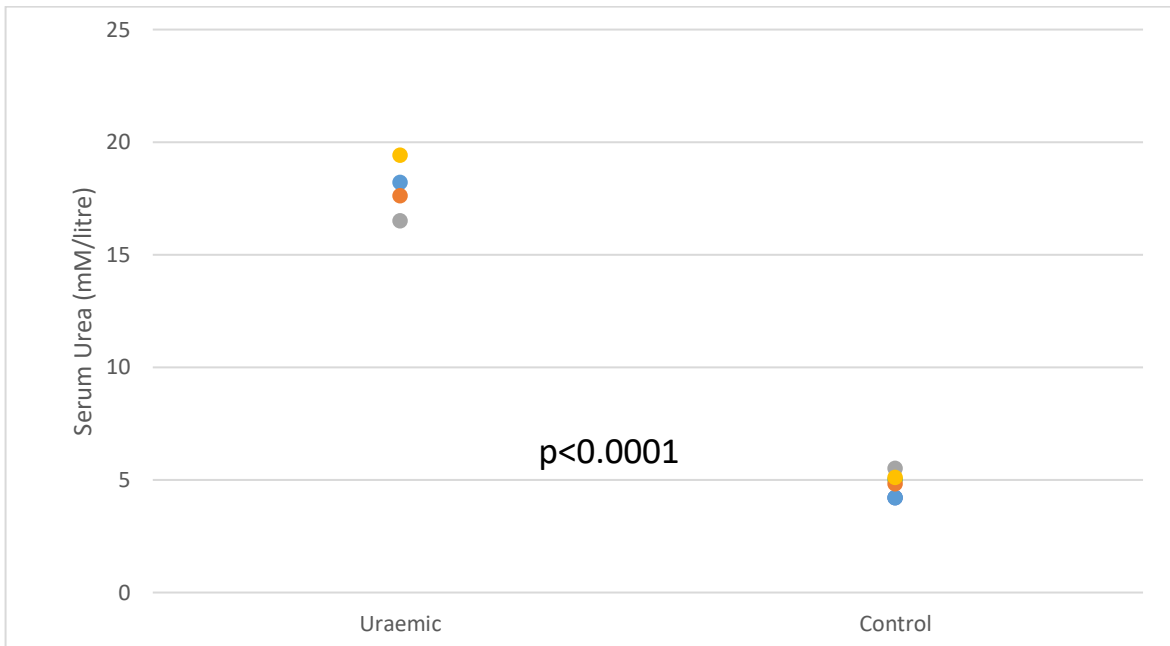


Figure 4.4 Serum urea levels at 12 weeks post nephrectomy or sham procedure

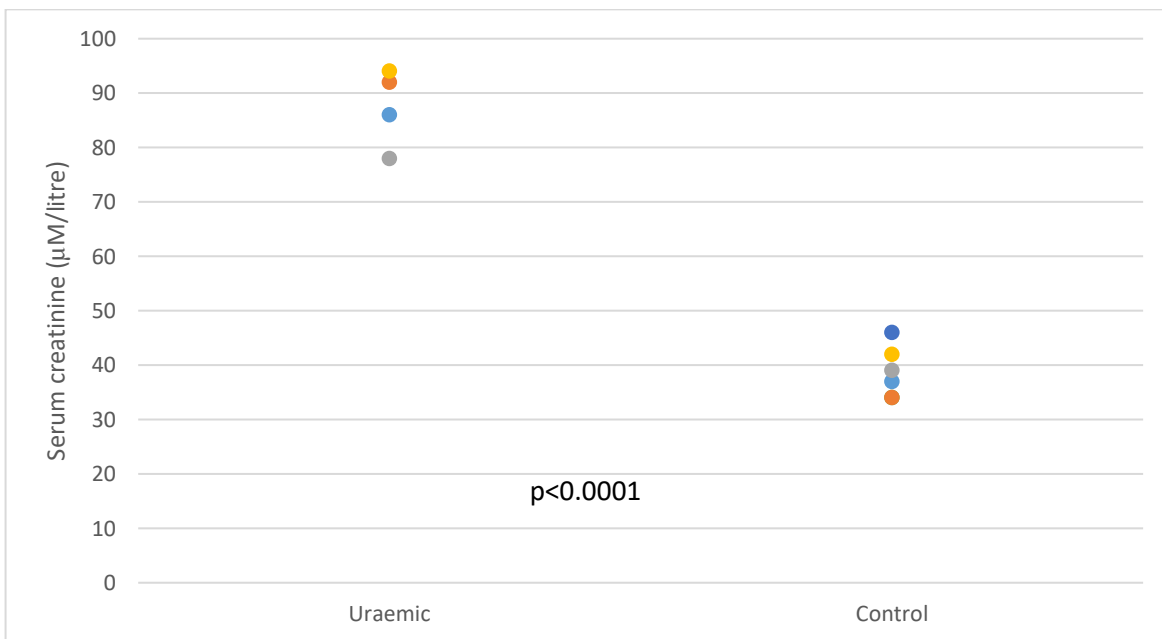


Figure 4.5 Serum creatinine levels at 12 weeks post nephrectomy and their controls

4.5.3 Assessment of cardiac function

There was no difference in left ventricular systolic pressure (126mmHg vs 124.2mmHg, $p=0.66$), or LV developed pressure (122mmHg vs 121mmHg $p=0.87$) between uraemic and control hearts at 12 weeks post subtotal nephrectomy. Similarly, there was no difference in rate pressure product (41580 vs 40975, $p=0.67$) between the two groups (Table 4.2, figure 4.6).

	Systolic pressure (mmHg) Mean (S.E)	LV developed pressure (mmHg) Mean (S.E)	Rate pressure product (mmHg•bpm) Mean (S.E)
Uraemic (n=4)	126 (2.04)	122 (2.3)	41580 (652.37)
Control (n=5)	124.17 (3.83)	121 (3.75)	40975 (1224.37)

Table 4.2 Comparison of *in vitro* left ventricular pressure recordings LV-left ventricular, S.E.-standard error, mmHg-millimetres of mercury, bpm- beats per minute

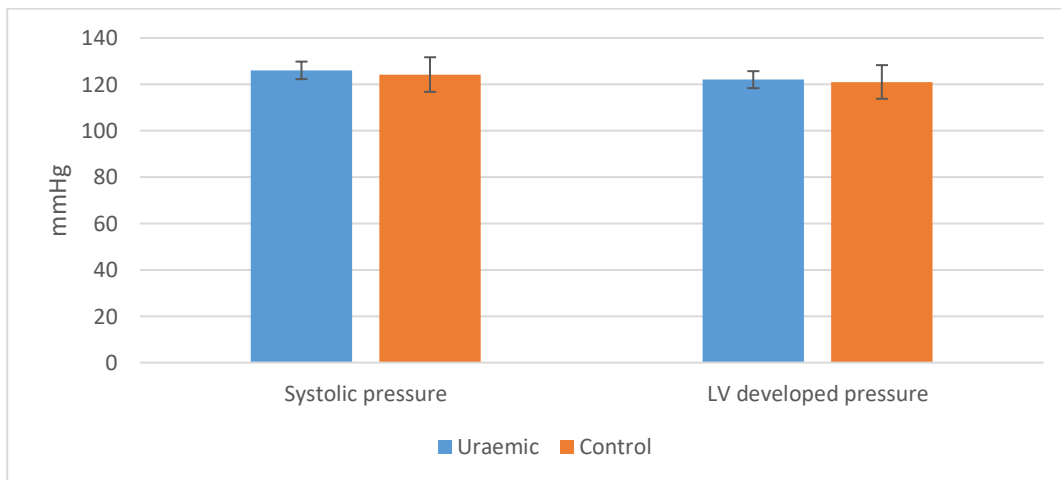


Figure 4.6 *In vitro* left ventricular pressure recordings of 12 week uraemic and control rat hearts

There was no difference in the derived rate of pressure change, as measured by both dP/dt_{max} and dP/dt_{min} between the uraemic and control groups ($p=0.87$ and 0.59 respectively), table 4.3, figure 4.7.

4.5.4 Mitochondrial respiration

There was no significant difference in mean protein content of mitochondrial preparations between the uraemic and control hearts (3.8mg/ml vs 3.6mg/ml, $p=0.456$), measured using a Bio-rad protein determination assay.

	dP/dt _{max} (mmHg/s)	dP/dt _{min} (mmHg/s)
	Mean (S.E)	Mean (S.E)
Uraemic (n=4)	3702.5 (438.67)	-2930.5 (361.69)
Control (n=5)	3744.5 (371.15)	-2781.83 (435.1)

Table 4.3 *In vitro* derived rate of LV pressure change S.E.-standard error, mmHg/s-millimetres of mercury per second

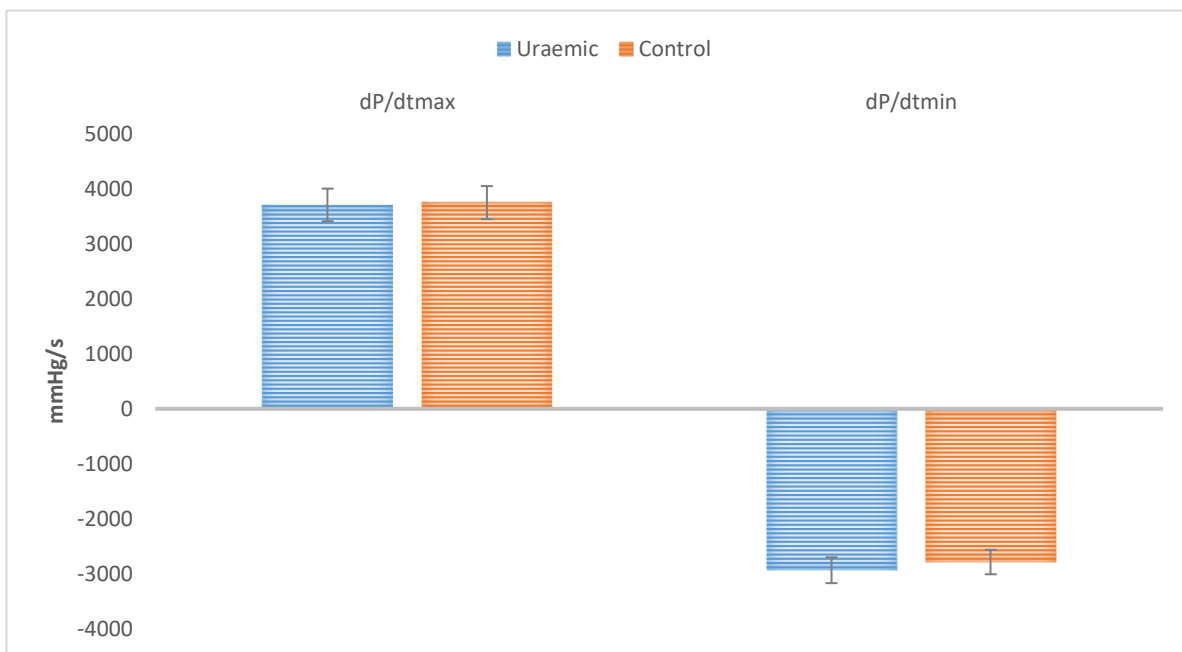


Figure 4.7 *In vitro* derived rate of LV pressure change of 12 week uraemic and control rat hearts

State 3 and 4 respiration rates, and respiratory control ratio are shown in table 4.4. There was no difference in mean state 3 respiration rates between uraemic and control hearts with glutamate/malate substrate, $p = 0.53$. The rate of state 4 respiration was higher in the uraemic

hearts compared with control, $p= 0.014$. This resulted in a lower mean respiratory control ratio in the uraemic arm compared with control, $p=0.032$.

	State 3 respiration (nmolO ₂ /min/mg protein) Mean (S.E.)	State 4 respiration (nmolO ₂ /min/mg protein) Mean (S.E.)	Respiratory control ratio
Uraemic (n=4)	216.25 (12.7)	44.50 (5.61) *	4.93 (0.23)
Control (n=5)	220.33 (11.9)	40.23 (5.24)	5.52 (0.17)

Table 4.4 State 3 and 4 respiration rates in the presence of glutamate/malate

In the succinate/rotenone group, there was no difference between state 3 respiration rates ($p=0.54$), state 4 respiration ($p=0.17$) or respiratory control ratio ($p=0.46$) between the uraemic and control arms (table 4.5, figures 4.8 and 4.9).

	State 3 respiration (nmolO ₂ /min/mg protein) Mean (S.E.)	State 4 respiration (nmolO ₂ /min/mg protein) Mean (S.E.)	Respiratory control ratio
Uraemic (n=4)	193.75 (8.6)	56.5 (1.73)	3.43 (0.15)
Control (n=5)	188.67 (4.9)	53.33 (1.94)	3.54 (0.28)

Table 4.5 State 3 and 4 respiration rates in the presence of succinate/rotenone

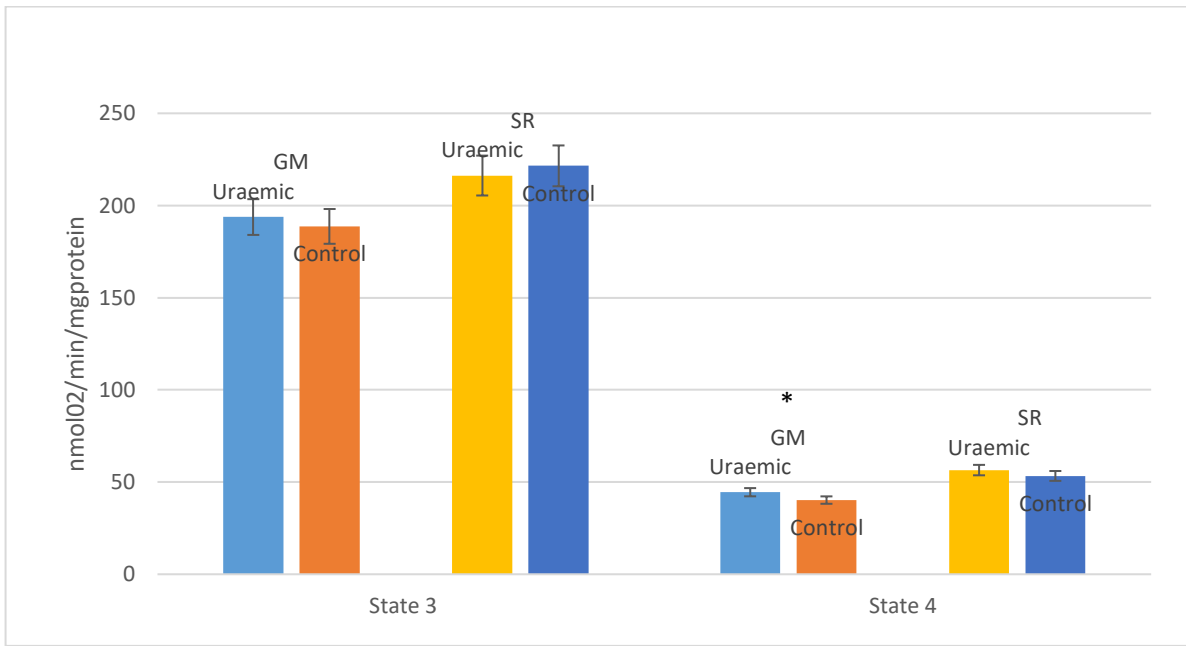


Figure 4.8 – State 3 and 4 cardiac mitochondrial respiration states with the addition of complex 1 and complex 2 substrates *p<0.05

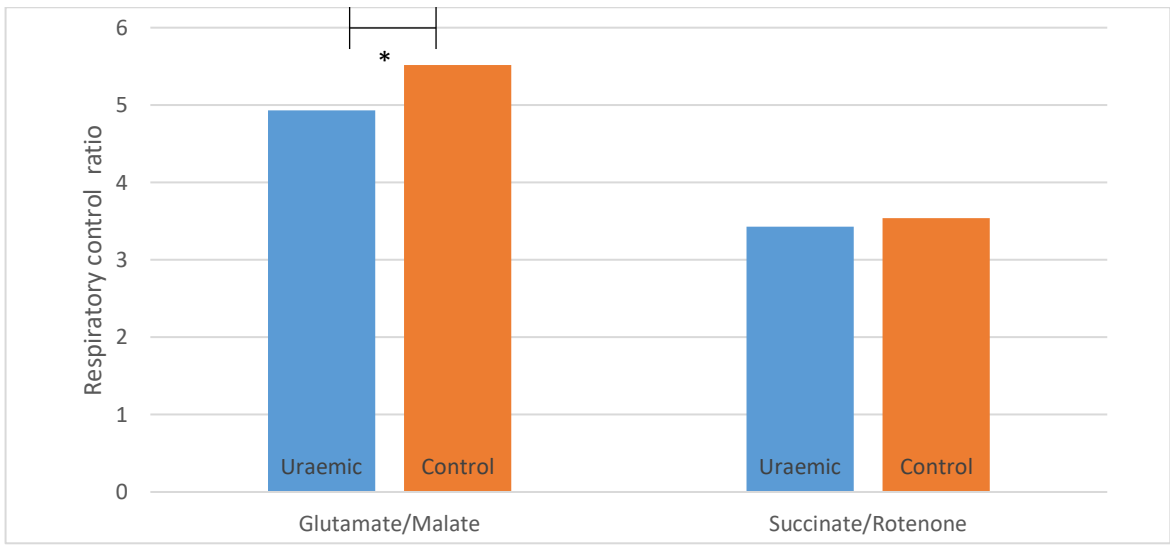


Figure 4.9 Respiratory control ratios with the addition complex I and II substrates *p<0.05

4.5.5 Mitochondrial enzyme activity

Citrate Synthase

The mean citrate synthase activity was lower in the uraemic group than the control arm, although the difference was not statistically significant by student t-test (p=.345), table 4.6.

	Enzyme activity (nmol/min/mg protein)		Enzyme activity (nmol/min/mg protein)
U1	99.63	S1	104.90
U2	90.44	S2	72.30
U3	72.42	S3	116.05
U4	76.25	S4	107.23
		S5	79.26
Mean (s.e.)	84.67 (10.93)		95.95 (17.03)

Table 4.6 – Citrate synthase activity in isolated mitochondria

Aconitase

Mean mitochondrial aconitase activity was lower in the uremic group was lower than the sham group, but this was not statistically significant ($p=0.3$), table 4.7.

Uraemic	Enzyme activity (nmol/min/mg protein)	Sham	Enzyme activity (nmol/min/mg protein)
U1	7.73	S1	7.29
U2	5.96	S2	7.38
U3	6.40	S3	9.60
U4	6.13	S4	7.11
		S5	5.78
Mean (s.e.)	6.56 (0.35)		7.43 (0.55)

Table 4.7 – Aconitase activity in isolated mitochondria from uraemic and non-uraemic rat hearts

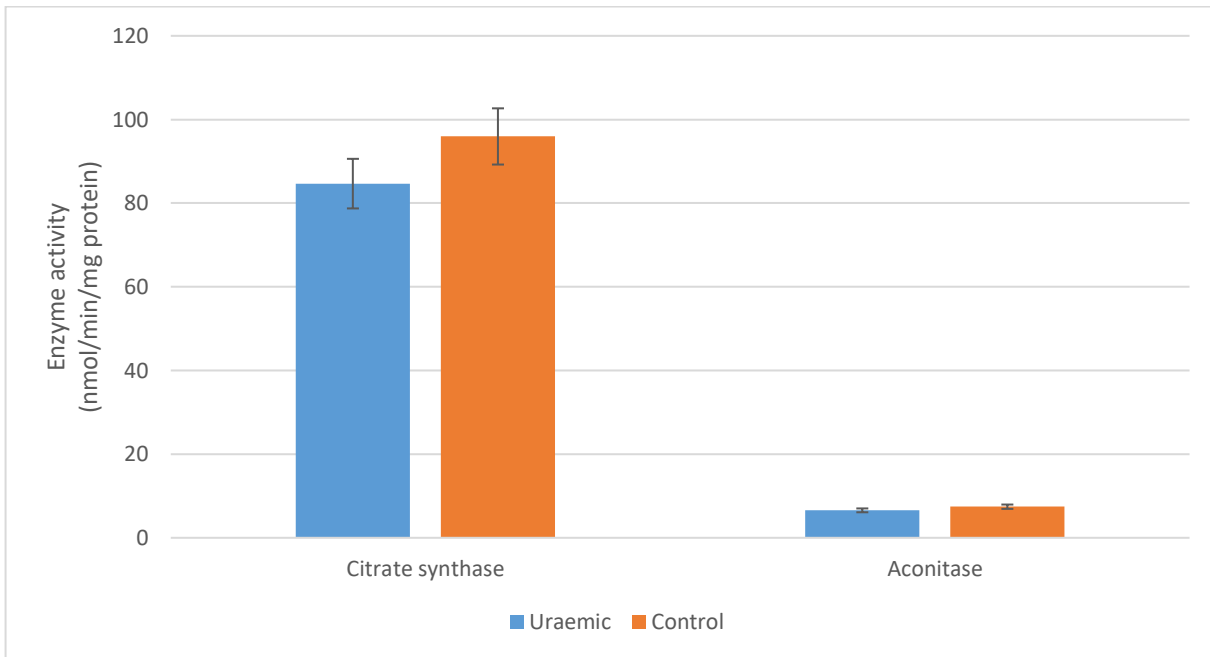


Figure 4.10 Citrate synthase and aconitase enzyme activity of isolated cardiac mitochondria

4.5.6 Respiratory complex assays

Respiratory complex I

Mean complex I activity was lower in the uraemic rats, compared with control. This did not achieve statistical significance, $p=0.06$ (table 4.8).

Respiratory complex II

The mean complex II activity in isolated uraemic mitochondria was lower than in control rats. This difference was not statistically significant, $p=0.099$ (table 4.9).

	Enzyme activity (nmol NADH/mg/min/mg protein)		Enzyme activity (nmol NADH/mg/min/mg protein)
U1	219.90	S1	209.42
U2	146.67	S2	260.28
U3	180.00	S3	236.35
U4	160.00	S4	242.33
		S5	173.52
Mean (s.e.)	176.64 (12.45)		224.38 (13.88)

Table 4.8 Respiratory complex I activity

Complex II and III

Mean complex 2 and 3 activity was lower in the isolated mitochondria of uremic rats, compared with control. This was statistically significant at the 5% level ($p=0.033$), table 4.10.

	Enzyme activity (nmol DPIP/mg/min/mg protein)		Enzyme activity (nmol DPIP/mg/min/mg protein)
U1	58.8	S1	69.23
U2	65.07	S2	56.46
U3	57.5	S3	69.12
U4	55.19	S4	70.3
		S5	66.09
Mean (s.e.)	59.14 (4.6)		66.24 (4.71)

Table 4.9 Respiratory complex II activity

Complex IV

The mean complex IV activity in the isolated cardiac mitochondria of uraemic rats was very similar to the control arm, $p=0.99$ (table 4.11)

	Enzyme activity (nmol cytochromec/mg/min/mg protein)		Enzyme activity (nmol cytochromec/mg/min/mg protein)
U1	62.1	S1	78.4
U2	63.44	S2	72.1
U3	55.89	S3	61.43
U4	50.85	S4	64.32
		S5	69.12
Mean (s.e.)	58.07 (3.85)		69.06 (3.29)

Table 4.10 Complex II and III activity

	Enzyme activity (nmol cytochromec/mg/min/mg protein)		Enzyme activity (nmol cytochromec/mg/min/mg protein)
U1	312.71	S1	298.12
U2	272.4	S2	264.9
U3	323.55	S3	299.43
U4	280.30	S4	302.18
		S5	322.29
Mean (s.e.)	297.24 (12.35)		297.39 (7.86)

Table 4.11 Complex IV

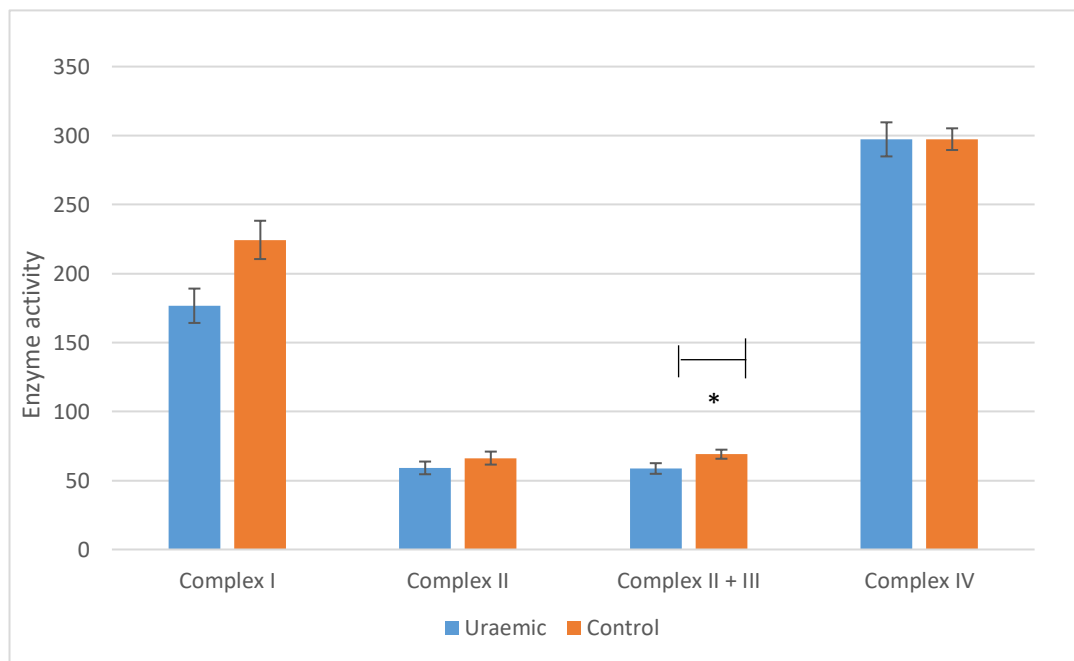


Figure 4.11 Complex enzyme activity of isolated cardiac mitochondria (* difference $p < 0.05$)

4.6 Discussion

The 5/6ths nephrectomy model of renal failure leads to structural and metabolic cardiac adaptations. Induction of renal failure was confirmed on biochemical analysis, where there was a 310% increase in serum urea and 210% increase in serum creatinine levels, compared with control. These changes are consistent with prior studies using the 5/6ths nephrectomy model within the department (Reddy *et al*, 2007; Smith *et al*, 2010). Serum creatinine is a commonly used marker of renal function in clinical practice, however it has a number of limitations. It is affected by a number of extra-renal factors, including age, gender, ethnicity and muscle mass. Furthermore it is an insensitive marker, as creatinine levels may remain within the normal range despite the loss of 50% of nephron function.

Novel biomarkers of chronic kidney disease, such as beta trace protein, and neutrophil gelatinase-associated lipocalin are postulated to be more sensitive markers of renal disease progression, but require clinical validation in larger cohorts (Nickolas 2008). Twenty four hour creatinine clearance is inversely correlated to glomerular filtration rate, although is similarly affected by muscle mass, age etc. Additionally, tubular secretion of 10-15% of

excreted creatinine leads to overestimation of true glomerular filtration, particularly in more severe renal disease (Kasiske and Keane, 2000).

Heart weight, and heart weight indexed to body weight were significantly elevated in the uraemic group. Heart weight / tibia length was also higher in the uraemic group, but this difference was not statistically significant, possibly due to the small numbers within each arm. Increased heart weight is a result of left ventricular hypertrophy, which is highly prevalent in patients with renal failure.

Approximately 40% of patients with chronic kidney disease and 75% with end stage renal failure have left ventricular hypertrophy by electrocardiographic and electrographic criteria (Foley *et al* 1995; Middleton *et al*, 2001). Systolic hypertension is common in renal failure, due to a combination of increased arterial stiffness, neurohumoral activation, and vascular calcification. Left ventricular pressure increases in order to overcome the increased afterload. This is frequently compounded by increased volume loading, anaemia, and the direct and indirect effects of abnormal calcium and phosphate handling that increase wall tension within the ventricular cavity.

Pressure overload activates signalling pathways, including angiotensin II, aldosterone, calcium regulatory proteins, heat-shock proteins and integrins, which stimulate cell proliferation, cardiomyocyte hypertrophy, and extracellular matrix protein expression (Cacciapuoti *et al*, 2011). This adaptive process initially leads to compensated hypertrophy, whereby systolic cardiac function is preserved. As the condition progresses, there is an increase in fibroblast deposition relative to myocyte hypertrophy, and neovascularization is unable to match the increased demand requirements of the hypertrophic muscle. This ultimately leads to a decompensated state, leading to overt systolic dysfunction, and portends a poor prognosis.

In our experimental model, *ex vivo* cardiac contractility was preserved at 12 weeks post induction of uraemia. This was seen consistently in previous studies of the 5/6ths nephrectomy model in our department. The model therefore allows us to assess alterations in mitochondrial function in the compensated hypertrophy state. Identifying therapeutic targets at this stage of the disease process have already been shown to induce regression of left ventricular hypertrophy, with attendant improvements in clinical outcomes.

Drugs targeting the renin- aldosterone-angiotensin system have the strongest evidence for LVH regression. As described earlier, pro-hypertrophic and fibrotic signalling pathways are activated by angiotensin 2 and aldosterone. Blocking these pathways with agents such as

angiotensin receptor blockers (ARBs), angiotensin converting enzyme inhibitors ACE-Is, and aldosterone antagonists (AAs) lead to regression of LVH independent of their blood pressure lowering effects. A large meta-analysis of the effect of antihypertensive treatments on LVH revealed that ARBs reduced LV mass index by 13%, ACE-Is 10%, whereas beta blockers lead to a 6% reduction (Klingbeil *et al*, 2003). Patients with advanced renal disease (stages 4 and 5) are commonly excluded from these trials. Although these treatments have been shown to slow progression of CKD at earlier stages of disease, they should not be used when creatinine levels exceed 220mmol/l. They can have particularly deleterious effects in patients with significant reno-vascular disease, and hyperkalaemia frequently precludes their use in patients with renal disease. This leaves limited treatment options for a group of patients with a very high prevalence of LVH and its adverse consequences. Treating anaemia with erythropoietin and intravenous iron leads to modest LVH regression, however this has only shown to be beneficial in patients with a haemoglobin of <100mg/dL, and there are well documented risks associated with overcorrection to levels >120mg/dL (Paoletti and Cannella, 2006).

An intriguing treatment that has shown to induce LVH regression without any antihypertensive effect is allopurinol. This agent has been in clinical use for decades as a treatment for gout. The active metabolite is oxypurinol, which inhibits xanthine oxidase, a key enzyme in purine metabolism. Inhibition leads to reduced production of uric acid. A significant, albeit modest reduction in LV mass was demonstrated in CKD stage 3 patients following 9 months treatment with allopurinol 300mg/day, compared with placebo (Kao *et al* 2011). Similar effects were seen in separate cohorts of patients with type 2 diabetes and ischaemic heart disease (Szwejkowski, *et al*, 2013; Rekhraj *et al*, 2013). A study of the xanthine oxidase inhibitor febuxostat also demonstrated LVH regression in an experimental model of volume overload induced hypertrophy in mice (Xu *et al*, 2014). The postulated mechanism of action is a reduction in oxidative stress.

In the respiratory complex activity assays, there was a significant reduction in complex II+III enzyme activity in the uraemic arm (Figure 4.11). There was a trend towards lower complex I and II activities in the uraemic group, but complex IV activity was very similar between groups. Complex III of the electron transport chain is particularly sensitive to the deleterious effects of oxidative stress. As described earlier, an increase in ROS production leads to damage to inner mitochondrial membrane protein units, including ETC complexes, leading to a reduction in oxidative phosphorylation. A reduction in complex III activity has also been identified in pacing-induced canine models of dilated cardiomyopathy, as well as in humans with dilated cardiomyopathy (Marin-Garcia *et al*, 2001, Jarreta *et al*, 2000). However, prior

studies of mitochondrial function at the compensated hypertrophy stage have not demonstrated a decrease in ETC complex activity (Matlib et al 1983, Abel and Doenst 2010). Aconitase levels were no different between arms, as seen in prior studies. This enzyme is also very sensitive to the effects of reactive oxygen species. If the reduction in complex III activity was due to oxidative stress, then one would also have expected a decrease in aconitase activity.

In the mitochondrial respiration studies, state 4 respiration rates in the presence of complex I substrates was higher in the uraemic arm when compared with control. This was not seen with complex II substrates, and state 3 respiration rates were unchanged with either substrate set. Increased state 4 respiration was also seen in a previous study from this department, using the same uraemic cardiomyopathy model (Taylor *et al*, 2014). This finding was also seen in a hyperthyroid heart model, and was associated with elevated levels of uncoupling proteins (Boehm *et al*, 2001).

It was postulated by Taylor (2014) that a chronic increase in mitochondrial uncoupling from oxidative phosphorylation would lead to a decrease in metabolic reserve. This would lead to preserved cardiac contractility at rest, but an inability to augment cardiac output with increased demand. Future studies could further evaluate *ex vivo* response to haemodynamic stress using the Langendorff perfusion mode, by altering the pacing heart rate, or increasing calcium concentration in the KH buffer, to the perfusate. Echocardiography and dynamic myocardial perfusion imaging studies could also be utilized to assess *in vivo* cardiac function in response to pharmacological stress.

4.7 Conclusion

The 5/6ths nephrectomy model produced biochemical evidence of renal dysfunction, and structural cardiac adaptations that mimic those seen in patients with chronic kidney disease. At 12 weeks post induction of uraemia, there is evidence of compensated cardiac hypertrophy, with preserved LV contractility. However, there were alterations in mitochondrial respiration and electron transport complex activity that may indicate impaired metabolic reserve, with oxidative stress as a possible mechanism. These findings require verification using larger samples, with mitochondrial activity measured in freshly isolated mitochondria.

Chapter 5: Technetium 99m Sestamibi Washout

5.1 Myocardial Perfusion Imaging

5.1.1 Technetium 99m sestamibi

Technetium 99m sestamibi, first introduced in the 1980s, is now established as the most widely used myocardial perfusion agent in clinical practice. It is a lipophilic cation that passively diffuses into healthy mitochondria via the negative membrane potential (Pinwica-Worms *et al*, 1990). One of its key properties is its prolonged myocardial retention with minimal redistribution (Okada *et al*, 1988). In contrast, Thallium-201 actively diffuses into cells via the ATP/potassium pump. This leads to rapid redistribution, particularly following exercise, meaning that imaging needs to be undertaken 5-10 minutes following tracer injection. Similarly, Technetium teboroxime is rapidly redistributed within the myocardium, and imaging should commence within 2 minutes of tracer injection. The stable retention of technetium sestamibi means that imaging can be delayed by several hours, without significantly affecting imaging quality. This avoids the need to commence imaging in the early recovery phase following exercise, where tachycardia and tachypnoea can lead to excessive cardiac and thoracic movement, leading to imaging artefact and reduced imaging resolution. It also affords the advantage of being able to repeat imaging in the event of significant artefact or technical issues.

5.1.2 Technetium washout

The discovery that impaired technetium retention is a marker of cell viability was first demonstrated in an experimental animal model (Beanlands *et al*, 1990). Myocardial clearance was significantly increased in the presence of sodium cyanide, a cytochrome c oxidase inhibitor, and Triton X, a sarcolemmal membrane detergent. An *in vitro* study using guinea pig cardiomyocytes demonstrated that calcium overload enhanced technetium washout, however this effect was inhibited by the addition of a mitochondrial calcium channel blocker, suggesting that washout was more specifically a marker of mitochondrial viability (Crane *et al*, 1993).

The first clinical utilisation of technetium washout was in tumour imaging. Technetium sestamibi is transported out of cells via the ATP dependent p-glycoprotein efflux pump, therefore higher p-glycoprotein expression is associated with enhanced washout. It has been used to evaluate lung malignancies, multiple myeloma, and musculoskeletal sarcomas, with increased washout associated with multi-drug resistance and thus altered clinical response to treatment (Kostakoglu *et al*, 1998; Burak *et al*, 2001; Pace *et al*, 2005). The differential washout rates of Technetium sestamibi in thyroid tissue and parathyroid adenomas also

allows accurate localisation for pre-operative planning in patients undergoing parathyroidectomy (Civelek *et al*, 2002).

Pre-clinical and clinical studies examining the effect of myocardial ischaemia on technetium retention demonstrate increased washout in normal myocardium, when compared with ischaemic tissue (Ayalew *et al*, 2000; Taillefer *et al*, 1991). This was hypothesised to be due to reduced wash-in, with retention being inversely proportional to coronary flow rates.

The first clinical evidence that Tc99m retention was impaired in diseased myocardium was identified by Morishita *et al* (2001) using Technetium 99m tetrofosmin in patients with hypertrophic cardiomyopathy (HCM). Washout rate was increased in patients with localised disease (apical HCM, asymmetric septal hypertrophy), and to a greater extent in those with echocardiographic evidence of global left ventricular involvement. Tc99m sestamibi washout was subsequently evaluated in patients with cardiomyopathy, predominantly the dilated phenotype. Increased washout was seen at 3 hours when compared with healthy controls. Furthermore, higher rates were associated with established markers of poorer cardiovascular prognosis, including higher NYHA class and BNP levels, and lower ejection fraction (Matsuo *et al*, 2007). A more recent study of patients with dilated cardiomyopathy demonstrated an association between higher washout and impaired contractile reserve in response to dobutamine stress, suggesting impaired mitochondrial energetics. Endomyocardial biopsy specimens revealed reduced mRNA expression of key mitochondrial proteins in the TGA cycle and respiratory complex chain, including alpha-ketoglutarate dehydrogenase, cytochrome c-oxidase, and NADH ubiquinone oxidoreductase. Patients with washout rates of greater than 25% at 4 hours had evidence of mitochondrial degeneration, increased glycogen deposition and reduced lipid droplets on electron microscopy (Hayashi *et al*, 2001).

Significantly enhanced technetium washout in patients with inherited mitochondrial myopathies has been demonstrated in case reports and a small case series (Matsuo *et al*, 2008; Noriyuki *et al*, 2009; Ikawa *et al*, 2007). There is an association between increased washout, and increased left ventricular wall thickness and reduced ejection fraction, the latter two being established markers of disease severity.

There is very limited data assessing the association between Tc99m washout and clinical outcomes. A trial of 16 patients treated with potentially cardiotoxic chemotherapeutic regimen, but with echocardiographically normal left ventricular systolic function were compared with a group of matched controls (Carboni, 2012). There was higher initial myocardial uptake in the chemotherapy treated group, with a greater reduction in counts on

delayed imaging, but no significant difference in the washout rate. Higher initial and delayed counts were both independently associated with cardiac morbidity and mortality. The majority of deaths were as a result of heart failure, despite the initial normal cardiac function and functional status. Chemotherapeutic agents hyperpolarize mitochondrial membranes, leading to increased membrane permeability, and consequently increased tracer uptake and impaired retention. Increased permeability can lead to uncoupling oxidative phosphorylation, ATP depletion and ultimately cell death (Oliveira *et al*, 2004). Impaired tracer kinetics may therefore provide an early clinical marker of cardiac dysfunction, and thus an opportunity to intervene prior to the onset of irreversible myocardial damage.

Technetium washout may also be useful for the assessment of response to pharmacological treatment. A prospective study of patients with coronary spastic angina revealed that washout was significantly enhanced in territories supplied by arteries with proven spasticity on coronary angiography (Ono *et al*, 2003). Repeat imaging following three months treatment with calcium channel blockers and nitrates revealed a substantial reduction in washout rate, demonstrating that impaired retention is a marker of dysfunctional, but ultimately viable myocardium.

The role of technetium washout in patients with type 4 cardiorenal syndrome has not been studied. Renal failure is associated with mitochondrial dysfunction through a range of mechanisms, including hyperlipidaemia, hyperglycaemia, volume overload, and increased reactive oxidative species production (Massy and Nguyen-Khoa, 2002). Due to the overlap between clinical signs and symptoms of heart failure and renal failure, there is frequently a delay in identifying underlying cardiac dysfunction, and thus many patients present at an advanced stage. There is therefore a need for the development of novel markers of early myocardial dysfunction, at a time where early intervention may slow, or even reverse disease progression. Additionally, a sensitive marker of cardiac mitochondrial function and myocardial energetics may serve as a useful tool in the evaluation of new therapeutic agents.

5.2 Objectives

The aim of this study was;

To establish a robust method of performing SPECT imaging on an isolated perfused rat heart model

Measure technetium 99m sestamibi washout in an isolated heart perfusion model

Assess the impact of a mitochondrial uncoupling agent on technetium washout in an isolated heart perfusion model

To assess in-vivo technetium 99m sestamibi washout in rats

Evaluate different methods of analysing technetium washout

5.3 Hypothesis

1. Technetium 99m sestamibi washout can be measured using in an isolated heart perfusion model.
2. Addition of a mitochondrial uncoupler will lead to a significant increase in washout rate.
3. Technetium 99m sestamibi washout in healthy control rats will demonstrate a consistent washout rate over a prolonged (90 minute) scanning period.

5.4 Methods

5.4.1 Developing an isolated perfusion system

The SPECT small animal imaging system incorporates a closed, temperature controlled imaging cell. This cell was modified to allow imaging of an isolated heart. A hole was cut into the Perspex cell in order to allow positioning of a right angled metal inflow cannula for delivery of perfusate. The cannula was secured using a specially designed plastic holder to ensure stable positioning. A glass collecting dish was fitted directly below the cannula connected to polyethylene tubing in order to collect the effluent (Figure 5.1).

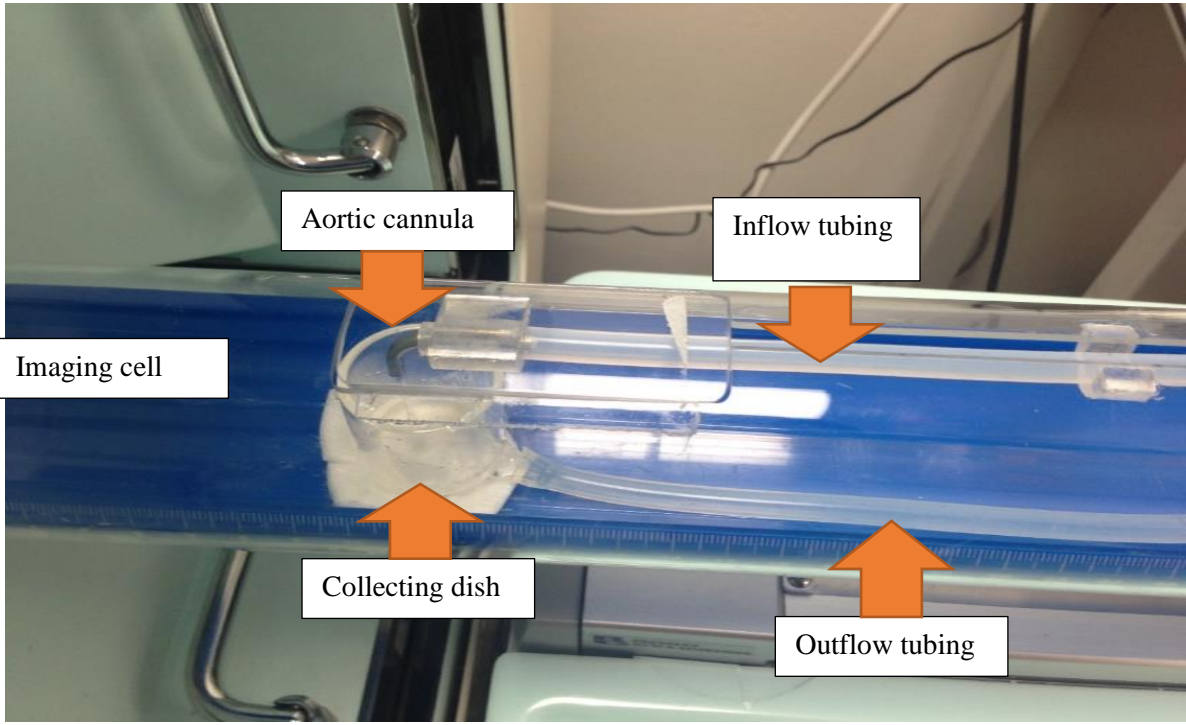


Figure 5.1 Modified imaging cell

Perfusate was driven around the system by two peristaltic pumps. A temperature controlled water bath was used to hold an Erlenmeyer flask containing perfusate. The perfusate was oxygenated using a 95% O₂/5% CO₂ mix via a glass diffuser. A bubble trap was incorporated into the outflow tubing in order to prevent air bubbles within the heart (Figure 5.2).

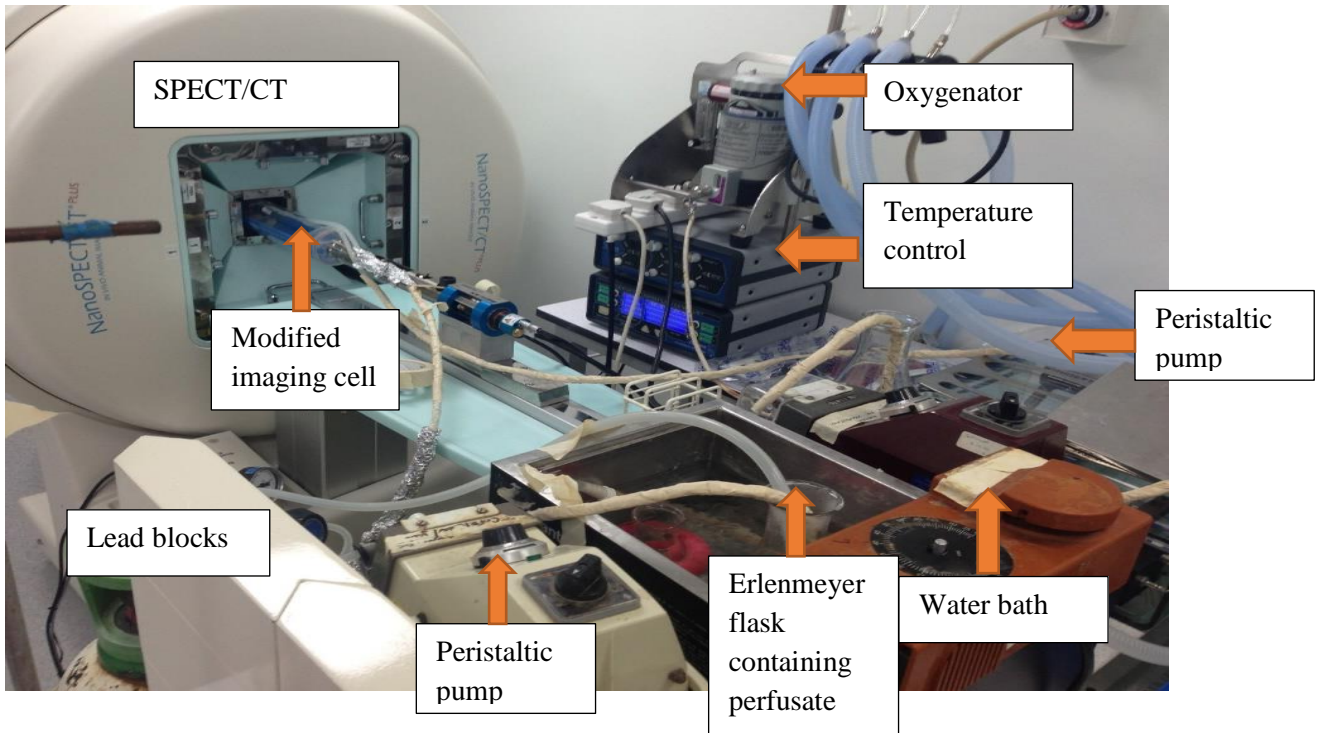


Figure 5.2 Isolated perfused heart system

Preliminary testing of the system revealed significant heat loss of perfusate between the flask and delivery at the metal outflow cannula. A temperature drop of 15 degrees Celsius resulted in marked impairment of cardiac function, and early organ loss. Initially, the temperature of the water bath was increased to compensate for the heat loss, however there was precipitation of some of the constituents of the K-H buffer above 50 degrees Celsius. Thicker walled polyethylene tubing was used, and the new tubing was wrapped in insulating tape and covered in reflective metal foil. The tubing was shortened to reduce transit time, whilst ensuring that there was sufficient tubing to ensure a full range of movement within the scanner. The model was switched from a recirculating model to a non-recirculating system due to significant heat loss of the perfusate returning to the flask. A recirculating system was initially preferred as this was felt to more accurately reflect the closed cardiovascular system. The first pass myocardial extraction fraction of technetium 99m sestamibi is 55-68%, and the majority of uptake (>98%) is extra-cardiac (Okada *et al*, 1988). Therefore, minimal additional uptake occurs on second and subsequent passes, and is unlikely to be clinically important in terms of overall count rates. Furthermore, delivery of a fixed concentration of tracer to the heart within a non-recirculating model will allow for better kinetic modelling. To minimise the radiation dose for operators, the effluent was pumped to a large conical flask housed behind lead bricks.

5.4.2 Mitochondrial uncoupling

CCCP is a lipid soluble protonophore that is used as a mitochondrial uncoupling agent. It is a weak acid that diffuses freely into phospholipid membrane of mitochondriae. It discharges the pH gradient, thus destroying the membrane potential that is essential for ATP synthesis via the electron transport chain (Rousset *et al*, 2004). The dose of CCCP chosen was 1mM in dimethyl sulfoxide solvent, diluted to 1 in 1000 in KH buffer. This dose had been used in prior isolated perfused heart studies, where a marked reduction in ATP and phosphocreatinine production was confirmed (Piwnica-Worms, 1990).

5.4.3 Phantom Studies

Phantom studies were used to determine the optimal technetium dose that would ensure adequate count rates and imaging resolution, whilst minimising radiation exposure for the animals and operators. A 1.5ml glass phantom was filled with Krebs-Henseliet buffer and Technetium pertechnetate at varying concentrations. A fixed pinhole SPECT camera was used at an angle of 90 degrees in order to simulate a standard projection of the anterior wall of the left ventricle in conventional imaging. Uptake was measured over five minutes.

A count rate of >100,000 per acquisition was considered adequate to achieve good image resolution. We planned to acquire 5 minute frames, and therefore a dose between 50 and 100Mbq would be appropriate. We assumed that the first pass myocardial extraction fraction would be around 50%, which is slightly lower than published data, but takes into account the potential for early myocardial dysfunction immediately after removal of the heart and incorporation into the modified Langendorff perfusion model. We therefore selected a dose of 150Mbq for the isolated heart experiments.

5.4.4 SPECT imaging of control hearts

Thirteen Male Sprague Dawley rats weighing between 370 and 587 grams were imaged for the isolated perfused heart experiments. We were unable to hang one heart on the perfusion rig as the aorta became very friable, therefore data for 12 animals was obtained for analysis. The hearts were removed and hung as described in the methods section. The following imaging protocol was used for 9 animals (Figure 5.3).

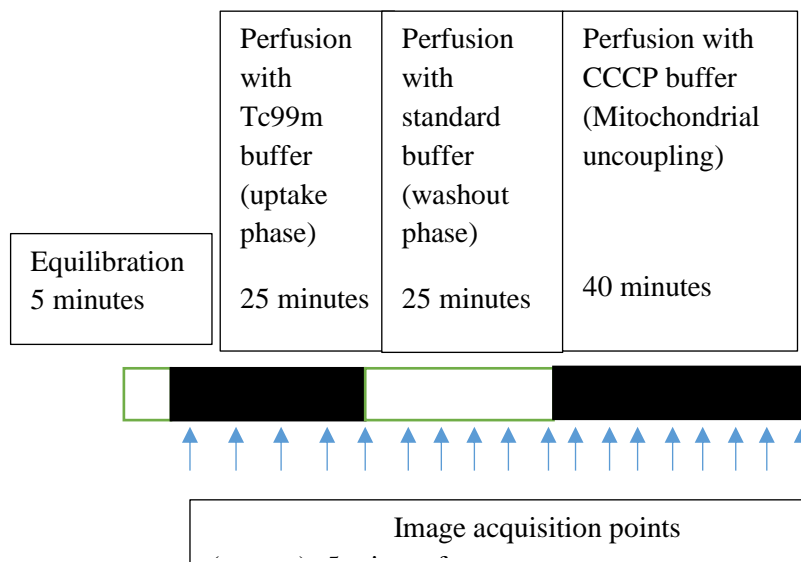


Figure 5.3 Technetium washout protocol, isolated rat hearts

Three animals were imaged without adding CCCP to the buffer, in order to assess prolonged washout rates in the absence of a mitochondrial uncoupler. (Figure 5.4)

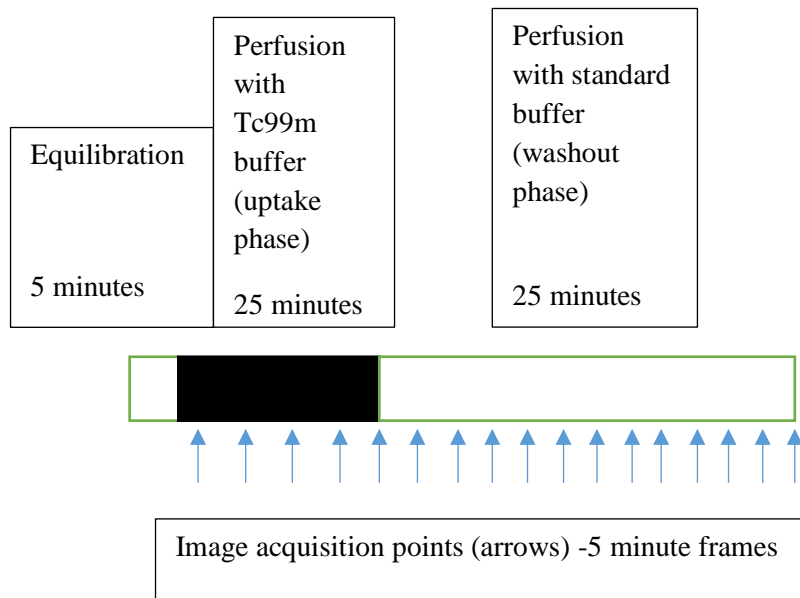


Figure 5.4 Technetium washout protocol – prolonged washout phase

Absolute counts were collected at 5 minute intervals, and the following decay correction was applied;

$$A_o = A_t \times e^{kt}$$

A_o = time A_t = raw data

k = decay constant t = time elapsed

The decay constant was calculated using the formula;

$$\text{Decay constant} = \ln(2) / \text{Technetium half time}$$

The half-life of Technetium is 6 hours, therefore the decay constant is 0.1155

To take into account of the variability in size of the hearts, the decay corrected counts were converted to counts per mm^2 .

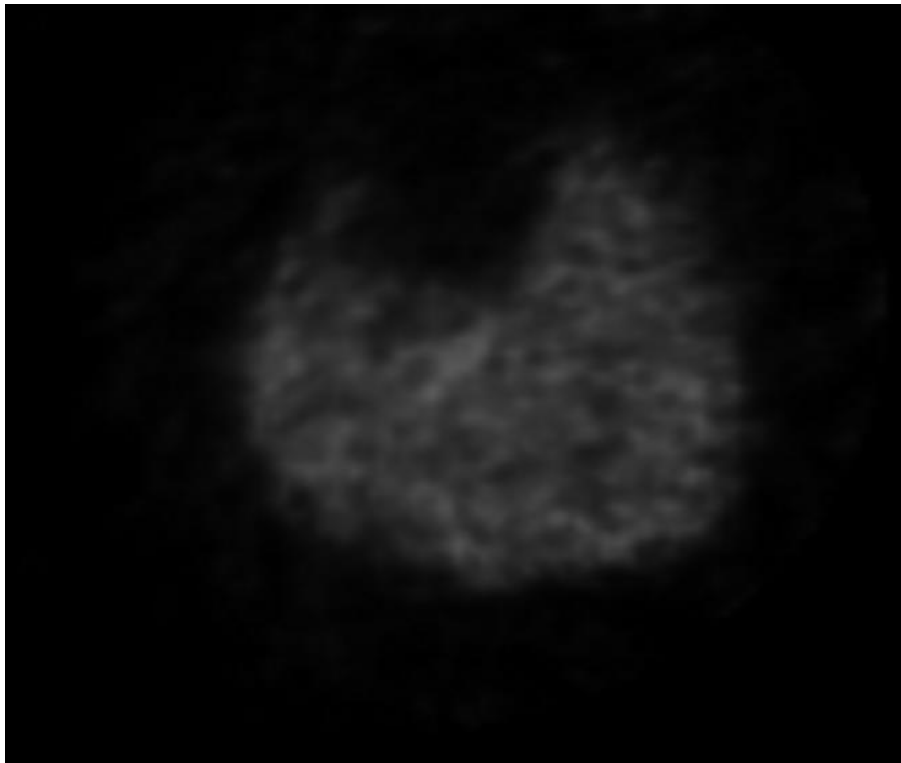


Figure 5.5 Example planar SPECT image from isolated heart perfusion

Washout rate was calculated using the following formula.

Washout rate (%/min) =

$$\frac{\text{Early decay corrected counts} - \text{Delayed decay corrected counts}}{\text{Early decay corrected counts} \times \text{Time in minutes}} \times 100$$

This formula was used in a preclinical study by Fukushima *et al.* They demonstrated a reduction in washout rates in the presence of mitochondrial dysfunction. This was confirmed by changes in mitochondrial density on electron microscopy, and impaired energetics through a reduction in ATP production. This formula was also used in clinical studies by Matsuo *et al.* and Inoie *et al.* It has the advantage of only requiring scans at two timepoints, making it a more acceptable method for patients than one which requires multiple studies.

Initially, the count rate at 25 minutes was used for early counts, i.e. the start of the washout phase, however at this point the majority of hearts had not reached peak counts, leading to spurious rates. Therefore the peak count was used to determine early counts, based on the individual data points for each heart. For post CCCP washout rate, counts at 50 minutes were used for early counts.

A line of best fit was drawn on each washout curve to establish the initial linear washout rate. This provided the rate of reduction in counts/mm²/min, which was then adjusted to take into

account of the initial count rate. Phase 1 refers to the initial washout period, and phase 2 is post CCCP (Figure 5.6). This method was used in a study by Okada *et al* in a pre-clinical study of ischaemia/reperfusion injury. The increase in Technetium washout was associated with markers of mitochondrial dysfunction. No clinical studies were identified that used the line of best fit method, likely due to the practical issues with serial scanning, as discussed above.

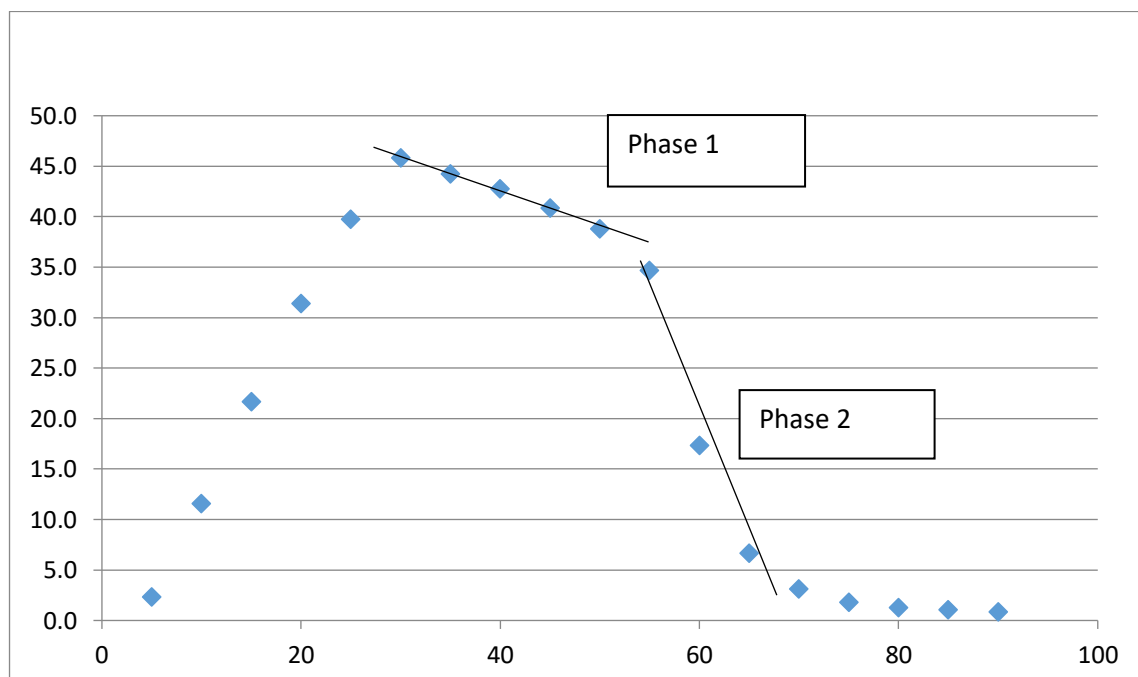


Figure 5.6 Example washout curve demonstrating lines of best fit for calculation of washout rate for isolated heart studies

5.4.5 In vivo SPECT imaging

Six male Wistar rats (Charles River, Kent UK) were scanned using the imaging protocol described in section 2.1. The animals were scanned for a total of 90 minutes, with 6 frames obtained at 15 minute intervals. Activity was measured in Megabecquerels (MBq), and converted to MBq/mm² to account for variation in heart size. A background region of interest was drawn close to, but not involving, the cardiac boundaries, and background activity was subtracted from the calculated left ventricular activity.

Standardised uptake values (SUV) were calculated to adjust for body weight and injected dose according to the following formula.

$$\text{SUV} = \frac{\text{Count activity (MBq)}}{\text{Injected dose (MBq)/Body Weight (g)}}$$

Injected dose was calculated by subtracting the residual activity within the syringe following injection from the total activity drawn up.

5.4.6 Alternative methods of analysis

A number of alternative methods were explored in order to determine which may be useful analysis techniques.

Peak intensity - Activity of the pixel with the highest activity within the left ventricle.

Measured in Kilobecquerels (KBq)

Peak intensity/ peak background - The ratio of the activity within the highest activity pixel in the LV to the highest intensity pixel within the background region of interest (KBq).

Modal intensity – The most frequent activity level per pixel within the left ventricle (KBq).

5.5 Results

5.5.1 Phantom studies

The results of phantom studies are shown below (Table 5.1).

Technetium pertechnetate activity/ 1.5ml buffer	Average counts per minute
10 Mbq	3325
50 Mbq	15040
100Mbq	29476
200Mbq	55782

Table 5.1 Count rates measured by SPECT using a range of Technetium activities within a phantom study

5.5.2 Washout data – ex vivo control hearts

The following wash in/washout curves were obtained from the 9 isolated hearts that were exposed to CCCP (Figures 5.7, 5.8).

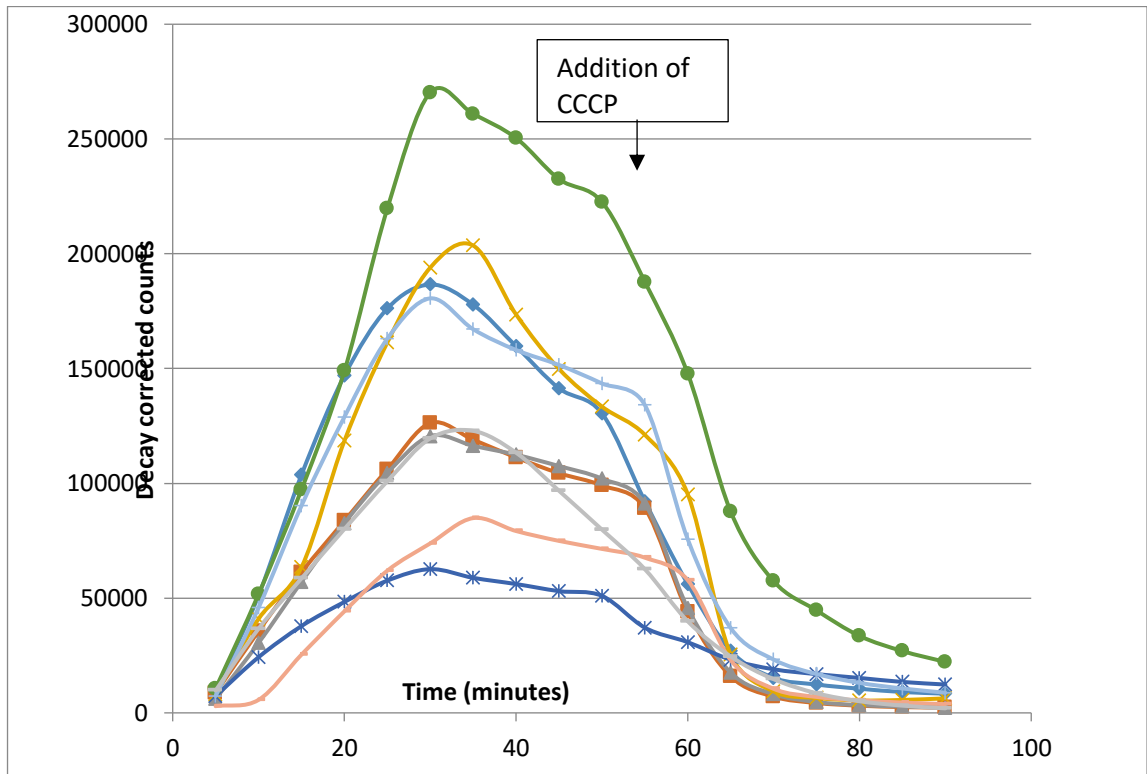


Figure 5.7 Decay corrected counts in control hearts Addition of CCCP at 55 minutes

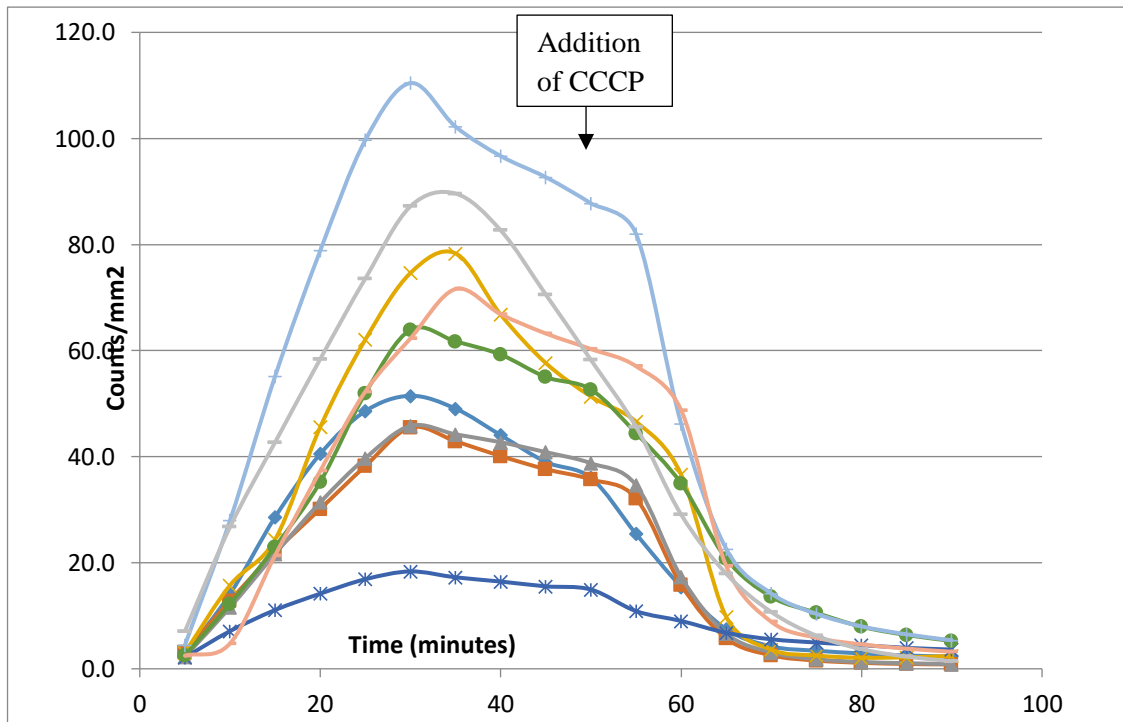


Figure 5.8 Decay corrected counts/mm² in isolated control hearts Addition of CCCP at 55 minutes

5.5.3 Alternative method of measuring washout rate

The following washout rates were obtained using the line of best fit model. Mean washout rate as calculated by this method was significantly higher following the addition of CCCP (1.36%/min vs 6.18%/min $p < 0.00001$).

Heart	Animal weight (g)	Washout rate Peak to 50 mins (%/minute)	Washout Rate CCCP 50-90 mins (%/minute)
1	378	1.51	2.33
2	343	1.08	2.44
3	370	0.77	2.45
4	373	1.55	2.47
5	371	0.93	1.90
6	515	0.88	2.25
7	587	1.04	2.37
8	498	1.05	2.39
9	510	2.33	2.46
Mean	438	1.24	2.33

Table 5.2 Washout rates before and after the addition of CCCP * $p < 0.00001$ vs peak to 50 minute washout rate

Heart	Change in count rate per minute/mm ² Phase 1	Initial counts/mm ² at peak intensity Phase 1	Washout rate min ⁻¹ Phase 1 %	Change in count rate per minute/mm ² Phase 2	Initial counts/mm ² at peak intensity Phase 2	Washout rate min ⁻¹ Phase 2 %
1	-0.84	51.5	1.64	-1.79	25.4	7.08
2	-0.66	45.5	1.16	-2.64	32.1	8.22
3	-0.33	45.8	0.71	-2.79	34.2	8.2
4	-1.80	78.3	2.27	-2.36	46.6	5.08
5	-0.18	18.4	1.04	-0.41	10.9	1.82
6	-0.59	63.9	0.91	-2.37	44.4	5.33
7	-1.18	110.4	1.07	-5.94	82	7.25
8	-0.75	71.6	1.05	-3.77	57	6.61
9	-2.12	89.6	2.37	-2.77	46	6.08
Mean	-0.94	63.89	1.36 (0.20)	-2.76	42.07	6.18*
(S.E.)	(0.22)	(9.11)		(0.50)	(6.74)	(0.66)

Table 5.3 Washout rates using line of best fit method *p <0.0001 vs phase 1

washout

5.5.4 Prolonged washout

Three studies were performed on isolated hearts without the addition of CCCP (figures 5.9, 5.10). There was no significant difference between washout rates from peak to 50 minutes, and 50-90 minutes (0.75 vs 0.84, p=0.46), table 5.4.

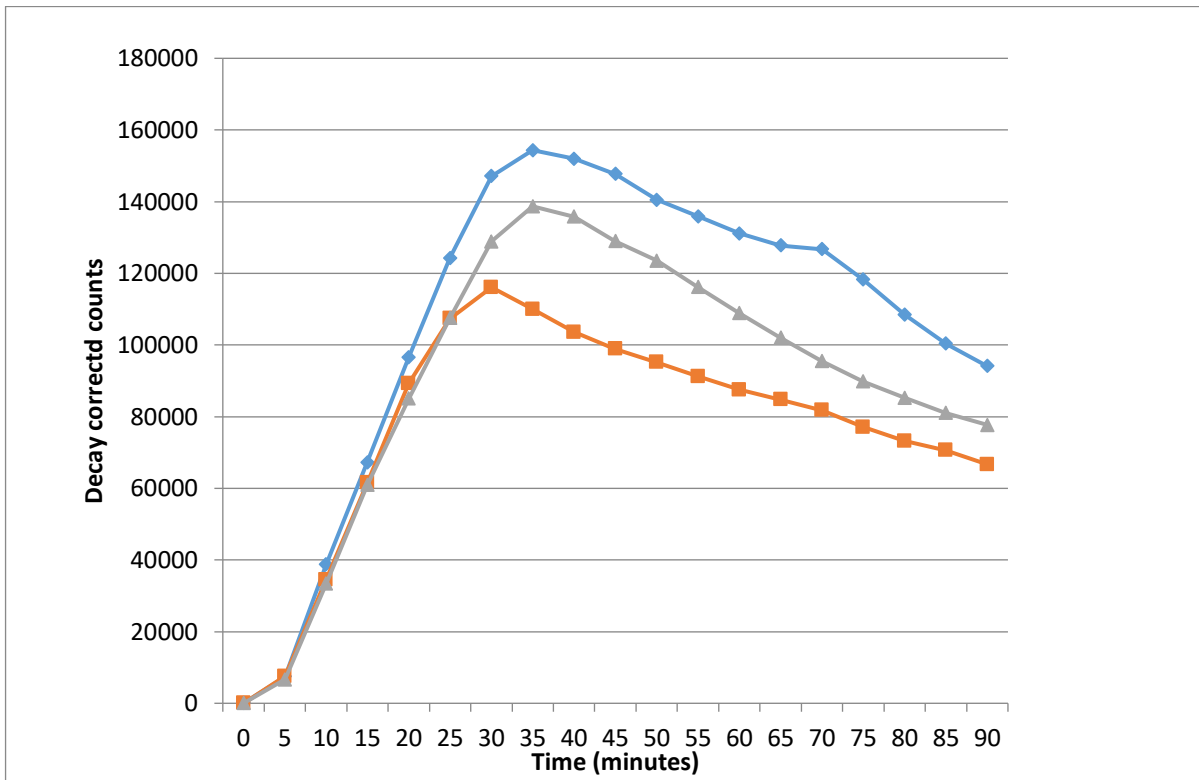


Figure 5.9 Washout curves of decay corrected counts with a prolonged washout phase

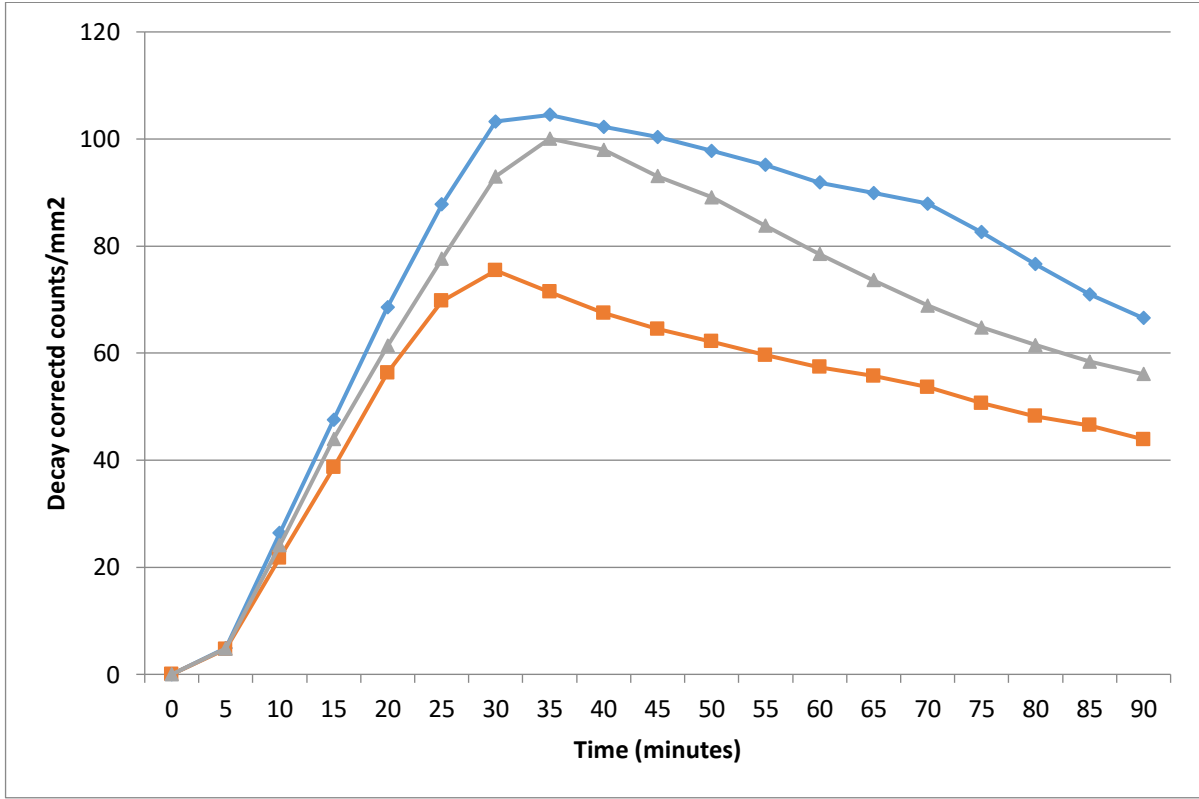


Figure 5.10 Washout curves of decay corrected counts with prolonged washout adjusted to heart size

Heart	Weight (g)	Washout rate Peak to 50 mins (%/minute)	Washout rate 50-90 mins (%/minute)
1	530	0.6	0.83
2	480	0.91	0.76
3	486	0.73	0.94
Mean (S.E.)	498.7 (18.2)	0.75 (0.1)	0.84 (0.06)

Table 5.4 Washout rate for prolonged washout studies

There was no difference in mean washout rates as measured by line of best fit model between peak to 50 minutes and 50 to 90 minutes in the prolonged washout studies (0.69%/min vs 0.86%/min, $p=0.31$), see table 5.5.

5.5.5 Comparing washout rates with and without CCCP

There was no significant difference in mean peak to 50 minute washout rates between CCCP studies and prolonged washout studies (1.11%/min vs 0.75%/min $p=0.12$).

	Change in count rate per minute/mm ² Phase 1	Initial counts/mm ² at peak intensity Phase 1	Washout rate min ⁻¹ Phase 1 %	Change in count rate per minute/mm ² Phase 2	Initial counts/m m ² at peak intensity Phase 2	Washout rate min ⁻¹ Phase 2 %
1	-0.44	104.5	0.42	-0.83	95.1	0.87
2	-0.67	95.2	0.89	-0.45	59.6	0.76
3	-0.75	100.1	0.75	-0.80	83.8	0.95
Mean (S.E.)	-0.62 (0.11)	99.93 (3.1)	0.69 (0.16)	-0.69 (0.14)	79.5 (12.1)	0.86 (0.06)

Table 5.5 Washout rate using line of best fit method for prolonged washout studies

There was, however, a significantly higher mean 50-90 minute washout rate washout when CCCP was added at 50 minutes than without (2.33% vs 0.84% $p < 0.00001$), figure 5.11.

These findings were also seen using the line of best fit method – no significant difference in mean peak to 50 minutes washout CCCP vs prolonged washout (0.60 vs 0.69, $p = 0.09$), but a significant increase in washout with CCCP (1.97%/min vs 0.86%/min, $p < 0.00001$).

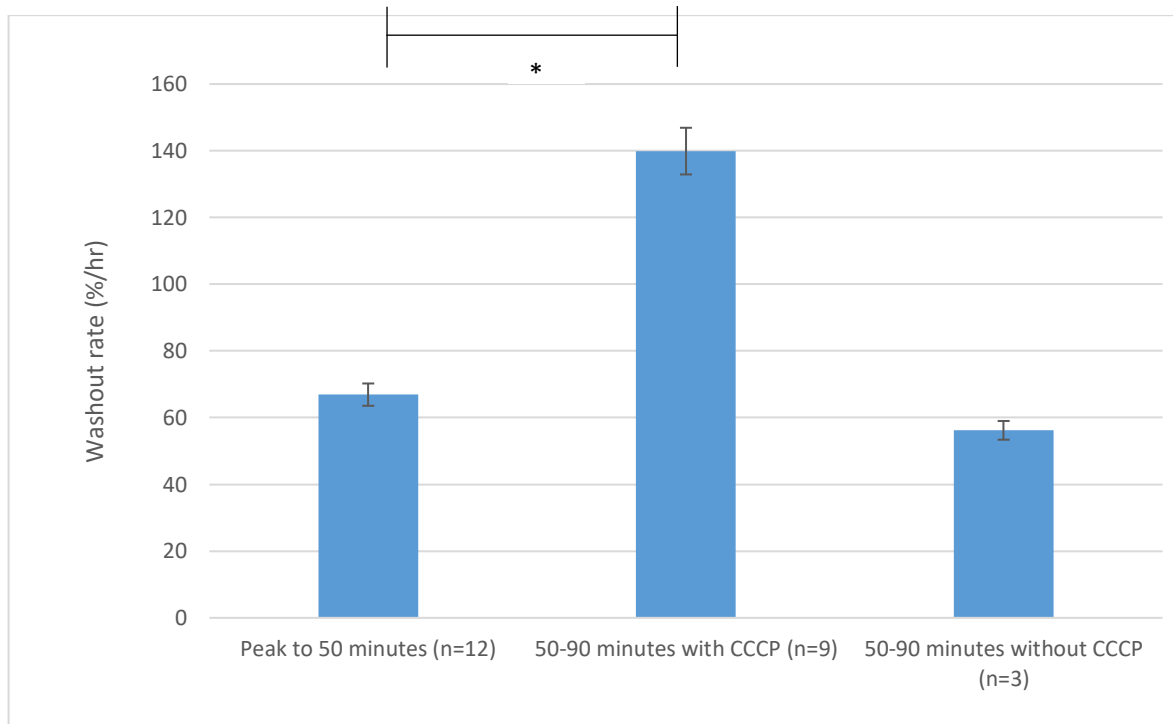


Figure 5.11 Graph displaying initial and late washout rates with and without the addition of CCCP * $p < 0.0001$ vs peak to 50 minutes, and 50-90 minutes without CCCP

5.5.6 In vivo Technetium SPECT washout studies

The following washout curves were obtained over a 90 minute scanning period (Figure 5.12).

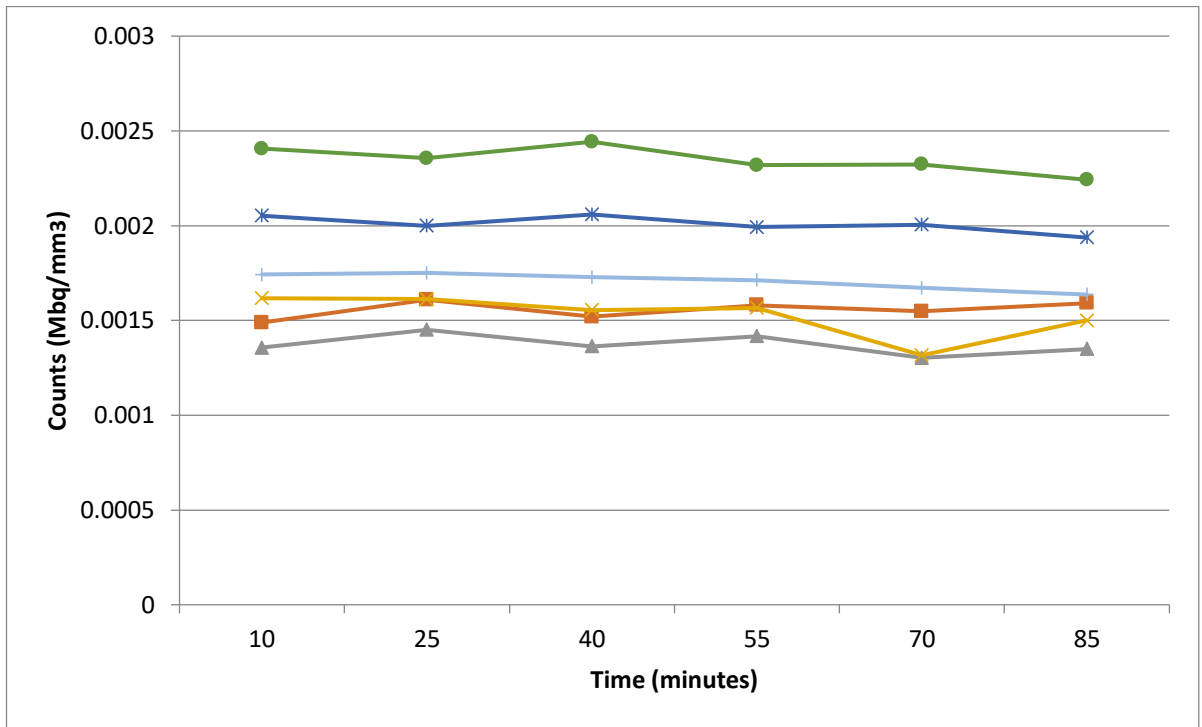


Figure 5.12 Technetium washout traces for *in vivo* SPECT imaging, control hearts

The standard uptake values over time are shown in figure 5.13.

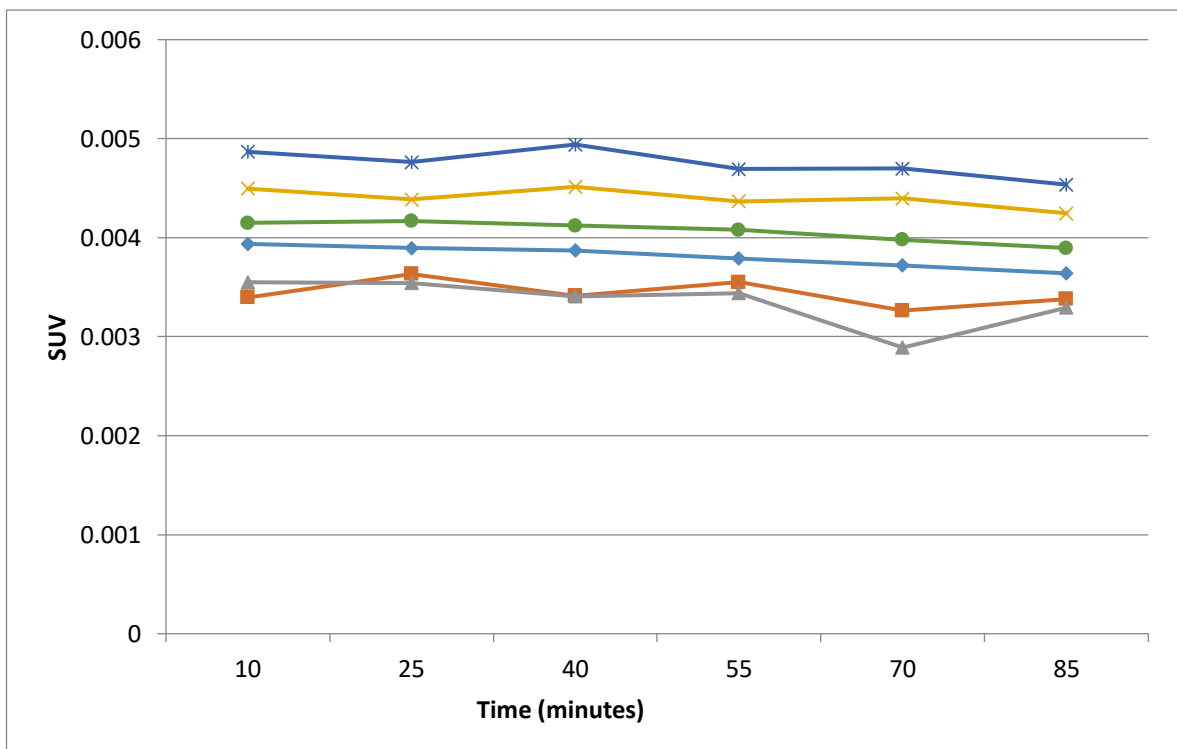


Figure 5.13 *In vivo* Technetium washout – standard uptake

Alternative methods of analysis of count activity are shown below (figures 5.14 – 5.17).

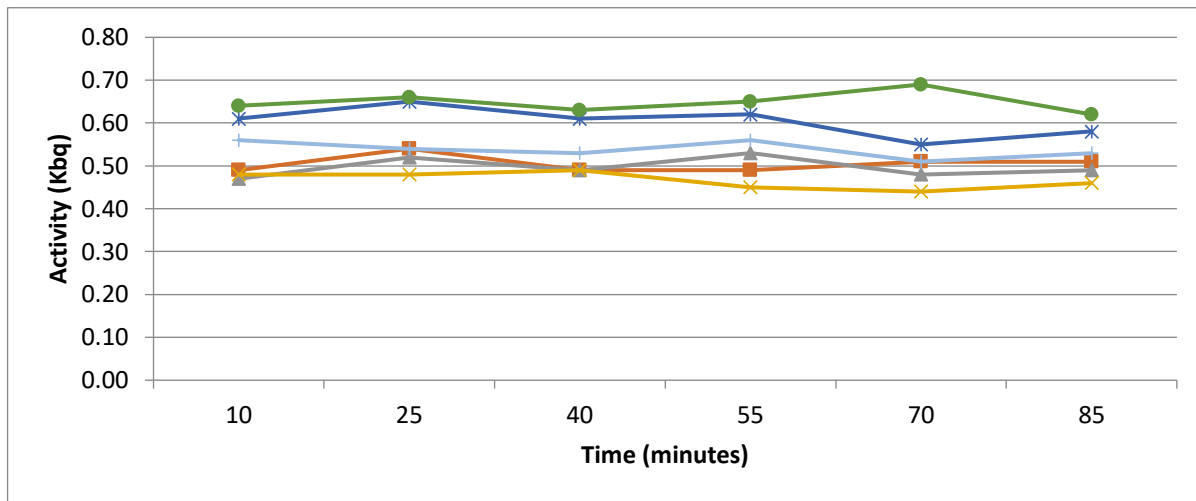


Figure 5.14 Graph of peak intensity - in vivo controls

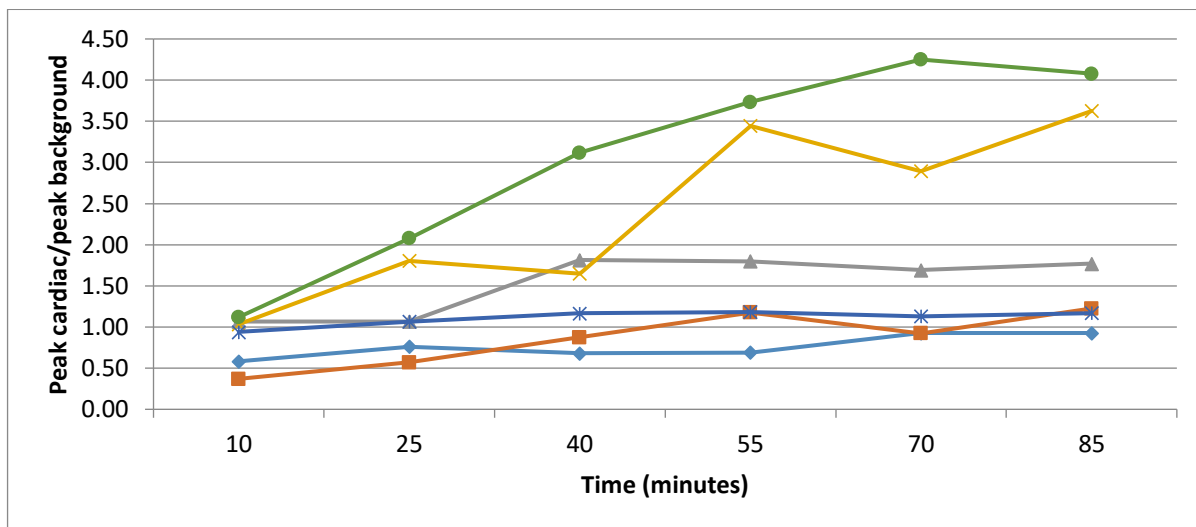


Figure 5.15 Ratio of peak cardiac to peak background counts

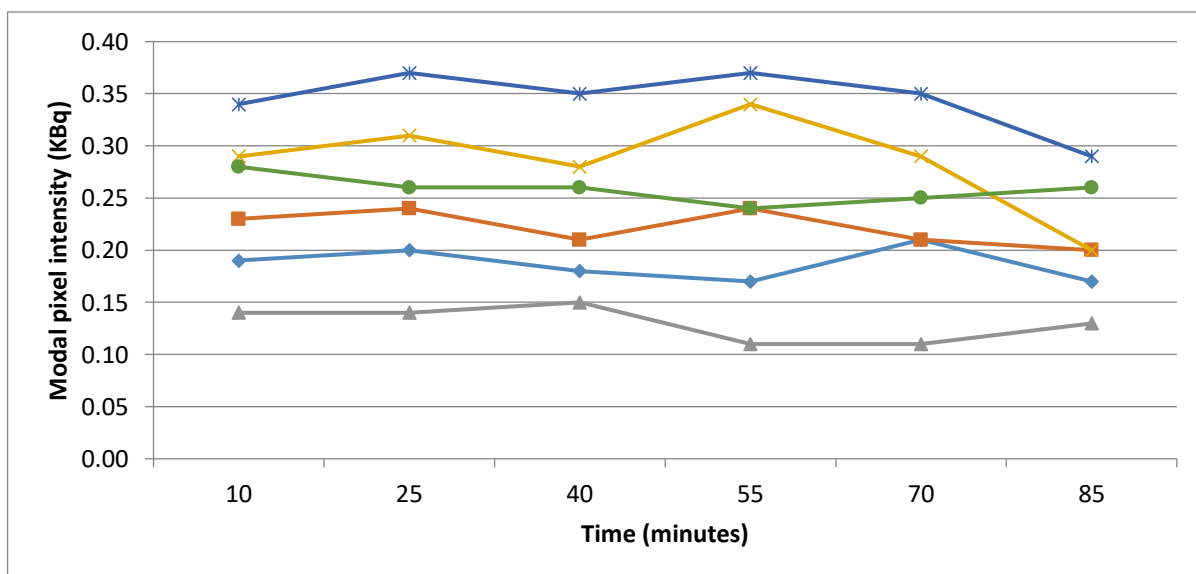


Figure 5.16 Modal intensity - in vivo controls

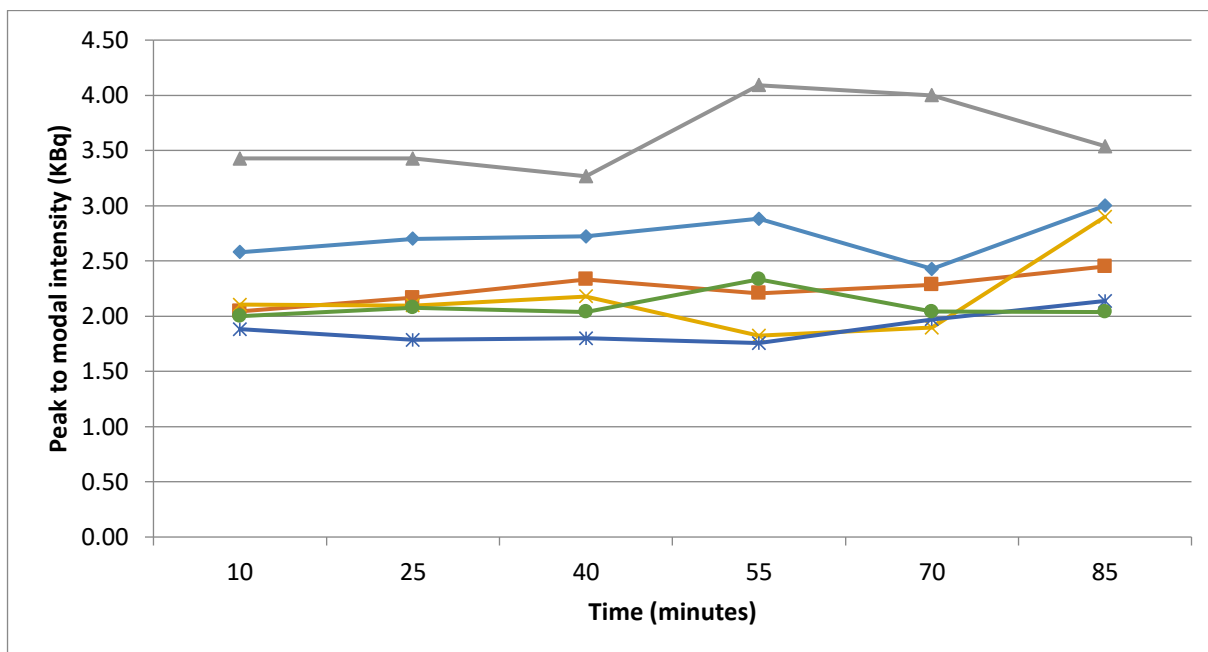


Figure 5.17 Peak intensity to modal intensity - in vivo controls

The mean washout rate in the *in vivo* studies was 0.09%/hour. This is significantly lower than the washout rate in the *ex vivo* prolonged washout studies, $p < 0.0001$ (table 5.6).

Heart	1	2	3	4	5	6
Washout rate Mbq/mm ² (%/min)	0.1	0.12	0.12	0.05	0.08	0.11
Washout rate SUV (%/min)	0.09	0.09	0.09	0.07	0.09	0.08

Table 5.6 Calculated washout rate for in vivo control studies

5.6 Discussion

We have developed an isolated heart perfusion system that can be used to perform *ex vivo* SPECT imaging on isolated rat hearts. There was linear uptake of tracer during the wash-in phase, which would indicate preserved myocardial viability when the heart was incorporated into the perfusion rig. There was marked heterogeneity in tracer uptake between hearts. In particular, one of the hearts demonstrated limited uptake and washout, and was visibly dysfunctional following scanning. There was no clearly identifiable cause for this outlier; there was a short ischaemic time between removal of the heart and incorporation into the perfusion rig, and no protocol deviations. Uptake and washout curves were more uniform in

later scans: this is likely to reflect increasing proficiency, and familiarity with a complex protocol that included multiple time-sensitive steps.

Technetium sestamibi washout was greater in our study compared with previous studies using isolated rat hearts in a Langendorff perfusion mode (Fukushima *et al*, 2007; Fukushima *et al*, 2010). The perfusion systems were similar in terms of buffer constituents, oxygenation, temperature control, and perfusate flow rate. The rats used in our study were older and heavier than prior studies, although I do not believe that this will have greatly altered uptake, given that we were scanning healthy controls. The time from heart extraction to cannulation was less than 30 seconds in the studies by Fukushima *et al*, which is shorter than in our experiments. This is likely to have meant that the hearts in our study had more prolonged myocardial ischaemia, and thus affected tracer uptake and retention within the stunned myocardium. The previous studies were able to incorporate heart rate and pressure monitoring within their system, as counts were collected using an external gamma well counter. The limited space within the closed SPECT scanner meant that we were unable to perform external pacing, nor insert an adjustable balloon into the left ventricle to maintain ventricular end-diastolic pressure. These factors may have also affected myocardial viability, and the lack of monitoring was a significant limitation of our perfusion model.

Technetium washout was significantly increased by perfusion with buffer containing the mitochondrial uncoupling agent CCCP. This is in keeping with prior studies, and strongly suggests that Technetium retention within mitochondria is dependent upon an intact mitochondrial membrane potential (Beanlands *et al*, 1990, Crane *et al*, 1993). It also confirms that our perfusion model is sensitive to changes in experimental conditions. In order to determine the sensitivity of the model, further studies are required in which the concentration of the mitochondrial uncoupler is varied, or the heart is exposed to a range of conditions such as variable periods of ischaemia.

The *in vivo* SPECT imaging of control hearts revealed minimal technetium washout over the 90 minute scanning period. This is in keeping with multiple prior studies, which have demonstrated excellent tracer retention in healthy myocardium. Prior clinical studies have examined retention for up to 4 hours, however to recreate this it would have meant prolonged or repeated anaesthesia of animals. Prolonged anaesthesia with isoflurane has been shown to lead to impaired cardiac contractility. As discussed in section 2.2, this was in higher concentrations than used in our study, and on older animals. The stable Technetium retention would indicate that cardiac function was not impaired in our study.

5.6.1 Methods of analysis

The planar SPECT imaging protocol provided data in the form of absolute count rate. Dynamic SPECT imaging gave data as count activity, measured in megabecquerels. There was no method of converting this data to absolute counts, or *vice versa*, for direct comparison. The calculated washout rate for each method is, however, directly comparable as it is not dependent on the unit of measurement, and therefore this discrepancy did not materially affect the results.

Adjusting the data to take into account of the heart area did produce more uniform washout curves, as compared with using absolute counts alone. For example, heart 8 initially provided relatively low absolute counts, but when adjusted the count rates per mm² were very close to median values. For the *in vivo* experiments, calculation of a standard uptake value, which incorporates body weight and injected dose, produced values that were more greatly spread than those obtained using megabecquerels per mm² (standard deviation 1.78% vs 1.59%).

The line of best fit method of measuring washout was used to measure the initial washout during each period. The rates obtained were similar for the initial washout period (74.2% vs 81.6% mean washout rate per hour for data over complete period vs initial rate respectively). In contrast the line of best fit model provided substantially higher rates for post CCCP data, compared with the original method (371% vs 140% per hour respectively). This is unsurprising, given that during the first washout phase rates were linear, whereas the post CCCP washout produced a negative exponential curve, with a substantial reduction in rates when counts fell to less than 20% of peak activity. The line of best fit method is more appropriate in experimental conditions where there are multiple data points, and producing a washout curve would help to determine appropriate timing for delayed imaging. In clinical practice, a pragmatic washout protocol would typically provide only two data points- early and delayed counts, and therefore the original calculation would be used.

Alternative measures of count activity were evaluated. Peak and modal intensity are measures that have been utilised in prior clinical studies, principally when examining differences in regional washout (Ono *et al*, 2003; Chua *et al*, 1993). There was a greater reduction in modal count intensity over the scanning period when compared with peak intensity, which exhibited minimal change. There was heterogeneity in the intensity curves for both measures, more marked in the modal values. Evaluation of these outputs was only possible for the *in vivo*

SPECT imaging, and not for the planar data acquisition. It would be interesting to see how these measures vary with more dynamic washout, as the information obtained was only for the *in vivo* control hearts that exhibited relatively stable retention. Adjusting for background counts by calculating a ratio produced highly variable results that are difficult to interpret. In some of the studies, the cannula and tubing used to administer the activity was within the background field of view, which produced very high counts, particularly in the early scan period. This led to the progressive increase in count ratio seen in some of the studies. Use of a peak heart to background ratio may be of use when determining the optimal time for scan interpretation in terms of minimising attenuation from other organs/structures, but for the purposes of examining washout it is of limited value. Furthermore, use of peak and modal values alone disregards much of the obtained data, and will be more prone to errors due to sampling variability. Uraemic cardiomyopathy is typically a generalised process, with minimal differences in regional washout in the absence of significant coronary artery disease. Use of measures of global activity would therefore appear to be the most appropriate, incorporating much of the available data as possible.

5.7 Conclusion

We have successfully developed a method of assessing Technetium 99m sestamibi myocardial washout in isolated rat hearts using SPECT imaging. This has not previously been described in the literature. We confirmed that the model was sensitive to changes in experimental conditions through the use of mitochondrial uncoupling agents. The system could be improved by reducing the time between removal of the heart and aortic cannulation, and potentially through external pacing and left ventricular pressure monitoring. We have also developed a protocol for dynamic SPECT imaging that can be used to examine technetium washout *in vivo*, which will allow assessment of longitudinal changes in technetium washout over time. Total count activity within the left ventricle, measured as either total absolute counts per mm² or Mbq per mm² depending on the imaging protocol used, appear to be the most suitable measures for assessing washout rates.

Chapter 6: Early Technetium 99m sestamibi kinetics in clinical practice

6.1 Early Technetium Kinetics

One of the key properties of Tc 99m sestamibi is its prolonged retention in cardiomyocytes, as demonstrated in a number of pre-clinical and clinical studies (Carvalho *et al*, 1992, Pinwica-Worms *et al*, 1989, Wackers *et al*, 1990). This is clinically advantageous, for reasons outlined in the chapter 5. Studies designed to specifically assess Technetium washout have performed the early scan at 30- 60 minutes, and the delayed scan at between 2 and 4 hours (Kumita *et al*, 2002; Sugiura *et al*, 2006; Matsuo *et al*, 2007). The washout rates in the control arms have ranged between 25 and 32%. The counts were not decay corrected in any of the clinical studies. The half-life of Tc sestamibi is 6 hours, therefore the reduction in counts observed will predominantly be due to radioactive decay. Calculating washout rates without decay correction will not affect the comparative analysis between arms, however it is more challenging to evaluate the direct effects of mitochondrial dysfunction on Tc retention using only the raw count data.

From a practical viewpoint, a successful imaging test must be acceptable to patients, and ensure efficient throughput within the department. To facilitate this, the duration of a test needs to be as short as possible, without compromising its sensitivity. Prior washout studies have waited between 30 and 60 minutes before measuring early counts. Technetium 99m sestamibi exhibits rapid clearance from the blood pool, with a blood concentration of 0.3% of the injected dose at 10 minutes. The *in vivo* washout studies described in the previous chapter identified minimal redistribution from the first image, taken at 10 minutes. This was also seen in the control arm of canine models examining the effects of ischaemia on myocardial kinetics. There is no published data on early technetium kinetics using contemporary imaging techniques. If we are able to demonstrate that very early imaging (10 minutes post injection) was a reliable indicator of peak count activity, then it could be used in the measurement of Technetium washout. This could potentially lead to reduced scan times, making it more acceptable for patients and reduce waiting times within the department.

6.2 Objectives

- To measure early technetium uptake in human subjects referred for MPI without end stage renal disease
- Measure decay corrected technetium washout within the first hour post injection

6.3 Hypothesis

1. In healthy controls there is no significant difference in tracer counts between early (10 minutes) and delayed (45 minutes) initial scan, indicating that peak count activity occurs at an early stage.
2. The presence of myocardial ischaemia will increase early technetium washout rates.

6.4 Methods

The subjects were part of a separate study designed to examine the utility of immediate image acquisition following technetium 99m sestamibi injection, when compared with the current protocol of waiting 40-45 minutes before image acquisition (unpublished).

A delay in scanning is commonly employed to allow hepatobiliary clearance of tracer and thus improve image quality; the original study assessed the image quality and interpretability of immediate acquisition when compared with standard imaging. This provided 2 sets of images that could be used to assess technetium washout over a 45 minute period.

Patients were referred for myocardial perfusion studies on clinical grounds to look for evidence of myocardial ischaemia. Patients underwent symptom limited exercise stressing according to the standard Bruce protocol (Bruce and Lovejoy, 1949). Technetium 99m sestamibi was injected intravenously at peak stress followed by a 20ml saline flush. The dose of technetium was determined by patient weight (range 750 -985 MBq). Following a 10 minute recovery period, patients underwent a gated SPECT study (early scan), as described in the methods section. The second scan was performed after 50 minutes (late scan), patients were rescanned using the same protocol.

Planar views from 40 degree left anterior oblique (projection 1) and anteroposterior projections (projection 2) were used to assess washout. A region of interest was drawn around the left ventricle, and corrected for decay and background counts. Washout rate was measured using the following calculation;

Washout rate (%/hour) =

$$\frac{\text{Number of counts (early)} - \text{Number of counts (delayed)}}{\text{Number of counts (early)} \times \text{time (hours)}} \times 100$$

Number of counts (early) x time (hours)

The patients were stratified according to whether they were above or below median age, median left ventricular ejection fraction (a measure of left ventricular function) and sum stress score (a semi-quantitative measure of perfusion defects, typically indicating ischaemia or infarction, with higher scores indicating larger defects).

Ejection fraction was calculated using the following formula

Ejection fraction % =

$$\frac{\text{End-diastolic LV volume (ml)} - \text{End-systolic volume (ml)}}{\text{End-diastolic volume (ml)}} \times 100$$

(Masani *et al*, 2011)

6.5 Results

Fifty-five patients were enrolled into the study, 4 patients were excluded (2 required pharmacological stress, 1 suffered extravasation of tracer, 1 unable to have both scans due to time constraints) therefore 51 sets of images were included in the final analysis. The median age was 62, and 65% of subjects were male. The early scans were taken after a mean delay of 15 minutes, the delayed scans were taken at a mean of 58 minutes post tracer injection.

Using decay corrected activity, there was a net increase in counts between the early and delayed scans, which produced a negative washout rate (-4.96%/hr in projection 1, -1.03% in projection 2). There was no significant difference between early and delayed count activity in either projection. There was no difference in washout rates between the two projections (p=0.39), table 6.1.

	Mean counts early scan – corrected (S.E.)	Mean counts delayed scan – corrected (S.E.)	Washout rate - corrected %/hr (S.E.)	P value (Early counts vs delayed counts)
Projection 1	7046 (302)	7153 (317)	-4.96 (2.9)	0.18
Projection 2	7394 (273)	7308 (273)	-1.03 (3.3)	0.59

Table 6.1 Technetium activity and washout rates, with decay correction

Measuring count activity without applying decay correction resulted in a significant reduction in mean count activity between early and delayed scans in both projections (p=0.0073 and

p=0.00032 respectively). This produced negative washout rates (6.61% projection 1, 10.3% projection 2), table 6.2. There was again no difference in washout rates between the two projections (p=0.39).

	Mean counts early scan (S.E.)	Mean counts delayed scan (S.E.)	Washout rate – corrected %/hr (S.E.)	P value (Early counts vs delayed counts)
Projection 1	7033 (319)	6778 (298)	6.61(2.7)	0.0073
Projection 2	7336 (279)	6925 (256)	10.32 (3.2)	0.00032

Table 6.2 Technetium washout without decay correction

	N	Mean washout rate (S.E) P1	Mean washout rate (S.E.) P2	P Value
Washout	51	6.61 (2.7)	10.32 (3.2)	-----
SSS<4	29	2.64 (2.45)	4.64 (3.41)	P1 0.44
SSS≥4	22	6.86 (2.48)	17.81 (2.62)	P2 0.049
Age ≤62	26	5.98 (3.23)	10.07 (3.19)	P1 0.86
Age> 62	25	7.22(3.46)	10.57 (3.26)	P2 0.94
EF ≤ 60	26	4.86 (2.45)	12.86 (1.95)	P1 0.52
EF >60	25	8.43 (2.9)	7.68 (4.2)	P2 0.45

Table 6.3 Technetium washout stratified by clinical variables EF – ejection fraction SSS - sum stress score

There was no significant difference in washout rates, stratified by age, and ejection fraction. Patients with sum stress scores greater or equal to 4 had a higher washout rate, reaching borderline statistical significance (p=0.049) in projection 2 (table 6.3). Figure 6.1 clearly

shows the increase in Technetium washout when a sum stress score was greater than 4 from projection 2, from which the early scan was taken at mean time of 21 minutes, and the delayed scan at 64 minutes. This suggests that myocardial ischaemia leads to augmented washout as early as 1 hour post tracer injection.

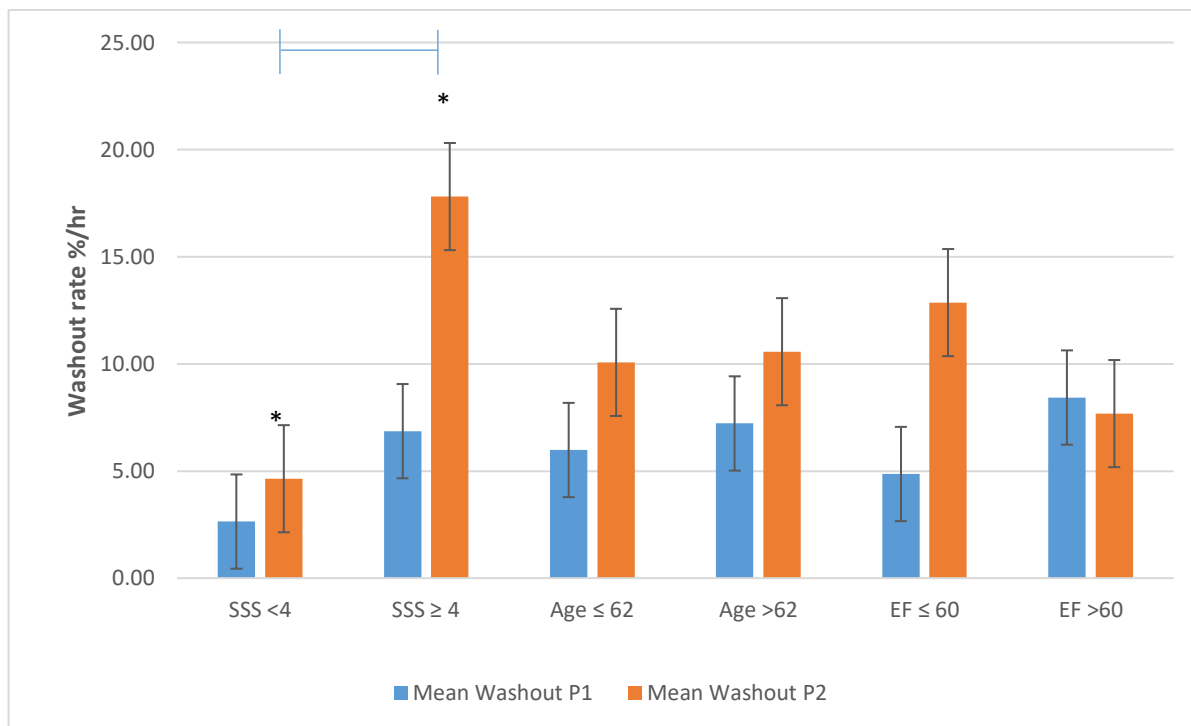


Figure 6.1 Washout rates from 2 projections, according to SSS, age and EF
 SSS Sum Stress Score, EF Ejection Fraction

6.6 Discussion

There was a trend towards increasing Technetium activity between 15 minutes and 50 minutes when a decay correction was applied, however this was not statistically significant. An early study by Wackers *et al* (1989), which was influential in developing our understanding of Technetium sestamibi kinetics in clinical practice, found that there was an initial plateau in cardiac activity from 5 minutes post tracer injection to approximately 40 minutes, at which point there was a linear decline. The count activity in their study was not decay corrected. Given the nature of Technetium 99m sestamibi decay, one would expect approximately a 9% reduction in count activity over the first hour once a steady state had been achieved. A plateau in early activity would suggest that there is ongoing tracer uptake during the first 40 minutes that offsets the expected decrease in count activity over time.

When our data was evaluated without decay correction, there was a significant reduction in counts between the early and delayed images. The washout rates are in keeping with the expected reduction in count activity due to Technetium decay. Therefore, in contrast to the study by Wackers *et al*, it would appear that there is negligible cardiac uptake beyond the first 15 minutes. This would also be in keeping with our *in vivo* Technetium washout studies in rats, and other published animal work from Beanlands *et al*, and Liu *et al* (see figure 6.2).

There are no published clinical studies that have measured Technetium prior to 30 minutes for the initial scan. Therefore this may represent a novel imaging protocol that reduces the overall scanning period.

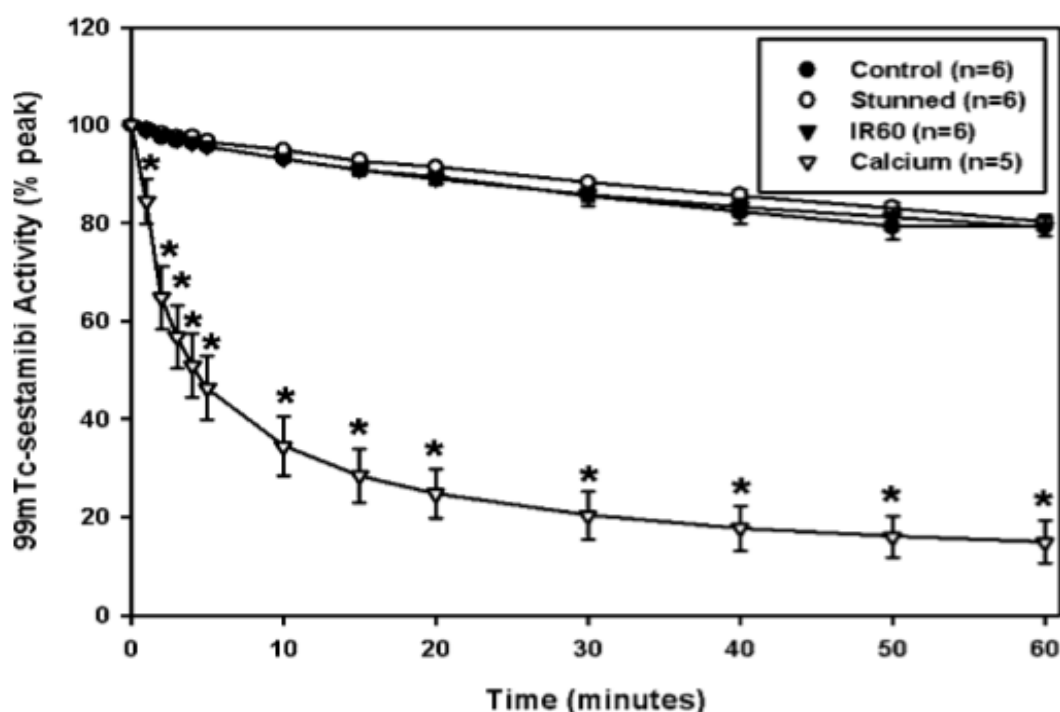


Figure 6.2 Tracer washout curves from Liu et al, 2008 This demonstrates rapid early uptake within the first few minutes following tracer injection.

Left ventricular function, measured by ejection fraction, did not affect washout rates in this study. Prior studies have shown that ejection fraction is inversely associated with washout rate (Sugiura *et al*, 2006; Matsuo *et al*, 2007). In these studies the severity of cardiac dysfunction was more severe, with an EF of < 40%, whereas in our study only 1 patient had an EF below this level. Furthermore, washout was monitored over a more prolonged period, which is likely to have enhanced its sensitivity.

Patients with greater than mild perfusion defects, as measured by sum stress score, had higher washout rates. Technetium retention has shown to be impaired in patients with significant coronary stenoses, and following myocardial infarction (Shin *et al* 1995, Takeishi *et al*, 1996). These findings are also in keeping with the study by Okada *et al*, which specifically assessed the effects of ischaemia on Technetium washout. The delayed scans in that study were performed at 3 hours. Our findings suggest that the delayed scan could be performed at an earlier time, whilst retaining its sensitivity for detecting changes in mitochondrial function. Uptake of sestamibi is dependent on the mitochondrial membrane potential, which is coupled to ATP production. After a period of ischaemia, ATP production reduces after 10- 60 minutes, depending on the degree of reduction blood flow (Massy *et al*, 2002). This would suggest initial tracer uptake into mitochondria in ischaemic territories, followed by impaired retention as the membrane potential decreases.

6.7 Conclusion

There was no significant net change in Technetium 99m sestamibi activity between 15 and 50 minutes following tracer injection in a group of unselected patients referred for MPI. This suggests that for the purposes of washout calculations, early count activity could be measured as early as 15 minutes following tracer injection. Given the large individual variability in washout rates, further studies are required that measure serial Technetium activity at multiple time points in order to determine optimal scan timing.

Chapter 7: Discussion and future work

7.1 Project findings

The main findings of this project were;

- In patients with end stage renal failure undergoing MPI as part of a renal transplant evaluation, the presence of fixed perfusion defects were independently associated with a 2.3 times increase in the relative risk of all-cause mortality. Moderate to severe stress perfusion defects were associated with a 1.7 times increased relative risk of all-cause mortality and cardiovascular events. However, the finding of an abnormal scan did not add additional prognostic information beyond traditional clinical risk factors and ECG abnormalities for predicting medium to long term cardiovascular outcomes. An abnormal baseline ECG was the most powerful predictor of both all-cause mortality (16.2 times increase relative risk, and mortality and cardiovascular events combined (3.4 times increased relative risk). Perfusion scan abnormalities correlated with angiographic stenosis in only 40% of patients who were referred for invasive coronary angiography, suggesting poor agreement between the two techniques.
- A rat model of uraemic cardiomyopathy led to structural and mitochondrial cardiac adaptations at 12 weeks following 5/6ths nephrectomy. There was a 310% increase in serum urea level, and 210% in serum creatinine level, when compared with controls. The mean heart weight increased by 13%, suggesting the development of left ventricular hypertrophy. Blood pressure and cardiac contractility were unchanged at 12 weeks vs control. There was a 9.6% increase in state 4 respiration rates in the presence of complex I substrate in the uraemic animals, suggesting a greater degree of mitochondrial uncoupling. There was also a 16% reduction in complex II and III enzyme activity in uraemic hearts, when compared with control.
- An isolated perfused heart system was developed that can be used for assessing *ex vivo* Technetium 99m sestamibi washout. Technetium washout was increased by 2.8 times in the presence of the mitochondrial uncoupling agent CCCP, suggesting that Technetium retention is linked to mitochondrial function. A method for measuring *in vivo* Technetium washout was developed. We demonstrated stable Technetium retention in control animals up to 90 minutes post injection.
- Patients without renal failure referred for stress perfusion imaging exhibit, on average, minimal Technetium washout between 15 minutes and 1 hour post tracer injection. There was large individual variability in washout rates, between 1 and 20% in a 45 minute period. Patients with stress induced ischaemia, as measured by sum stress

score, exhibited higher Technetium washout compared with those without significant ischaemia (17.1% with SSS>4 vs 6.86% with SSS≤4).

7.2 Limitations

7.2.1 Clinical Studies

Retrospective audit

Documentation from clinic and discharge letters was generally of high quality, however there may have been co-morbidities and clinical events that were not recorded, particularly if the events occurred at different hospitals. We were unable to establish the smoking history from the information available, which is clearly an important cardiovascular risk factor. This was a retrospective, observational study, and therefore causation cannot be established. The number of patients included in the retrospective analysis was too small to produce a validated risk prediction tool, particularly given the relatively low event rate. A larger sample, including data from other centres would be required to produce an adequate sample size.

Early technetium kinetics study

There was significant variability between washout rates of individual patients, which was largely unexplained. There were many clinical variables that were not recorded, such as diabetes and hypertension that may account for the variability seen. Patients move off the imaging table between scans, hence they may be in a slightly different position for the second scan. This may mean that the early and delayed projections are not taken at exactly the same angle, and therefore affect count measurements. All scans were assessed prior to analysis to ensure that there was no visible positional change. Furthermore the findings were consistent in both projections suggesting that this was not a significant factor.

There was a delay of 6 minutes between obtaining projections 1 and 2, however this time period was too short to observe a significant change in count activity, and therefore they could not be studied meaningfully as 4 discrete time points. In order to gain a more detailed insight into Technetium kinetics we would require imaging acquisition at a number of time points to develop a time/activity curve.

7.2.2 Animal studies

Unfortunately, we were not able to perform the planned *in vivo* perfusion studies on uraemic rats. This was due to a major fault with the preclinical SPECT scanner that could not be rectified in time to scan a prepared batch of 12 week uraemic animals. There was insufficient time and resources to repeat these experiments during the research period. It would be interesting to perform this set of experiments as part of a future project to determine whether the abnormalities of mitochondrial function seen *in vitro* translate into measurable differences in Technetium sestamibi washout rates.

The number of animals used in the washout studies was low, therefore they are likely to have been underpowered to detect differences between arms. A key principle of animal studies is to minimise the number of animals used where possible, but clearly there needs to be sufficient numbers to provide valid results. Resource constraints, and the equipment issues described above contributed to the low numbers studied.

Technetium washout rates were higher our isolated perfused heart studies those recorded by other groups (Fukushima et al, 2007; Fukushima et al, 2010). This may have been due to a longer delay between heart explantation and incorporation into the perfusion rig in our study, which lead to increased myocardial injury. There may have been limitations of our perfusion system that contributed to the deterioration in cardiac function. There were issues with maintaining the temperature within the system, and we were unable to pace the hearts, as described in 5.4.1. Furthermore we were not able to directly visualise the hearts during the scan. Future work should focus on methods of optimising the perfusion conditions and monitoring process within the limited confines of the scanning area.

The mitochondrial samples that I used were freeze-thawed, and this has been shown to reduce cardiolipin levels (Quigley et al, 2000), which is necessary for inner mitochondrial membrane function, and may therefore have affected measured complex activity. The control and uraemic samples were stored and prepared in an identical manner, so this would not explain the difference between the groups. Citrate synthase levels was not statistically different between the two arms, which indicates that the quantity of intact mitochondria was similar. We can surmise, therefore, that the reduction in complex activity was not due to a reduction in mitochondrial density

7.3 Implications for clinical practice

The retrospective analysis of MPI in patients referred for renal transplantation highlighted its utility, as well as its limitations. The clinical value of the test depends upon the question that you wish to answer. In patients with symptoms suggestive of cardiac ischaemia and cardiovascular risk factors, MPI is a reliable imaging test for identifying significant obstructive coronary disease (Berman *et al*, 2001). Its role as a perioperative screening tool in asymptomatic patients undergoing non-cardiac surgery is less well established, although the presence of reversible perfusion defects is associated with perioperative cardiac events (Hendel *et al*, 1992). The 30 day perioperative cardiac event rate in our cohort was very low, which may indicate that our current screening methods appropriately identify high risk patients, who are then either not considered for transplant, or appropriately revascularised. The role of revascularisation in asymptomatic patients undergoing non-cardiac surgery is itself a matter of considerable debate.

If a clinician wishes to determine an individual's long term cardiovascular risk, in order to help determine the potential benefit of transplantation, MPI appears to be less helpful. In agreement with prior studies, the presence of fixed defects did predict worse longer term outcomes, but overall the MPI findings did not add to a prognostic model comprising of clinical risk factors and ECG abnormalities. The prognostic utility of MPI in certain groups, such as diabetics, is only valid for up to 2 years (Giri *et al*, 2002). In the unique population of ESRD patients, there are multiple factors that will impact on longer term outcomes, such as whether they receive a renal transplant, immunosuppressive regimes and rejection rates. It would therefore be extremely difficult for any test to accurately predict longer term outcomes in this group.

In our analysis, the vast majority of patients were asymptomatic, which lowers the pre-test probability of identifying significant cardiac disease. In patients without key risk factors (older age, diabetes, history of CV disease) the event rates were very low, hence the yield from non-invasive testing is limited. This was seen in the study by De Lima (2013), who found that low risk patients had favourable outcomes irrespective of the MPI findings.

I would therefore advocate a more selective approach to cardiovascular assessment in transplant candidates. In low risk, asymptomatic patients further testing is not beneficial. For symptomatic patients, or those at intermediate to high risk, it would be reasonable to perform MPI. Those with significant stress or resting perfusion abnormalities should be investigated

further with coronary angiography, where appropriate. The semi-quantitative summed scores should be quoted in scan reports, and their significance discussed between the cardiology and nephrology teams. Ultimately the findings are just one facet of a complex, multidisciplinary assessment to determine transplant suitability, weighing up all of the potential risks and benefits.

7.4 Future pre-clinical studies

The isolated heart perfusion technique was shown to be a reliable method for assessing Technetium washout. The washout rates were higher than previous studies; the viability of hearts may be improved by reducing cold-ischaemic times during excision of the heart and incorporation into the perfusion system. In order to improve the model, it would be interesting to develop the system in order to incorporate cardiac pacing, and potentially an intraventricular balloon to provide a consistent preload. These modifications need to be balanced against the risk of introducing artefact within the small imaging field, which may affect the reliability of the test. With appropriate technical proficiency, the current model provides reproducible washout curves that could be used to assess *ex vivo* washout in uraemic hearts, and examine the effect of changes in conditions, such as increasing cardiac workload or ischaemia.

A method for assessing technetium 99m sestamibi washout *in vivo* was established, which confirmed minimal redistribution in healthy myocardium. Various methods of assessing washout were examined; decay corrected count activity measured in MBq/mm² appeared to be the most suitable for planar SPECT imaging, and is a measure that can be translated from pre-clinical to clinical studies. At 12 weeks post subtotal nephrectomy, there was evidence of compensated cardiac hypertrophy. Subtle changes in mitochondrial respiration and enzyme activity were identified, but this may not result in measurable changes in technetium washout rates. Adapting the model to produce a more advanced form of renal failure, such as introducing a high salt diet or maintaining the animal for a longer duration, would enable longitudinal studies examining changes in washout rate in the transition from compensated to decompensated cardiac hypertrophy.

7.5 Future clinical work

There was limited scope within the project time-frame to perform a clinical study of technetium washout in patients with renal failure. I had data that enabled me to assess early Technetium kinetics in a group of unselected patients referred for MPI. There was significant individual variability in washout rates, and cardiac ischaemia was shown to be associated with greater washout. A formal pilot study examining serial changes in decay-corrected count activity at multiple time points is required to determine the optimal timing for measuring Technetium washout in clinical practice, as this has not been studied previously.

If this novel clinical indicator is proven to be a useful indicator of cardiac mitochondrial dysfunction, it could be utilised to assess treatments targeted at metabolic function.

7.5.1 Perhexilene

Perhexilene alters myocardial substrate utilisation by inhibition of carnitine palmitoyl transferase 1 and 2 (Jeffrey *et al*, 1995). This leads to a reduction in free fatty acid utilisation and a switch towards glucose metabolism, which results in more efficient ATP production. It is used in selected patients with refractory angina or chronic heart failure, but requires therapeutic drug level monitoring to minimise the occurrence of side effects. There is evidence of symptomatic benefit in a small randomised controlled trial with short term use. A review of 5 year multi-centre clinical experience suggests that it is safe and efficacious for longer term use in chronic heart failure and angina (Phan *et al*, 2009). A switch from fatty acid oxidation to glucose utilisation has been postulated as a causative mechanism in the transition from compensated to decompensated cardiac hypertrophy, as described in chapter 3. It would therefore be interesting to perform a longitudinal study that evaluates Technetium washout in patients with uraemic cardiomyopathy treated with perhexilene.

7.5.2 Sacubitril- Valsartan

This agent is a combination of Valsartan, an angiotensin receptor blocker, and sacubitril, a neprilysin inhibitor. It is the first drug in a class of agents termed ARNis (Angiotensin Receptor Blocker Neprilysin Inhibitor). As described in Chapter 1, angiotensin receptor blockers induce LVH regression and attenuate fibrosis in left ventricular hypertrophy. Neprilysin is responsible for the enzymatic cleavage of an array of peptides responsible for

maintaining cardiorenal homeostasis, including natriuretic peptides and substance P. Inhibition of neprilysin has a number of effects, including vasodilation and positive cardiac remodelling. In a recent landmark randomised clinical trial, sacubitril-valsartan was shown to be superior to the ACE-inhibitor enalapril in the treatment of chronic heart failure with reduced ejection fraction (McMurray *et al*, 2014). Trials are underway to examine its effects in heart failure with preserved ejection, which has many phenotypic similarities to uraemic cardiomyopathy. A recent study of a sub-total nephrectomy model of uremic cardiomyopathy found that treatment with sacubitril-valsartan had reno-protective effects, assessed through reduction in serum creatinine and urinary protein excretion, and cardioprotective effects through reduction in LVH, fibrosis and improved fractional shortening. This effect was greater than that seen with an ARB alone (Ushijima *et al*, 2017). Assessing the effect of this intriguing new agent on mitochondrial function *in vivo* using Technetium washout may provide useful mechanistic insights into its metabolic effects.

References

2008 Nuclear Medicine: Market Summary Report. Des Plaines, Ill: IMV Medical Information Division; 2008:IV19–IV30 42(1), pp.61-68

Abel ED, Doenst T (2011). Mitochondrial adaptations to physiological vs. pathological cardiac hypertrophy. *Cardiovasc Res*, 90(1), pp. 234–242

Aksentijević D, Bhandari S, Seymour AM. (2009). Insulin resistance and altered glucose transporter 4 expression in experimental uremia. *Kidney Int.* 75(7), pp. 711-8

Al Banchaabouchi M, Marescau B, D’Hooge R, Van Marck E, Van Daele A, Levillain O. (1998). Biochemical and histopathological changes in nephrectomized mice. *Metabolism.* 47(4-5), pp. 355–61

Alhaj E, Alhaj N, Rahman I, Niazi TO, Berkowitz R, Klapholz M. (2013). Uremic cardiomyopathy: an underdiagnosed disease. *Congest Heart Fail.* 19(4), pp. E40-50.

Al-Jaroudi W, Iskandrian AE. (2009) Regadenoson: A new myocardial stress agent. *J Am Coll Cardiol* 54(1), pp. 1123-30

Amann K, Mall G, Ritz E. (1994) Myocardial interstitial fibrosis in uraemia: is it relevant? *Nephrol Dial Transplant* 9(2), pp. 127-128

American Diabetes Association. (2010) Diagnosis and classification of diabetes mellitus. *Diabetes Care* 33(Suppl. 1) pp. S62–S69

Anavekar, N.S., McMurray, J.J., Velazquez, E.J. (2004) Relation between renal dysfunction and cardiovascular outcomes after myocardial infarction. *N Engl J Med.* 351: pp. 1285–1295

Ankur Gupta GZ, Hage FG. (2016) Pharmacologic stress testing. In: Garcia AE, editor. Nuclear cardiac imaging principles and applications. New York: McGraw-Hill; pp. 196-224

Armstrong AC, Gidding S, Gjesdal O, Wu C, Bluemke DA, Lima JC. (2012). LV Mass Assessed by Echocardiography and CMR, Cardiovascular Outcomes, and Medical Practice. *J Am Coll Cardiol Img*, 5(8), pp. 837-848.

Aubertin G, Choquet P, Dheu C, Constantinesco A, Ratomponirina C, Zaloszcyc A, Passlick-Deetjen J, Fischbach M. (2012). The impact of dialysis solution biocompatibility on ultrafiltration and on free water transport in rats. *Pediatric Nephrology*, 27(1), pp. 131–138

- Aurigemma GP, Zile MR, Gassch WH. (2006). Contractile behaviour of the left ventricle in diastolic heart failure: With emphasis on regional systolic function. *Circulation*, 113(296), pp. 108-112
- Auerbach AD, Goldman L. (2002). B-Blockers and reduction of cardiac events in non-cardiac surgery: scientific review. *JAMA*, 287(1), pp. 1435-44
- Ayalew A, Marie P Y, Menu P, Mertes PM, Hassan N, Danchin N, Olivier P, Karcher G, Bertrand A. (2000). A comparison of the overall first-pass kinetics of thallium-201 and technetium-99m MIBI in normoxic and low-flow ischaemic myocardium. *European journal of nuclear medicine* 27(11), pp. 1632-40
- Barger PM, Brandt JM, Leone TC, Weinheimer CJ, Kelly DP. (2000) Deactivation of peroxisome proliferator-activated receptor-alpha during cardiac hypertrophic growth. *J Clin Investig* 105(12), pp. 1723–1730
- Barger PM, Brandt JM, Leone TC, Weinheimer CJ, Kelly DP. (2000). Deactivation of peroxisome proliferator-activated receptor- α during cardiac hypertrophic growth. *J. Clin. Invest*, 105(1), pp. 1723–1730
- Bateman TM, Berman DS, Heller GV. (1999). American society of nuclear cardiology position statement on electrocardiographic gating of myocardial perfusion SPECT scintigrams. *J Nucl Cardiol*, 6(3), pp. 470-479
- Baudino TA, Carver W, Giles W, Borg TK. (2006). Cardiac fibroblasts: friend or foe? *Am J Physiol Heart Circ Physiol*, 291(3), pp. 1015-26
- Beanlands RS, Dawood F, Wen WH, McLaughlin PR, Butany J, D'Amati G, et al. (1990). Are the kinetics of technetium-99m methoxyisobutyl isonitrile affected by cell metabolism and viability? *Circulation*, 82(4), pp. 1802-14
- Bell RM, Mocanu MM, Yellon DM . (2011). Retrograde heart perfusion: The Langendorff technique of isolated heart perfusion. *Journal of Molecular and Cellular Cardiology*, 50(6), pp. 940-950
- Bergmann SR, Clarck RE and Sobel BE. (1979). An improved isolated heart preparation for external assessment of myocardial metabolism. *American Journal of Physiology*, 236, pp. 644-651

- Berman DS, Hayes SW, Germano G. (2001). Assessment of myocardial perfusion and viability with technetium-99m perfusion agents. In: Depuey EG, Garcia EV, Berman DS Cardiac SPECT Imaging. Philadelphia: Lippincott Williams & Wilkins. pp.179–210
- Blaber M. (2001). Skeletal Muscle Myosin and Muscle Contraction. Biochemistry I. A Virtual Textbook. Lecture 31
<http://mikeblaber.org/oldwine/BCH4053/Lecture31/Lecture31.htm>
- Bliziotis IA, Destounis A, Stergiou GS. (2012). Home versus ambulatory and office blood pressure in predicting target organ damage in hypertension: a systematic review and meta-analysis. *J Hypertens*, 30, pp. 1289–1299
- Boehm EA, Jones BE, Radda GK, Veech RL, Clarke K. (2001). Increased uncoupling proteins and decreased efficiency in palmitate-perfused hyperthyroid rat heart. *AJP – Heart*, 280(3), pp. 977–983
- Boehm EA, Jones BE, Radda GK, Veech RL, Clarke K. (2001). Increased uncoupling proteins and decreased efficiency in palmitate-perfused hyperthyroid rat heart. *Am J Physiol Heart Circ Physiol*, 280(2), pp. H977–H983
- Booth, J. (1977). A short history of blood pressure measurement. *Proceedings of the Royal Society of Medicine*, 70(11), pp. 793–799.
- Brown N. (2013). Contribution of aldosterone to cardiovascular and renal inflammation and fibrosis. *Nat Rev Nephrology*, 9(8), pp. 459-69
- Bruce RA, Lovejoy FR. (1949). Normal respiratory and circulatory pathways of adaptation in exercise. *J Clin Invest*, 28(6), pp. 1423-30
- Brunson D. (1997). Pharmacology of inhalation anesthetics, In: Anesthesia and analgesia in laboratory animals, (Kohn D, Wixson S, White W, Benson J, eds). New York: Academic Press, pp. 29-40.
- BS 350: Part 1: 1974 – Conversion factors and tables. British Standards Institution. 1974. pp. 49
- Burak Z, Ersoy O, Moretti J, L, Erinc R, Ozcan Z, Dirlik A, Sabah D, Basdemir G. (2001). The role of 99mTc-MIBI scintigraphy in the assessment of MDR1 overexpression in patients with musculoskeletal sarcomas: comparison with therapy response. *European journal of nuclear medicine*. 28(9), pp. 1341-1350

Cabezas M, Comellas A, Ramón Gómez J, López Grillo L, Casal H, Carrillo N, Camero R, Castillo R . (1997). Comparison of the sensitivity and specificity of the electrocardiography criteria for left ventricular hypertrophy according to the methods of Romhilt-Estes, Sokolow-Lyon, Cornell and Rodríguez Padial. *Rev Esp Cardiol*, 50(1), pp. 31-5

Cacciapuoti F. (2011). Molecular mechanisms of left ventricular hypertrophy (LVH) in systemic hypertension (SH)—possible therapeutic perspectives. *Journal of the American Society of Hypertension*, 5(6), pp. 449-455

Canadian Organ Replacement Register: Annual Report 1998, Volume 1: Dialysis and Renal Transplantation. Ottawa, Ontario, Canadian Institute for Health Information

Carboni GP. (2012). A novel clinical indicator using cardiac technetium-99m sestamibi kinetics for evaluating cardiotoxicity in cancer patients treated with multiagent chemotherapy. *American Journal of Cardiovascular Disease*, 2(4), pp. 293-300

Carvalho PA, Chiu ML, Kronauge JF, Kawamura M, Jones AG, Holman BL. (1992) Subcellular distribution and analysis of technetium- 99m-MIBI in isolated perfused rat hearts. *J Nucl Med*, 33(3), pp. 1516-22

Cerqueira MD, Verani MS, Schwaiger M, Heo J, Iskandrian AS. (1994) Safety profile of adenosine stress perfusion imaging: Results from the Adenoscan Multicenter Trial Registry. *J Am Coll Cardiol*, 23, pp. 384-9

Cha H, Jeong HJ, Jang SP. (2010) Parathyroid hormone accelerates decompensation following left ventricular hypertrophy. *Experimental & Molecular Medicine*.

Chanutin A, Ferris EB. (1932). Experimental renal insufficiency produced by partial nephrectomy. *Arch Intern Med*, 49(2), pp. 767–87

Chew CG, Unger S, Shakib S. (2013) Value of myocardial perfusion imaging in renal transplant evaluation. *Nephrology*, 18(2), pp. 376-381

Chow CK, Teo KK, Rangarajan S, Islam S, Gupta R, Avezum A, Bahonar A, Chifamba J, Dagenais G, Diaz R, Kazmi K, Lanus F, Wei L, Lopez Jaramillo P, Fanghong L, Ismail NH, Puoane T, Rosengren A, Szuba A, Temizhan A, Wielgosz A, Yusuf R, Yusufali A, McKee M, Liu L, Mony P, Yusuf S. (2012) PURE Study Investigators. Prevalence, awareness, treatment, and control of hypertension in rural and urban communities in high-, middle-, and low-income countries. *JAMA* 310(4), pp. 959–968.

- Chua T, Kiat H, Germano G, Palmas W, Takemoto K, Friedman J, Berman DS. (1993). Technetium-99m teboroxime regional myocardial washout in subjects with and without coronary artery disease. *Am J Cardiol*, 72(9), pp. 728-34
- Churchill DN, Taylor DW, Cook RJ, LaPlante P, Barre P, Cartier P, Fay WP, Goldstein MB, Jindal K, Mandin H. (1992) Canadian hemodialysis morbidity study. *Am J Kidney Dis*, 19(2), pp. 214-234
- Civelek AC, Ozalp E, Donovan P, Udelsman R. (2002). Prospective evaluation of delayed technetium-99m sestamibi SPECT scintigraphy for preoperative localization of primary hyperparathyroidism. *Surgery*, 131(2), pp. 149-57
- Cogan MG: (1991) Normal water homeostasis. In *Fluid & Electrolytes, Physiology and Pathophysiology*. Edited by Cogan MG. Norwalk: Appleton & Lange, 98.
- Coleman V, Martin JF. (1994) The role of animal experimentation in cardiovascular therapeutic discovery. *Cardiovasc Res*, 28(2), pp. 1102–1118
- Combet S, Ferrier ML, Van Landschoot M, Stoeniu M, Moulin P, Miyata T, Lameire N, Devuyst O. (2001) Chronic uremia induces permeability changes, increased nitric oxide synthase expression, and structural modifications in the peritoneum. *J Am Soc Nephrol*, 12(10), pp. 2146-57
- Conway MA, Allis J, Ouwerkerk R, Niioka T, Rajagopalan B, Radda GK. (1991) Detection of low phosphocreatine to ATP ratio in failing hypertrophied human myocardium by ³¹P magnetic resonance spectroscopy. *Lancet*, 338(8773), pp. 973-6
- Costacou T, Lopes-Virella MF, Zgibor JC. (2005). Markers of endothelial dysfunction in the prediction of coronary artery disease in type 1 diabetes. The Pittsburgh Epidemiology of Diabetes Complications Study. *J Diabetes Complications* 19(3), pp. 183–193
- Cowie MR, Wood DA, Coats AJ. (2000) Survival of patients with a new diagnosis of heart failure: a population based study. *Heart*, 83(5), pp. 505–510
- Crane P, Laliberté R, Heminway S, Thoolen M, Orlandi C. (1993) Effect of mitochondrial viability and metabolism on technetium-99m-sestamibi myocardial retention. *Eur J Nucl Med*, 20(1), pp. 20-25
- Crawford ES, Husain SS. 2003. *Nuclear Cardiac Imaging: Terminology and Technical Aspects*. Reston, VA: Society of Nuclear Medicine

- Dabelea D, Kinney G, Snell-Bergeon JK. (2006) Coronary Artery Calcification in Type 1 Diabetes Study. Effect of type 1 diabetes on the gender difference in coronary artery calcification: a role for insulin resistance? The Coronary Artery Calcification in Type 1 Diabetes (CACTI) Study. *Diabetes*, 52, pp. 2833–2839
- De Lima JGG, Gowdak LHW, de Paula FJ, Ramires JAF, Bortolotto LA . (2012). The role of myocardial scintigraphy in the assessment of cardiovascular risk in patients with end-stage chronic kidney disease on the waiting list for renal transplantation. *Nephrol Dial Transplant*, 27(7), pp. 2979-2984
- de Vries SO, Heesen WF, Beltman FW, Kroese AH, May JF, Smit AJ, Lie KI. (1996). Prediction of the left ventricular mass from the electrocardiogram in systemic hypertension. *Am J Cardiology*, 77(11), pp. 974-8
- DeLuca AJ, Kaplan S, Aronow WS. (2006). Comparison of prevalence of unrecognized myocardial infarction and of silent myocardial ischemia detected by a treadmill exercise sestamibi stress test in patients with versus without diabetes mellitus. *Am J Cardiol*, 98(1), pp. 1045-1047
- Desvergne B, Wahli W. (1999). Peroxisome proliferator-activated receptors: nuclear control of metabolism. *Endocr Rev*, 20(2), pp. 649–688
- Devereux RB, Alonso DR, Lutas EM, Gottlieb GJ, Campo E, Sachs I, Reichek N. (1986) Echocardiographic assessment of left ventricular hypertrophy: comparison to necropsy findings. *Am J Cardiol*, 57(5), pp. 450-458
- Dikow R, Kihm LP, Zeier M, Kapitza J, Törnig J, Amann K, Tiefenbacher C, Ritz E. (2004). Increased infarct size in uremic rats: reduced ischemia tolerance? *J Am Soc Nephrol*, 15(6), pp. 1530-6
- Djaberi R, Schuijf JD, Boersma E. (2009) Differences in atherosclerotic plaque burden and morphology between type 1 and 2 diabetes as assessed by multislice computed tomography. *Diabetes Care*, 32(12), pp. 1507–1512
- Doenst T, Nguyen TD, Abel ED. (2013). Cardiac metabolism in heart failure: implications beyond ATP production. *Circ Res*, 113(6), pp. 709-24
- Doggrell S, Brown L (1998). Rat models of hypertension, cardiac hypertrophy and failure. *Cardiovascular Research*, 39(1), pp. 89–105

- Dounousi E, Papavasiliou E, Makedou A, Ioannoua K, Katopodis KP, Tselepis A., Siamopoulos KC, Tsakiris D. (2006). Oxidative stress is progressively enhanced with advancing stages of CKD. *Am J Kidney Dis*, 48(2), pp. 752-60.
- Dudley C, Harden P. Assessment of the potential kidney transplant recipient. UK Renal Association 2011
- Eliahou HE, Avinoach I, Shahmurov M, Shahar C, Ben-David A, Matas Z, Zimlichman A. (2000). Advantage of angiotensin-ii receptor antagonists over calcium channel blockers in experimental chronic renal failure-prevention of mesangial hypertrophy in glomeruli. *American Journal of Hypertension*, 13(S2), pp. 281A
- El-Hajj S, Hage FG. (2014). Risk stratification for coronary artery disease using pharmacological stress tests. *Leban Med J*, 62(1), pp. 69-75
- Etchells E, Meade M, Tomlinson G, Cook D. (2002). Semiquantitative dipyridamole myocardial stress perfusion imaging for cardiac risk assessment before non-cardiac vascular surgery: a meta-analysis. *J Vasc Surg*, 36(3), pp. 534-40
- Fansler B, Lowenstein JM. (1969). Aconitase from pig heart. *Methods in Enzymology* 13(7), pp. 26-30
- Fedorova L, Tamirisa A, Kennedy DJ, Haller ST, Budnyy B, Shapiro JI, Malhotra D. (2013). Mitochondrial impairment in the five-sixth nephrectomy model of chronic renal failure: proteomic approach. *BMC Nephrology*, 14(2), pp. 209-16
- Fernández MAG, de Diego JJG. (2011). Transthoracic echocardiography. In: Galiuto L, Badano L, Fox K, Sicari R, Zamorano JL EAE Textbook of Echocardiography, 2011. 2nd ed. London: Oxford University Press 48.
- Floras JS. (2003). Sympathetic activation in human heart failure: Diverse mechanism, therapeutic opportunities. *Acta Physiol Scand*, 177(391), pp. 361-370
- Fine L. (1986) The biology of renal hypertrophy. *Kidney international*, 29(3), pp. 619-634
- Foley RN, Parfrey PS, Harnett JD, Kent GM, Martin CJ, Murray DC et al. (1995). Clinical and echocardiographic disease in patients starting end-stage renal disease therapy. *Kidney Int*, 47(1), pp. 186–192
- Foley RN, Parfrey PS, Sarnak MJ. (1998) Clinical epidemiology of cardiovascular disease in chronic renal disease. *Am J Kidney Dis*, 32(S3), pp. S112-119

Foppa, M., Duncan, B. B., & Rohde, L. E. (2005). Echocardiography-based left ventricular mass estimation. How should we define hypertrophy? *Cardiovascular Ultrasound*, 3(17), pp. 1476-77

Forouzanfar MH, Liu P, Roth GA, Ng M, Biryukov S, Marczak L, Alexander L, Estep K, Hassen Abate K, Akinyemiju TF, Ali R, Alvis-Guzman N, Azzopardi P, Banerjee A, Barnighausen T, Basu A, Bekele T, Bennett DA, Biadgilign S, Catala-Lopez F, Feigin VL et al (2017). Global burden of hypertension and systolic blood pressure of at least 110 to 115 mm Hg, 1990-2015. *JAMA*, 317(3), pp. 165–182

Frank D, Frey N (2011) Cardiac Z-disc Signalling Network. *J Biol Chem*, 286(35), pp. 9897–9904.

Frank O (1899) Die Grundform des Arteriellen Pulses. *Z Biol* 37:483–526 (translated by Sagawa K, Lie RK, Schaefer J, 1990, *J Mol Cell Cardiol*, 22(4), pp. 253–277)

Franklin SS, Khan SA, Wong ND, Larson MG, Levy D. (1999). Is pulse pressure useful in predicting risk for coronary heart disease? The Framingham heart study. *Circulation* 100, pp. 354–360

Frey N, Olson EN (2003) Cardiac hypertrophy: the good, the bad, and the ugly. *Annu Rev Physiol*, 65(4), pp. 45–79

Friedman SE, Palac RT, Zlotnick DM, Chobanian MC, Costa SP. (2011). A call to action: variability in guidelines for cardiac evaluation before renal transplantation. *Clin J Am Soc Nephrol*, 6(2), pp. 1185-91

Fukushima K, Momose M, Kondo C, Higuchi T, Kusakabe K, Hagiwara N. (2010). Myocardial ^{99m}Tc-sestamibi extraction and washout in hypertensive heart failure using an isolated rat heart. *Nucl Med Biol*, 37(8), pp. 1005-12

Fukushima K, Momose M, Kondo C, Kusakabe K, Kasanuki H . (2007). Myocardial kinetics of (201)Thallium, (99m)Tc-tetrofosmin, and (99m)Tc-sestamibi in an acute ischemia-reperfusion model using isolated rat hearts. *Ann Nucl Med*, 21(5), pp. 267-73

Gagnon RF and Gallimore B. (1988). Characterization of a mouse model of chronic uremia. *Urol Res*, 16(1), pp.119-126

Gamble WJ, Conn PA, Kumar AE, Plenge R and Monroe RG. (1970). Myocardial oxygen consumption of blood-perfused, isolated, supported, rat heart. *American Journal of Physiology*, 219(4), pp. 604-612

- Garnier A, Fortin D, Delomenie C, Momken I, Veksler V, Ventura-Clapier R (2003) Depressed mitochondrial transcription factors and oxidative capacity in rat failing cardiac and skeletal muscles. *J Physiol*, 551(2), pp. 491–501
- Gava A, Freitas P, Balarini F, Vasquez C, Meyrelles E (2012). Effects of 5/6 nephrectomy on renal function and blood pressure in mice. *International journal of physiology, pathophysiology and pharmacology*, 4(3), pp. 167-73
- Gill JB, Ruddy TD, Newell JB, Finkelstein DM, Strauss HW, Boucher CA. (1987). Prognostic Importance of Thallium Uptake by the Lungs during Exercise in Coronary Artery Disease. *N Engl J Med*, 317(1), pp. 1485-1489
- Giri S, Shaw LJ, Murthy DR, Travin MI, Miller DD, Hachamovitch R. (2002). Impact of diabetes on the risk stratification using stress single-photon emission computed tomography myocardial perfusion imaging in patients with symptoms suggestive of coronary artery disease. *Circulation*, 105(3), pp. 32-40
- Goldberg M (1975) Water control and the dysnatremias. In *The Sea Within Us*. Edited by Bricker NS. New York: Science and Medicine Publishing Co. 20.
- Gottlieb R, Magnus R. (1904). Digitalis und Herzarbeit. Nach Versuchen an uberlebenden Warmbluterherzen. *Path Pharamakol*, 51(1), pp. 30– 63
- Granata S, Zaza G, Simone S, Villani G, Latorre D, Pontrelli P, Carella M, Schena FP, Grandaliano G, Pertosa G. (2009). Mitochondrial dysregulation and oxidative stress in patients with chronic kidney disease. *BMC Genomics*, 21(10), pp. 388-94
- Gray WA, Gewirtz H. (1991). Comparison of Tc-99 m-teboroxime with thallium for myocardial imaging in the presences of coronary artery stenosis. *Circulation*, 84(2), pp. 1796-807
- Griffith T, Reddan DN, Klassen PS, and Owen WF. (2003). Left ventricular hypertrophy: a surrogate end point or correlate of cardiovascular events in kidney disease? *Nephrol. Dial. Transplant*, 18(12), pp. 2479-2482
- Gross ML, Ritz E. (2008). Hypertrophy and fibrosis in the cardiomyopathy of uremia--beyond coronary heart disease *Semin Dial*, 21(4), pp. 308-18

Gross O, Schulze-Lohoff E, Koepke ML, Beirowski B, Addicks K, Bloch W, Smyth N, Weber M. (2004). Antifibrotic, nephroprotective potential of ACE inhibitor vs AT1 antagonist in a murine model of renal fibrosis. *Nephrol Dial Transplant*, 19(7), pp. 1716-23

Grossman W, Jones D, McLaurin LP. (1975). Wall stress and patterns of hypertrophy in the human left ventricle. *J. Clin. Invest.* 56(1), pp. 56–64

Gupta PK, Gupta H, Sundaram A. (2011) Development and validation of risk calculator for prediction of cardiac risk after surgery. *Circulation*, 124(4), pp. 381–387

Hacot JP, Bojovic M, Delonca J (1993) Comparison of planar imaging and single-photon emission computed tomography for the detection and localization of coronary artery disease. *Int J Cardiac Imag*, 9(1) pp. 113-114

Hage FG. (2014) Regadenoson for myocardial perfusion imaging: Is it safe? *J Nucl Cardiol.* 21(5), pp. 871-6

Hakeem A, Bhatti S, Dillie KS, Cook JR, Samad Z, Roth-Cline MD, Chang SM . (2008). Predictive value of myocardial perfusion single-photon emission computed tomography and the impact of renal function on cardiac death. *Circulation*, 118(24), pp. 2540-9

Harvey RP, Rosenthal N. Heart development. Estados Unidos:Academic Press; 1999. pp. 234.

Hayashi D, Ohshima S, Isobe S, Cheng XW, Unno K (2001). Increased (99m)Tc-sestamibi washout reflects impaired myocardial contractile and relaxation reserve during dobutamine stress due to mitochondrial dysfunction in dilated cardiomyopathy patients. *Journal of the American College of Cardiology.* 61(19), pp. 2007-17

Hedenqvist P. (2008). Anaesthesia and analgesia for surgery in rabbits and rats: A comparison of the effects of different compounds. Thesis submission to the Karolinska Institutet, Stockholm, Sweden.

Hein S, Amon E, Kostin S. (2003). Progression from compensated hypertrophy to failure in the pressure-overloaded human heart. Structural deterioration and compensatory mechanisms. *Circulation*, 107(984), pp. 253-61

Hendel RC, Berman DS, Di Carli MF, Heidenreich PA, Henkin RE, Pellikka PA, Pohost G, Williams K ACCF/ASNC/ACR/AHA/ASE/SCCT/SCMR/SNM appropriate use criteria for cardiac radionuclide imaging: a report of the American College of Journal of Nuclear Cardiology/Cardiology Foundation Appropriate Use Criteria Task Force 2009

- Hendel RC, Whitfield SS, Villegas BJ. (1992). Prediction of late cardiac events by dipyridamole thallium imaging in patients undergoing elective vascular surgery. *Am J Cardiol*, 70(4), pp. 1243–9
- Hood B, Attman P, Ahlmen J, Jagenburg R. (1971). Renal haemodynamics and limitations of creatinine clearance in determining filtration rate in glomerular disease. *Scand J Urol Nephrol*, 5(2), pp. 154-161
- Hindler K, Shaw AD, Samuels J, Fulton S, Collard CD, Riedel B. (2006). Improved postoperative outcomes associated with preoperative statin therapy. *Anaesthesiology*, 105(2-3), pp. 1260-72
- Holmuhamedov EL, Oberlin A, Short K, Terzic A, Jahangir A. (2012). 1. Cardiac subsarcolemmal and interfibrillar mitochondria display distinct responsiveness to protection by diazoxide. *PLoS One*, 7(9), pp. 446-67
- Hsu CY, McCulloch CE, Darbinian J, Go AS, Iribarren C. (2005). Elevated blood pressure and risk of end-stage renal disease in subjects without baseline kidney disease. *Arch Intern Med*, 165(8), pp. 923-8
- Hunold P, Vogt FM, Heemann UW, Zimmermann U, Barkhausen J.. (2003). Myocardial mass and volume measurement of hypertrophic left ventricles by MRI--study in dialysis patients examined before and after dialysis. *J Cardiovasc Magn Reson*, 5(4), pp. 553-61
- Huss JM, Levy FH, Kelly DP. (2001). Hypoxia inhibits the PPAR α /RXR gene regulatory pathway in cardiac myocytes. *J. Biol Chem*, 276(1) pp. 27605–27612
- Husain SS. (2007). Myocardial perfusion imaging protocols: is there an ideal protocol? *J Nucl Med Technol*, 35(1), pp. 3-9
- Ikawa M, Kawai Y, Arakawa K, Tsuchida T, Miyamori I, Kuriyama M, Tanaka M, Yoneda M. (2007). Evaluation of respiratory chain failure in mitochondrial cardiomyopathy by assessments of ^{99m}Tc-MIBI washout and ^{123I}-BMIPP/^{99m}Tc-MIBI mismatch. *Mitochondrion*, 7(1-2), pp. 164-70
- Imai M & Kokko JP. (1974). Sodium chloride, water and urea transport in the thin ascending limb of Henle. Generation of gradients by passive diffusion of solutes. *J Clin Invest* 53(2), pp. 393-402

- Iozzo RV, Zoeller JJ, Nyström A. (2009) Basement membrane proteoglycans: modulators Par Excellence of cancer growth and angiogenesis. *Mol Cells*, 27(5), pp. 503-13
- Isobe S, Ohshima S, Unno K, Izawa H, Kato K, Noda A, Hirashiki A. (2010). Relation of ^{99m}Tc-sestamibi washout with myocardial properties in patients with hypertrophic cardiomyopathy. *Journal of Nuclear Cardiology*, 17(6), pp. 1082–1090
- Jacobson HR (1981) Functional segmentation of the mammalian nephron. *Am J Physiol*, 1981, 241(4) pp. 203-205
- Jarreta D, Orus J, Barrientos A, Miro O, Roig E, Heras M. (2000). Mitochondrial function in heart muscle from patients with idiopathic dilated cardiomyopathy. *Cardiovasc Res*, 45(4), pp. 860–865
- Jeffrey FM, Alvarez L, Diczku V, Sherry AD, Malloy CR. (1995). Direct evidence that perhexiline modifies myocardial substrate utilization from fatty acids to lactate. *J Cardiovasc Pharmacol*, 25(2), pp. 469–472
- Jing L, Jin C, Li S et al. (2012). Chronic alcohol intake-induced oxidative stress and apoptosis: role of CYP2E1 and calpain-1 in alcoholic cardiomyopathy. *Mol Cell Biochem*, 359(1-2), pp. 283-89
- K/DOQI Workgroup, K/DOQI clinical practice guidelines for cardiovascular disease in dialysis patients 2012
- Kahn MR, Fallahi A, Kim MC, Esquitin R, Robbins MJ. (2011). Coronary Artery Disease in a Large Renal Transplant Population: Implications for Management. *American Journal of Transplantation*, 11(12), pp. 2665-2674
- Knepper MA, Roch-Ramel F (1987) Pathways of urea transport in the mammalian kidney. *Kidney Int*, 31(6), pp. 629
- Karthikeyn V, Lip G (2007). Matrix metalloproteinases and hypertension. A link between left ventricular hypertrophy and diastolic dysfunction? *Tohoku J Exp Med*, 208(2), pp. 93-97
- Kao MP, Ang DS, Gandy SJ, Nadir MA, Houston JG, Lang CC, Struthers AD . (2011). Allopurinol benefits left ventricular mass and endothelial dysfunction in chronic kidney disease. *J Am Soc Nephrol*, 22(7), pp. 1382-9

Kasiske BL, Keane WF. (2000). Laboratory assessment of renal disease: clearance, urinalysis, and renal biopsy. In: BM Brenner The Kidney. 6th ed. Philadelphia: WB Saunders Company. pp.1129-1170

Kearney PM, Whelton M, Reynolds K, Muntner P, Whelton PK, He J. (2005). Global burden of hypertension: analysis of worldwide data. *Lancet*, 365 pp. 217–223

Kennedy D, Omran E, Periyasamy SM, Nadoor J, Priyadarshi A, Willey JC, Malhotra D, Xie Z, Shapiro JI. (2003). Effect of chronic renal failure on cardiac contractile function, calcium cycling, and gene expression of proteins important for calcium homeostasis in the rat. *J Am Soc Nephrol*, 14(1), pp. 90-7

Kinugawa S , Tsutsui H , Hayashidani S , Ide T , Suematsu N , Satoh S , Utsumi H , Takeshita A. (2000). Treatment with dimethylthiourea prevents left ventricular remodeling and failure after experimental myocardial infarction in mice: role of oxidative stress. *Circ Res* 87(6), pp. 392-398

Klingbeil AU, Schneider M, Martus P, Messerli FH, Schmieder RE. (2003). A meta-analysis of the effects of treatment on left ventricular mass in essential hypertension. *Am J Med*, 115(1), pp. 41-6

Klocke FJ, Baird MG, Lorell BH, Bateman TM, Messer JV, Berman DS, O'Gara PT, Carabello BA, Russell RO Jr, Cerqueira MD et al. (2003). American College of Cardiology; American Heart Association; American Society for Nuclear Cardiology. ACC/AHA/ASNC guidelines for the clinical use of cardiac radionuclide imaging--executive summary. *J Am Coll Cardiol*, 42(7), pp. 1318-33

Kokko J, Rector F. (1972). Countercurrent multiplication system without active transport in inner medulla. *Kidney Int*, 114(6), pp. 232-236

Kostakoglu L, Kiratli P, Ruacan S, Hayran M, Emri S, Ergün EL, Bekdik CF. (1998). Association of tumor washout rates and accumulation of technetium-99m-MIBI with expression of P-glycoprotein in lung cancer. *Journal of nuclear medicine*, 39(2), pp. 228-234

Knoll R, Hoshijima M, Hoffman HM. (2002). The cardiac mechanical stretch sensor machinery involves a z-disc complex that is defective in a subset of human dilated cardiomyopathy. *Cell*, 111 pp. 943-945

Kumano K, Kogure K, Tanaka T, Sakai T. (1986). A new method of inducing experimental chronic renal failure by cryosurgery. *Kidney Int*, 30(1), pp. 433–6

- Kumita S, Seino Y, Cho K, Nakajo H, Toba M, Fukushima Y. (2002). Assessment of myocardial washout of Tc-99m-sestamibi in patients with chronic heart failure: comparison with normal control. *Ann Nucl Med*, 4(3), pp. 237-42
- Langendorff O (1895) Untersuchungen am uberlebenden Saugethierherzen . *Pflügers Arch*, 61(1), pp. 291– 332
- Larsen JR, Brekke M, Bergengen L. (2005) Mean HbA1c over 18 years predicts carotid intima media thickness in women with type 1 diabetes. *Diabetologia* 48(5), pp. 776–779
- LeBleu VS, Macdonald B, Kalluri R. (2007). Structure and function of basement membranes. *Exp Biol Med*, 232(9), pp. 1121-29
- Lee TH, Marcantonio ER, Mangione CM (1999). Derivation and prospective validation of a simple index for prediction of cardiac risk of major non cardiac surgery. *Circulation*, 146(2), pp. 2131–2134
- Lee J, Iskandrian B, Cassel D, Heo J, Iskandrian AS. (1991). Agreement between thallium and sestamibi in the quantitative assessment size of the perfusion abnormality. *Circulation*, 84(Suppl 11), pp. 295–302
- Lee L, Campbell R, Scheuermann-Freestone M, Taylor R, Gunaruwan P, Williams L, Ashrafian H, Horowitz J, Fraser AG, Clarke K, Frenneaux M.. (2005). Metabolic modulation with perhexiline in chronic heart failure: a randomized, controlled trial of short-term use of a novel treatment. *Circulation*, 112(21), pp. 3280-8
- Lentine KL, Brennan DC, Schnitzler MA. (2005). Incidence and predictors of myocardial infarction after kidney transplantation. *J Am Soc Nephrol*, 16(1), pp. 496-506
- Lentine KL, Hurst FP, Jindal RM, Villines TC, Kunz JS, Yuan CM, Hauptman PJ, Abbott KC. (2010). Cardiovascular risk assessment among potential kidney transplant candidates: approaches and controversies. *Am J Kidney Dis*, 55(1), pp. 152-67
- Leppo JA, Meerdink DJ. (1989). Comparison of the myocardial uptake of a technetium-labeled isonitrite analogue and thallium. *Circ Res*, 65(7), pp. 632–9
- Leslie W, Tully S, Yogendran M, Ward L. (2005). Prognostic Value of Automated Quantification of 99mTc-Sestamibi Myocardial Perfusion Imaging. *J Nucl Med*, 46(2), pp. 204-211

- Lewington S, Clarke R, Qizilbash N, Peto R, Collins R. (2002). Age-specific relevance of usual blood pressure to vascular mortality: a meta-analysis of individual data for one million adults in 61 prospective studies. *Lancet*, 360, pp. 1903–1913
- Lewis O. (1994) Stephen Hales and the measurement of blood pressure. *J Hum Hypertens*. 8(12), pp. 865-71
- Li JM, Poolman RA, Brooks G. (1998). Role of G1 phase cyclins and cyclin-dependent kinases during cardiomyocyte hypertrophic growth in rats. *Am J Physiol*, 275(5), pp. 814-22
- Liang F, Wang F, Zhang S, Gardner DG. (2003). Peroxisome proliferator activated receptor (PPAR) alpha agonists inhibit hypertrophy of neonatal rat cardiac myocytes. *Endocrinology*, 144(9), pp. 4187-94
- Liu Z, Okada DR, Johnson G 3rd, Hocherman SD, Beju D, Okada RD. (2008). 99mTc-sestamibi kinetics predict myocardial viability in a perfused rat heart model. *Eur J Nucl Med Mol Imaging*, 35(3), pp. 570-8
- Liu ZC, Chow KM, Chang TM. (2003). Evaluation of two protocols of uremic rat model: partial nephrectomy and infarction. *Ren Fail*, 25(6), pp. 935-43
- London GM. (2003). The Clinical Epidemiology of Cardiovascular Disease in Chronic Kidney Disease. *Seminars in Dialysis*, 16(2), pp. 85-94
- Long J, Maa J, Luo C, Mo X, Sun L, Zang W, Liu J. (2009). Comparison of two methods for assaying complex I activity in mitochondria isolated from rat liver, brain and heart. *Life Sciences*, 85(7–8), pp. 276-280
- Lorell BH, Carabello BA. (2000). Left ventricular hypertrophy: pathogenesis, detection, and prognosis. *Circulation*, 102(1), pp. 470-476
- Lubowitz H, Slatopolsky S, Shankel S. (1967). Glomerular filtration rate: Determination in patients with chronic kidney disease. *JAMA* 199, pp. 252-256
- Mall G (1990). Diffuse intermyocardiocytic fibrosis in uraemic patients. *Nephrology Dialysis Transplantation*, 5(1), pp. 39-44
- Manske CL, Wang Y, Rector T, Wilson RF, White CW. (1992). Coronary revascularisation in insulin-dependent diabetic patients with chronic renal failure. *Lancet*, 340(8826), pp. 998-1002

- Marik PE, Preiser JC. (2010) Toward understanding tight glycemic control in the ICU: a systematic review and meta-analysis. *Chest*, 137(5), pp. 544–551
- Marin-Garcia J, Goldenthal MJ, Moe GW. (2001). Abnormal cardiac and skeletal muscle mitochondrial function in pacing induced cardiac failure. *Cardiovasc Res*, 52(1), pp. 103-110
- Marin-Garcia, J. (2005). Mitochondrial Bioenergetics and the Heart. In: Marin-Garcia, J Mitochondria and the Heart. London: Springer. pp. 27-62
- Mark PB, Johnston N, Groenning J, Foster JE, Blyth KG, Martin TN, Steedman T, Dargie HJ and Jardine AG. (2006). Redefinition of uremic cardiomyopathy by contrast-enhanced cardiac magnetic resonance imaging. *Kidney International*, 69(1), pp.1839-1845
- Masani N, Wharton G, Allen J, Chambers J, Graham J, Jones R, Rana B, Steeds R. (2011) Echocardiography: Guidelines for Chamber Quantification. British Society of Echocardiography Education Committee
- Massy ZA, Nguyen-Khoa T. (2002). Oxidative stress and chronic renal failure: markers and management. *J Nephrol*, 15(4), pp. 336-41
- Mathew J, Sleight P, Lonn E. (2001). Reduction of cardiovascular risk by regression of electrocardiographic markers of left ventricular hypertrophy by the angiotensin converting enzyme inhibitor, Ramipril. *Circulation*. 104(1), pp. 1615–1621
- Matlib MA, Rembert JC, Millard RW, Ashraf M, Rouslin W, Asano G, Greenfield JC Jr, Schwartz A . (1983) Mitochondrial function in canine experimental cardiac hypertrophy. *J Mol Cell Cardiol*, 15(2), pp. 221–23
- Matsuo S, Nakae I, Tsutamoto T, Okamoto N, Horie M. (2007). A novel clinical indicator using Tc-99m sestamibi for evaluating cardiac mitochondrial function in patients with cardiomyopathies. *J Nucl Cardiol*, 14(2), pp. 215-20
- Matsuo S, Nakajima K, Kinuya S, Sato Y, Matsumoto N, Horie M. (2008). Cardiac scintigraphic findings of mitochondrial myopathy, encephalopathy, lactic acidosis and stroke-like episodes: A case report. *Exp Clin Cardiol*, 13(2), pp. 93-5
- Mautner SL, Lin F, Roberts WC. (1992) Composition of atherosclerotic plaques in the epicardial coronary arteries in juvenile (type I) diabetes mellitus. *Am J Cardiol* 70(6), pp. 1264–1268

- McCain ML, Parker KK (2011) Mechanotransduction: the role of mechanical stress, myocyte shape, and cytoskeletal architecture on cardiac function. *Eur J Physiol*, 462(34), pp. 89–104
- McFalls EO, Ward HB, Moritz TE, Goldman S, Krupski WC, Littooy F, Pierpont G, Santilli S, Rapp J, Hattler B, Shunk K, Jaenicke C, Thottapurathu L, Ellis N, Reda DJ, Henderson WG. (2004). Coronary-artery revascularization before elective major vascular surgery. *N Engl J Med*, 351(4), pp. 2795-2804
- McLaughlin DP, Beller GA, Linden J, Ayers CR, Ripley ML, Taylor H (1994). Hemodynamic and metabolic correlates of dipyridamole-induced myocardial thallium-201 perfusion abnormalities in multivessel coronary artery disease. *Am J Cardiol*, 73(6) pp. 1159-64
- McLaughlin M, Danias PG. (2002). Transient ischemic dilation: A powerful diagnostic and prognostic finding of stress myocardial perfusion imaging. *Journal of Nuclear Cardiology*, 9(6), pp. 663–667
- McMullen J, Jennings GL. (2007) Differences between pathological and physiological cardiac hypertrophy: Novel therapeutic strategies to treat heart failure. *Clinical and experimental pharmacology and physiology*, 34(4), pp. 255-262
- McMurray JJ, Packer M, Desai AS, Gong J, Lefkowitz MP, Rizkala AR, Rouleau JL, Shi VC, Solomon SD, Swedberg K, Zile MR. (2014). PARADIGM-HF Investigators and Committees. Angiotensin-neprilysin inhibition versus enalapril in heart failure . *N Engl J Med*, 371(11), pp. 993-1004
- Middleton RJ, Parfrey PS, Foley RN. (2001). Left ventricular hypertrophy in the renal patient. *J Am Soc Nephrol*, 12(5), pp. 1079–1084
- Morishita S, Kondo Y, Nomura M, Miyajima H, Nada T, Ito S, Nakaya Y. (2001). Impaired retention of technetium-99m tetrofosmin in hypertrophic cardiomyopathy. *Am J Cardiol*, 87(6), pp. 743-7
- Morrish NJ, Wang SL, Stevens LK, Fuller JH, Keen H. (2001). Mortality and causes of death in the WHO Multinational Study of Vascular Disease in Diabetes. *Diabetologia*, 44 Suppl(2), pp. S14-21
- Mow VC, Wang CC, Hung CT. (1999). The extracellular matrix, interstitial fluid and ions as a mechanical signal transducer in articular cartilage. *Osteoarthritis Cartilage*, 7(1), p. 41

Myung SK, Ju W, Cho B, Oh SW, Park SM, Koo BK, Park BJ; Korean Meta-Analysis Study Group. (2013). Efficacy of vitamin and antioxidant supplements in prevention of cardiovascular disease: systematic review and meta-analysis of randomised controlled trials. *BMJ*, 346(10), pp. 221-32

Narahara KA, Villanueva-Meyer J, Thompson CJ, Brizendine M, Mena I. (1990). Comparison of thallium-201 and technetium-99 m hexakis 2-methoxyisobutyl isonitrile singlephoton emission computed tomography for estimating the extent of myocardial ischemia and infarction in coronar. *Am J Cardiol*, 66(4), pp. 1438–44

Nardi E, Palermo A, Mulè G, Cusimano P, Cottone S, Cerasola G. (2009). Left ventricular hypertrophy and geometry in hypertensive patients with chronic kidney disease. *J Hypertens*. 27(3), pp. 633-641

Navare SM, Mather JF, Shaw LJ, Fowler MS, and Heller GV. (2004). Comparison of risk stratification with pharmacologic and exercise stress myocardial perfusion imaging: a meta-analysis. *Journal of Nuclear Cardiology*, 11(5), pp. 551-561

Neely JR, Liebermeister H, Battersby EJ, Morgan HE (1967). Effect of pressure development on oxygen consumption by isolated rat heart. *Am J Physiol*, 212(2), pp. 804– 814

Nickolas TL, Barasch J, Devarajan P. (2008). Biomarkers in acute and chronic kidney disease. *Curr Opin Nephrol Hypertens*, 17(2), pp. 127-32

Nielsen S, Di Giovanni SR Christensen EL. (1993). Cellular and subcellular immunolocalization of vasopressin-regulated water channel in rat kidney. *Proc Natl Acad Sci US*, 90(5), pp. 11663-11667

Nishio ML, Ornatsky OI, Craig EE, Hood DA (1995) Mitochondrial biogenesis during pressure overload induced cardiac hypertrophy in adult rats. *Can J Physiol Pharmacol*, 73(5), pp. 630–637

Noriyuki Yajima Yoshikazu Yazaki Kunihiro Yoshida Uichi Ikeda. (2009). A case of mitochondrial cardiomyopathy with pericardial effusion evaluated by 99mTc-MIBI myocardial scintigraphy. *Journal of Nuclear Cardiology*, 16(6), pp. 989-94

O'Hare AM, Choi AI, Bertenthal D, Bacchetti P, Garg AX, Kaufman JS, Walter LC, Mehta KM, Steinman MA, Allon M, McClellan WM, Landefeld CS. (2007). Age affects outcomes in chronic kidney disease. *J Am Soc Nephrol*, 18(4), pp. 2758-2765

- Ojo AO. (2006). Cardiovascular complications after renal transplantation and their prevention. *Transplantation*, 82(3), pp. 603-11
- Okada RD, Glover DK, Nguyen KN, Johnson G 3rd. (1995). Technetium-99m sestamibi kinetics in reperfused canine myocardium. *Eur J Nucl Med*, 22(7), pp. 600-7
- Okuda S, Oh Y, Tsuruda H, Onoyama K, Fujimi S, Fujishima M. (1986). Adriamycin-induced nephropathy as a model of chronic progressive glomerular disease. *Kidney Int*, 29(70), pp. 502–10
- Oliveira PJ, Bjork JA, Santos MS, Leino RL, Froberg MK, Moreno AJ, Wallace KB. (2004). Carvedilol-mediated antioxidant protection against doxorubicin-induced cardiac mitochondrial toxicity. *Toxicol Appl Pharmacol*, 200(2), pp. 159-68
- Olson RE. (1959) Myocardial metabolism in congestive heart failure. *J Chron Dis*, 9(1), pp. 442–447
- Ono S, Takeishi Y, Yamaguchi H, Abe S, Tachibana H, Sato T, Kubota I. (2003). Enhanced regional washout of technetium-99m-sestamibi in patients with coronary spastic angina. *Ann Nucl Med*. 17(5), pp.393-8
- Opie LH (2005). Mechanism of cardiac contraction and relaxation. In Zipes, DP, Libby P, Bonow R, Braunwald E: Heart Disease: A textbook of cardiovascular medicine. 7th Ed, Philadelphia, Elsevier Saunders, 457-489.
- Opie LH (2004). Heart Physiology: From Cell to Circulation. 4th Ed. Philadelphia. Lippincott, Williams and Wilkins
- Opie LH, Commerford PI, Gersch BJ, Pfeffer MA. (2006). Controversies in ventricular remodelling. *Lancet*. 367(356), pp. 287-292
- Osorio JC, Stanley WC, Linke A, Castellari M, Diep QN, Panchal AR, Hintze TH, Lopaschuk GD, Recchia FA. (2002). Impaired myocardial fatty acid oxidation and reduced protein expression of retinoid X receptor-alpha in pacing-induced heart failure. *Circulation*. 106 (5), 606-12
- Pace L, Catalano L, Del Vecchio S. (2005). Washout of [99mTc] sestamibi in predicting response to chemotherapy in patients with multiple myeloma. *The Quarterly Journal of Nuclear Medicine and Molecular Imaging*. 49(3), pp. 281-285

- Pacher P, Mabley JG, Liaudet L, Evgenov OV, Marton A, Hasko G. (2004). Left ventricular pressure–volume relationship in a rat model of advanced aging-associated heart failure. *Am J Physiol Heart Circ Physiol*, 287(1), pp. 2132-2137
- Paluch EK, Nelson CM, Biais N, et al. (2015) Mechanotransduction: use the force(s). *BMC Biology* 13(47) pp. 36.
- Paoletti E, Cannella G. (2006). Left ventricular hypertrophy in chronic kidney disease. *G Ital Nefrol.* 23(6), pp. 560–568
- Papaioannou GI, Heller GV. (2003). Risk assessment by myocardial perfusion imaging for coronary revascularization, medical therapy, and non-cardiac surgery. *Cardiol Rev.* 11(2), pp. 60-72
- Parfrey PS, Foley RN, Harnett JD, Kent GM, Murray DC, Barre PE. (1996). Outcome and risk factors for left ventricular disorders in chronic uraemia. *Nephrol Dial Transplant* 11(1), pp. 1277–1285
- Parwani P, Ryan J. (2012). Heart Failure Patients With Low Blood Pressure How Should We Manage Neurohormonal Blocking Drugs? *Circulation: Heart Failure.* 5(6) pp. 81-83
- Pelliccia A, Maron BJ, De Luca R. (2002). Remodelling of left ventricular hypertrophy in elite athletes after long term deconditioning. *Circulation* 105, pp. 944-949
- Peterson GE, de Backer T, Gabriel A . (2007). Prevalence and correlates of left ventricular hypertrophy in the African American Study of Kidney Disease Cohort Study. *Hypertension.* 50(6), pp. 1033-1039
- Peterson OH. (2007). Cardiovascular System – The Heart. In *Human Physiology 5th Edition*. Oxford, Blackwell pp. 335-371
- Phan TT, Shivu GN, Choudhury A, Abozguia K, Davies C, Naidoo U, Ahmed I, Yousef Z, Horowitz J, Frenneaux M. (2009). Multi-centre experience on the use of perhexiline in chronic heart failure and refractory angina: old drug, new hope. *Eur J Heart Fail.* 11(9), pp. 881-6
- Piascik MT (2008). G-protein coupled receptor systems. University of Kentucky lecture series. PHA 622. <http://www.uky.edu/~mtp/PHA622lec2.htm>

- Piwnica-Worms D, Kronauge JF, Chiu ML. (1990). Uptake and retention of hexakis (2-methoxyisobutyl isonitrate) technetium(I) in cultured chick myocardial cells. Mitochondrial and plasma membrane potential dependence. *Circulation*. 82(4), pp. 1826-38
- Poldermans D, Bax JJ, Boersma E, De Hert S, Eeckhout E, Fowkes G et al. (2009). Preoperative risk assessment and perioperative cardiac management in non-cardiac surgery. *Eur Heart Journal*. 30(2), pp. 2769-2812
- Poldermans D, Schouten O, Vidakovic R, Bax JJ, Thomson IR, Hoeks SE, Feringa HH, Dunkelgrun M, de Jaegere P, Maat A, van Sambeek MR, Kertai MD, Boersma E. (2007). A clinical randomized trial to evaluate the safety of a non-invasive approach in high-risk patients undergoing major vascular surgery: the DECREASE-V Pilot Study. *J Am Coll Cardiol*. 49(3), pp. 1763-1769
- Pon L, Schon E (2007). *Mitochondria*. 2nd ed. Columbia University: Academic Press
- Port FK, Wolfe RA, Mauger EA, Berling DP, Jiang K. (1993). Comparison of survival probabilities for dialysis patients vs cadaveric renal transplant recipients. *JAMA*. 270(2), pp. 1339-45
- Pritchard JB, Miller DS. (1992). Proximal tubular transport of organic anions and cations. In Seldin DW, Giebisch GH : *The Kidney: Physiology and Pathophysiology Volume 2*. New York, Raven Press, p. 2921
- Quigley AF, Kapsa RM, Esmore D, Hale G, Byrne E. (2000). Mitochondrial respiratory chain activity in idiopathic dilated cardiomyopathy. *J Cardiac Fail* 6(1), pp. 47–55
- Rabbat CG, Treleaven DJ, Russell JD, Ludwin D, Cook DJ. (2003). Prognostic value of myocardial perfusion studies in patients with end-stage renal disease assessed for kidney or kidney-pancreas transplantation: a meta-analysis. *J Am Soc Nephrol*. 14(2), pp. 431-439
- Ranhosky A, Kempthorne-Rawson J.(1990). The safety of intravenous dipyridamole thallium myocardial perfusion imaging. Intravenous Dipyridamole Thallium Imaging Study Group. *Circulation*. 81, pp. 1205-9.
- Raine AE, Seymour AM, Roberts AF, Radda GK, Ledingham JG. (1993). Impairment of cardiac function and energetics in experimental renal failure. *J Clin Invest*. 92(6), pp. 2934-40
- Ravizzini GC, Hanson MW, Shaw LK, Wong TZ, Hagge RJ, Pagnanelli RA, Jain D, Lima HS, Coleman RE, Borges-Neto S. (2002). Efficiency comparison between 99mTc-tetrofosmin

and ^{99m}Tc-sestamibi myocardial perfusion studies. *Nuclear Medicine Communications*. 23(3), pp. 203-8

Recchia FA, McConnell PI, Bernstein RD, Vogel TR, Xu X, Hintze TH. (1998). Reduced nitric oxide production and altered myocardial metabolism during the decompensation of pacing-induced heart failure in the conscious dog. *Circ Res*. 83(2), pp. 969-979

Reddy AK, Namiranian K, Lloyd EE, Bryan RM, Taffet GE, Hartley CJ. (2009). Effect of isoflurane on aortic impedance in mice. *Conf Proc IEEE Eng Med Biol Soc*. 2009 pp. 1104-1105

Reddy V, Bhandari S, Seymour AM . (2007). Myocardial function, energy provision, and carnitine deficiency in experimental uremia. *J Am Soc Nephrol*. 18(1), pp. 84-92

Rekhray S, Gandy SJ, Szejewski BR, Nadir MA, Noman A, Houston JG, Lang CC, George J, Struthers AD. (2013). High-dose allopurinol reduces left ventricular mass in patients with ischemic heart disease. *J Am Coll Cardiol*. 61(9), pp. 926-32

Reyes E, Loong CY, Harbinson M, Shelley Rahman S, Prvulovich E, Ell PJ, Anagnostopoulos C, Underwood R. (2006). A comparison of Tl-201, Tc-99m sestamibi, and Tc-99m tetrofosmin myocardial perfusion scintigraphy in patients with mild to moderate coronary stenosis. *Journal of Nuclear Cardiology*. 13(4), pp. 488–494

Ronco C, Haapio M, House AA, Anavekar N, Bellomo R. (2008). Cardiorenal syndrome. *J Am Coll Cardiol*. 52(19), pp. 1527-39

Rose BD: (1994) Antidiuretic hormone and water balance. In *Clinical Physiology of Acid Base and Electrolyte Disorders*, edn. 4. New York: McGraw Hill,

Ross RS (2004) Molecular and mechanical synergy: cross-talk between integrins and growth factor receptors. *Cardiovascular Res* 63(37), pp. 381–390

Rostand SG, Brunzell JD, Cannon RO 3rd, Victor RG. (1991). Cardiovascular complications in renal failure. *J Am Soc Nephrol*. 2 (2), pp. 1053-62

Rousset S, Alves-Guerra MC, Mozo J, Miroux B, Cassard-Doulier AM, Bouillaud F, Ricquier D. (2004). The biology of mitochondrial uncoupling proteins. *Diabetes*. 53 (Suppl 1), pp S130-5

- Rozanski A, Gransar H, Hayes SW, Min J, Friedman JD, Thomson LE. (2013). Temporal trends in the frequency of inducible myocardial ischemia during cardiac stress testing: 1991 to 2009. *J Am Coll Cardiol* 61, pp. 1054-65
- Sadoshima J, Izumo S. (1997). The cellular and molecular response of cardiac myocytes to mechanical stress. *Annu Rev Physiol.* 59(1), pp. 551-71.
- Sánchez-Lozada LG, Tapia E, Soto V, Avila-Casado C, Franco M, Wessale JL, Zhao L, Johnson RJ. (2008). Effect of febuxostat on the progression of renal disease in 5/6 nephrectomy rats with and without hyperuricemia. *Nephron Physiol.* 108(4), pp. 69-78
- Santos PC, Krieger JE, Pereira AC. (2012). Renin-angiotensin system, hypertension, and chronic kidney disease: pharmacogenetic implications. *J Pharmacol Sci.* 120(2), pp. 77-88
- Sarnak MJ, Levey AS, Schoolwerth AC. (2003). Kidney disease as a risk factor for development of cardiovascular disease: a statement from the American Heart Association Councils on Kidney in Cardiovascular Disease, High Blood Pressure Research, Clinical Cardiology, and Epidemiology and Prevention. *Hypertension.* 42, pp. 1050-1065
- Scarhag J, Schneider G, Urhausen A. (2006). Athlete's heart: Right and left ventricular mass and function in male endurance athletes and untrained individuals determined by MRI. *J Am Coll Cardiol* 40, p.1856
- Schnuelle P, Lorenz D, Trede M, Van Der Woude FJ. (1998). Impact of renal cadaveric transplantation on survival in end-stage renal failure: evidence for reduced mortality risk compared with haemodialysis during long-term follow-up. *J Am Soc Nephrol.* 9(3), pp. 2135-42
- Schölin A, Siegbahn A, Lind L. (2004). Diabetes Incidence Study in Sweden group. CRP and IL-6 concentrations are associated with poor glycemic control despite preserved beta-cell function during the first year after diagnosis of type 1 diabetes. *Diabetes Metab Res Rev* 20, pp. 205–210
- Secrest AM, Becker DJ, Kelsey SF, Laporte RE, Orchard TJ. (2010). Cause-specific mortality trends in a large population-based cohort with long-standing childhood-onset type 1 diabetes. *Diabetes.* 59, pp. 3216–3222
- Seddon M, Looi YH, Shah AM. (2007). Oxidative stress and redox signalling in cardiac hypertrophy and heart failure. *Heart.* 93(8), pp. 903-907

- Sengupta, P. (2013). The Laboratory Rat: Relating Its Age With Human's. *International Journal of Preventive Medicine*, 4(6), pp. 624–630.
- Sequeira V, van der Velden J. (2005). Historical perspective on heart function: the Frank-Starling Law. *Biophys Rev*. 7(4), pp. 421-447
- Shan K, Bick RJ, Poindexter BJ . (2000). Relation of tissue Doppler derived myocardial velocities to myocardial structure and beta-adrenergic receptor density in humans. *J Am Coll Cardiol*. 36(2),pp. 891-896
- Shapiro RJ. (1993). Catabolism of low-density lipoprotein is altered in experimental chronic renal failure. *Metabolism*. 42(1),pp. 162–9
- Sharir T, Kang X, Germano G, Bax JJ, Shaw LJ, Gransar H. (2006). Prognostic value of post-stress left ventricular volume and ejection fraction by gated myocardial perfusion SPECT in women and men: gender-related differences in normal limits and outcomes. *J Nucl Cardiol*. 13(3), pp. 495–506
- Sheridan D. (1998). Left Ventricular Hypertrophy - Alterations in Myocyte Number, Size, Shape and Structure. In: Sheridan D Left Ventricular Hypertrophy. London: Churchill - Livingston. pp. 79 - 85.
- Shin WJ, Miller K, Stipp V, Mazour S . (1995). Reverse redistribution on dynamic exercise and dipyridamole stress technetium- 99m-MIBI myocardial SPECT. *J Nucl Med*. 36(4), pp. 2053-2055
- Shub C, Cueto-Garcia L, Sheps SG, Ilstrup DM, Tajik AJ. (1986). Echocardiographic findings in pheochromocytoma. *Am J Cardiol*. 57(1), pp. 971–975.
- Silberberg JS, Barre PE, Prichard SS, Sniderman AD. (1989). Impact of left ventricular hypertrophy on survival in end-stage renal disease. *Kidney Int*. 36(2), pp. 286-90
- Sjostrom PA, Odland BG, Wolgast M. (1988). Extensive reabsorption and secretion of creatinine in humans. *Scand J Urol Nephrol* 22, pp. 129-131
- Smith K, Semple D, Aksentijevic D, Bhandari S, Seymour A-M (2010). Functional and metabolic adaptations in uraemic cardiomyopathy *Front Biosci*. 2(Elite Ed), pp. 1492-501
- Soedamah-Muthu SS, Fuller JH, Mulnier HE, Raleigh VS, Lawrenson RA, Colhoun HM. (2006) High risk of cardiovascular disease in patients with type 1 diabetes in the U.K.: a cohort study using the general practice research database. *Diabetes Care* 29(5), pp. 798–804

- Spinale FG , Coker ML , Thomas CV , Walker JD , Mukherjee R , Hebbar L. (1998). Time-dependent changes in matrix metalloproteinase activity and expression during the progression of congestive heart failure: relation to ventricular and myocyte function. *Circ Res* 82, pp. 482-495,
- Stanley WC, Lopaschuk GD, Hall JL, McCormack JG. (1997). Regulation of myocardial carbohydrate metabolism under normal and ischaemic conditions. *Cardiovasc Res.* 33(3), pp. 243–257
- Stratmann G, Sall JW, May LD, Bell JS, Magnusson KR, Rau V, Visrodia KH, Alvi RS, Ku B, Lee MT, Dai R. (2009). Isoflurane differentially affects neurogenesis and long-term neurocognitive function in 60-day-old and 7-day-old rats. *Anesthesiology.* 110(4), pp. 834-48
- Steffey EP. (1996). Inhalation anesthetics, In: Lumb and Jones veterinary anesthesia, 3rd ed (Thurmon J, Tranquilli W, Benson J). Baltimore, Williams and Wilkins, pp. 297-329
- Sugiura T, Takase H, Toriyama T, Goto T, Ueda R, Dohi Y. (2006). Usefulness of Tc-99m methoxyisobutylisonitrile scintigraphy for evaluating congestive heart failure. *J Nucl Cardiol.* 13(1), pp. 64-8
- Szwejkowski BR, Gandy SJ, Rekhraj S, Houston JG, Lang CC, Morris AD, George J, Struthers AD (2013). Allopurinol reduces left ventricular mass in patients with type 2 diabetes and left ventricular hypertrophy. *J Am Coll Cardiol.* 62(24), pp. 2284-93
- Tada M, Katz AM. (1982). Phosphorylation of the sarcoplasmic reticulum and sarcolemma. *Ann Rev Physiol.* 44, pp. 401-408
- Taddei S, Nami R, Bruno RM, Quatrini I, Nuti R. (2011). Hypertension, left ventricular hypertrophy and chronic kidney disease. *Heart Fail Rev.* 16(1), pp. 615–620
- Taillefer R, Primeau M, Costi P, Lambert R, Léveillé J, Latour Y. (1991). Technetium-99m-sestamibi myocardial perfusion imaging in detection of coronary artery disease: comparison between initial (1-hour) and delayed (3-hour) post-exercise images. *J Nucl Med.* 32(10), pp. 1961-5
- Takeishi Y, Sukekawa H, Fujiwara S, Ikeno E, Sasaki Y, Tomoike H, et al. (1996). Reverse redistribution of technetium- 99m-sestamibi following direct PTCA in acute myocardial infarction. *J Nucl Med.* 37(1), pp. 1289-1294

- Taylor D, Bhandari S, Seymour AM. (2015). Mitochondrial dysfunction in uremic cardiomyopathy. *Am J Physiol Renal Physiol.* 308(6), pp. F579-87
- Tian R, Musi N, D'Agostino J, Hirshman MF, Goodyear LJ. (2001) Increased adenosine monophosphate-activated protein kinase activity in rat hearts with pressure-overload hypertrophy. *Circulation.* 104, pp.1664–1669
- Tripepi G, Benedetto FA, Mallamaci F, Tripepi R, Malatino L, Zoccali C. (2007). Left atrial volume in end-stage renal disease: A prospective cohort study. *J Am Soc Nephrol.* 18, pp. 1316-22
- Tsutsui H, Kinugawa S, Matsushima S. (2011). Oxidative stress and heart failure. *Am J Physiol Heart Circ Physiol.* 301(6), pp. H2181-90
- Tsutsui H, Kinugawa S, Matsushima S. (2011). Oxidative stress and heart failure. *American Journal of Physiology - Heart and Circulatory Physiology.* 301(6), pp. H2181-H2190
- Ullrich KJ, Rumrich G. (1993). Renal transport mechanisms for xenobiotics. *Clin Invest* 71(843) pp. 23-28
- Ushijima K, Ando H, Arakawa Y, Aizawa K, Suzuki C, Shimada K, Tsuruoka S. (2017). Prevention against renal damage in rats with subtotal nephrectomy by sacubitril/valsartan (LCZ696), a dual-acting angiotensin receptor-neprilysin inhibitor. *Pharmacol Res Perspect.* 5(4), e03336
- Van Agtmael T, Bruckner-Tuderman L. (2010). Basement membranes and human disease. *Cell Tissue Res.* 339(1), pp. 167-88.
- Van Koppen A, Verhaar MC, Bongartz LG, Joles JA. (2013). 5/6th Nephrectomy in Combination with High Salt Diet and Nitric Oxide Synthase Inhibition to Induce Chronic Kidney Disease in the Lewis Rat. *J Vis Exp.* 77 (50398), Online
- Van HeerebeekL, Borbely A, Niessen HW.(2006). Myocardial structure and function differ in systolic and diastolic heart failure. *Circulation.* 113, pp. 1966-1970
- Vander A (1980) In *Renal Physiology*. New York: McGraw Hill, p. 89.
- Vander Heide RS, L'Ecuyer TJ. (2007). Molecular basis of Anthracycline induced cardiotoxicity. *Heart Metab.* 35(1), pp.1-4
- Victor VM, Rocha M, Herance R, Hernandez-Mijares A. (2011). Oxidative stress and mitochondrial dysfunction in type 2 diabetes. *Curr Pharm Des.* 17(36), pp. 3947-58

Vítola JV, Wanderley MR, Cerci RJ, Pereira Neto CC, Korman O, Neto OF, da Silva JA, da Cunha CL, Shin-Ike I, Stier AL. (2016). Outcome of patients with high-risk Duke treadmill score and normal myocardial perfusion imaging on spect. *J Nucl Cardiol.* 23(6), pp. 1291-1300

Wackers FJ, Berman DS, Maddahi J, Watson DD, Beller GA, Strauss HW et al. (1989). Technetium-99m hexakis 2-methoxyisobutyl isonitrile: human biodistribution, dosimetry, safety, and preliminary comparison to thallium-201 for myocardial perfusion imaging. *J Nucl Med.* 30(4), pp. 301-11

Wackers FJ, Berman DS, Maddahi J, Watson DD, Beller GA, Strauss HW. (1989). Technetium-99m hexakis 2-methoxyisobutylisonitrile: human biodistribution, dosimetry, safety, and preliminary comparison to thallium-201 for myocardial perfusion imaging. *J Nucl Med.* 30(1), pp. 301-11

Wehrens XH, Lehnart SE, Reiken S. (2005). Enhancing calastabin binding to ryanodine receptors improves cardiac and skeletal muscle function in heart failure. *Proc Natl Acad Sci.* 102(9607), pp. 126-133

Wiggers CJ. (1915) *Modern Aspects of Circulation in Health and Disease.* Philadelphia, Lea and Febiger.

Williams G, Pickup JC. (1998) *Handbook of Diabetes.* Oxford: Blackwell Science Inc

Williams B, Mancia G, Spiering W, Rosei E, Azizi M, Burnier M, Clement DL, Coca A, de Simone G et al. (2018). ESC Scientific Document Group; 2018 ESC/ESH Guidelines for the management of arterial hypertension, *European Heart Journal,* 39(3), pp. 3021–3104,

Wilson RF, Wyche K, Christensen BV, Zimmer S, Laxson DD.(1990) Effects of adenosine on human coronary arterial circulation. *Circulation* 82, pp.1595-606.

Winther S, Svensson M, Jørgensen HS, Bouchelouche K, Gormsen LC, Pedersen BB. (2015). Diagnostic Performance of Coronary CT Angiography and Myocardial Perfusion Imaging in Kidney Transplantation Candidates. *JACC Cardiovasc Imaging.* 8(5), pp. 553-62

World Health Organization. Part 1, Diagnosis and classification of diabetes mellitus. Geneva: World Health Organization; (1999). Definition, diagnosis and classification of diabetes mellitus and its complications: Report of a WHO consultation.

- Worthley L. (2000). Shock: A Review of Pathophysiology and Management. *Critical Care and Resuscitation*. 2(2) pp. 55-65
- Xiao G, Mao S, Baumgarten G, Serrano J, Jordan MC, Roos KP, Fishbein MC, MacLellan WR. (2001). Inducible activation of c-Myc in adult myocardium in vivo provokes cardiac myocyte hypertrophy and reactivation of DNA synthesis. *Circ Res*. 89(12), pp.1122-9
- Xie Y-W, Shen W, Zhao G, Xu XB, Wolin MS, Hintze TH. (1996). Role of endothelium-derived nitric oxide in the modulation of canine myocardial mitochondrial respiration in vitro. *Circ Res*. 79(1), pp. 381–387
- Xu X, Hu X, Lu Z, Zhang P, Zhao L, Wessale JL, Bache RJ, Chen Y. (2008). Xanthine oxidase inhibition with febuxostat attenuates systolic overload-induced left ventricular hypertrophy and dysfunction in mice. *J Card Fail*. 14(9), pp. 746-53
- Yang CF, Chen MYC, Chen TI, Cheng CF. (2014). Dose-dependent effects of isoflurane on cardiovascular function in rats. *Tzu Chi Medical Journal*. 26(3), pp. 119-122
- Yap L, Arshad W, Jain A, Kurbaan AS. (2005). Significance of ST depression during exercise treadmill stress and adenosine infusion myocardial perfusion imaging. *The International Journal of Cardiovascular Imaging*. 21(3), pp. 253-8
- Yokozawa T, Zheng PD, Oura H, Koizumi F. (1986). Animal models of adenine induced chronic renal failure in rats. *Nephron* 44(2), pp. 230-4
- Zak R. Growth of the Heart in Health and Disease. Raven Press, New York. 1984, pp 194-198
- Zaragoza C, Gomez-Guerrero C, Martin-Ventura JL. (2011) Animal Models of Cardiovascular Diseases. *Journal of Biomedicine and Biotechnology*. 2011, 497841 (Online).
- Zaret B, Beller G. Clinical Nuclear Cardiology. 3rd ed. Philadelphia, PA: Mosby; 2005, pp. 216-218
- Zhong W, Mao S, Tobis S, Angelis E, Jordan MC, Roos KP, Fishbein MC, de Alborán IM, MacLellan WR. (2005). Hypertrophic growth in cardiac myocytes is mediated by Myc through a Cyclin D2-dependent pathway. *EMBO J*. 25(16), pp. 3869-79
- Zimmer HG, Kolbeck-Ruhmkorff C, Zierhut W. (1995). Cardiac hypertrophy induced by alpha- and beta-adrenergic receptor stimulation. *Cardioscience*. 6(1), pp. 47-57.

Zorov DB, Filburn CR, Klotz LO, Zweier JL, Sollott SJ. (2000). Reactive oxygen species (ROS)-induced ROS release: a new phenomenon accompanying induction of the mitochondrial permeability transition in cardiac myocytes. *J Exp Med.* 192, pp. 1001-14